Synthesis, Characterisation and Polymerisation Behaviour of Novel α-Diimine Iron Catalysts

by

Laura E. N. Allan

A thesis submitted for the degree of Doctor of Philosophy at Imperial College London

September 2007

Statement of Copyright

The copyright of this thesis rests with the author. No quotation from it should be published without the prior written consent of the author and information derived from it should be acknowledged.

Declaration

The work described in this thesis was carried out in the Department of Chemistry at Imperial College London between October 2003 and May 2007. The entire body of work is my own, unless otherwise stated to the contrary, and has not been submitted previously for a degree at this or any other university.

Acknowledgements

My time in the Harwood Lab began more or less accidentally, after a meeting with Vernon about something else entirely. However, I enjoyed immensely my time in the VCG group and owe a great debt of thanks to my inspirational supervisor of the last 4 years, Professor Vernon Gibson.

The EPSRC provided the funding for this work, and thanks must also go to those who have helped me collect the data for this thesis, both at Imperial and on my travels. At Imperial, Dick and Pete helped with NMR, John and Geoff ran mass spectra, Prof. Henry Rzepa did the calculations and Dr. Andrew White spent a lot of time on the crystal structures (particularly the nasty, twinned samples!) In terms of other institutions I've visited over the years, Stephen Boyer from the London Metropolitan University ran the elemental analyses and Dr. Dave Evans from the John Innes Centre, Norwich obtained and analysed the Mössbauer spectra. From the University of Manchester, Drs. Joanna Wolowska and Floriana Tuna collected the EPR and SQUID data, and Professors Eric McInnes and David Collison are also thanked for invaluable discussions.

Thanks to Sue, who not only keeps the lab running efficiently but also finds time to organise the many mulled wine parties, fireworks, Christmas parties and Vernon-funded trips to the pub.

There are many people who have helped me out over the years; far too many to list here. However, a particular mention for those who took pity on a young and inexperienced PhD student: Missy, Kilian, Rich and Andrew (the original Grumpy Whinging Northerner!)

Special thanks go to "Professor Mike" Shaver, who arrived during my 2nd year and made a big difference, not just to my project, but to the way I approach my chemistry. Happily, most of our disagreements were settled without resorting to physical violence. Thanks also to Mike for his trans-Atlantic proof-reading.

Many thanks to those who made the social side of a chemistry PhD so much fun, particularly those veterans of Southside, the Holland Club and the Union: Andrew, Andy C, Atanas, Cas, Charlie, Chris, Damien, DJD, DJJ, Dom, Ed, George, Humpo, Ian, James, Juan, Juri, Kilian, Keith, Linsey, Lisa, Lizzie, Mike, Missy, MvM, Paddy, Pete, Phil, Pimpa, Por, PZ, Renan, Rich, Richie, Rob, Russell, (Cheers!) Tang and Theo.

A special mention to Pete, Trudi and Ian of the (now sadly closed) Radnor Arms, where Friday night quizzes soon became tradition. And to my fellow Team Sb members: Lisa, Mike, Paddy, Richie and Mr Monkey.

And finally...it would have been very difficult to get through the past 8 years at Imperial without the support of my family. When I announced I wanted to stay on for a PhD, they took it very well and have continued to love me, even in my perpetual studenthood.

Thanks!

Abstract

This thesis describes the synthesis and characterisation of a series of novel α-diimine Fe^{II} and Fe^{III} complexes and explores the controlled radical polymerisation behaviour of the Fe^{II} complexes.

Chapter 1 gives an introduction to the field of iron catalysis, with emphasis on the development of controlled radical polymerisation and the relevant mechanisms discussed in later chapters. The evolution of these mechanisms and the importance of the interplay between them are covered.

Chapter 2 reports the synthesis of a family of novel 2,3-substituted α-diimine ligands, bearing electron-withdrawing groups at the 2,3-positions of the backbone. The synthesis, characterisation and polymerisation behaviour of the Fe^{II} chloride complexes is described.

Chapter 3 reports the synthesis and characterisation of Fe^{III} chloride complexes bearing electron-withdrawing groups at the 2,3-positions of the ligand backbone. The prevalent polymerisation mechanism exhibited by the Fe^{II} dichloride complexes in Chapter 2 is shown to correlate to the metal spin-state of the analogous Fe^{III} trichloride complexes. Computational studies are used to rationalise these findings.

Chapter 4 investigates structure-activity relationships for the α-diimine iron complexes, through the synthesis of an extended family of 2,3-phenyl-substituted ligands, varying at the *para* position of the aromatic ring. Hammett plots illustrate the linear relationship between the substituent constant and both the rate of reaction and polymer molecular weight.

Chapter 5 is a detailed discussion of mechanistic studies carried out to elucidate the polymerisation mechanisms in which the α-diimine iron catalysts participate. A series of reactivity studies, the role of organometallic mediated radical polymerisation, and the catalytic reactivity in terms of radical concentrations is discussed.

Chapter 6 looks at exploiting the low toxicity and economic viability of iron α-diimine catalysts through moving towards atom transfer radical polymerisation in aqueous media. A range of novel complexes are synthesised and tested in polymerisation reactions.

Chapter 7 gives experimental details for Chapters 2-6.

Abbreviations

δ	chemical shift	J	coupling constant
$\mu_{eff.}$	effective magnetic moment	$k_{obs.}$	observed rate of polymerisation
Å	angstrom	MALDI-MS	matrix assisted laser desorption / ionisation mass spectrometry
acac	acetyl acetonate	mmol	millimoles
a.m.u.	atomic mass units	M_n	number average molecular weight
ATRP	atom transfer radical polymerisation	$M_{n,th}$	theoretical molecular weight, based on monomer conversion
Ar	generic aryl group	M_p	molecular weight at peak maximum
B. M.	Bohr magneton	M_w	weight average molecular weight
COSY	correlation spectroscopy	M_w/M_n	molecular weight distribution
Cp	cyclopentadienyl	NMR	nuclear magnetic resonance
Cp^*	pentamethyl cyclopentadienyl	OMRP	organometallic mediated radical polymerisation
cm^{-1}	wave number	PDI	polydispersity index
CI-MS	chemical ionisation mass spectrometry	PMMA	poly(methyl methacrylate)
CCT	catalytic chain transfer	ppm	parts per million
Da	Daltons	PS	polystyrene
EI-MS	electron ionisation mass spectrometry	R	generic alkyl group
eq. / equiv.	equivalents	RAFT	reversible addition fragmentation chain transfer
FAB-MS	fast atom bombardment mass spectrometry	SFRP	stable free radical polymerisation
g	grams	T	Tesla
GPC	gel permeation chromatography	UV-vis	ultra-violet / visible spectroscopy
GC	gas chromatography	*vs.*	versus
GC-MS	gas chromatography-mass spectrometry	v/v	volume for volume
h	hours	w/w	weight for weight
Hz	hertz	X	generic anionic, monodentate donor
IR	infra-red spectroscopy		

All other abbreviations are described in the text as they occur.

Table of Contents

Statement of Copyright 2

Declaration 2

Acknowledgements 3

Abstract 4

Abbreviations 5

Table of Contents 6

List of Tables 10

Chapter 1 - Introduction 12

1.1 - Living Polymerisations 14

1.2 - Controlled Radical Polymerisation 15

1.3 - Atom Transfer Radical Polymerisation 17

1.3.1 Detailed mechanism 21

1.4 - Iron ATRP catalysts 22

1.5 - Stable Free Radical Polymerisation 27

1.6 - Organometallic Mediated Radical Polymerisation 29

1.6.1 Detailed mechanism 30

1.7 - Catalytic Chain Transfer 31

1.8 - Catalysts Operating by more than 1 Mechanism 34

1.9 - Conclusions 37

1.10 - References 38

Chapter 2 - Synthesis, Characterisation and Polymerisation Studies using Fe^{II} α-Diimine Complexes 46

2.1 - Introduction 47

2.2 - Results and Discussion 50

2.2.1 - Synthesis of Fe^{II} compounds 50

2.2.2 - Polymerisation data 60

2.2.2.1 - N-alkyl complexes 7-10 60

2.2.2.2 - N-aryl complexes 11-12 67

2.2.2.3 - End group analysis 69

*2.2.2.4 - MMA polymerisation using N-alkyl complexes **7-10*** 72

2.3 - Conclusions 73

2.4 - References 74

Chapter 3 - Correlation between Metal Spin-State and Catalytic Reactivity 76

3.1 - Introduction 77

3.2 - Results and Discussion 79

3.2.1 - Synthesis of Fe^{III} compounds 79

*3.2.1.1 - X-ray structure of ^{tBu,H}[N,N]$FeCl_3$, **15**.* 81

3.2.1.2 - Attempted X-ray structure determination of other Fe^{III} derivatives. 82

3.2.2 - The magnetic behaviour of 14 and 15. 87

3.2.2.1 - Solution and solid state EPR spectroscopy studies. 87

3.2.2.2 - SQUID magnetometry studies. 91

3.2.2.3 - Mössbauer spectroscopy studies. 102

3.2.3 - Computational studies. 108

3.3 - Conclusions 112

3.4 - References 113

Chapter 4 - Structure-Activity Relationships for α-Diimine Iron Complexes 117

4.1 - Introduction 118

4.2 - Results and Discussion 120

4.2.1 - Synthesis of Fe^{II} compounds 120

4.2.2 - Polymerisation data 127

4.2.2.1 - Styrene polymerisation 127

4.2.2.2 - MMA polymerisation 139

4.2.3 - Synthesis of Fe^{III} compounds 146

4.2.4 - SQUID magnetometry 147

4.2.5 - Correlation of para substituent with reactivity for $^{R';R''}$[N,N]$FeCl_2$ catalysts 150

4.3 - Conclusions 155

4.4 - References 156

Chapter 5 - Investigating the Polymerisation Mechanism of α-Diimine Iron Complexes 158

5.1 - Introduction 159

5.2 - Results and Discussion 163

5.2.1 - β-H elimination versus direct H-transfer 163

5.2.1.1 - Alkylation experiments 163

5.2.1.2 - Radical trapping experiments 166

5.2.1.3 - Catalyst loading 167

5.2.2 - Radical concentrations and the role of OMRP for $^{R';R''}$[N,N]$FeCl_2$ catalysts 168

5.2.2.1 - Mixed catalyst systems 173

5.3 - Conclusions 178

5.4 - References 180

Chapter 6 - Towards ATRP in Aqueous Media using New α-Diimine Iron Complexes 183

6.1 - Introduction 184

6.2 - Results and Discussion 188

6.2.1 - Synthesis and polymerisation behaviour of amino-functionalised Fe^{II} complexes 188

6.2.1.1 - Aryl amino substituents 188

6.2.1.2 - Alkyl amino substituents 190

6.2.1.3 - Polymerisation studies using the amino-substituted complexes 194

6.2.1.4 - Next generation amino substituents 207

6.2.1.5 - Polymerisation studies using the new amino complexes 209

6.2.2 - Synthesis and polymerisation behaviour of hydroxy-substituted Fe^{II} complexes. 213

6.2.2.1 – Synthesis of Fe^{II} oxime complexes 214

6.2.2.2 - Polymerisation studies using Fe^{II} oxime complexes 219

6.3 - Conclusions and Further Work 223

6.4 - References 226

Chapter 7 - Experimental 229

7.1 -General experimental details 230

7.2 - Solvents and reagents 231

7.3 - Polymerisation procedures 231

7.4 – General procedure for alkyl decomposition experiments 232

7.5 - Solution magnetic susceptibility measurements 232

7.6 - Synthetic procedures 233

7.6.1 - Experimental details for Chapter 2 233

7.6.1.1 - Ligand synthesis 233

7.6.1.2 - Synthesis of Fe^{II} complexes 235

7.6.2 - Experimental details for Chapter 3 237

7.6.2.1 - Synthesis of Fe^{III} complexes 237

7.6.3 - Experimental details for Chapter 4 239

7.6.3.1 - Ligand synthesis 239

7.6.3.2 - Synthesis of Fe^{II} complexes 242

7.6.3.3 - Synthesis of Fe^{III} complexes 245

7.6.4 - Experimental details for Chapter 5 247

7.6.5 - Experimental details for Chapter 6 248

7.6.5.1 - Synthesis of amine-substituted compounds 248

7.6.5.2 - Synthesis of hydroxy-substituted compounds 255

7.7 - References 258

Chapter 8 - Appendices 259

8.1 - Appendix 1: Crystal Structure Data 260

8.1.1 - Crystal structure data for Chapter 2 260

8.1.2 - Crystal structure data for Chapter 3 266

8.1.3 - Crystal structure data for Chapter 4 272

8.1.4 - Crystal structure data for Chapter 6 277

8.2 - Appendix 2: Hammett Substituent Constants 283

8.2.1 - Substituent constant data for Chapter 4 283

List of Tables

Table 2.1 Selected bond lengths (Å) and angles (°) for complex **7**. 54

Table 2.2 Selected bond lengths (Å) and angles (°) for the two disordered orientations (**major** *ca.* 58%, **minor** *ca.* 42% occupancy) of the C_S-symmetric complex **8**. 56

Table 2.3 Selected bond lengths (Å) and angles (°) for the three crystallographically independent complexes (**I**, **II** and **III**) present in the crystals of **9**. 57

Table 2.4 Selected bond lengths (Å) and angles (°) for the two crystallographically independent C_S-symmetric complexes (**I** and **II**) present in the crystals of **10**. 58

Table 2.5 Selected bond lengths (Å) and angles (°) for complex **11**. 59

Table 3.1 Selected bond lengths (Å) and angles (°) for the two crystallographically independent C_S-symmetric complexes (**I** and **II**) present in the crystals of **15**. 82

Table 3.2 Selected bond lengths (Å) and angles (°) for **17a**. 84

Table 3.3 Selected bond lengths (Å) and angles (°) for **16a** and **16b**. 85

Table 3.4 Mössbauer parameters for complex **15**. 105

Table 3.5 Mössbauer parameters for complex **14**. 106

Table 4.1 Selected bond lengths (Å) and angles (°) for **31**. 124

Table 4.2 Selected bond lengths (Å) and angles (°) for the two crystallographically independent complexes (**I** and **II**) present in the crystals of **35** (major occupancy orientations). 126

Table 4.3. Magnetic moments at selected temperatures for complexes **13-15**, **36-39**. 150

Table 5.1 Radical concentrations for ATRP and OMRP of styrene using $^{R',R''}[N,N]FeCl_2$. 171

Table 6.1 Selected bond lengths (Å) and angles (°) for complex **45**. 189

Table 6.2 Selected bond lengths (Å) and angles (°) for complex **52**. 193

Table 6.3 Selected bond lengths (Å) and angles (°) for complex **53**. 194

Table 6.4 Selected data for styrene polymerisation using complexes **52-54**. 198

Table 6.5 Selected data for styrene polymerisation using complexes **55-57**. 204

Table 6.6 Selected data for MMA and 2-HPMA polymerisation using complexes **55-57**. 206

Table 6.7 Selected data for polymerisation using complexes **62** and **63**. 213

Table 6.8 Selected bond lengths (Å) and angles (°) for complex **66**. 216

Table 6.9 Selected bond lengths (Å) and angles (°) for complex **67**. 218

Table 6.10 Selected data for polymerisation using complexes **66-69**. 219

Chapter 1

Introduction

Radical polymerisations are perhaps the most commonly employed industrial technique for the synthesis of polymeric materials, allowing the facile polymerisation of a wide variety of vinyl monomers under mild conditions. The versatility of radical polymerisations results from their tolerance to functional groups, both within the monomer and in terms of external impurities. The highly active, neutral, growing radical species enable rapid polymerisation but do not react with polar compounds. However, this high activity results in bimolecular termination reactions between the neutral species, such as recombination and disproportionation. Initiation is slow, relative to the extremely fast propagation rate, and the fast termination reactions mean that new chains are continually generated and control over the polymer molecular weight and polydispersity index is poor.[1]

Polymeric materials, including 'pure' linear, branched or cross-linked polymers (gels, rubbers, etc.) and polymer blends and composites, where polymers are combined with other materials such as metals, clays and ceramics, are used in every branch of life, science and technology. The properties and application of a polymer depend on the molecular weight distribution and molecular structure; the composition, topology and functionality of the polymer are all important.[2] Synthetic procedures which allow control over these parameters are therefore of great significance, particularly those which are not industrially demanding. One such process is controlled radical polymerisation which, through virtual elimination of the side-reactions, has allowed the synthesis of novel functionalised materials with well-controlled molecular weights and molecular weight distributions.

The work reported in the rest of this thesis details investigation into the mechanism by which an α-diimine Fe system polymerises styrene, the interplay of the various polymerisation mechanisms and the application of the mechanistic understanding obtained to the design of new catalysts. The rest of this chapter details the development of controlled radical polymerisation techniques, which combine the precision polymer synthesis of a living polymerisation with the versatility and tolerance of a free radical polymerisation. Of particular interest are the recent reports of catalysts which are able to operate through more than one polymerisation mechanism, paving the way for greater exploitation of the techniques through an understanding of the mechanistic details.

1.1 Living Polymerisations.

A "living" polymerisation is one which proceeds in the absence of irreversible termination or chain transfer reactions, affording polymers with well-defined compositions and architectures. Propagation occurs without chain transfer or termination reactions and so all chain ends remain active during the reaction. Chain extension continues until an external reagent is added in to irreversibly terminate the polymerisation. Living polymerisations allow the synthesis of macromolecular materials with excellent control over molecular weight and microstructure, and the synthesis of well-defined copolymers and end-functionalised polymers. The polymer chains all grow at the same rate and molecular weights increase linearly with conversion, with the number of growing chains determined by the concentration of the initiator. The molecular weight distribution in a living polymerisation is narrow (low polydispersity index), close to a Poisson distribution.

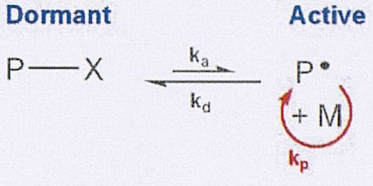
The first living polymerisation was reported in 1956 by Szwarc[3] who used the reaction between sodium and naphthalene to initiate the living anionic polymerisation of styrene and to perform block copolymerisations of styrene and isoprene.[4,5] He noted that addition of new monomer feed after the polymerisation was complete resulted in chain extension, thus proving that the chain ends were living. For more than a decade, living anionic polymerisation was the only method by which chain transfer and termination reactions could be eliminated from chain growth polymerisation. Other living polymerisations were to follow, beginning with cationic ring opening polymerisation,[6-9] and eventually extending to living cationic polymerisation.[10,11]

Until recently, only these living ionic polymerisations were able to offer precise control over the structure and architecture of vinyl polymers. Although anionic and cationic polymerisation techniques allowed the synthesis of low polydispersity materials, control over molecular weights and well-defined chain ends, they were unsuitable for a wide range of functionalised monomers. The anionic or cationic growing polymer chain end is incompatible with certain functional groups and monomer families, and these techniques also necessitate stringent reaction conditions; ultra-pure reagents and the total exclusion of water and oxygen from the system are required. In order to overcome these limitations, synthetic polymer chemists developed new processes, resulting in the development of free radical polymerisations which display all the characteristics of a living process[12,13] but

which are tolerant of a wide range of functional groups and the presence of water, oxygen and other impurities.

1.2 Controlled Radical Polymerisation.

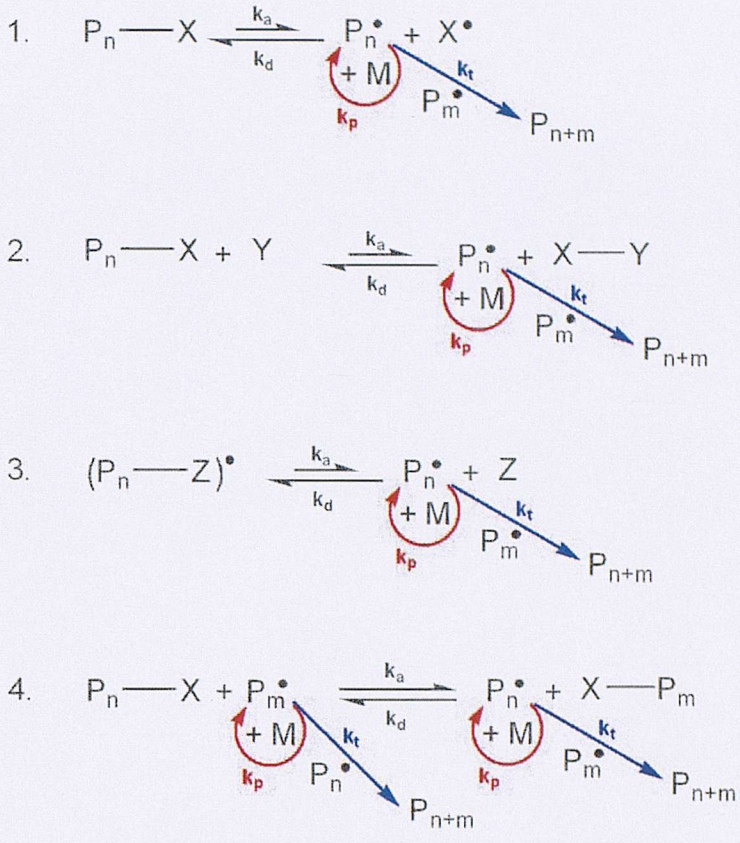
Controlled radical polymerisation (CRP), or controlled/living radical polymerisation, techniques use the principle of equilibration between a growing free radical and a dormant species (Scheme 1.1) to reduce chain breaking reactions and ensure quantitative initiation, resulting in good control over molecular weights, polydispersities and end functionalities. Although termination is minimised, it is not eliminated and the presence of unavoidable termination reactions means that a truly living free radical polymerisation is still a goal aspired to by polymer chemists.



Scheme 1.1 General scheme for reversible activation.

The position and dynamics of the equilibrium between the dormant and active species defines the rate of reaction, the molecular weight and the polydispersity of the polymer formed during a CRP. Mechanistically, there are four different types of CRP,[14] illustrated in Scheme 1.2. P_n–X represents the dormant, non-propagating species, $P_n^{\bullet}$ is the active species and $X^{\bullet}$, $XY^{\bullet}$ and Z are the radical traps.

The first system (see **1** in Scheme 1.2) involves spontaneous homolytic cleavage of the dormant species into a propagating radical chain and a "stable" (or persistent) free radical ($X^{\bullet}$). The early reports were of the versatile nitroxide-mediated polymerisations (NMP), which used persistent radicals such as 2,2,6,6-tetramethylpiperidine-1-oxyl (TEMPO) as the radical trap.[15] Much recent work has focused on organometallic mediated radical polymerisation (OMRP) which allows control over polymerisations based on the reversible homolytic cleavage of the weak bond between an alkyl group and a transition metal catalyst.[16-22]



Scheme 1.2 Different types of controlled radical polymerisation.

The second mechanism, atom transfer radical polymerisation (ATRP, see **2** in Scheme 1.2), involves a redox-active transition metal species. Reversible homolytic cleavage of carbon-halogen bonds generates the active species, while the propagating radicals are temporarily deactivated through a halogen-transfer reaction with the oxidised metal complex.[23,24] In this system the persistent radical is $XY^\bullet$.

The third system involves the reversible formation of persistent radicals through the reaction of the propagating radical with a species containing an even number of electrons (see **3** in Scheme 1.2). Phosphites,[25] reactive but non-polymerisable alkenes such as stilbene,[26] and transition metal compounds with an even number of electrons[27] have been used as the reversible radical trap. The persistent radical should neither react with itself nor the monomer. This mechanism is very similar to the first system described, except that the dormant species has an odd number of electrons and the radical trap (Z) is not a radical, meaning that the role of "persistent radical" in this system is actually played by a non-radical species.

The fourth process (**4** in Scheme 1.2) is based on a thermodynamically neutral bimolecular exchange between a low concentration of growing radical chains and a

dormant species. An example of this category is degenerative transfer (DT) polymerisations using alkyl iodides,[28,29] organotelluriums,[30] organostibenes[31] and organobismuthines.[32] Reversible addition fragmentation chain transfer (RAFT) polymerisation[33] and macromolecular architecture design by interchange of xanthates (MADIX)[34] also utilise this mechanism. This system is very different to the other three described above, as it does not involve a persistent radical.

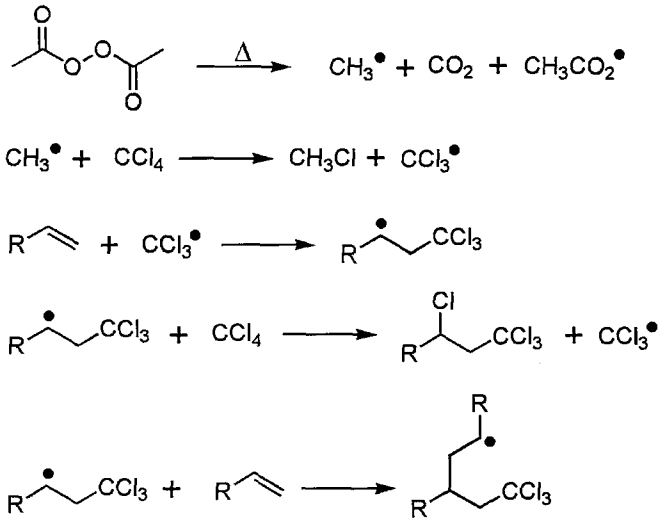
The polymerisation mechanisms which are relevant to the work reported in this thesis will be discussed further in the following sections. One of the most interesting facets of current study in this field is in recognising the interplay between these mechanisms, as illustrated in a recent review article on the relationship between 1-electron transition metal reactivity and radical polymerisation processes.[22]

1.3 Atom Transfer Radical Polymerisation.

Atom transfer radical polymerisation (ATRP) is perhaps the most versatile controlled radical polymerisation technique, and allows polymerisation of a wide variety of monomers,[35] including styrene,[36,37] methacrylates[38,39] and acrylates.[40] The ATRP process expresses all of the experimental characteristics of a living polymerisation[41] and facilitates control of chain topology, composition and functionality. A wide range of initiators can be used and experimental conditions are relatively simple, but excellent control of both the molecular weight and the molecular weight distribution of the resulting polymers is possible. Furthermore, it has been demonstrated that polymerisation can be carried out in water,[42] in the presence of oxygen,[43] and even at room temperature,[44] if the relevant conditions are met. Another important advantage of ATRP is that the end-group of the polymer chain is typically an inexpensive halogen, and thus can easily be converted to other functional groups including azides, amines, alkenes, sulfides and thiols.[41] ATRP has attracted much industrial interest because of its robust nature, such as the low requirement of monomer purity and tolerance towards trace amounts of oxygen and water. Much research into understanding the reaction mechanism and expanding the areas of application[45] has already been completed, in the hope of utilising the process in the design of novel materials and polymer architectures.[46]

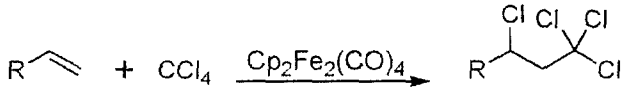
ATRP is an extension of atom transfer radical addition (ATRA) which was developed from the Kharasch addition. Kharasch showed that addition of an olefin to an excess of CCl_4 or $CHCl_3$ and heating the reaction with a small amount of

dibenzoyl or diacetyl peroxide resulted in addition of the haloalkane across the double bond.[47] He noted that effective repetition of the cycle only occurred when R = alkyl (Scheme 1.3, **A**), as if R = aryl (e.g. styrene was used) the radical tended to react with the alkene to form polymers (Scheme 1.3, **B**).



Scheme 1.3 Radical mechanism of the Kharasch addition.

A number of metal complexes were subsequently shown to catalyse the addition of a halocarbon to an olefin, without the need for a radical initiator.[48] The dinuclear Fe^{I} complex, $Cp_2Fe_2(CO)_4$, was found to be a more efficient catalyst for the addition of halocarbon to olefin than both mononuclear systems and Kharasch's original peroxides.[49] During the reaction (Scheme 1.4) one of the metal centres undergoes reversible redox between the monovalent and divalent states, in a similar manner to the reactions reported in the literature for complexes of Ru^{II}, Ni^{II}, Cu^{I} and Mo^{0}, which have been shown to catalyse a variety of carbon-carbon bond forming processes.[50-52]

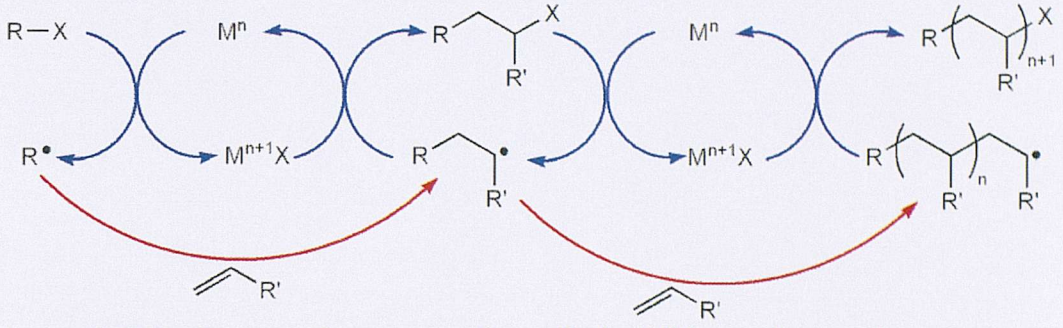


Scheme 1.4 Metal-catalysed addition of a haloalkane across an alkene double bond.

Both ATRP and ATRA involve the generation of radicals from dormant halogenated derivatives via reversible redox processes, catalysed by transition metal compounds. If the olefin is introduced in a relatively small amount, close to the stoichiometry of the halogenated compound, the formation of a single addition product is favoured, and the reaction is referred to as an ATRA. However, in the

presence of an excess of olefin with respect to the haloalkane, multiple insertion of the unsaturated monomer leads to a macromolecular chain, and the process is referred to as ATRP.[53] Control of polymerisation is achieved by maintaining a low concentration of active radical species and reducing the probability of termination via bimolecular coupling.

Although the Kharasch reaction was first discovered over 60 years ago,[54] and extensive research has been carried out on the carbon-carbon and carbon-halogen bond-forming processes it facilitates,[51,55] it was not until the 1990s that atom transfer radical polymerisation (Scheme 1.5) was discovered.[56,57]



Scheme 1.5 Mechanism of atom transfer radical addition and extension to atom transfer radical polymerisation.

The ATRP system comprises the monomer, an organic initiator (usually a molecule with a carbon-halogen bond which can be readily homolytically cleaved), and a transition metal catalyst with a suitable redox potential.

The quantity of initiator added to the reaction determines the number of growing polymer chains. In ATRP it is assumed that there is negligible termination, and that initiation is fast, with the result that the concentration of growing chains is constant and of a value approximately equal to the initiator concentration. Many organic compounds can act as an initiator, including alkyl halides, α-haloesters and sulfonyl halides (Figure 1.1).[58] Potentially, any alkyl halide with an activating group on the α-carbon can act as an initiator, but it is essential that the correct initiator for a particular reaction is used in order to minimise side reactions. For the ATRP system to be effective, X must migrate quickly and selectively between the growing polymer chain and the transition metal catalyst. Generally, best control of the molecular weight is achieved when X = Cl or Br.

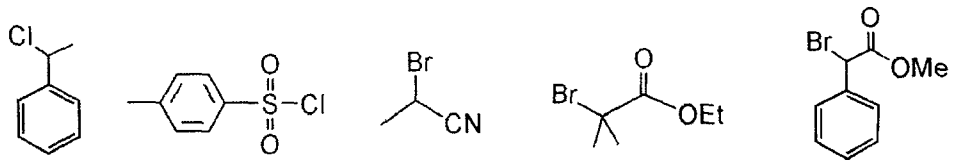


Figure 1.1 Common ATRP initiators: 1-phenylethyl chloride (1-PECl), toluene sulfonyl chloride (TosCl), 2-bromopropionitrile (2-BPN), ethyl-α-bromoisobutyrate (EBrB), methyl α-bromophenylacetate (MBPA).

The most "tunable" component of ATRP is the catalyst, which principally determines the position of the atom transfer equilibrium and controls the dynamics of exchange between the active and dormant species. In order to function effectively, two readily accessible oxidation states, separated by one electron, must be available to the metal. The transition metal should also have a high affinity for halogen atoms, and space within its coordination sphere to accommodate the extra halogen atom upon oxidation. Since the initial discovery of ATRP by Sawamoto[56] and Matyjaszewski,[57] using ruthenium and copper based catalysts respectively, many other systems have been investigated, incorporating a wide variety of transition metal centres. Whilst copper[58] and ruthenium[1] remain the most extensively studied metals in ATRP catalysis (Figure 1.2) other systems examined include those based on nickel,[59-65] palladium,[66,67] rhodium,[68,69] rhenium,[70,71] molybdenum[18,72-78] and iron.[79-86] More recently, systems based on titanium,[87-89] cobalt[90,91] and osmium[92] have been reported.

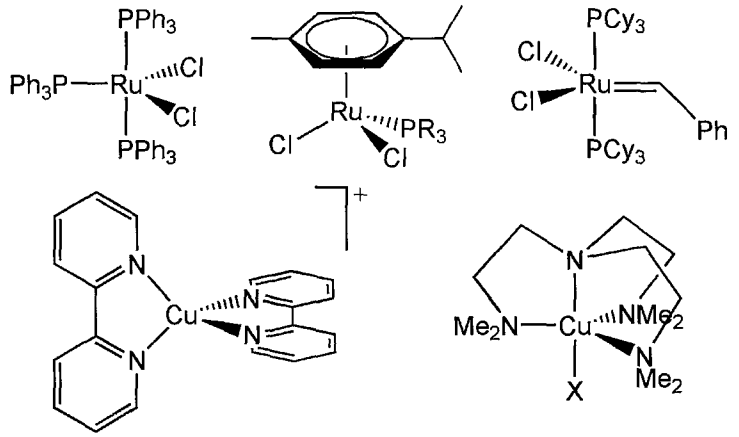
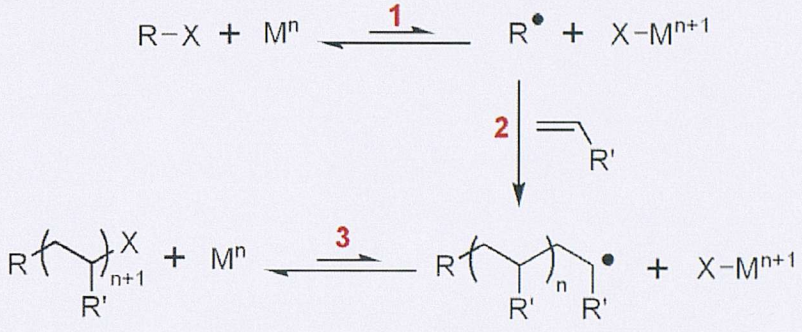


Figure 1.2 Examples of copper- and ruthenium-based ATRP catalysts.

1.3.1 Detailed mechanism.

There are three main steps in the ATRP mechanism - initiation, propagation and deactivation (Scheme 1.6). The polymer is generated by the sequential addition of monomer to the growing, radical-terminated chain, which exists in equilibrium with a deactivated, halogen-terminated chain. In order to maintain control of the polymerisation and produce polymers with low polydispersities, it is important that the number of monomer repeat units added during any one activation step is low. Controlled ATRP results in polymer chains with M_w/M_n values of 1.0-1.4.



Scheme 1.6 Atom transfer radical polymerisation mechanism.

During initiation, **1**, the metal complex, M^n, reversibly abstracts a halogen from the initiator, RX. This produces a carbon-centred radical, $R^\bullet$, and a metal complex where the oxidation state has increased by one, $M^{n+1}X$. In the propagation stage, **2**, the carbon-centred radical, $R^\bullet$, initiates polymerisation by successive addition of monomer units until deactivation. Deactivation, **3**, occurs when the propagating radical reacts reversibly with the oxidised metal complex, $M^{n+1}X$, to re-form the original complex, M^n, and a temporarily dormant, halogen-capped polymer chain.

To prevent recombinant termination from becoming significant, it is important that the equilibrium constants of initiation and deactivation are such that the concentration of radical species remains very low. If this is the case, the number of active centres in the reaction mixture remains approximately constant throughout, and such polymerisations are typically termed pseudo-living or controlled.[93] It is possible to change the position of the equilibria, and hence the steady state radical concentration, by altering the initiator (RX) and the redox potential of the metal (by variation of the ancillary ligands).

1.4 Iron ATRP catalysts.

Iron is not only one of the most abundant metals on earth, it is also one of the least toxic and most economically viable transition metals.[94] Many iron salts and complexes are commercially available, inexpensive, and thus have become widely used for a variety of catalytic reactions.[95] In terms of organic reactions, iron was a much under-used element until relatively recently. In the last 10 years its efficacy has become apparent, not only as a C-H oxidation catalyst,[96-106] but also as a tool in forming C-C bonds, through aldol reactions,[107-110] Michael additions,[111-117] carbometalations,[118-121] and the synthetically useful allylation of aldehydes.[122-124]

In ATRP, iron has been relatively well-studied although it is not as commonly used as the ubiquitous copper and ruthenium systems. The low toxicity and biocompatibility of iron makes it an attractive choice in the search for low cost catalysts and the more interesting features of these systems are described herein.

Monomer choice is an important factor in optimising polymerisation via ATRP, as each monomer possesses its own intrinsic radical propagation rate. In order to maintain a controlled polymerisation, the concentration of propagating radicals and the rate of deactivation needs to be adjusted for each different monomer. Some systems are active for several different monomers, whilst some are more selective. Figure 1.3 shows one of the simplest iron-based catalysts.

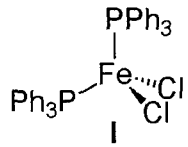


Figure 1.3 Simple iron dichloride diphosphine complex used in ATRP.

$FeCl_2(PPh_3)_2$ was first reported in 1997 as an efficient ATRP catalyst for the polymerisation of methyl methacrylate (MMA),[79] requiring an activated halide initiator such as CCl_4 or ethyl 2-bromoisobutyrate (EBrB). In contrast to its 4-d analogue, $RuCl_2(PPh_3)_3$,[56] the iron complex does not require a Lewis acid additive to induce smooth living polymerisation, and the reaction proceeds at a fast rate. Polymers had unimodal and relatively narrow molecular weight distributions and molecular weight increased linearly with conversion, although at higher monomer conversions there was some deviation from the theoretical values. However, this system was inactive as a catalyst for the polymerisation of styrene.

Recently, a closely related compound $FeCl_2(PPh_3)_2.4H_2O$ was reported to catalyse the polymerisation of acrylates[83] in both bulk and solution. A range of initiators were studied, with bromo compounds proving to be the more effective. Optimised conditions allowed the synthesis of polymers with high molecular weights and low polydispersities (1.2), and also the preparation of diblock copolymers.

Changing the ligands on the iron centre can have a dramatic effect on both the rate and molecular weight distribution of a polymerisation, as well as the range of susceptible monomers. Figure 1.4 shows variations in the simple iron system, where the nature of the ligands strongly affects the kinetics of the polymerisation and the polydispersity by influencing the thermodynamics and kinetics of the halogen atom exchange process. The more nucleophilic ligands stabilise the Fe^{III} species more effectively and accelerate the polymerisation rates. The exchange process is sufficiently fast to maintain a low polydispersity, and each of the complexes in Figure 1.4 are active catalysts for the polymerisation of MMA and styrene by ATRP.[80]

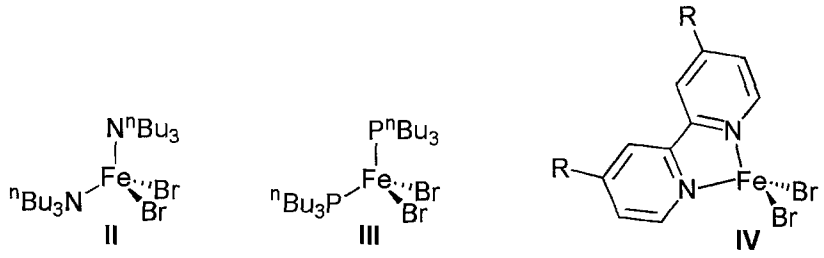


Figure 1.4 Variations of the simple Fe^{II} halide system.

Polymerisations using $Fe(N^nBu_3)_2Br_2$, **II**, were heterogeneous, but polystyrene with controlled molecular weights and low polydispersities of approximately 1.2 were nonetheless obtained. The initiator used was 1-phenylethyl bromide (1-PEBr), although it was found that for the polymerisation of MMA, tosyl chloride (TosCl) was more efficient. Although the polymerisation of MMA had molecular weights which increased linearly with conversion, the polydispersity was relatively high ($\approx$1.5). Using the more soluble tri-*n*-octylamine complex resulted in lower PDIs of 1.4, indicating that the broad molecular weight distribution was probably partly due to the heterogeneous nature of the catalyst.

Polymerisations using the related phosphine complex, $Fe(P^nBu_3)_2Br_2$, **III**, and 1-PEBr as the initiator gave a homogeneous system which polymerised styrene smoothly, and rapidly, although the polydispersities were relatively high (1.3-1.4).

The polymerisation of MMA also proceeded with good molecular weight control and polymerisation rate. Choice of initiator was again shown to be important, with the best results from a fast initiation step using TosCl, EBrB or 2-bromopropionitrile (BPN).

Employing the bidentate coordinating ligand often used in Cu^{I} ATRP, 4,4'-dinonyl-2,2'-bipyridine (dNbipy), resulted in polystyrene molecular weights close to the theoretical values, and relatively narrow PDIs ($\approx$1.3). The polymerisation rate with **IV** was slow, requiring 21 hours to reach 64% conversion. Interestingly, the polymerisation rate could be dramatically increased if dNbipy was mixed with $P^{n}Bu_3$ or $N^{n}Bu_3$, giving polymers with better molecular weight control and lower polydispersities (<1.2). When dNbipy was mixed with $P^{n}Bu_3$ in a 1:1 ratio, the polymerisation reached 82% conversion in 5 hours. Polymerisation of MMA using Fe(dNbipy)Br_2 in conjunction with BPN as an initiator gave a homogeneous reaction mixture which yielded polymers with relatively low polydispersities of <1.3.

Changing the coordinating ligand can also be used to impart desirable properties upon the catalyst. For example, several half-metallocene iron complexes (Figure 1.5) are stable to air and moisture. The anionic Cp ring coordinates to the metal ion more tightly than neutral ligands such as PR_3 or NR_3. This makes them more active and efficient catalysts, leading to increased rates of polymerisation whilst maintaining excellent control over the polymerisation.

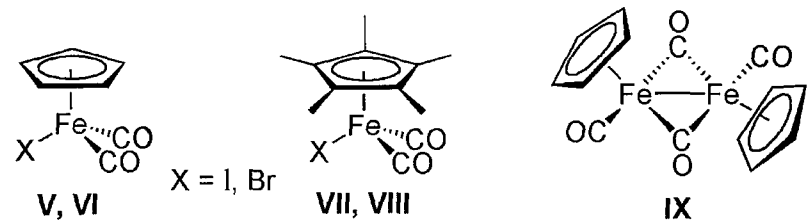


Figure 1.5 Half-metallocene iron complexes used in ATRP.

$CpFe(CO)_2I$, **V**, proved to be a good catalyst for the ATRP of styrene when used with an iodide initiator, $Me_2C(CO_2Et)I$, and yielded polymers with narrow polydispersities of 1.1.[81] Changing the initiator to the bromide analogue, **VI**, increased the polymerisation rate, although the polydispersity was slightly compromised (1.3 for **VI**, *cf.* 1.1 for **V**).[125]

Using the bulkier Cp* ligand resulted in a slower polymerisation for both iodide and bromide complexes, **VII** and **VIII**, with their respective initiators. The PDIs of

the polystyrene formed using the Cp* complexes were narrower than those of their Cp analogues because the rate of polymerisation was slower due to the increase in electron density on the Fe^{II} centre.[125] These complexes also catalyse the suspension ATRP of acrylates (*n*-butyl acrylate, ^{n}BA, methyl acrylate, MA and *t*-butyl acrylate, ^{t}BA) and styrene in water and toluene (50% v/v) at 80°C, using an iodo initiator, $Me_2C(CO_2Et)I$.[42] These systems gave good control of molecular weight distribution (M_w/M_n ~ 1.2-1.3), with the addition of water to the system increasing the polymerisation rates, potentially through the formation of a highly active catalyst/activator species. As seen with the purely organic systems, the rate of polymerisation increased in the order $Cp^*FeI(CO)_2$ < $CpFeI(CO)_2$ < $CpFeBr(CO)_2$, with the Cp complexes reaching 90% conversion in 2-4 hours. These systems have also been used to produce block copolymers of acrylates and styrene under suspension conditions.

A catalyst system comprising of the dinuclear iron half-sandwich complex, $[CpFe(CO)_2]_2$, **IX**, and $Me_2C(CO_2Et)I$ is active for the ATRP of styrene, with faster polymerisation rates than the mononuclear FeCp complexes and narrow PDIs (1.2).[125] This system is also active for the ATRP of vinyl acetate at 60°C in anisole, although low polydispersities are only produced at low monomer conversion.[126] At monomer conversions above 60%, the PDIs broaden from 1.4 to 1.9. Addition of $Ti(O^iPr)_4$ or other Lewis acid additives increased the rate of polymerisation.

As the importance of the ancillary ligand system was realised, more complicated organic moieties were introduced (Figure 1.6) and their effect on ATRP catalysis assessed. Since it appears that the electron donating ability of the ligands plays an important role in the activity of ATRP catalysts this is one area where the catalyst can be 'tuned'.

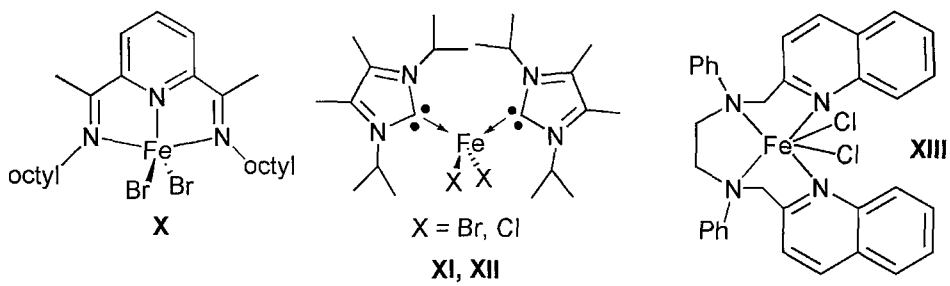


Figure 1.6 More complicated iron ATRP catalysts.

The tridentate dialkyl*bis*(imino)pyridine (BIP) ligand was not as effective as the bidentate dNbipy system, presumably because of the crowding of the coordination

sphere upon oxidation to the Fe^{III} species. $BIPFeBr_2$, **X**, was active for the polymerisation of MMA, using 2-BPN as an initiator, although the polymerisation only reached 42% conversion in 9 hours. The PDI increased during the reaction, from 1.21 at 5% conversion to 1.68 at 42%.[127] Deviation from linearity on the semilogarithmic plot indicated that the concentration of growing radicals decreased during the polymerisation due to termination reactions. This catalyst was inactive with respect to the polymerisation of styrene and MA. One advantage of this system is that variation of the imino substituents could provide a source of electronic-tuning, which could also be used to control the activity.

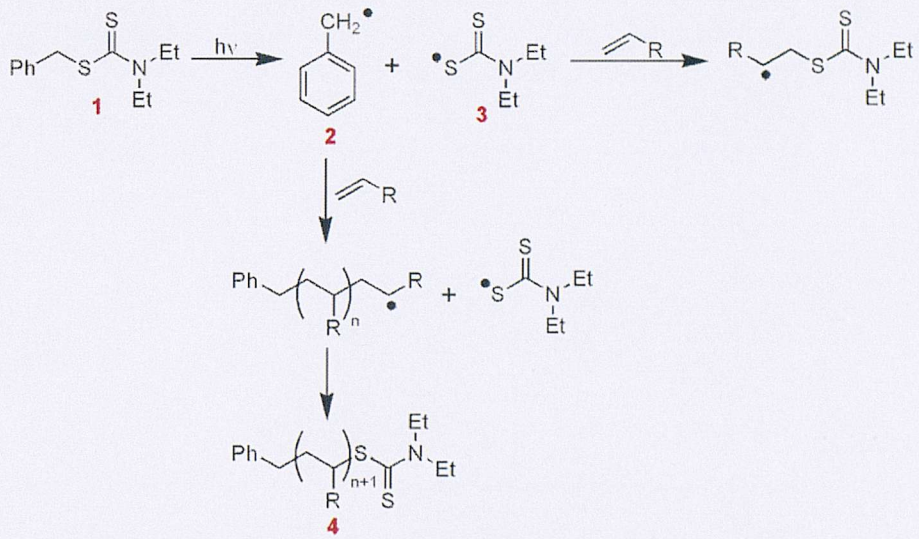
The Fe^{II} halide complexes of the highly electron donating imidazolylidene ligand were extremely active ATRP catalysts for both styrene and MMA.[82] Polymers with PDIs of <1.1 were obtained, molecular weights increased linearly with conversion and agreed well with theoretical values. In addition, these complexes had rate constants among the highest reported for metal catalysed ATRP in organic systems. The bromide analogue, **XI**, was faster than the chloride complex, **XII**, due to the difference in the iron-halide bond dissociation energies. The high Lewis basicity of the imidazolylidene unit was thought to lower the redox potential of the Fe^{II} complex, which facilitates the abstraction of a halogen atom from the dormant polymer chains. This would shift the equilibrium towards the growing polymer radicals and increase the rate of polymerisation. The increased donating ability of the ligands may also stabilise the Fe^{III} species and enhance the rapid exchange of halogen atoms between the dormant and active polymer chain ends.

The same principles of increased donating ability facilitating rapid halogen exchange were applied in the development of the tetradentate amine complex, **XIII**.[128] Amines are the ligands of choice in copper-mediated ATRP but have been less widely used with iron. However, the complex shown in Figure 1.6 was an efficient ATRP catalyst for the polymerisation of MMA, reaching 88% in 90 minutes with a PDI of 1.35. Molecular weights increased linearly with conversion, although were somewhat higher than the theoretical values. There were two possible reasons suggested for this; either a slow initiation relative to propagation, or the discrepancy between using polystyrene standards for PMMA samples. However, the M_n values calculated by ^1H NMR were also significantly higher than theoretical, making it unlikely that the difference in hydrodynamic volume between the PS standards and PMMA samples could be solely responsible for the inconsistencies. Slow initiation

relative to propagation also seems unlikely since the molecular weights did not approach theoretical at high conversions, and it is more likely that the initiator efficiency is low, coupled with a slow deactivation rate.[22]

1.5 Stable Free Radical Polymerisation.

Early work on "iniferters" (*ini*tiator trans*fer* agent *ter*minator) during the 1980s led to the development of the first successful controlled/living radical polymerisation in the early 1990s. Research by Otsu *et al* used disulfides such as benzyl *N,N*-diethyldithiocarbamate as photochemical initiators (Scheme 1.7) for the polymerisation of monomers including styrene and MMA.[129,130] Benzyl *N,N*-diethyldithiocarbamate was found to be a particularly effective thermal photoinitiator for styrene polymerisation because the benzyl radical, formed through homolytic cleavage of the C-S bond, is very similar in structure to the propagating styrene radical.[131]



Scheme 1.7 Mechanism of early attempts at controlled radical polymerisation, using "iniferters".

The photochemical initiator, **1**, is cleaved at the C-S bond to give a carbon-based propagating radical, **2**, and the mediating thio-radical, **3**. The propagating radical, **2**, can undergo monomer addition then recombine with **3** to give the dormant species, **4**. However, **2** can also undergo chain transfer to the initiator, resulting in the formation of relatively low molecular weight polymer. The iniferter mechanism

results in a linear increase in molecular weight with conversion and other characteristics typical of a living system. However, the molecular weight cannot accurately be controlled and PDIs are generally not particularly narrow since the mediating thio-radical, **3**, can also initiate polymerisation.

In order for a more successful controlled/living radical polymerisation, the mediating radical must undergo reversible termination of the propagating chain end without acting as an initiator. The chain transfer and irreversible termination reactions, such as combination and disproportionation, should also be minimal. In the absence of other reactions leading to the initiation of new polymer chains, the concentration of reactive chain ends is very low and the irreversible termination reactions are minimised. All of the growing chains are initiated by the desired initiating species and chain growth occurs in a living fashion, allowing good control over the polymerisation process and resulting in the synthesis of well-defined polymers. The identity of the mediating radical is critical to the success of a living free radical polymerisation, and a variety of different persistent radicals have been investigated. These include (arylazo)oxy,[132] substituted phenyls,[133] verdazyl,[134] triazolinyl[135] and nitroxides[136] (Figure 1.7).

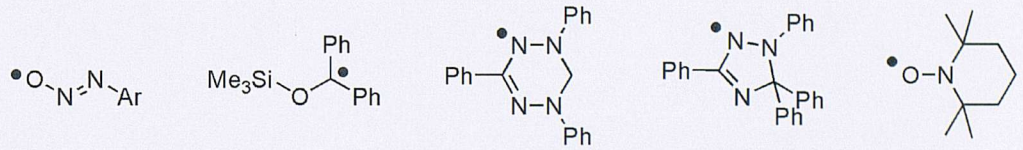
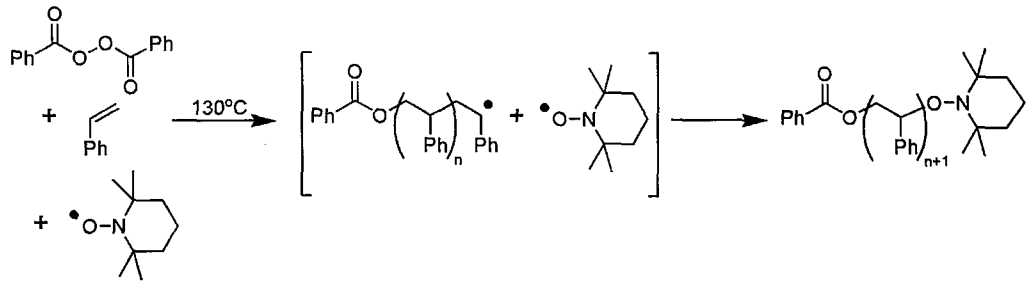


Figure 1.7 Persistent radicals which have been used to mediate radical polymerisations.

A particularly successful example of the 'stable' free radical polymerisation mechanism has been nitroxide mediated radical polymerisation (NMP), which allowed the first synthesis of polystyrene with controlled molecular weights and narrow PDIs.[137] This bimolecular initiation system used benzoyl peroxide (BPO) as the radical source and TEMPO as the persistent radical (Scheme 1.8). Combination of these reagents (1.3:1 ratio) in bulk styrene at 130°C allowed the synthesis of high molecular weight polystyrene derivatives with PDIs of 1.2-1.3. At these high temperatures, the C-ON bonds are unstable and are reversibly cleaved, allowing the nitroxide to successfully mediate the polymerisation. The linear increase in molecular weights with conversion and the narrow PDIs are typical of a living system.



Scheme 1.8 Example of the stable free radical polymerisation mechanism.

Since this early work, nitroxide mediated polymerisation has been extensively investigated. The use of unimolecular initiators has improved control over the polymerisation, and a wide range of nitroxides have been developed; these allow facile, high yielding syntheses of these initiators, lower temperature reactions, shorter reaction times and polymerisation of a wide range of monomers.[15] However, it is another subsection of this type of polymerisation mechanism which uses organometallic compounds as the radical trap which has most relevance to the work described in this thesis.

1.6 Organometallic Mediated Radical Polymerisation.

Transition metals, especially cobalt, have shown efficacy in controlling radical polymerisations through an entirely organometallic pathway. This mechanism proceeds using the same principles as a reversible addition-cleavage mechanism, with the transition metal acting as a reversible spin-trap. OMRP offers control over polymerisations based on the reversible homolytic cleavage of the weak bond between an alkyl group and a metal catalyst and is initiated using conventional free radical initiators such as azobisisobutyronitrile (AIBN) or 2,2'-azobis(4-methoxy-2,4-dimethyl valeronitrile) (V70) (Figure 1.8).

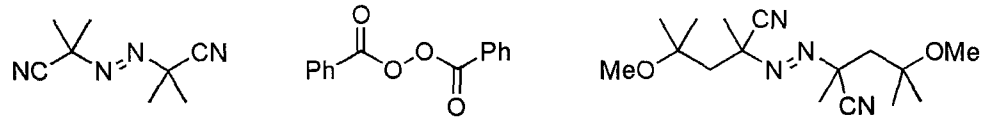
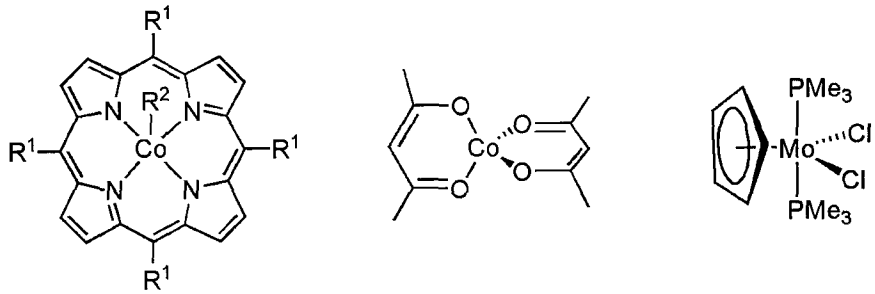


Figure 1.8 Typical radical initiators used in OMRP and SFRP: azobisisobutyronitrile (AIBN), benzoyl peroxide (BPO), 2,2'-azobis(4-methoxy-2,4-dimethyl valeronitrile) (V70).

Cobalt systems (Figure 1.9) supported by judiciously chosen porphyrin ligands were first able to yield high molecular weight acrylate polymers with very low polydispersities (M_w/M_n ~ 1.1).[16,17,138] Recently this work has expanded to include the controlled polymerisation of vinyl acetate (VOAc), a notoriously difficult monomer to achieve control over. While $Co(acac)_2$ is unable to mediate the polymerisation of acrylate monomers, it can effectively control the polymerisation of vinyl acetate in bulk,[19] suspension[20] and mini-emulsion,[139] and has led to the development of end-functionalised[21] and block copolymers of poly(vinyl acetate) with poly(vinyl alcohol)[140] and poly(*n*-butyl acrylate).[141] Supported systems have allowed the synthesis of poly(vinyl acetate) without the coloured metal residues, and also allow facile recycling of the catalyst.[142] However, detailed mechanistic investigations conducted recently have provided evidence that some cobalt-porphyrin mediated polymerisations actually proceed through degenerative transfer as well as OMRP.[143] Similarly, the controlled radical polymerisation of VOAc by $Co(acac)_2$ is also proposed to occur via a degenerative transfer mechanism, with OMRP playing only a minor role in the polymerisation.[144]

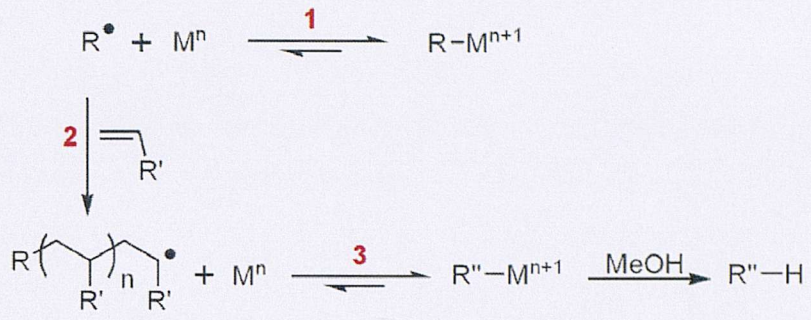


R^1 = Mes
R^2 = CH_2CMe_3
= $CH(CO_2Me)CH_3$

Figure 1.9 Complexes active in organometallic mediated radical polymerisation.

1.6.1 Detailed mechanism.

As in ATRP, there are three main steps which comprise the OMRP mechanism. The growing, radical-terminated chain exists in equilibrium with the dormant species, which in the case of OMRP is metal-terminated. A low concentration of radical species present at any one time allows control over the molecular weight and PDI, and so the equilibrium should favour the formation of the M-C bonds of the deactivated polymer chain (Scheme 1.9).

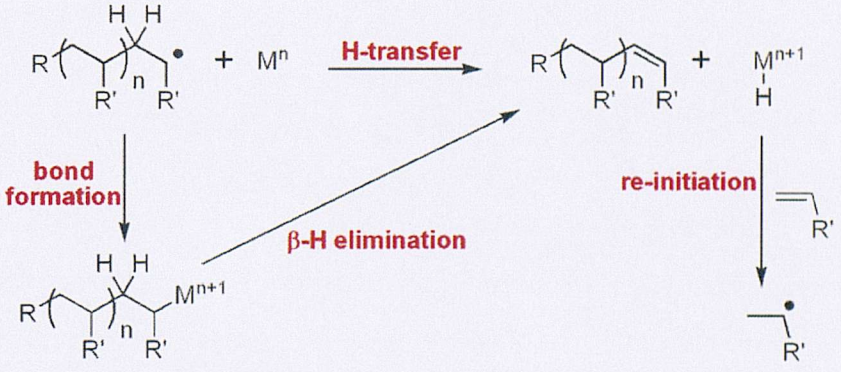


Scheme 1.9 Organometallic mediated radical polymerisation mechanism.

The free radical initiator decomposes thermally to release carbon-based radicals. These either react reversibly with the transition metal complex to form a dormant species with a weak metal-carbon bond, **1**, or enter the propagation stage, **2**. Propagation continues until the growing, radical-terminated polymer chain reacts with the metal complex to form the dormant species in the deactivation step, **3**. Quenching the polymer samples with MeOH hydrolyses the metal-carbon bonds and gives polymer with saturated end groups.

1.7 Catalytic Chain Transfer.

Catalytic chain transfer (CCT) to a monomer in radical polymerisations was first reported in 1975 by Smirnov and Marchenko using cobalt porphyrin catalysts.[145,146] CCT is a non-living process, resulting from intermolecular transfer of a hydride between the propagating radical and a metal complex. The mechanism is thought to involve conventional hydrogen transfer, but the possibility of bond formation followed by β-elimination has not been discounted (Scheme 1.10).[147]



Scheme 1.10 Catalytic chain transfer mechanism.

Abstraction of hydrogen from the growing polymer radical and transfer to another molecule of the monomer initiates a new propagating radical chain. Thus, unlike the controlled radical polymerisations, the amount of initiator (usually AIBN) does not determine the number of growing radical chains. CCT produces short-chain, olefin-terminated oligomers, with molecular weights largely independent of conversion. CCT is an efficient way to control the molecular weight during a free radical polymerisation, as cobalt chain transfer agents typically have chain transfer constants of 10^2-10^4 (k_{tr}/k_p, where k_{tr} is the rate constant for chain transfer by a growing polymer chain and k_p is the rate constant for addition of another monomer unit to the growing polymer chain). This means that reactions are exceptionally fast when compared to the uncatalysed polymerisation and those using organic chain transfer agents such as thiols, which have much lower chain transfer constants of 10^{-2}-10.[148,149] The use of transition metal CCT catalysts allows the synthesis of very low molecular weight polymers, with only ppm quantities of catalyst required.[146]

There are many Co-based CCT agents,[146-151] the most common of which are the cobalt porphyrins and cobaloximes (Figure 1.10). These catalysts are used for the synthesis of macromonomers and are important in many industrial applications, particularly in the automotive, paper and printing industries. The cobaloximes such as bis(boron difluorodimethylglyoximate) cobaltate(II), COBF (Figure 1.10), are among some of the most active CCT catalysts, with chain transfer constants of up to 10^5 for MMA and 10^4 for styrene.[152]

A range of other transition metals have been studied for use in catalytic chain transfer polymerisation, although the chain transfer constants tend to be much lower than in the cobalt systems. These include a range of bimetallic half-sandwich complexes of Mo, Fe, Cr, W, Ru and Os with CO and PR_3 ligands reported in a patent by DuPont.[153] More recently, chromium-based systems such as $C_5R_5Cr(CO)_3$ (where R = H, Me, Ph, see Figure 1.10) have shown CCT activity, and have allowed the synthesis, isolation and characterisation of the hydride intermediate, $C_5R_5Cr(CO)_3H$.[154,155] The related phosphine systems, $C_5R_5Cr(CO)_2PMe_3$ are also moderately active CCT catalysts, as are some molybdenum trispyrazole borate complexes, including $TpMo(CO)_3$ and $Tp^*Mo(CO)_3$.[156] However, CCT can also interfere with the chain growth process in a pseudo-living polymerisation such as OMRP or ATRP. This is the case for several Mo half-sandwich complexes which act

as catalysts for both ATRP and OMRP, with CCT occurring under ATRP conditions with certain ancillary ligands.[18,72]

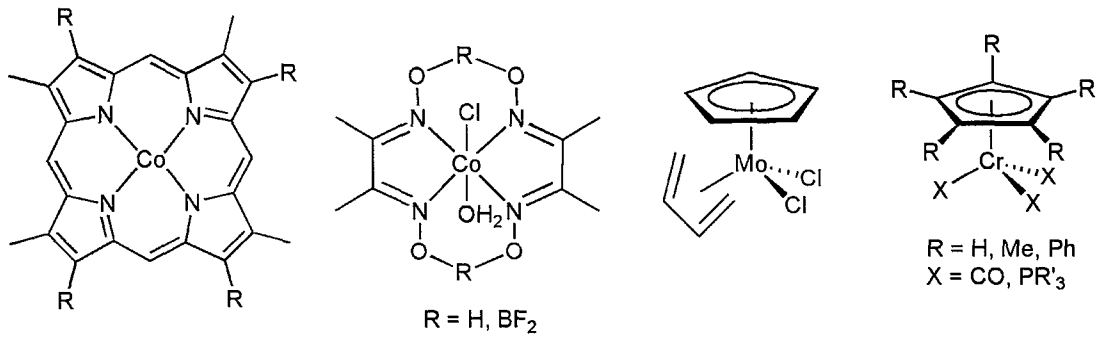


Figure 1.10 Metal complexes reported to be catalytic chain transfer catalysts.

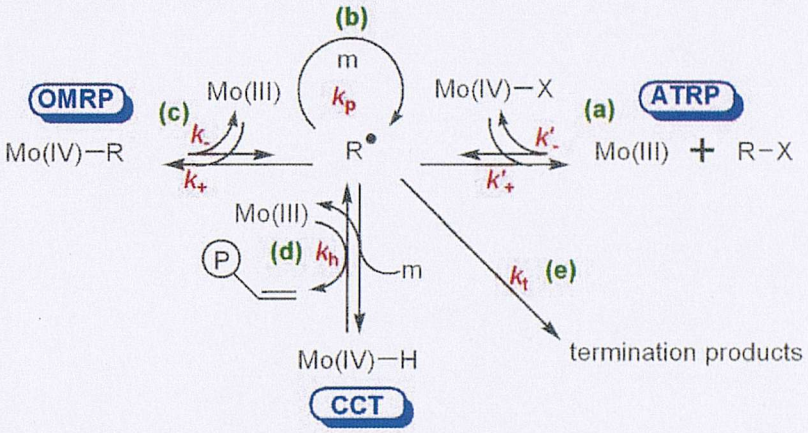
There are two conditions which particularly favour CCT in a controlled/living polymerisation. Under OMRP conditions, a low M-C bond dissociation energy will result in a relatively high radical concentration. The concentration of catalyst will also be high, thus favouring a β-hydrogen abstraction reaction. Under ATRP conditions, assuming that the trapping of radicals by the catalyst is minimal, the atom transfer equilibrium will be shifted towards the dormant species, where there is a high concentration of the reduced form of the catalyst. Providing the OMRP trapping is negligible, a radical reacting with the catalyst will undergo β-hydrogen abstraction.

The ability of a transition metal complex to abstract a β-H and to form a metal-carbon bond is dependent on the propagating radical. Certain radicals have a greater propensity for transferring a β-H, and the particular metal complex in question also plays an important role in affecting the trapping / transfer ratio.[22] Steric effects are also important, as an H-transfer reaction is generally regarded as less sterically demanding than formation of an organometallic species. The work of Norton *et al* showed that by increasing the steric bulk of the ligand in their Cr system, the H-transfer process was favoured over M-M or M-C bond formation.[156] There is an important balance to be found, as too much steric hindrance on the metalloradical decreases its effectiveness as a chain transfer catalyst. However, without some steric protection on the metal centre, the side reactions including metal complex dimerisation, M-C bond formation and transfer of $H^{\bullet}$ to the propagating radical, $R^{\bullet}$, rather than to the monomer can have a significant effect on the chain transfer constants. These side reactions are less common for tertiary radicals such as those

derived from MMA, but M-C bond formation and net hydrogenation are often observed in the styrene polymerisation reactions.

1.8 Catalysts operating by more than 1 mechanism.

One of the most interesting and mechanistically important catalyst systems in the literature are the half-sandwich molybdenum compounds reported by Poli *et al.*[18,72-74,77] $CpMoCl_2(PMe_3)_2$ and $CpMoCl_2$(dppe) are active catalysts for the polymerisation of styrene under both ATRP and OMRP conditions,[18,72] affording a linear increase in molecular weight with conversion, moderate PDIs, and end-groups consistent with the proposed mechanisms. As it has been shown that Mo^{III} can reversibly trap the propagating radical under OMRP conditions, and since the concentration of Mo^{III} remains high under ATRP conditions, both trapping mechanisms can occur simultaneously (Scheme 1.11). Closely related complexes $CpMoCl_2(\eta^4\text{-}C_4H_6)$ and $CpMo(SiMe_3)_2(\eta^4\text{-}C_4H_6)$ operate by another mechanism under standard ATRP conditions, generating short-chain, olefin-terminated oligomers, with molecular weights independent of conversion, *i.e.* via CCT.[18]



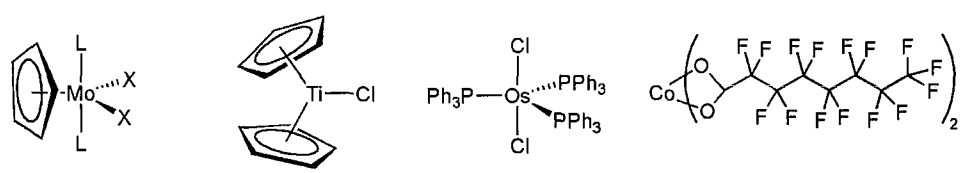
Scheme 1.11 Comprehensive mechanistic scheme for polymerisations mediated by the Mo^{III}/Mo^{IV} redox couple.

Another example of a catalyst system which is capable of controlling the polymerisation of MMA through both ATRP and OMRP mechanisms is that based on Cp_2TiCl.[157,158] Thermal decomposition of AIBN in the presence of Cp_2TiCl_2 generates the active species, and the broadened PDIs are attributed to the various side reactions which occur. A related system uses the Cp_2TiCl-induced ring opening of an oxirane as the initiation step, and involves reversible formation of Ti^{IV} capped dormant species.[159,160] The initiation process is an ATRP-like activation which

irreversibly gives $Cp_2ClTi\text{-}OCH_2CH_2^{\bullet}$ because the oxophilic nature of titanium results in high homolytic strength of the Ti-O bonds. Control in the polymerisation of styrene is derived from the OMRP-type trapping of the propagating radicals by additional Cp_2TiCl.

$OsCl_2(PPh_3)_3$ can also control the radical polymerisation of styrene under both ATRP and OMRP conditions.[161] The somewhat broadened PDIs and bimodal molecular weight distribution were explained by the early presence of low molecular weight dead chains, formed from the rapid AIBN initiation and subsequent bimolecular coupling. As seen for the half-sandwich Mo complexes, under OMRP conditions there are no halogen end groups observed, and under ATRP conditions, no Os-terminated polymer is seen. There is therefore no 'contamination' of OMRP with ATRP. Although there must be some OMRP trapping under ATRP conditions, the system is most energetically stable as an Os^{II} catalyst and halogen-capped dormant species, and so only chlorine end groups are observed under ATRP conditions.[22]

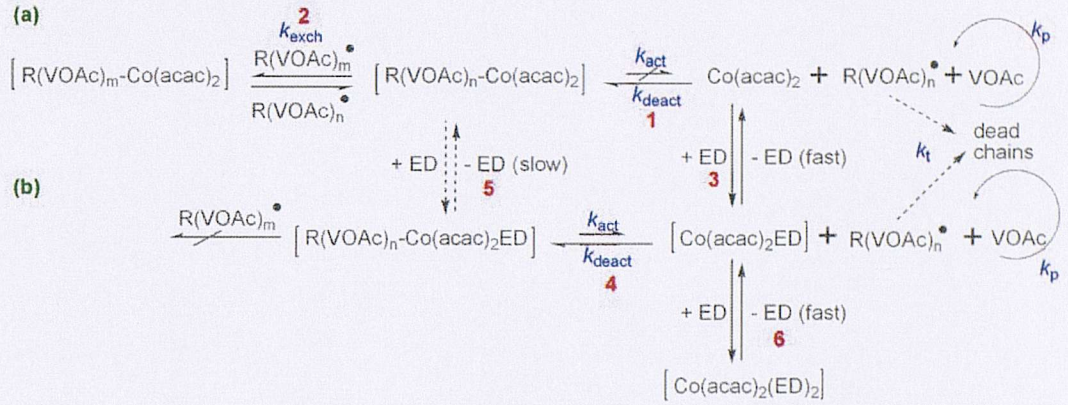
Cobalt is a metal which has previously shown great efficiency in both CCT and OMRP reactions, however Co ATRP catalysts are rare. A recent report into the controlled radical polymerisations of styrene and MMA by cobalt perfluorooactanoate initiated by 1-PEBr and AIBN showed that this catalyst can exert control through both ATRP and OMRP mechanisms.[91] The authors incorrectly labelled the polymerisation initiated by AIBN as reverse-ATRP, whereas the absence of halogens in the system (the metal precursor $CoCl_2$ is transformed into $Co(O_2CC_7F_{15})_2$ using sodium perfluorooctanoate) means that the control must be derived from OMRP. For polymerisations initiated by 1-PEBr, control may be through OMRP only or through a combination of OMRP and ATRP. End group analysis should provide the answer to this, but the observation of *only* halogen end groups (even for polymerisations initiated with AIBN) suggests that the treatment of the polymer with acidified MeOH resulted in the decomposition of any Co end groups.



X = Cl; L = PMe_3, dppe, η^4-C_4H_6
X = $SiMe_3$; L = η^4-C_4H_6

Figure 1.11 Metal catalysts active under both ATRP and OMRP conditions.

The polymerisation of vinyl acetate by $Co(acac)_2$ has recently been proposed to occur via a degenerative transfer mechanism, with OMRP playing only a minor role in the polymerisation (route a, Scheme 1.12).[144] Experiments which included an electron donor (ED) such as NEt_3 or pyridine resulted in polymerisation by OMRP only (route b, Scheme 1.11), leading to less control over the polymerisation, and without the induction period previously observed with this system.[19] The electron donor blocks the coordination site on the cobalt which is required for an associative radical exchange during the degenerative transfer mechanism. In the absence of the electron donor group the polymerisation is believed to proceed by degenerative transfer but with the influence of OMRP.



Scheme 1.12 Proposed mechanisms for the controlled radical polymerisation of vinyl acetate using $Co(acac)_2$, in the (a) presence and (b) absence of an electron donor.

The radical initiator V70 has a $t_{1/2}$ of 10 h under the polymerisation conditions of 30°C. In the absence of an electron donor group, $R^\bullet$ slowly converts the $Co(acac)_2$ catalyst into $Co(acac)_2R$, **1**. This conversion of Co^{II} into Co^{III} is essentially irreversible. Towards the end of this transformation, the concentration of $Co(acac)_2$ is low, and so the new $R^\bullet$ are not efficiently trapped. These radicals begin to propagate, quickly generating polymer chains, and explaining the observation of a rapid polymerisation process after the induction period. The intervention of a degenerative transfer process ensures that the polymerisation remains controlled, **2**. In the presence of an electron donor group, $Co(acac)_2ED$ is formed, **3**, meaning that when the organometallic dormant species $RCo(acac)_2ED$ forms, **4**, the coordination site needed for the degenerative transfer is blocked. The dissociation of the ED from dormant species, **5**, will be slow, as the low-spin d^6 complex is relatively inert.

Degenerative transfer will therefore only take place if the ED doesn't bind very strongly to the Co^{III} dormant species and a significant amount of $Co(acac)_2R$ remains present at equilibrium. With a strong ED, when polymerisation is occurring predominantly through OMRP, the electron donor addition / dissociation equilibrium, **6**, between $Co(acac)_2ED$ and $Co(acac)_2(ED)_2$ stabilises the Co^{II} spin trap and accelerates the polymerisation.

1.9 - Conclusions

The development of controlled radical polymerisation techniques such as ATRP, SFRP and OMRP illustrates the similarities between these mechanisms. Although these methods differ in the nature of the moderating species and the mechanism by which a dormant species is produced, the same radical intermediates are responsible for consumption of the monomer. Transition metals capable of this type of 1-electron process can also participate in catalytic chain transfer, leading to non-living polymerisation behaviour. In order for the catalytic behaviour of a particular complex to be predicted, a thorough understanding of each of the possible 1-electron reactions is required.

The last section of this introduction described several catalyst systems which are efficient in radical polymerisation using two different mechanisms, usually ATRP and OMRP. However, the half-sandwich molybdenum complexes illustrate the potential for complexes which may incorporate three different mechanisms, with the inclusion of CCT. Small differences in the ligand structure appear to greatly influence the polymerisation mechanism, although the reasons behind these switches in mechanism have not been satisfactorily explained. Work in this laboratory led to the development of α-diimine Fe^{II} halide complexes, which proved to be effective ATRP catalysts with an alkyl *N*-substituent. With *N*-aryl substituents, however, the complexes were CCT agents.[86,162] These complexes will be discussed in more detail in the introduction to the subsequent chapter, and the remainder of this thesis will detail the most recent work into the observed mechanism switches for novel α-diimine Fe^{II} complexes. The results of investigations into the relationship between the ligand substituents and the effect on the polymerisation mechanisms, and the intimate relationships between the OMRP, ATRP and CCT equilibria will be described.

1.10 - References

(1) Kamigaito, M.; Ando, T.; Sawamoto, M., *The Chemical Record* **2004,** *4*, 159.

(2) Tsarevsky, N.; Matyjaszewski, K., *J. Polym. Sci. A: Polym. Chem.* **2006,** *44*, 5098.

(3) Scott, N. D., *US Patent 2181771* **1939**.

(4) Szwarc, M., *Nature* **1956,** *178*, 1168.

(5) Szwarc, M.; Levy, M.; Milkovich, R., *J. Am. Chem. Soc.* **1956,** *78*, 2656.

(6) Matyjaszewski, K.; Kubisa, P.; Penczek, S., *J. Polym. Sci., Polym. Chem. Ed.* **1974,** *12*, 1333.

(7) Matyjaszewski, K.; Penczek, S., *J. Polym. Sci., Polym. Chem. Ed.* **1974,** *12*, 1905.

(8) Matyjaszewski, K.; Kubisa, P.; Penczek, S., *J. Polym. Sci., Polym. Chem. Ed.* **1975,** *13*, 763.

(9) Penczek, S.; Matyjaszewski, K., *J. Polym. Sci., Polym. Symp.* **1976,** *56*, 255.

(10) Sawamoto, M., *Prog. Polym. Sci.* **1991,** *16*, 111.

(11) Matyjaszewski, K.; Lin, C. H.; Pugh, C., *Macromolecules* **1993,** *26*, 2649.

(12) Goto, A.; Fukuda, T., *Prog. Polym. Sci.* **2004,** *29*, 329.

(13) Braunecker, W. A.; Matyjaszewski, K., *Prog. Polym. Sci.* **2007,** *32*, 93.

(14) Matyjaszewski, K., *Controlled/living radical polymerization: progress in ATRP, NMP and RAFT.* Matyjaszewski, K., ed.; Oxford University Press: ACS: Washington, D.C., 2000.

(15) Hawker, C. J.; Bosman, A. W.; Harth, E., *Chem. Rev* **2001,** *101*, 3661.

(16) Wayland, B. B.; Poszmik, G.; Mukerjee, S. L.; Fryd, M., *J. Am. Chem. Soc.* **1994,** *116*, 7943.

(17) Davis, T. P.; Kukulj, D.; Haddleton, D. M.; Maloney, D. R., *Trends Polym. Sci.* **1995,** *3*, 7943.

(18) Grognec, E. L.; Claverie, J.; Poli, R., *J. Am. Chem. Soc.* **2001,** *123*, 9513.

(19) Debuigne, A.; Caille, J.-R.; Jérôme, R., *Angew. Chem. Int. Ed.* **2005,** *44*, 1101.

(20) Debuigne, A.; Caille, J.-R.; Detrembleur, C.; Jérôme, R., *Angew. Chem. Int. Ed.* **2005,** *44*, 3439.

(21) Debuigne, A.; Caille, J.-R.; Willet, N.; Jérôme, R., *Macromolecules* **2005,** *38*, 5452.

(22) Poli, R., *Angew. Chem. Int. Ed.* **2006,** *45*, 5058.

(23) Kamigaito, M.; Ando, T.; Sawamoto, M., *Chem. Rev.* **2001,** *101*, 3689.

(24) Matyjaszewski, K.; Xia, J., *Chem. Rev.* **2001,** *101*, 2921.

(25) Greszta, D.; Mardare, D.; Matyjaszewski, K., *Polym. Prepr. (Am. Chem. Soc., Div. Polym. Chem.)* **1994,** *35*, 466.

(26) Harwood, H. J.; Christov, L.; Guo, M.; Holland, T. V.; Huckstep, A. Y.; Jones, D. H.; Medsker, R. E.; Rinaldi, P. L.; Soito, T.; Tung, D. S., *Macromol. Symp.* **1996,** *111*, 25.

(27) Espenson, J. H., *Acc. Chem. Res.* **1992,** *25*, 222.

(28) Iovu, M. C.; Matyjaszewski, K., *Macromolecules* **2003,** *36*, 9346.

(29) Gaynor, S. G.; Wang, J.-S.; Matyjaszewski, K., *Macromolecules* **1995,** *28*, 8051.

(30) Kwak, Y.; Tezuka, M.; Goto, A.; Fukuda, T.; Yamago, S., *Macromolecules* **2007,** *40*, 1881.

(31) Yamago, S., *J. Polym. Sci. Part A: Polym. Chem.* **2006,** *44*, 1.

(32) Yamago, S.; Kayahara, E.; Kotani, M.; Ray, B.; Kwak, Y.; Goto, A.; Fukuda, T., *Angew. Chem. Int. Ed.* **2007,** *46*, 1304.

(33) Monteiro, M. J., *J. Polym. Sci. A: Polym. Chem.* **2005,** *43*, 3190.

(34) Quiclet-Sire, B.; Zard, S. Z., *Pure & Appl. Chem.* **1997,** *69*, 645.

(35) Richel, A.; Delfosse, S.; Cremasco, C.; Delaude, L.; Demonceau, A.; Noels, A. F., *Tetrahedron Lett.* **2003,** *44*, 6011.

(36) Matyjaszewski, K.; Patten, T. E.; Xia, J. H., *J. Am. Chem. Soc.* **1997,** *119*, 674.

(37) Berthier, D.; Perrier, S.; Willoughby, I.; Batt-Coutrot, D.; Haddleton, D. M., *Macromolecules* **2002,** *35*, 2941.

(38) Haddleton, D. M.; Crossman, M. C.; Dana, B. H.; Duncalf, D. J.; Heming, A. M.; Kukulj, D., *Macromolecules* **1999,** *32*, 2110.

(39) Patten, T. E.; Matyjaszewski, K., *Acc. Chem. Res.* **1999,** *32*, 895.

(40) Coca, S.; Davis, K.; Miller, P.; Matyjaszewski, K., *Polym. Prepr. (Am. Chem. Soc., Div. Polym. Chem.)* **1997,** *213*, 321.

(41) Garamszegi, L.; Donzel, C.; Carrot, G.; Nguyen, T. Q.; Hilborn, J., *React. Funct. Polym.* **2003,** *55*, 179.

(42) Fuji, Y.; Ando, T.; Kamigaito, M.; Sawamoto, M., *Macromolecules* **2002,** *35*, 2949.

(43) Matyjaszewski, K.; Coca, S.; Gaynor, S. G.; Wei, M.; Woodworth, B. E., *Macromolecules* **1998,** *31*, 5967.

(44) Xia, J.; Gaynor, S. G.; Matyjaszewski, K., *Macromolecules* **1998,** *31*, 5958.

(45) Matyjaszewski, K., *Macromol. Symp.* **2002,** *182*, 209.

(46) Hawker, C. J., *Acc. Chem. Res.* **1997,** *30*, 373.

(47) Kharasch, M. S.; Jensen, E. V.; Urry, W. H., *Science* **1945,** *102*, 128.

(48) Nesmeyanov, A. N.; Freidlina, R. K.; Chukovskaya, E. C.; Petrova, R. G.; Belyavsky, A. B., *Tetrahedron* **1962,** *17*, 61.

(49) Susuki, T.; Tsuji, J., *J. Org. Chem.* **1970,** *35*, 2982.

(50) Iqbal, J.; Bhatia, B.; Nayyar, N. K., *Chem. Rev.* **1994,** *94*, 519.

(51) Asscher, M.; Vofsi, D., *J. Chem. Soc.* **1961**, 2261.

(52) Simal, F.; Demonceau, A.; Noels, A. F., *Tetrahedron Lett.* **1999,** *40*, 5689.

(53) Minisci, F., *Acc. Chem. Res.* **1975,** *8*, 165.

(54) Karasch, M. S.; Jensen, E. V.; Urry, W. H., *Science* **1945,** *102*, 128.

(55) Kochi, J. K., *Acc. Chem. Res.* **1974,** *7*, 351.

(56) Kato, M.; Kamigaito, M.; Sawamoto, M.; Higashimura, T., *Macromolecules* **1995,** *28*, 1721.

(57) Wang, J.-S.; Matyjaszewski, K., *J. Am. Chem. Soc.* **1995,** *117*, 5614.

(58) Pintauer, T.; Matyjaszewski, K., *Coord. Chem. Rev.* **2005,** *249*, 1155.

(59) Granel, C.; Dubois, P.; Jérome, R.; Teyssié, P., *Macromolecules* **1996,** *29*, 8576.

(60) Uegaki, H.; Kotani, Y.; Kamigaito, M.; Sawamoto, M., *Macromolecules* **1997,** *30*, 2249.

(61) Uegaki, H.; Kotani, Y.; Kamigaito, M.; Sawamoto, M., *Macromolecules* **1998,** *31*, 6756.

(62) Uegaki, H.; Kamigaito, M.; Sawamoto, M., *J. Polym. Sci. Part A: Polym. Chem.* **1999,** *37*, 3003.

(63) Moineau, G.; Minet, M.; Dubois, P.; Teyssié, P.; Senninger, T.; Jérôme, R., *Macromolecules* **1999,** *32*, 27.

(64) Li, P.; Qiu, K.-Y., *Polymer* **2002,** *43*, 5873.

(65) O'Reilly, R. K.; Shaver, M. P.; Gibson, V. C., *Inorg. Chim. Acta* **2006,** *359*, 4417.

(66) Lecomte, P.; Drapier, I.; Dubois, P.; Tessiyé, P.; Jérome, R., *Macromolecules* **1997,** *30*, 7631.

(67) Hong, S. C.; Jia, S.; Teodorescu, M.; Kowalewski, T.; Matyjaszewski, K.; Gottfried, A.; Brookhart, M., *J. Polym. Sci. Part A: Polym. Chem.* **2002,** *40*, 2736.

(68) Percec, V.; Barboiu, B.; Neumann, A.; Ronda, J. C.; Zhao, M., *Macromolecules* **1996,** *29*, 3665.

(69) Moineau, G.; Granel, C.; Dubois, P.; Teyssié, P.; Jérôme, R., *Macromolecules* **1998,** *31*, 542.

(70) Kotani, Y.; Kamigaito, M.; Sawamoto, M., *Macromolecules* **1999,** *32*, 2420.

(71) Kotani, Y.; Kamigaito, M.; Sawamoto, M., *Macromolecules* **2000,** *33*, 6746.

(72) Stoffelbach, F.; Poli, R.; Richard, P., *J. Organomet. Chem.* **2002,** *663*, 269.

(73) Stoffelbach, F.; Claverie, J.; Poli, R., *C.R. Acad. Sci., Ser. IIc: Chim.* **2002,** *5*, 37.

(74) Stoffelbach, F.; Haddleton, D. M.; Poli, R., *Eur. Polym. J.* **2003,** *39*, 2099.

(75) Poli, R.; Stoffelbach, F.; Maria, S.; Mata, J., *Chem. Eur. J.* **2005,** *11*, 2537.

(76) Maria, S.; Stoffelbach, F.; Mata, J.; Daran, J.-C.; Richard, P.; Poli, R., *J. Am. Chem. Soc.* **2005,** *127*, 2537.

(77) Mata, J.; Maria, S.; Daran, J.-C.; Poli, R., *Eur. J. Inorg. Chem.* **2006,** *13*, 2624.

(78) Stoffelbach, F.; Richard, P.; Poli, R.; Jenny, T.; Savary, C., *Inorg. Chim. Acta* **2006,** *359*, 4447.

(79) Ando, T.; Kamigaito, M.; Sawamoto, M., *Macromolecules* **1997,** *30*, 4507.

(80) Matyjaszewski, K.; Wei, M.; Xia, J.; McDermott, N. E., *Macromolecules* **1997,** *30*, 8161.

(81) Kotani, Y.; Kamigaito, M.; Sawamoto, M., *Macromolecules* **1999,** *32*, 6877.

(82) Louie, J.; Grubbs, R. H., *Chem. Commun.* **2000,** *16*, 1479.

(83) Ibrahim, K.; Lofgren, B.; Seppala, J., *Eur. Polym. J.* **2003,** *39*, 939.

(84) Gibson, V. C.; O'Reilly, R. K.; Wass, D. F.; White, A. J. P.; Williams, D. J., *Dalton Trans.* **2003**, 2824.

(85) Gibson, V. C.; O'Reilly, R. K.; White, A. J. P.; Williams, D. J., *J. Am. Chem. Soc.* **2003,** *125*, 8450.

(86) Gibson, V. C.; O'Reilly, R. K.; Reed, W.; Wass, D.; White, A. J. P.; Williams, D. J., *Chem. Commun.* **2002**, 1850.

(87) Kabachii, Y. A.; Kochev, S. Y.; Bronsteinl, L. M.; Blagodatskikh, I. B.; Valetsky, P. M., *Polym. Bull.* **2003,** *50*, 271.

(88) Grishin, D. F.; Semyonycheva, L. L.; Telegina, E. V.; Smirnov, A. S.; Nevodchikovc, V. 1., *Russ. Chem. Bull., Int. Ed.* **2003,** *52*, 505.

(89) Grishin, D. F.; Ignatov, S. K.; Shchepalov, A. A.; Razuvaev, A. G., *Appl. Organomet. Chem.* **2004,** *18*, 271.

(90) Wang, B.; Zhuang, Y.; Luo, X.; Xu, S.; Zhou, X., *Macromolecules* **2003,** *36*, 9684.

(91) Weiser, M. S.; Lhaupt, R. M., *J. Polym. Sci. Part A: Polym. Chem.* **2005,** *43*, 3804.

(92) Braunecker, W. A.; Itami, Y.; Matyjaszewski, K., *Macromolecules* **2005,** *38*, 9402.

(93) Bellus, D., *Pure Appl. Chem.* **1985,** *57*, 1827.

(94) Cotton, F. A.; Wilkinson, G., *Advanced Inorganic Chemistry* **1980,** *4th Ed.*, 749.

(95) Bolm, C.; Legros, J.; Paih, J. L.; Zani, L., *Chem. Rev.* **2004,** *104*, 6217.

(96) Barton, D. H. R.; Doller, D., *Acc. Chem. Res.* **1992,** *25*, 504.

(97) Barton, D. H. R., *Chem. Soc. Rev.* **1996,** *25*, 237.

(98) Barton, D. H. R., *Tetrahedron* **1998,** *54*, 5805.

(99) Sawyer, D. T.; Sobkowiak, A.; Matsushita, T., *Acc. Chem. Res.* **1996,** *29*, 409.

(100) MacFaul, P. A.; Wayner, D. D. M.; Ingold, K. U., *Acc. Chem. Res.* **1998,** *31*, 159.

(101) Walling, C., *Acc. Chem. Res.* **1998,** *31*, 155.

(102) Goldstein, S.; Meyerstein, D., *Acc. Chem. Res.* **1999,** *32*, 547.

(103) Fontecave, M.; Menage, S.; Duboc-Toia, C., *Coord. Chem. Rev.* **1998,** *178*, 1555.

(104) Costas, M.; Chen, K.; Que, L., *Coord. Chem. Rev.* **2000,** *200*, 517.

(105) Costas, M.; Mehn, M. P.; Jensen, M. P.; Que, L., *Chem. Rev.* **2004,** *104*, 939.

(106) Tshuva, E. Y.; Lippard, S. J., *Chem. Rev.* **2004,** *104*, 987.

(107) Colombo, L.; Ulgheri, F.; Prati, L., *Tetrahedron Lett.* **1989,** *30*, 6435.

(108) Bach, T.; Fox, D. N. A.; Reetz, M. T., *Chem. Commun.* **1992**, 1634.

(109) Kobayashi, S.; Nagayama, S.; Busujima, T., *J. Am. Chem. Soc.* **1998,** *120*, 8287.

(110) Aoyama, N.; Manabe, K.; Kobayashi, S., *Chem. Lett.* **2004,** *33*, 312.

(111) Fei, C. P.; Chan, T. H., *Synthesis* **1982,** *6*, 467.

(112) Kocovaky, P.; Dvorak, D., *Tetrahedron Lett.* **1986,** *27*, 5015.

(113) Laszlo, P.; Montaufier, M.-T.; Lalatiana Randriamahefa, S., *Tetrahedron Lett.* **1990,** *31*, 4867.

(114) Christoffers, J., *J. Chem. Soc., Perkin Trans. 1* **1997**, 3141.

(115) Christoffers, J., *Chem. Commun.* **1997**, 943.

(116) Christoffers, J., *Synlett* **2001**, 723.

(117) Shimizu, K.-i.; Miyagi, M.; Kan-no, T.; Kodama, T.; Kitayama, Y., *Tetrahedron Lett.* **2003,** *44*, 7421.

(118) Caporusso, A. M.; Giacomelli, G.; Lardicci, L., *J. Chem. Soc., Perkin Trans. 1* **1979**, 3139.

(119) Corey, E. J.; Barnes-Seeman, D.; Lee, T. W., *Tetrahedron Lett.* **1997,** *38*, 4351.

(120) Nakamura, M.; Hirai, A.; Nakamura, E., *J. Am. Chem. Soc.* **2000,** *122*, 978.

(121) Hojo, M.; Murakami, Y.; Aihara, H.; Sakuragi, R.; Baba, Y.; Hosomi, A., *Angew. Chem. Int. Ed.* **2001,** *40*, 621.

(122) Watahiki, T.; Oriyama, T., *Tetrahedron Lett.* **2002,** *43*, 8959.

(123) Durandetti, M.; Meignein, C.; Perichon, J., *J. Org. Chem.* **2003,** *68*, 3121.

(124) Watahiki, T.; Akabane, Y.; Mori, S.; Oriyama, T., *Org. Lett.* **2003,** *5*, 3045.

(125) Kotani, Y.; Kamigaito, M.; Sawamoto, M., *Macromolecules* **2000,** *33*, 3543.

(126) Wakioka, M.; Baek, K.-Y.; Ando, T.; Kamigaito, M.; Sawamoto, M., *Macromolecules* **2002,** *35*, 330.

(127) Gobelt, B.; Matyjaszewski, K., *Macromol. Chem. Phys.* **2000,** *201*, 1619.

(128) Ibrahim, K.; Yliheikkila, K.; Abu-Surrah, A.; Lofgren, B.; Lappalainen, K.; Leskela, M.; Repo, T.; Seppala, J., *Eur. Polym. J.* **2004,** *40*, 1095.

(129) Otsu, T.; Yoshida, M., *Makromol. Chem. Rapid Commun.* **1982,** *3*, 127.

(130) Otsu, T., *J. Polym. Sci., Polym. Chem.* **2000,** *38*, 2121.

(131) Otsu, T.; Yoshida, M.; Kuriyama, A., *Polym. Bull.* **1982,** *7*, 45.

(132) Druliner, J. D., *Macromolecules* **1991,** *24*, 6079.

(133) León-Sáenz, E. D.; Morales, G.; Guerrero-Santos, R.; Gnanou, Y., *Macromol. Chem. Phys.* **2000,** *201*, 74-83.

(134) Yamada, B.; Nobukane, Y.; Miura, Y., *Polym. Bull.* **1998,** *41*, 539.

(135) Steenbock, M.; Klapper, M.; Müllen, K., *Macromol. Chem. Phys.* **1998,** *199*, 763-769.

(136) Moad, G.; Rizzardo, E.; Solomon, D. H., *Polym. Bull.* **1982,** *6*, 589.

(137) Georges, M. K.; Veregin, R. P. N.; Kazmaier, P. M.; Hamer, G. K., *Macromolecules* **1993,** *26*, 2987.

(138) Lu, Z.; Fryd, M.; Wayland, B. B., *Macromolecules* **2004,** *37*, 2686.

(139) Detrembleur, C.; Debuigne, A.; Bryaskova, R.; Charleux, B.; Jérôme, R., *Macromol. Rapid Commun.* **2006,** *27*, 37.

(140) Debuigne, A.; Caille, J.-R.; Willet, N.; Jérôme, R., *Macromolecules* **2005,** *38*, 9488.

(141) Kaneyoshi, H.; Matyjaszewski, K., *Macromolecules* **2005,** *38*, 8163.

(142) Sciannamea, V.; Debuigne, A.; Piette, Y.; Jerome, R.; Detrembleur, C., *Chem. Commun.* **2006**, 4180.

(143) Wayland, B. B.; Peng, C.-H.; Fu, X.; Lu, Z.; Fryd, M., *Macromolecules* **2006,** *39*, 8219.

(144) Maria, S.; Kaneyoshi, H.; Matyjaszewski, K.; Poli, R., *Chem. Eur. J.* **2007,** *13*, 2480.

(145) Enikolopyan, N. S.; Smirnov, B. R.; Ponomarev, G. V.; Bel'govskii, I. M., *J. Polym. Sci., Polym. Chem. Ed.* **1981,** *19*, 879.

(146) Gridnev, A., *J. Polym. Sci., Polym. Chem. Ed.* **2000,** *38*, 1753.

(147) Gridnev, A. A.; Ittel, S. D.; Wayland, B. B.; Fryd, M., *Organometallics* **1996,** *15*, 5116.

(148) Chiu, T. Y. J.; Heuts, J. P. A.; Davis, T. P.; Stenzel, M. H.; Barner-Kowollik, C., *Macromol. Chem. Phys.* **2004,** *205*, 752.

(149) Wang, W.; Stenson, P. A.; Marin-Becerra, A.; McMaster, J.; Schroder, M.; Irvine, D. J.; Freeman, D.; Howdle, S. M., *Macromolecules* **2004,** *37*, 6667.

(150) Heuts, J. P. A.; Forster, D. J.; Davis, T. P., *Macromolecules* **1999,** *32*, 2511.

(151) Gridnev, A.; Ittel, D. S., *Chem. Rev.* **2001,** *101*, 3611.

(152) Heuts, J. P.; Roberts, G. E.; Biasutti, J. D., *Aust. J. Chem.* **2002,** *55*, 381.

(153) Janowicz, A. H. (Dupont) Bimetallic catalytic chain transfer agents for molecular weight control in free radical polymerization. US Patent 4746713, May 24th, 1988.

(154) Abramo, G. P.; Norton, J. R., *Macromolecules* **2000,** *33*, 2790.

(155) Tang, L.; Papish, E. T.; Abramo, G. P.; Norton, J. R.; Baik, M.-H.; Friesner, R. A.; Rappe, A., *J. Am. Chem. Soc.* **2003,** *125*, 10093.

(156) Tang, L.; Norton, J. R., *Macromolecules* **2004,** *37*, 241.

(157) Grishin, D. F.; Semyonycheva, L. L.; Telegina, E. V.; Smirnov, A. S.; Nevodchikovc, V. I., *Russ. Chem. Bull., Int. Ed.* **2003,** *52*, 505.

(158) Grishin, D. F.; Ignatov, S. K.; Shchepalov, A. A.; Razuvaev, A. G., *Appl. Organometal. Chem.* **2004,** *18*, 271.

(159) Asandei, A. D.; Moran, I. W., *J. Am. Chem. Soc.* **2004,** *126*, 15932.

(160) Asandei, A. D.; Gobinda Saha, *Macromol. Rapid Commun.* **2005,** *26*, 626.

(161) Braunecker, W. A.; Itami, Y.; Matyjaszewski, K., *Macromolecules* **2005,** *38*, 9402.

(162) Gibson, V. C.; O'Reilly, R. K.; Wass, D. F.; White, A. J. P.; Williams, D. J., *Macromolecules* **2003,** *36*, 2591.

Chapter 2

Synthesis, Characterisation and Polymerisation Studies using Fe^{II} α-Diimine Complexes

2.1 - Introduction

Whilst transition metal complexes of molybdenum, titanium, osmium and cobalt have previously been shown to control radical polymerisation through both ATRP and OMRP mechanisms (Chapter 1), this work focuses on an α-diimine iron system which is also capable of participating in more than one mechanism. The basis for the work detailed in this thesis was the discovery that the α-diimine iron system can participate in controlled ATRP or CCT reactions depending on the ligand substituents.[1]

The simple, bidentate 1,4-diaza-1,3-butadiene (or α-diimine) ligands are readily synthesised through facile condensation reactions between a dialdehyde or diketone and a primary amine, and have been extensively investigated for a profusion of catalytic reactions.[2] The most prominent application of this ligand type is the use of bulky α-diimine complexes of nickel and palladium as effective catalysts for ethylene polymerisation.[3-6] These ligands have also been successfully applied in a variety of other catalytic processes. Vanadium and copper α-diimine complexes have also been reported as ethylene polymerisation catalysts,[7,8] while platinum complexes are also active in hexene isomerisation.[9] Platinum and palladium C-H activation catalysts have been extensively studied[10-12] and Pd α-diimines are also important in the copolymerisation of CO and aromatic olefins.[13,14] Half-sandwich molybdenum α-diimine complexes proved to be effective catalysts for both stable free radical and atom transfer radical polymerisation,[15] while the analogous tantalum complexes catalysed the living anionic polymerisation of MMA.[16] Iron α-diimine catalysts have been used in the dimerisation of dienes,[17-19] the oligomerisation of ethylene[20] and, with limited success, for olefin hydrogenation.[21]

The efficiency of α-diimine Fe^{II} complexes as catalysts for the controlled atom transfer radical polymerisation of styrene and MMA was reported by our group.[1,22-24] A wide variety of α-diimine ligands were prepared and the Fe^{II} halide complexes were synthesised and tested for ATRP (Figure 2.1).

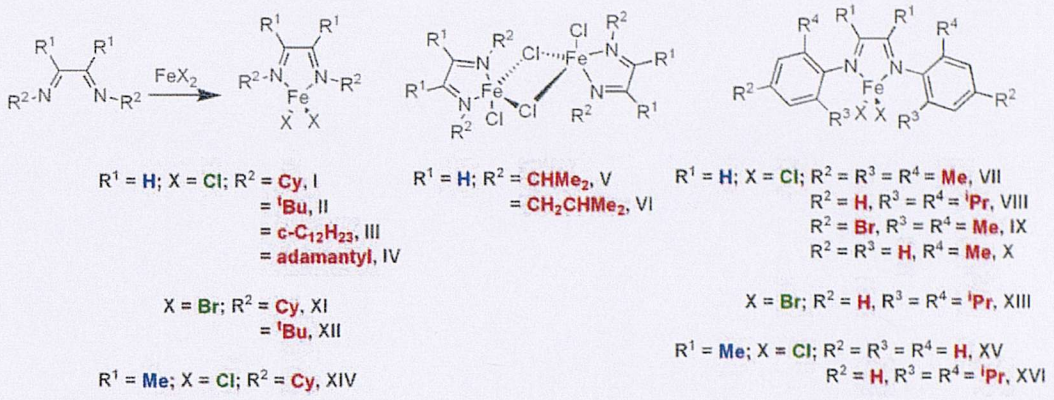


Figure 2.1 α-Diimine Fe^{II} complexes previously tested for ATRP.

The monomeric alkyl α-diimine Fe^{II} chloride complexes, **I-IV**, were effective ATRP catalysts[23,24] for the polymerisation of styrene and MMA, yielding polymers with low polydispersities and molecular weights close to the theoretical values. Complexes **V** and **VI** had dimeric structures, attributed to their less bulky alkyl substituents, and this resulted in less effective catalysts for ATRP. Both complexes produced polymers with molecular weights higher than the theoretical values and broad polydispersities. Their 5-coordinate geometry was proposed to be less favourable for ATRP, due to the steric crowding around the metal centre on going from five- to six- coordination upon oxidation.[1]

The *N*-aryl substituted $FeCl_2$ compounds, **VII-X,** were ineffective catalysts for the ATRP of styrene and MMA. Low molecular weight polymers were isolated and there was little control over polymerisation, as evidenced by the broad PDIs (1.6-2.1). The semi-logarithmic plots of $\ln([M]_o/[M]_t)$ versus time were non-linear, M_n did not increase linearly with monomer conversion and theoretical molecular weight values were vastly different to the experimental molecular weights measured by GPC. The polymer obtained was olefin-terminated, and the polymerisation mechanism was hypothesised to occur via catalytic chain transfer processes.[23,24]

The difference between the polymerisation behaviour with alkyl and aryl diimines was attributed to the accessibility of the Fe^{II}/Fe^{III} redox couple. In the case of alkyl substituents, where the complexes were efficient ATRP catalysts, the Fe^{II} centre was easily oxidised. Cyclic voltammagrams indicated that the redox couple was reversible and readily accessible. However, the aryl substituted diimines were much less reducing than their alkyl counterparts, and were suggested to have inaccessible or irreversible redox potentials.[1,25]

Complexes **XI-XIII,** the bromide analogues of **I, II** and **VIII**, were poor ATRP catalysts in comparison to their chloride counterparts. Polymerisations were slower and less controlled although, like the chloride complexes, **XI** and **XII** did proceed via an ATRP mechanism. The redox potentials of the bromide analogues were higher than the chloride complexes, which was thought likely to contribute to the poor ATRP performance.[1]

The polymerisation results for these catalysts indicated that the presence of electron-donating *N*-alkyl groups resulted in more effective ATRP catalysts than electron-withdrawing *N*-aryl groups. An electron-donating group may lower the redox potential, making the higher oxidation state more accessible and the atom transfer equilibrium faster. It was therefore hypothesised that inclusion of an electron-donating alkyl group on the diimine backbone would promote ATRP relative to CCT. Complexes **XIV-XVI** contained methyl groups on the diimine backbone, and complex **XIV** indeed gave reasonable polymerisation results, although there was a slight loss of control when compared to the analogous aldimine complex, **I**. The steric environments of **XIV** and **I** are somewhat different and the electrochemistry of **XIV** is actually less favourable than that of **I**, as it exhibits a significantly higher redox potential. The aryl diimines **XV** and **XVI** were poor ATRP catalysts, similar to the aryl α-diimines with non-substituted backbones such as **VIII**, and gave the low molecular weight polymers consistent with CCT processes.[1]

Although this work represented a significant contribution to the field of controlled radical polymerisation using α-diimine iron catalysts, much still remained to explore. The evidence suggests that polymerisation reactions using these complexes occur through two separate mechanisms, ATRP and CCT. The *N*-alkyl-substituted α-diimines are efficient ATRP catalysts, whereas their *N*-aryl counterparts give rise to polymerisation through CCT. An important question remaining to be answered was whether the difference in mechanism arises primarily due to steric or electronic factors, or a combination of these. The reasons behind the apparent switch in the polymerisation mechanism, and the interplay between the two mechanisms also remained to be investigated.

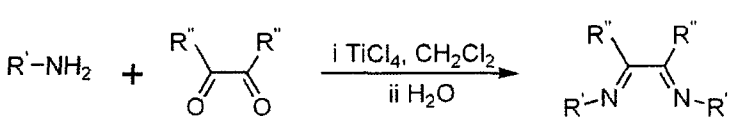
An apparently highly significant effect is the nature of the substituent attached to the imino *N*-donor atoms, with electron-donating groups favouring ATRP and electron-withdrawing groups favouring CCT. An initial objective for this study was

the preparation and characterisation of α-diimine Fe^{II} complexes analogous to the efficient *N*-alkyl ATRP catalysts, but containing electron-withdrawing substituents attached to the carbon atoms of the α-diimine ligand backbone. The rest of this chapter details the synthesis, characterisation and polymerisation behaviour of a series of novel α-diimine Fe^{II} complexes, exploring the effect of substituting electron-withdrawing groups into the 2,3-positions of the diimine backbone.

2.2 - Results and Discussion

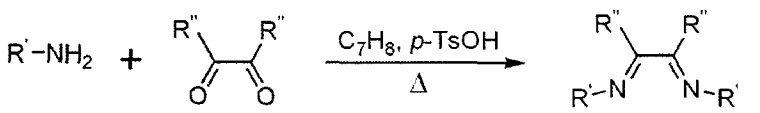
2.2.1 - Synthesis of Fe^{II} compounds.

The *N*-alkyl substituted α-diimine ligands, $^{R',R''}[N,N]$, (where $^{R',R''}[N,N]$ = R'-N=CR''-CR''=N-R', R' = *tert*-butyl (^{t}Bu), cyclohexyl (Cy), and R'' = phenyl (Ph), *para*-fluorophenyl (F-Ph)), **1-4**, were prepared through $TiCl_4$-mediated condensation reactions, modifying a literature procedure[26] (Scheme 2.1). After aqueous workup, separation and removal of the organic solvent, the sticky crude residues were recrystallised from hot alcohol to give the desired products as crystalline materials in moderate to good yields (45-85%). Attempts to synthesise these ligands using more conventional techniques, such as Dean-Stark, $Si(OEt)_4$-mediated and acid-catalysed condensations were unsuccessful, resulting in isolation either of mono-substituted product or starting materials. The *N*-aryl substituted α-diimine ligands, $^{R',R''}[N,N]$, (where R' = phenyl (Ph) and mesityl (Mes), and R'' = phenyl (Ph) and *para*-fluorophenyl (F-Ph)) were synthesised using the same $TiCl_4$-activated route in the case of the Mes-substituted ligand, **6**, and using Dean-Stark apparatus and *p*-toluenesulfonic acid (TsOH) as a catalyst in the case of the Ph-substituted ligand, **5** (Scheme 2.2). Recrystallisation of the crude material gave the disubstituted products in yields of 55-65 %, significantly improving the literature yield of 35% reported for **5**.[27]



	R'	R''
1	Cy	Ph
2	Cy	F-Ph
3	^{t}Bu	Ph
4	^{t}Bu	F-Ph
6	Mes	F-Ph

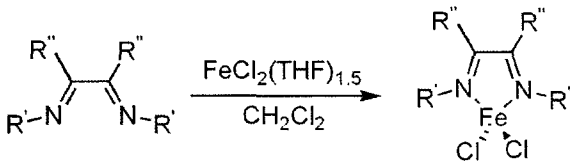
Scheme 2.1 Synthesis of novel 2,3-substituted α-diimine ligands.



	R'	R''
5	Ph	Ph

Scheme 2.2 Dean-Stark method for synthesis of phenyl-substituted α-diimine ligand.

The Fe^{II} chloride complexes, **7-12** (Scheme 2.3), were readily synthesised and isolated in good yields (64-77%). Addition of CH_2Cl_2 to an intimate mixture of ligand and $FeCl_2(THF)_{1.5}$ produced a deep blue solution, except in the case of **11** and **12** which were green and brown, respectively. After stirring overnight the solution was filtered and concentrated, before the desired product was obtained as a purple (**7-10**), green (**11**) or brown (**12**) solid after precipitation with pentane.



	R'	R''
7	Cy	Ph
8	Cy	F-Ph
9	^{t}Bu	Ph
10	^{t}Bu	F-Ph
11	Ph	Ph
12	Mes	F-Ph

Scheme 2.3 Synthesis of novel 2,3-substituted Fe^{II} chloride complexes.

Despite the paramagnetism of the complexes, contact-shifted ^{1}H NMR spectra could be obtained for compounds **7-10** and assigned on the basis of integrated signal intensities and chemical shifts. Spectra obtained for complexes **11** and **12** were not meaningful. As an example, the spectra obtained for complexes **7** and **9** are shown in Figures 2.2 and 2.3. The spectrum of complex **7**, ^{Cy,Ph}[*N,N*]$FeCl_2$ (Figure 2.2), is relatively complicated when compared to the analogous ^{t}Bu-substituted complex, **9**. The most highly deshielded resonance is that of H_d, whose axial position and close proximity to the paramagnetic Fe centre results in a large shift downfield, to 192 ppm. The most highly shielded resonances are those of the methylene ring protons, H_e, H_f and H_g (δ -6 to -48) where it is notable that the axial and equatorial sites are inequivalent. The aromatic protons H_a, H_b and H_c appear between 6.5 and 16 ppm and are least affected by the local magnetic field of the paramagnetic centre. The ^{1}H NMR spectrum obtained for **9**, ^{tBu,Ph}[*N,N*]$FeCl_2$ (Figure 2.3), shows the aromatic signals H_a, H_b and H_c in a similar region to complex **7** (δ 7-19), while the most highly shielded resonance is that of H_d (-17 ppm), the ^{t}Bu protons which are closest in proximity to the metal centre. Spectra obtained for complexes **8** and **10** were

similar in most respects to those described for **7** and **9**, allowing for the absence of the *para* protons on the phenyl rings.

FAB-MS of **7-12** showed the expected $[M+H]^+$ peaks as well as common fragments, such as $[M-Cl]^+$. In the infra-red spectra the imine $\nu_{C=N}$ stretches for **7-12** were visible between 1590-1610 cm^{-1}. In each case, the stretch for the Fe^{II} complex appeared at a lower frequency than that of the free ligand, indicating that the imine bond is weaker in the metal complex.

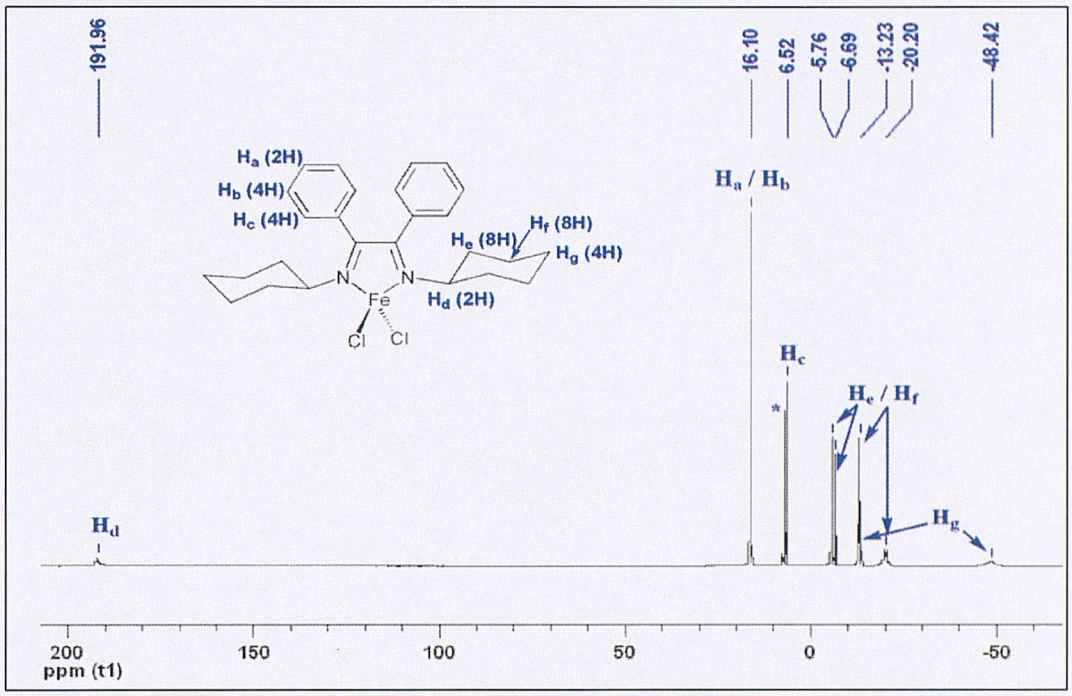


Figure 2.2 ^1H NMR spectrum obtained for $^{Cy,Ph}[N,N]FeCl_2$, **7**. * indicates residual proton signal in $CDCl_3$.

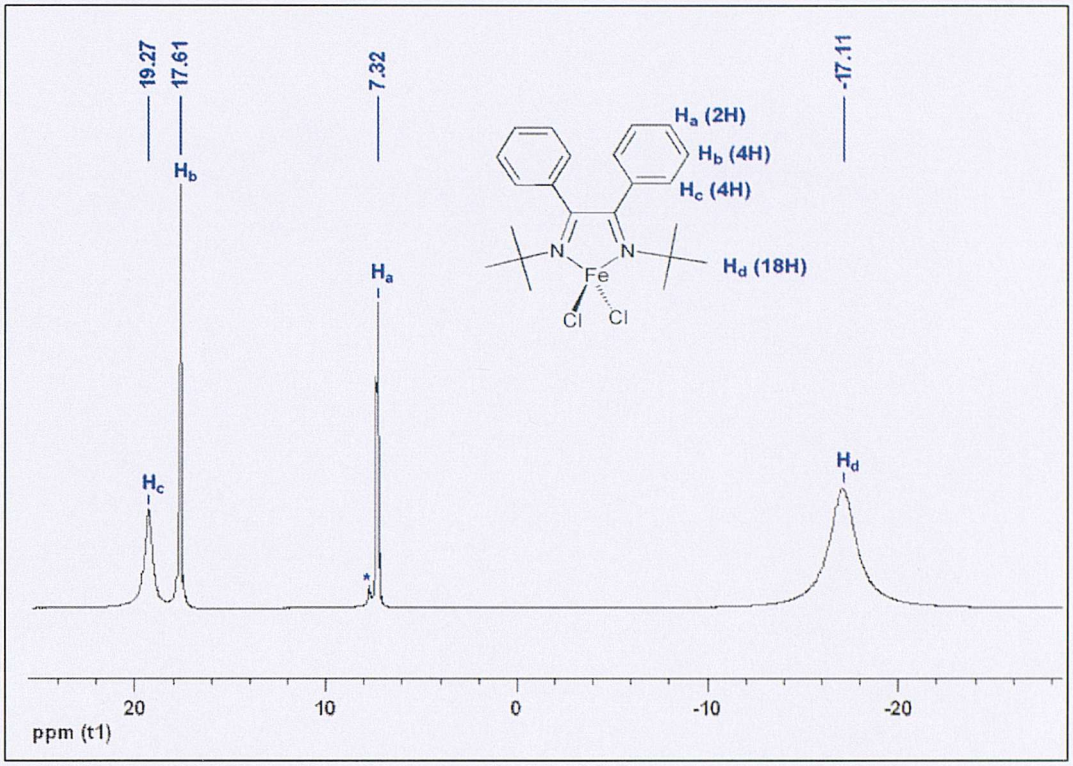


Figure 2.3 ^{1}H NMR spectrum obtained for $^{tBu,Ph}[N,N]FeCl_2$, **9**. * indicates residual proton signal in $CDCl_3$.

Crystals suitable for X-ray structure analysis of complexes **7**-**11** were obtained. The complexes all had similar, monomeric solid-state structures with 4-coordinate metal centres, and distorted tetrahedral iron centres. Crystals of $^{Cy,Ph}[N,N]FeCl_2$, **7**, were obtained through slow cooling of a saturated solution of **7** in toluene. The X-ray crystal structure revealed a C_S-symmetric complex with a highly distorted tetrahedral iron centre. The *cis* angles were in the range 78.43(15)-125.62(7)°, with the most acute angle being the bite angle of the chelating *N,N'* ligand (Figure 2.4). The crystallographic mirror plane includes the iron centre and the two chlorines, and bisects the C(1)–C(1A) single bond (1.521(6) Å) between the two imine units (C(1)–N(1) 1.284(4) Å). The two imines are perfectly coplanar (a consequence of the mirror symmetry), and the iron "perches" above this plane by *ca.* 0.59 Å in the direction of Cl(1). The angle between the two chlorine atoms is substantially enlarged from ideal tetrahedral, at 125.62(7)° and the aryl rings on the backbone are slightly twisted away from orthogonal. The torsion angle about the C(1)–C(Ph) bond is *ca.* 102° and the top (Cl(1) side) of the phenyl rings are rotated away from the mirror plane.

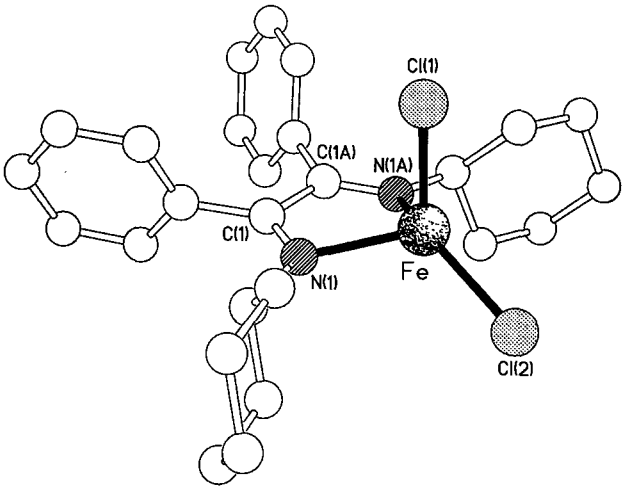


Figure 2.4 The molecular structure of the C_S-symmetric complex **7**.

Table 2.1 Selected bond lengths (Å) and angles (°) for complex **7**.

Fe–Cl(1)	2.2551(16)	Cl(1)–Fe–Cl(2)	125.62(7)
Fe–Cl(2)	2.2183(15)	Cl(1)–Fe–N(1)	101.79(9)
Fe–N(1)	2.077(3)	Cl(1)–Fe–N(1A)	101.79(9)
Fe–N(1A)	2.077(3)	Cl(2)–Fe–N(1)	119.24(9)
N(1)–C(1)	1.284(4)	Cl(2)–Fe–N(1A)	119.24(9)
C(1)–C(1A)	1.521(6)	N(1)–Fe–N(1A)	78.43(15)

Crystals of $^{Cy,F\text{-}Ph}[N,N]FeCl_2$ suitable for X-ray analysis were obtained through slow diffusion of pentane into a saturated CH_2Cl_2 solution of **8**, and were badly twinned. Numerous attempts were made to isolate the twinning (through repeating the crystallisation, physically cutting the crystals, and trying to separate the contributions of multiple overlapping lattices to the whole data set), as this structure was important in determining whether the steric or electronic properties of the ligand substituents had a greater effect on the solid state structures. Despite these efforts, the twinning in **8** was never fully resolved and the refinement of two slightly different locations of the complete molecule (which has crystallographic C_S symmetry) in an orthorhombic space group gave the structure shown in Figure 2.5. The good fit between this model of the structure and the observed X-ray diffraction pattern allowed the atom connectivity of the complex to be established with confidence.

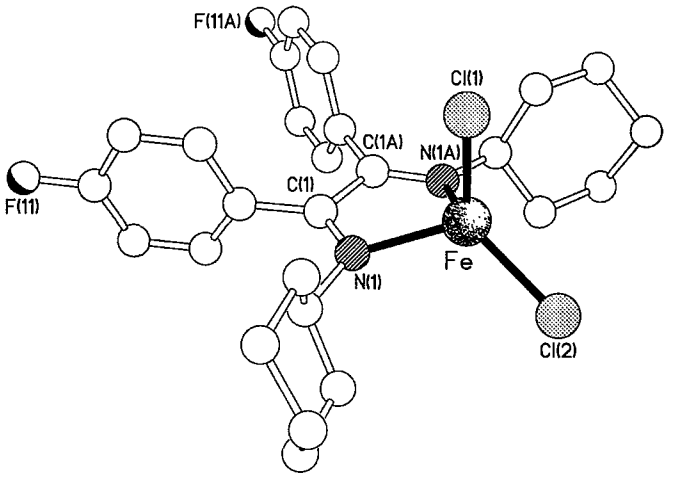


Figure 2.5 The molecular structure of the major occupancy (*ca.* 58%) orientation C_S-symmetric complex present in the crystals of **8**.

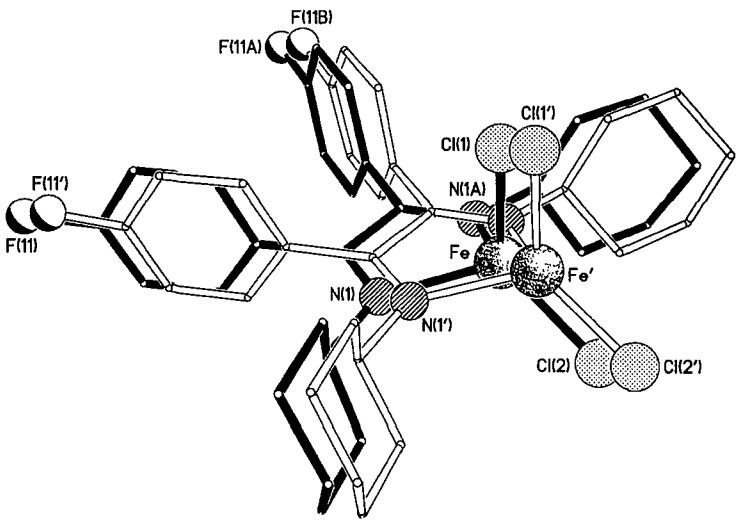


Figure 2.6 Overlay of the two orientations of the C_S-symmetric complex present in the crystals of **8**. The major occupancy (*ca.* 58%) orientation is shown with dark bonds, the minor occupancy (*ca.* 42%) orientation is shown with open bonds, and the two orientations are shown in their correct relative positions.

Table 2.2 Selected bond lengths (Å) and angles (°) for the two disordered orientations (**major** *ca.* 58%, **minor** *ca.* 42% occupancy) of the C_S-symmetric complex **8**.

	major	**minor**		**major**	**minor**
Fe–Cl(1)	2.209(5)	2.278(8)	Cl(1)–Fe–Cl(2)	121.1(2)	121.0(3)
Fe–Cl(2)	2.247(6)	2.145(8)	Cl(1)–Fe–N(1)	105.6(2)	102.3(4)
Fe–N(1)	2.064(8)	2.094(11)	Cl(1)–Fe–N(1A)	105.6(2)	102.3(4)
Fe–N(1A)	2.064(8)	2.094(11)	Cl(2)–Fe–N(1)	118.7(2)	122.4(4)
N(1)–C(1)	1.302(12)	1.280(15)	Cl(2)–Fe–N(1A)	118.7(2)	122.4(4)
C(1)–C(1A)	1.517(15)	1.58(3)	N(1)–Fe–N(1A)	79.0(4)	76.9(6)

A comparison of the solid state structure of $^{Cy,Ph}[N,N]FeCl_2$, **7**, with the analogous complexes containing proton and methyl groups on the diimine backbone, $^{Cy,H}[N,N]FeCl_2$ and $^{Cy,Me}[N,N]FeCl_2$, reported in the literature,[1] indicates a clear trend. Increasing the steric bulk on the diimine backbone causes an increase in the C=N bond lengths, from 1.239(6) Å (H) to 1.277(3) Å (Me) to 1.284(4) Å (Ph). Similarly, a decrease in the Fe–N bond lengths is observed, from 2.125(4) Å in the aldimine derivative to 2.102(2) Å in the methyl ketimine derivative and to 2.077(3) Å in the phenyl ketimine derivative. There is also an enlargement of the Cl–Fe–Cl angle, from 120.08(10)° to 123.87(4)° to 125.62(7)° on proceeding from the proton to methyl to phenyl substituents.

X-ray quality crystals of $^{tBu,Ph}[N,N]FeCl_2$ were obtained through slow cooling of a solution of **9** in hot toluene. Compound **9** crystallised with three independent complexes (**I**, **II** and **III**) in the asymmetric unit, along with one disordered toluene molecule (Figure 2.7, Table 2.3). The tetrahedral iron centres are highly distorted, with *cis* angles in the range 78.45(12)-124.53(5)°, again the most acute is the bite angle of the chelating *N,N'* ligand. The geometry at the iron centre is C_1 and the structure is unusual in that the N=C–C=N unit is not planar - instead, the chelate ring is puckered, with a torsion angle of *ca.* 14° between the imine units.

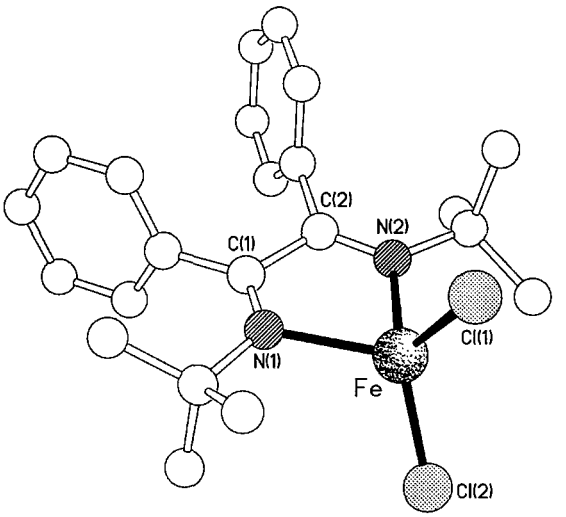


Figure 2.7 The molecular structure of one (**I**) of the three crystallographically independent complexes present in the crystals of **9**.

Table 2.3 Selected bond lengths (Å) and angles (°) for the three crystallographically independent complexes (**I**, **II** and **III**) present in the crystals of **9**.

	Mol I	**Mol II**	**Mol III**
Fe–Cl(1)	2.2460(12)	2.2450(12)	2.2451(14)
Fe–Cl(2)	2.2390(12)	2.2630(12)	2.2428(13)
Fe–N(1)	2.130(3)	2.115(3)	2.121(3)
Fe–N(2)	2.112(3)	2.114(3)	2.120(3)
C(1)–N(1)	1.283(5)	1.285(5)	1.269(5)
C(1)–C(2)	1.532(6)	1.525(5)	1.532(5)
C(2)–N(2)	1.282(5)	1.282(5)	1.284(5)
Cl(1)–Fe–Cl(2)	122.11(5)	124.53(5)	122.63(6)
Cl(1)–Fe–N(1)	113.71(9)	114.47(9)	117.11(9)
Cl(1)–Fe–N(2)	107.11(10)	110.09(9)	110.98(10)
Cl(2)–Fe–N(1)	110.56(9)	107.55(9)	104.92(10)
Cl(2)–Fe–N(2)	116.79(9)	112.15(9)	114.19(10)
N(1)–Fe–N(2)	78.45(12)	78.95(12)	78.75(12)

Crystals of $^{tBu,F\text{-}Ph}[N,N]FeCl_2$ were grown from a solution of **10** in CH_2Cl_2 / toluene (Figure 2.8, Table 2.4). The crystals of compound **10** contain two independent C_S-symmetric molecules (**I** and **II**), each of which has crystallographic mirror symmetry

about a plane which includes the iron, the two chlorines and bisects the C–C bond between the two C=N moieties. The *cis* angles are in the range 79.39(13)-121.56(6)°, and the metal atom sits *ca.* 17° (0.62 Å) above the diimine plane.

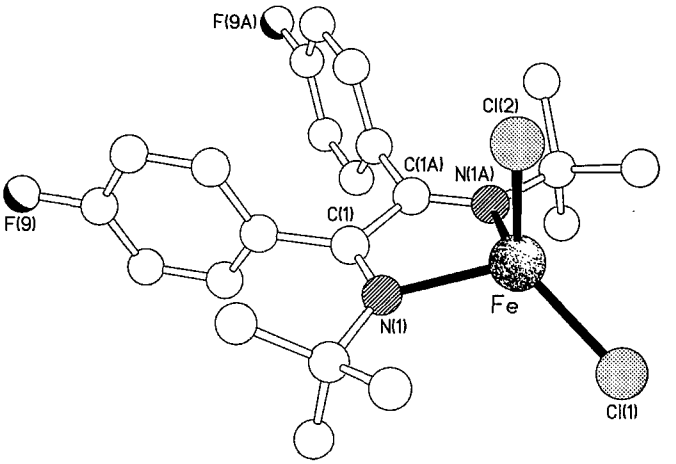


Figure 2.8 The molecular structure of one (**I**) of the two crystallographically independent C_S-symmetric complexes present in the crystals of **10**.

Table 2.4 Selected bond lengths (Å) and angles (°) for the two crystallographically independent C_S-symmetric complexes (**I** and **II**) present in the crystals of **10**.

	Mol I	**Mol II**		**Mol I**	**Mol II**
Fe–Cl(1)	2.2393(13)	2.2474(13)	Cl(1)–Fe–Cl(2)	121.56(6)	118.44(5)
Fe–Cl(2)	2.2329(14)	2.2341(13)	Cl(1)–Fe–N(1)	119.57(8)	122.50(8)
Fe–N(1)	2.103(2)	2.100(2)	Cl(1)–Fe–N(1A)	119.57(8)	122.50(8)
Fe–N(1A)	2.103(2)	2.100(2)	Cl(2)–Fe–N(1)	104.16(8)	103.17(8)
N(1)–C(1)	1.280(4)	1.285(4)	Cl(2)–Fe–N(1A)	104.16(8)	103.17(8)
C(1)–C(1A)	1.521(6)	1.521(6)	N(1)–Fe–N(1A)	79.39(13)	79.45(13)

The C=N double bonds in **10** are extremely similar in length to those obtained for complex **9**: 1.280(4)-1.285(4) Å for **10** *cf.* 1.269(5)-1.284(5) Å for **9**. However, the Fe–N bond lengths in **10** are noticeably shorter than in **9**, which may be attributed to the stronger electron-withdrawing ability of the ligand. The slight decrease in Cl–Fe–Cl angle from 122.11(5)° in **9** to 121.56(6)° in **10** is also consistent with the trends discussed above for the Cy-substituted complexes. These effects can be related directly to the electronics of the ligand, as the steric differences between **9** and **10** are negligible, and imply that the increased electron-withdrawing ability of

the substituents at the 2,3-positions of the ligand backbone play an important role in determining the solid state structure of the complexes.

Crystals of **11** suitable for X-ray structure determination were obtained through slow cooling of a saturated solution of $^{Ph,Ph}[N,N]FeCl_2$ in benzene and confirmed that the complex exhibited the expected monomeric structure (Figure 2.9, Table 2.5).

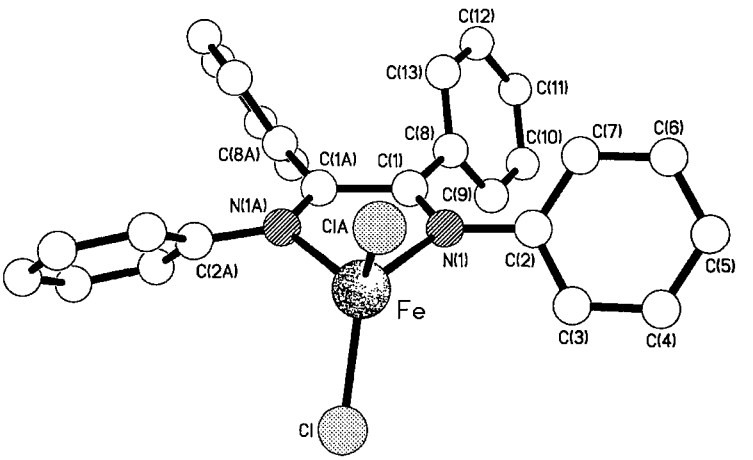


Figure 2.9 The molecular structure of the C_2 complex **11**.

Table 2.5 Selected bond lengths (Å) and angles (°) for complex **11**.

Fe–Cl	2.2253(11)	Cl(1)–Fe–Cl(A)	120.29(7)
Fe–Cl(A)	2.2253(11)	Cl–Fe–N(1)	117.98(8)
Fe–N(1)	2.116(3)	Cl(1)–Fe–N(1A)	108.16(8)
Fe–N(1A)	2.116(3)	Cl(A)–Fe–N(1)	108.16(8)
N(1)–C(1)	1.293(4)	Cl(A)–Fe–N(1A)	117.98(8)
C(1)–C(1A)	1.507(7)	N(1)–Fe–N(1A)	76.71(16)

Complex **11** has crystallographic C_2 symmetry about an axis which bisects the C(1)–C(1A) bond and passes through the metal centre. The geometry at iron is distorted tetrahedral with inter-bond angles in the range 76.71(16)-120.29(7)°, with the acute angle associated with the bite of the *N,N'* ligand. The bonding within the essentially planar five-membered chelate ring shows a distinct pattern of bond ordering where the C=N linkages are shorter than the C–C bond (1.293(4) Å compared with 1.507(7) Å), indicating an absence of bond delocalisation. There are 2 disordered benzene molecules within the unit cell and this structure is unique

within those reported thus far as the chelate ring and the metal centre are almost coplanar. The torsion angle between the imine units is 0.6°, with the Fe atom sitting 0.5° above the C=N bonds. The aryl rings on the backbone are significantly twisted away from orthogonal; the torsion angle about the C(1)–C(Ph) bond is *ca.* 120°, potentially due to the lesser steric bulk of having an aryl group as the *N*-substituent.

The C=N bond lengths in **11** are similar to those in **7** or **9**; 1.293(4) Å *cf.* 1.284(4) Å for **7** and 1.269(5)-1.285(5) Å for **9**. The Fe–N bond lengths are significantly longer than those observed in the Cy derivative, **7**, but are similar to those of the ^{t}Bu substituted complex, **9**: 2.116(3) Å for **11**, 2.077(3) Å for **7** and 2.112(3)-2.130(3) Å for **9**. At 120.29(7)°, the Cl–Fe–Cl angle in **11** is somewhat distorted from ideal tetrahedral geometry; however, it is closer than the analogous Cy and ^{t}Bu substituted complexes (125.62(7)° and 122.11(5)° for **7** and **9**, respectively).

2.2.2 - Polymerisation data.

Compounds **7**-**12** were tested for the ATRP of styrene (200 equiv., bulk), under inert atmosphere at 120°C, using 1-phenylethyl chloride (1-PECl) as the initiator. To ensure meaningful, reproducible data was obtained, the polymerisations were carried out in a glovebox in order to minimise the degradation of the complexes. Samples were removed at the required times during the polymerisation, typically every 1-2 hours for the first 10 h, and these crude samples were analysed by ^{1}H NMR and GPC to give the conversion and molecular weight. Once polymerisation was complete, the crude polymer was dissolved in THF and precipitated into acidified MeOH to give the clean polymer used for end-group analysis.

2.2.2.1 - N-alkyl complexes 7-10.

The polymerisation of styrene under ATRP conditions (200 equiv., bulk, 120°C, 1-PECl) using ^{Cy,Ph}[*N*,*N*]$FeCl_2$, **7**, proceeds relatively slowly, with $k_{obs.}$ = 0.03 h^{-1} (Figure 2.10). The aldimine derivative, ^{Cy,H}[*N*,*N*]$FeCl_2$, is an efficient ATRP catalyst,[23,24] with an observed rate of 0.25 h^{-1} and molecular weights which increase linearly with conversion, agreeing well with theoretical molecular weights. However, a comparison of these data with that obtained for complex **7** indicates that substitution of a phenyl group at the 2,3 positions has switched the polymerisation mechanism towards CCT. Molecular weights are independent of conversion, and are typically around 3500 Da (Figure 2.11), while end group analysis by ^{1}H NMR shows

that the polymer is olefin-terminated (this will be discussed fully in a later section). PDIs were broad throughout the polymerisation, from 1.4 at low conversions to 2.3 at 90%.

$^{Cy,F\text{-}Ph}[N,N]FeCl_2$, complex **8**, showed similar behaviour to **7** in the ATRP of styrene, with the increase in electron-withdrawing capabilities of the *para*-fluorophenyl substituted ligand resulting in an even slower rate of polymerisation ($k_{obs.}$ = 0.02 h^{-1}, see Figure 2.10) and formation of polymer of lower molecular weight (Figure 2.11). The "top-out" molecular weight (where the M_n stopped increasing with conversion) was around 1800 Da and the PDIs were broad throughout (1.4-2.0), with end group analysis again showing that the polystyrene isolated was olefin-terminated only.

The linear semilogarithmic plots obtained from kinetic experiments using complexes **7** and **8** indicated that radical concentrations were constant throughout the polymerisation (Figure 2.10), but that the polymerisations were significantly slower than the aldimine derivative, $^{Cy,H}[N,N]FeCl_2$. When ATRP predominates, the polymerisation proceeds rapidly, but as CCT becomes more prevalent the rate decreases significantly.

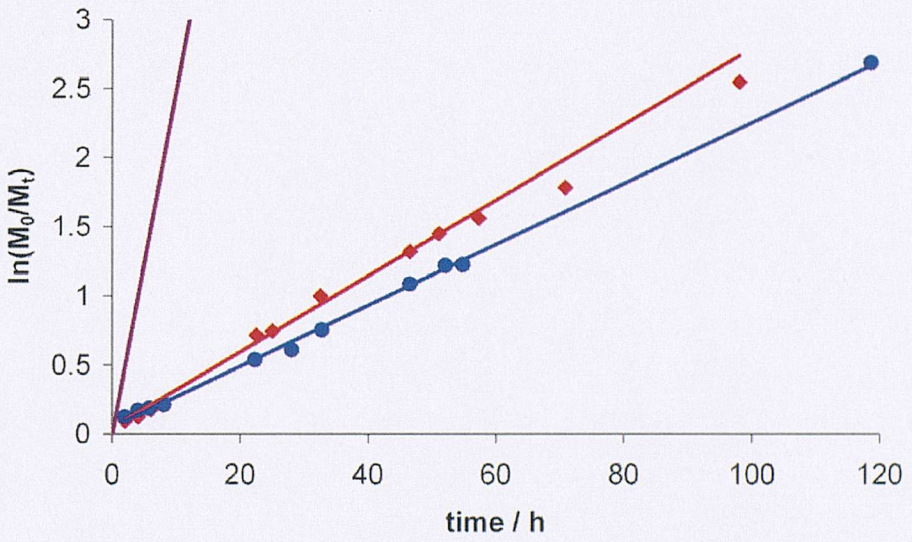


Figure 2.10 Rates for the bulk polymerisation of styrene (200 eq., 1-PECl, 120°C) by $^{Cy,R''}[N,N]FeCl_2$ complexes **7** and **8** (R″ = Ph, ◆; R″ = *p*-F-Ph, ●). $^{Cy,H}[N,N]FeCl_2$ ATRP rate (—) included for reference.[4]

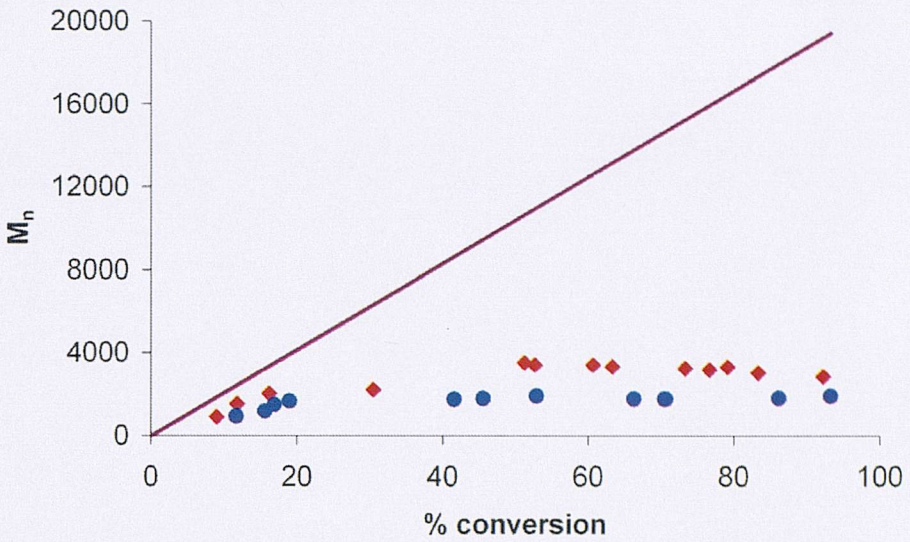


Figure 2.11 Molecular weight *versus* conversion for the bulk polymerisation of styrene (200 eq., 1-PECl, 120°C) by $^{Cy,R''}[N,N]FeCl_2$ complexes **7** and **8** (R″ = Ph, ◆; R″ = *p*-F-Ph, ●; $M_{n,th}$ = ▬).

The ^{t}Bu-substituted complexes, **9** and **10**, demonstrate similar behaviour to that discussed above for $^{Cy,Ph}[N,N]FeCl_2$ and $^{Cy,F\text{-}Ph}[N,N]FeCl_2$. Both catalysts exhibit slow kinetic behaviour for the polymerisation of styrene, and result in olefin-terminated polymer with molecular weights independent of conversion. PDIs are broad, typically ranging from 1.4-2.3 during the course of a polymerisation.

Using $^{tBu,Ph}[N,N]FeCl_2$, **9**, the polymerisation proceeded slowly, requiring 70 h to reach 80% conversion. The semilogarithmic plot of $\ln([M]_o/[M]_t)$ against time was linear up to 50% conversion indicating that the radical concentration was constant, with a pseudo-first order rate constant ($k_{obs.}$) of 0.013 h^{-1}. This is significantly slower than the rate constant of 0.19 h^{-1} reported for the aldimine derivative, substituted with protons on the backbone.[1] Molecular weights did not increase linearly with conversion and were much lower than theoretical (M_n = 1800-2000 Da), with extremely broad PDIs, typically ranging from 1.4-3.0. This catalyst appears to be sensitive to prolonged heating, as a colour change in the polymerisation solution after *ca.* 50 hours coincides with an increase in polymerisation rate (Figure 2.12). There is also an increase in molecular weight observed, from approximately 2000 to 2500 Da, although this is only particularly evident after 70 hours where the molecular weight approaches 5000 Da (Figure 2.13). These data are consistent with

decomposition of the catalyst, with some thermal polymerisation occurring as the number of active metal centres decreases.

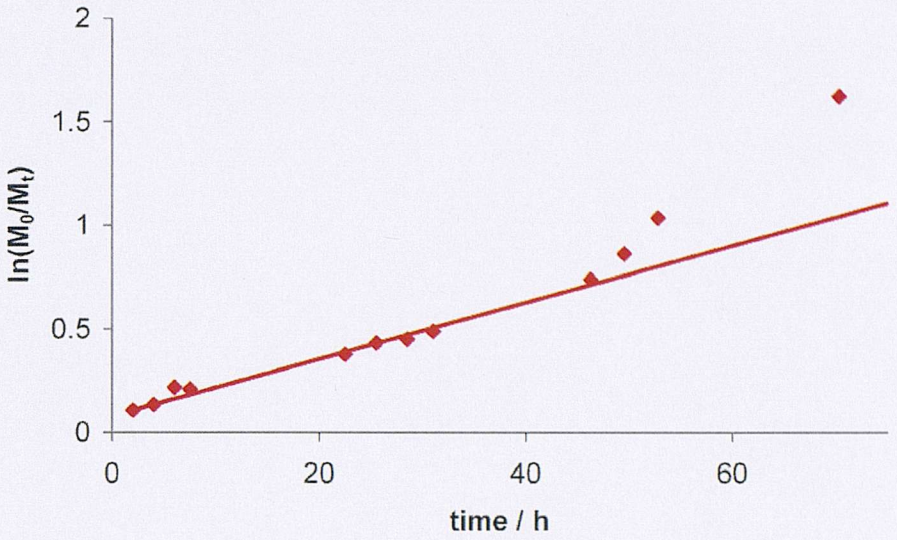


Figure 2.12 Rate for the bulk polymerisation of styrene (200 eq., 1-PECl, 120°C) by $^{tBu,Ph}[N,N]FeCl_2$, **9**.

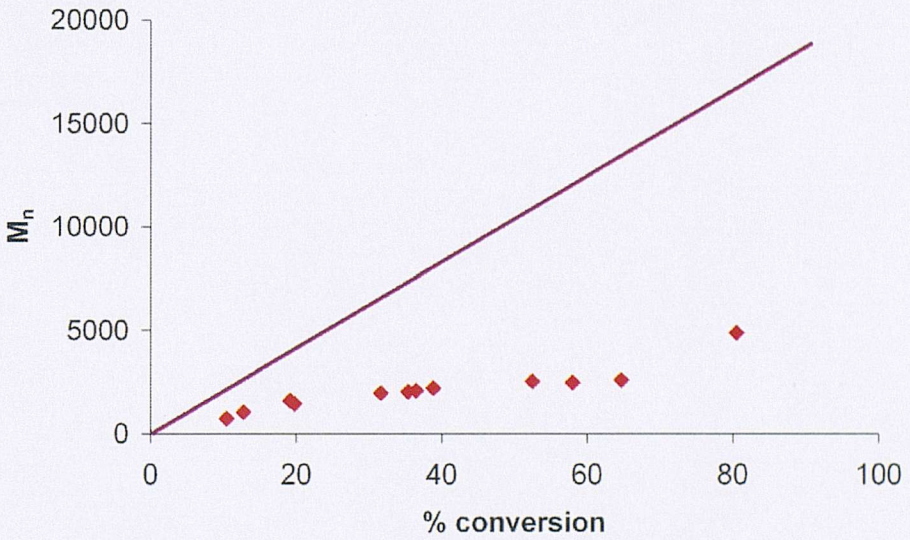


Figure 2.13 Molecular weight *versus* conversion for the bulk polymerisation of styrene (200 eq., 1-PECl, 120°C) by $^{tBu,Ph}[N,N]FeCl_2$, **9**. ($M_{n,th}$ = —).

Using the more electron-withdrawing substituent, $^{tBu,F\text{-}Ph}[N,N]FeCl_2$, **10**, again resulted in a decrease in the initial rate of polymerisation ($k_{obs.}$ = 0.008 h^{-1}) when compared to $^{tBu,Ph}[N,N]FeCl_2$, **9**. Molecular weights were independent of conversion, with the broad PDIs correlated to the CCT termination mechanism. Complex **10** also

shows evidence for the finite lifetime of the catalyst during the polymerisation, in both the kinetic and molecular weight plots. The slow polymerisation appears to reach a plateau at *ca.* 30% conversion, after 46 h. By 74 h the conversion has increased to 35%, and begins to rise sharply, deviating significantly from the initial polymerisation rate, until at 166 h the conversion has reached 91%. The effect is not observed in the molecular weight data until this final point, where the GPC trace shows a bimodal distribution, with a very high molecular weight component of 37,000 Da. Prior to this point, the M_n had remained relatively constant at 2000-2500 Da, throughout the polymerisation. This rapid increase in molecular weight is again consistent with catalyst decomposition (evidenced by a colour change from blue to yellow) and thermal polymerisation occurring as the catalyst dies. Figures 2.14 and 2.15 illustrate these points for complex **10**.

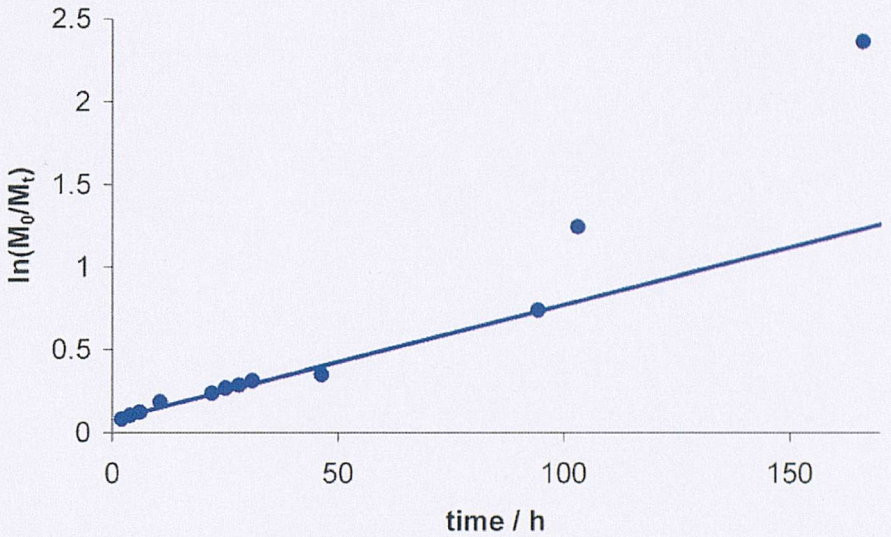


Figure 2.14 Rate for the bulk polymerisation of styrene (200 eq., 1-PECl, 120°C) by $^{tBu,F\text{-}Ph}[N,N]FeCl_2$, **10**.

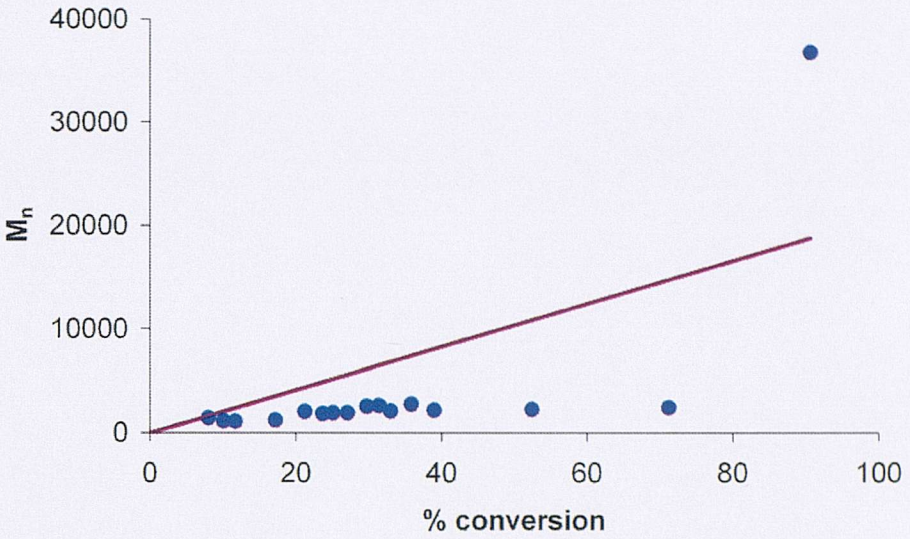


Figure 2.15 Molecular weight *versus* conversion for the bulk polymerisation of styrene (200 eq., 1-PECl, 120°C) by $^{tBu,F\text{-}Ph}[N,N]FeCl_2$, **10**. ($M_{n,th}$ = —).

It is interesting to note that while the $^{Cy,R''}[N,N]FeCl_2$ complexes **7** and **8** differ in both the rate of polymerisation and "top-out" molecular weight (illustrated in Figures 2.10 and 2.11), the analogous $^{tBu,R''}[N,N]FeCl_2$ complexes **9** and **10** only differ significantly in the rate of polymerisation (Figure 2.16). Polymerisation rates are extremely slow for both complexes **9** and **10**; significantly slower than the $k_{obs.}$ of 0.19 h^{-1} observed for the analogous aldimine complex, $^{tBu,H}[N,N]FeCl_2$. For both the Ph and F-Ph substituted complexes the "top-out" molecular weight is around 2000 Da, until decomposition of the catalyst occurs (Figure 2.17).

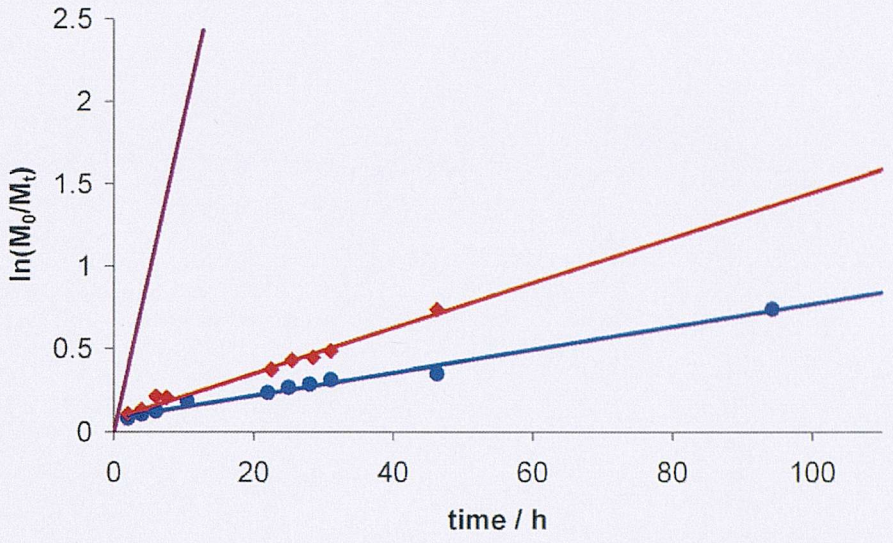


Figure 2.16 Rates for the bulk polymerisation of styrene (200 eq., 1-PECl, 120°C) by $^{tBu,R''}[N,N]FeCl_2$ complexes **9** and **10** (R″ = Ph, ◆; R″ = p-F-Ph, ●). $^{tBu,H}[N,N]FeCl_2$ rate (—) included for reference.[4]

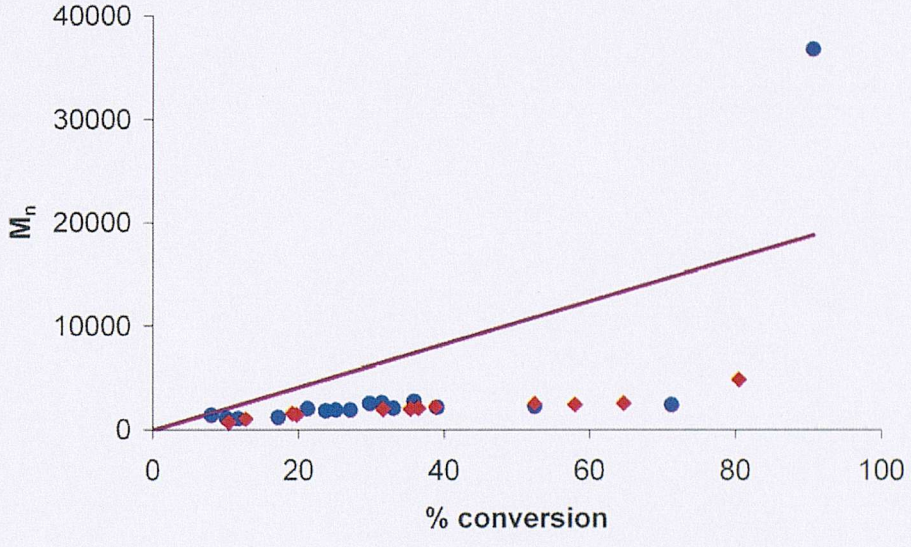


Figure 2.17 Molecular weight *versus* conversion for the bulk polymerisation of styrene (200 eq., 1-PECl, 120°C) by $^{tBu,R''}[N,N]FeCl_2$ complexes **9** and **10** (R″ = Ph, ◆; R″ = *p*-F-Ph, ●; $M_{n,th}$ = —).

2.2.2.2 - N-aryl complexes 11-12.

The *N*-aryl complex $^{Ph,Ph}[N,N]FeCl_2$, **11**, was tested under ATRP conditions for the polymerisation of styrene (200 equiv., 120°C, 1-PECl). The polymerisation proceeded relatively slowly, reaching only 50% conversion in 24 h ($k_{obs.}$ = 0.03 h^{-1}), and the polymer obtained was of low molecular weight with broad PDIs (1.4-2.1). Although the semilogarithmic plot of $ln([M]_o/[M]_t)$ against time approaches linear behaviour (Figure 2.18) the molecular weights of the polymer samples were much lower than theoretical (Figure 2.19), indicating that **11** is a CCT agent. The molecular weights obtained from polymerisations using complex **11** are lower and less variable than those obtained from the analogous complex with methyl groups on the backbone.[1,25] $^{Ph,Me}[N,N]FeCl_2$ catalyses faster styrene polymerisation (86% in 24 h, *cf.* 50% in 24 h for **11**) but the addition of electron-withdrawing phenyl rings to the backbone of the diimine ligand produces a more effective CCT catalyst.

The *para*-fluorophenyl substituted complex $^{Mes,F\text{-}Ph}[N,N]FeCl_2$, **12**, was also tested in styrene polymerisation. *N*-Mes is more electron-donating than *N*-Ph, and so a faster rate of polymerisation than **11** was expected. The related complex, $^{Mes,H}[N,N]FeCl_2$ reached 90% conversion in 24 h, with a non-linear semilogarithmic plot. Molecular weights were lower than theoretical, typically 4000-8000 Da, and PDIs were broad (1.7-2.2).[1] Complex **12** is a slower catalyst than $^{Mes,H}[N,N]FeCl_2$, requiring 48 h to reach 95% conversion ($k_{obs.}$ = 0.06 h^{-1}), but the linear semilogarithmic plot of $ln([M]_o/[M]_t)$ against time showed that the radical concentration remained constant throughout the polymerisation (Figure 2.18). Molecular weights were low throughout the polymerisation, ranging from 1300-3300 Da, and PDIs were broad (1.4-2.6). There was no evidence for chloro-end groups in the ^1H NMR spectra of the isolated polymer; only olefin end groups were observed.

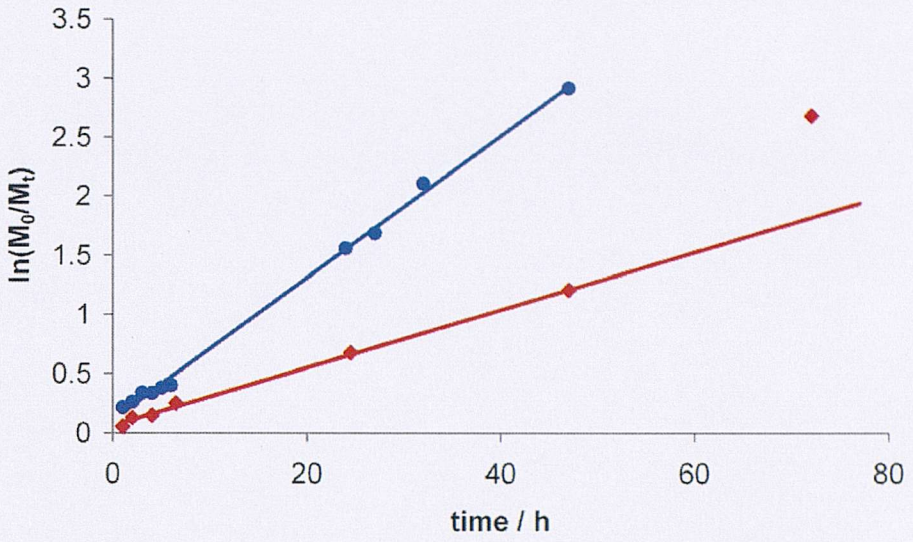


Figure 2.18 Rates for the bulk polymerisation of styrene (200 eq., 1-PECl, 120°C) by *N*-aryl complexes **11** and **12** (^{Ph,Ph}[*N*,*N*]$FeCl_2$, ◆; $^{Mes,F\text{-}Ph}$[*N*,*N*]$FeCl_2$, ●).

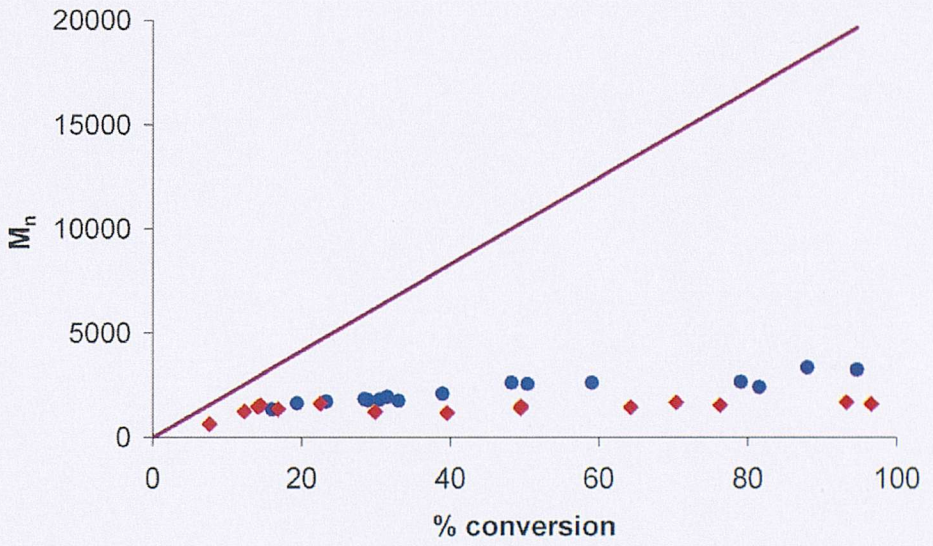


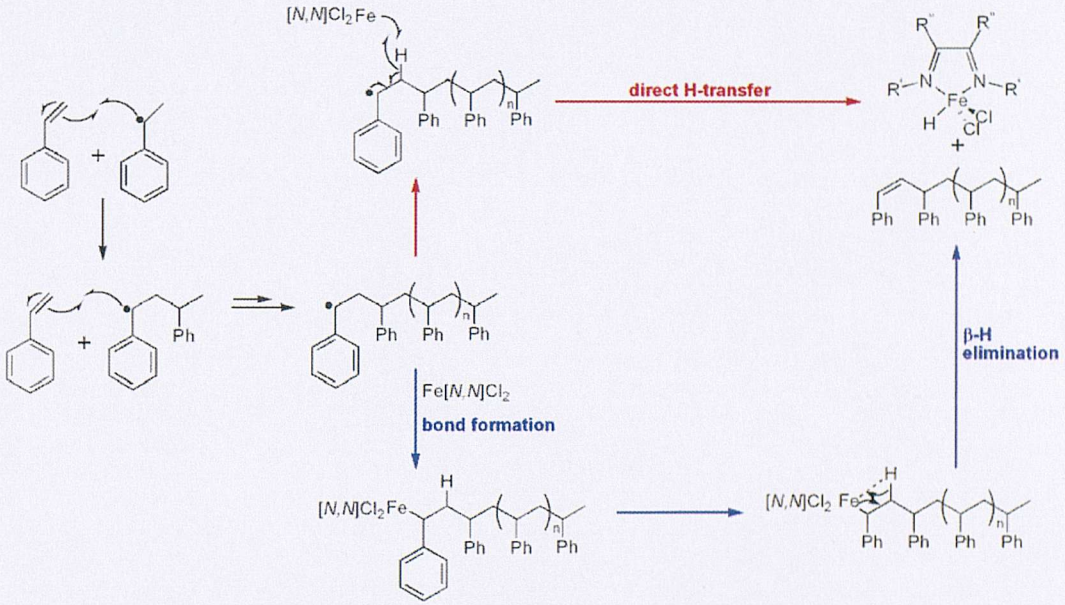
Figure 2.19 Molecular weight *versus* conversion for the bulk polymerisation of styrene (200 eq., 1-PECl, 120°C) by *N*-aryl complexes **11** and **12** (^{Ph,Ph}[*N*,*N*]$FeCl_2$, ◆; $^{Mes,F\text{-}Ph}$[*N*,*N*]$FeCl_2$, ●; $M_{n,th}$ = —).

The *N*-aryl complexes **11** and **12** reproduce the trends seen with the *N*-alkyl complexes. As the rate of polymerisation increases, so too does the "top-out" molecular weight. ^{Ph,Ph}[*N*,*N*]$FeCl_2$, **11**, is a slower catalyst than $^{Mes,F\text{-}Ph}$[*N*,*N*]$FeCl_2$, **12**, ($k_{obs.}$ = 0.03 h^{-1} for **11** *vs.* 0.06 h^{-1} for **12**) and the molecular weights are significantly lower (1200-1700 Da for **11** *vs.* 1400-3300 Da for **12**). The styrene

polymerisation data for complexes **7-12** and those in the literature[1,23] show that the ligand substituents at both the imine and backbone positions play an important role in determining the prevalent polymerisation mechanism. An electron-donating group as the *N*-substituent or at the 2,3-positions of the ligand backbone increases the rate of polymerisation. Inclusion of an electron-withdrawing group as the *N*-substituent or at the 2,3-positions increases the prevalence of CCT, slowing the polymerisation and resulting in polymer of lower molecular weight.

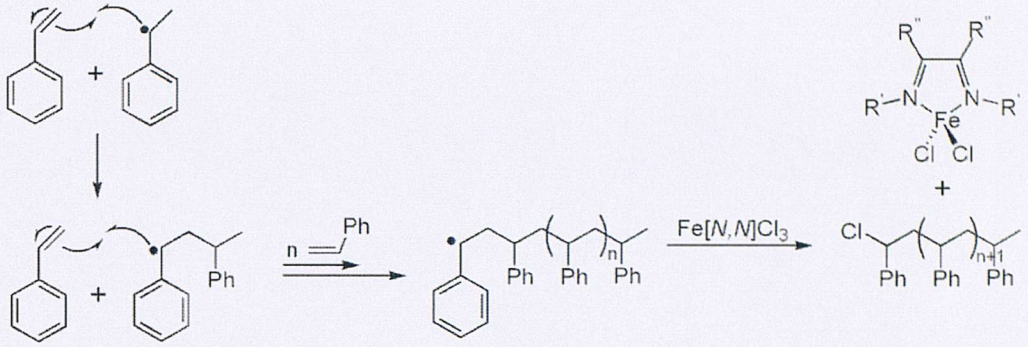
2.2.2.3 - End group analysis.

Formation of the low molecular weight polymers observed with the *N*-alkyl and *N*-aryl 2,3-substituted diimine CCT catalysts **7-12** is believed to occur in a manner analogous to that reported for the H-substituted *N*-aryl diimine catalysts[23,24,28] via formation of a metal-carbon bond, followed by β-hydrogen elimination (Scheme 2.4). It is also possible that the metal-hydride is formed through direct hydrogen abstraction. Differentiation between these two mechanistic pathways is a topic discussed in Chapter 4.



Scheme 2.4 Possible mechanisms for the formation of olefin-terminated polystyrene.

Polystyrene formed using complexes **7-12** showed no evidence for the chloro end groups (δ = 4.6 ppm) expected from an ATRP termination step (Scheme 2.5). Olefin signals at δ = 6.1-6.3 ppm, consistent with vinyl end groups, were clearly visible in the ^{1}H NMR spectra of the polymer samples obtained using complexes **7-12**.



Scheme 2.5 Mechanism for the formation of chloro-terminated polystyrene.

The lack of a broad resonance at 4.6 ppm in the ^{1}H NMR spectra of the polystyrene samples implies that the majority of the termination events occur through CCT. After initiation, radical propagation initially occurs through reaction of the styrene monomer with the radicals derived from the initiating species (1-PECl). The reaction of the propagating radical with the metal complex to form an olefin-terminated oligomer also generates a metal-hydride species (Scheme 2.4), which quickly reacts with a molecule of styrene to initiate a new propagating radical chain. This chain then enters the ATRP equilibrium until it reacts with the metal species, ultimately forming another olefin-terminated oligomer and new propagating chain. The potential chloro and olefin end groups, with characteristic ^{1}H NMR chemical shifts, for the polymer samples are shown in Figure 2.20.

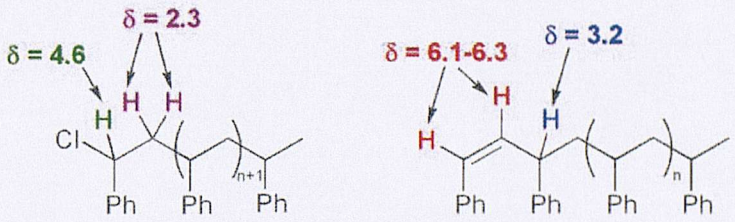


Figure 2.20 Structure of polystyrene samples obtained through ATRP and CCT.

In all cases, polymer samples from polymerisations using complexes **7-12** under ATRP conditions showed only olefin terminated signals in the ^{1}H NMR spectra. As a typical example, the ^{1}H NMR spectrum from polystyrene obtained using $^{Cy,Ph}[N,N]FeCl_2$, **7**, is shown in Figure 2.21. Correlation between the olefin peaks at δ = 6.1-6.2(**) ppm and the adjacent methine signal at 3.2(*) ppm was determined via COSY spectra (Figure 2.22).

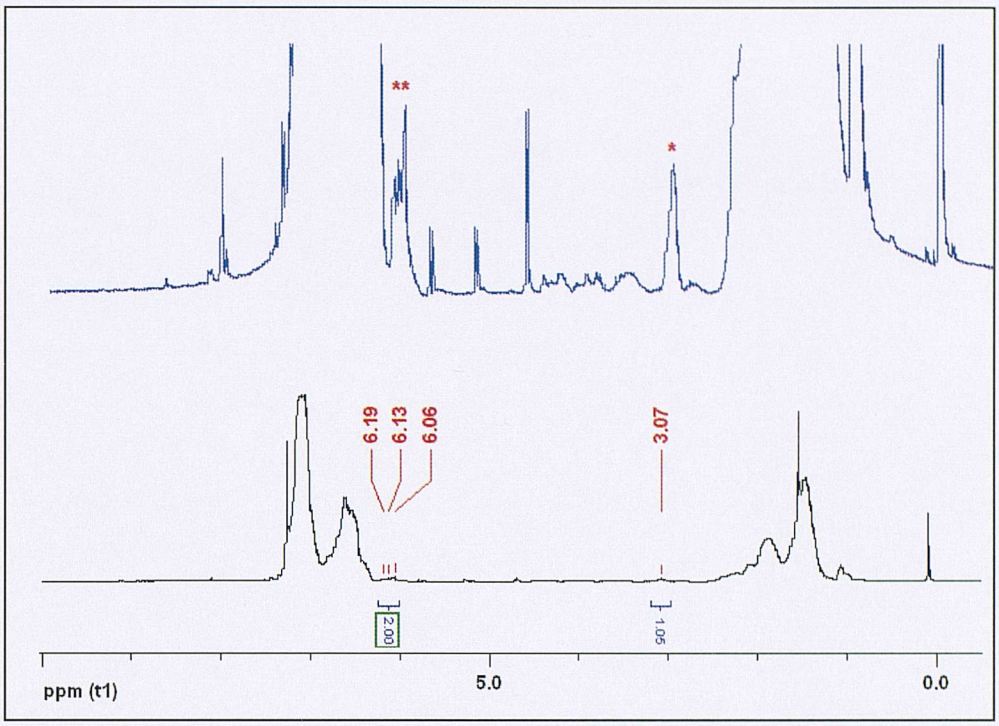


Figure 2.21 ^{1}H NMR of polystyrene formed using **7**, with expansion to show olefinic end-group signals.

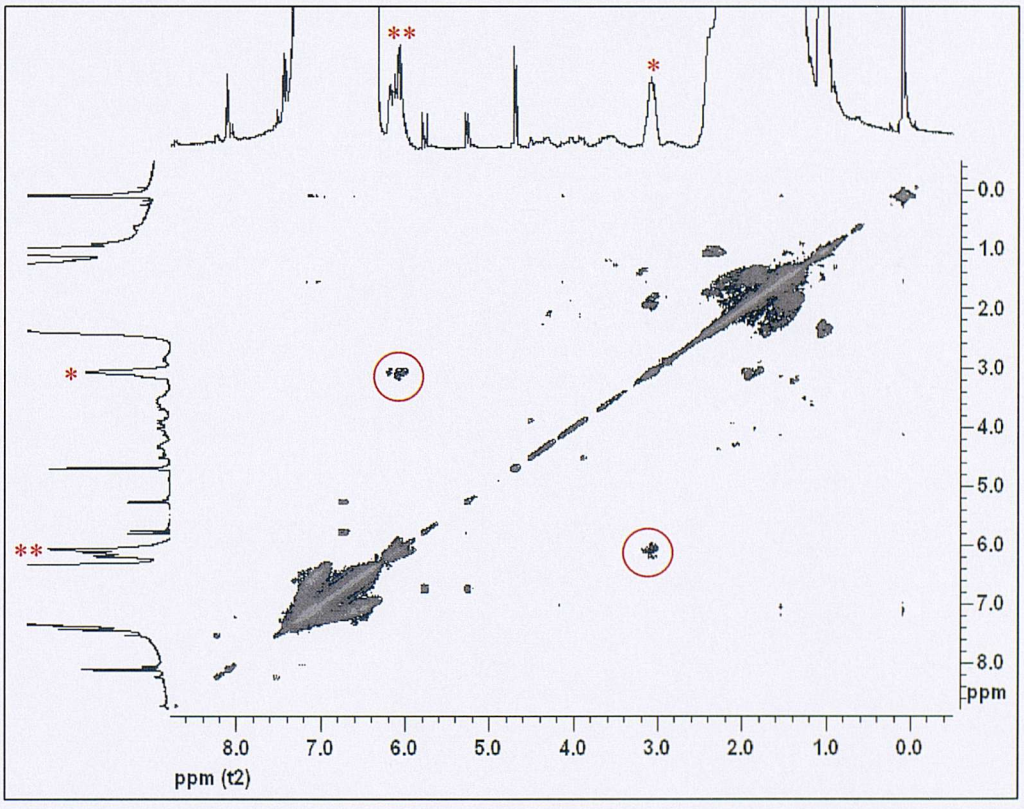


Figure 2.22 COSY spectrum of polystyrene showing olefin end groups obtained using **7**.

*2.2.2.4 - MMA polymerisation using N-alkyl complexes 7-**10**.*

1,1 Disubstituted olefins such as MMA readily undergo catalytic chain transfer, and there are many well-established CCT systems for acrylate monomers.[29-31] As discussed in Chapter 1, one of the most extensively studied CCT agents is bis(difluoroboryl)dimethylglyoximato cobalt (COBF). This is an extremely efficient CCT catalyst for the polymerisation of α-Me substituted monomers, with chain transfer rate coefficients of up to 3×10^7 $Lmol^{-1}s^{-1}$. However, greatly reduced chain transfer rate coefficients are obtained when using COBF for the polymerisation of styrene and acrylate monomers (9×10^5 $Lmol^{-1}s^{-1}$ for styrene and 7×10^5 $Lmol^{-1}s^{-1}$ for methyl acrylate).[32-37] There are two possible reasons given for the decrease in efficiency for the CCT polymerisation of monomers forming a secondary radical.[38,39] The absence of an α-methyl group means that H-abstraction must occur from the sterically and electronically unfavourable β-carbon. In addition, the formation of stable, reversible cobalt-carbon bonds with these monomers produces non-chain-transfer-active Co^{III}-R organometallic species. The decrease in chain transfer constants for monomers lacking an α-Me group is likely to be due to a combination of both of these mechanisms, with the size of the effect varying with the specific monomer.[40]

The α-diimine Fe catalysts may therefore be expected to be more efficient CCT catalysts for MMA polymerisation, when compared to styrene, as the H-abstraction step of CCT would be facilitated by the presence of the α-methyl group. However, MMA polymerisations under ATRP conditions (100 equiv., 10% w/w toluene, EBrB, 80°C) using the *N*-alkyl catalysts **7**-**10** revealed that these complexes were unsuitable catalysts for MMA. Molecular weights were higher than theoretical and PDIs were broad (typically 1.8-2.2). The polymerisations occurred relatively rapidly, consistent with the higher reactivity of the monomer, but the expected chain transfer reactions did not occur. This could be due to the bulkier nature of the propagating species. MMA is much more sterically hindered than styrene, and thus may be expected to undergo less facile β-H transfer (Scheme 2.4). This can be regarded as indirect evidence in support of the CCT mechanism in styrene polymerisation proceeding via bond formation and β-H elimination, rather than via direct H-transfer which is the widely accepted CCT mechanism for cobalt-based catalysts.

2.3 - Conclusions

This chapter has reported the synthesis and characterisation of a series of novel α-diimine Fe^{II} complexes containing electron-withdrawing phenyl and fluorophenyl groups at the 2,3-positions of the α-diimine backbone. Complexes with both electron-withdrawing *N*-aryl and electron-donating *N*-alkyl substituents have been prepared and the polymerisation behaviour of these complexes investigated.

Regardless of the *N*-substituent, complexes containing electron-withdrawing groups at the 2,3-positions of the α-diimine backbone result in styrene polymerisation terminated through CCT, with olefin-terminated polymer isolated in all cases. The presence of a more electron-withdrawing group, such as F-Ph, results in slower polymerisation rates and lower molecular weights. Conversely, including a potentially electron-donating group, such as *N*-Mes, increases the rate of polymerisation and the "top-out" molecular weight.

The $^{R',R''}[N,N]FeCl_2$ complexes reported in this chapter were unsuitable catalysts for the polymerisation of MMA, which resulted in uncontrolled reactions with molecular weights much higher than theoretical. This was proposed to be due to the bulkier nature of the tertiary propagating radical, which could hinder formation of the proposed organometallic intermediate and prevent β-H transfer.

Although the synthesis of new ligands and complexes has allowed trends to be observed in the styrene polymerisation behaviour of $^{R',R''}[N,N]FeCl_2$ complexes, the underlying reasons behind the switch in the polymerisation mechanism from ATRP to CCT remain to be identified. The synthesis of complexes containing electron-donating groups at the 2,3-positions of the ligand backbone and an assessment of their behaviour in styrene polymerisation is an obvious target. The synthesis of the analogous $^{R',R''}[N,N]FeCl_3$ complexes, in order to characterise all the components of the ATRP equilibrium, is also an important objective, and it is this which will be described in the following chapter.

2.4 - References

(1) O'Reilly, R. K. Synthesis of novel iron complexes and their use in atom transfer radical polymerisation. Ph.D. Thesis, University of London, 2003.

(2) Koten, G. v.; Vrieze, K., *Adv. Organomet. Chem.* **1982,** *21*, 157.

(3) Johnson, L. K.; Killian, C. M.; Brookhart, M., *J. Am. Chem. Soc.* **1995,** *117*, 6414.

(4) Feldman, J.; McLain, S. J.; Parthasarathy, A.; Marshall, W. J.; Calabrese, J. C.; Arthur, S. D., *Organometallics* **1997,** *16*, 1514.

(5) Tempel, D. J.; Johnson, L. K.; Huff, R. L.; White, P. S.; Brookhart, M., *J. Am. Chem. Soc.* **2000,** *122*, 6686.

(6) Lorber, C.; Choukroun, R.; Costes, J.-P.; Donnadieu, B., *C.R. Acad. Sci., Ser. IIc: Chim.* **2002,** *5*, 251.

(7) Gibson, V. C.; Tomov, A.; Wass, D. F.; White, A. J. P.; Williams, D. J., *J. Chem. Soc. Dalton Trans.* **2002**, 2261.

(8) Milione, S.; Cavallo, G.; Tedesco, C.; Grassi, A., *J. Chem. Soc. Dalton Trans.* **2002**, 1839.

(9) Fang, X.; Watkin, J. G.; Scott, B. L.; Kubas, G. J., *Organometallics* **2001,** *20*, 3351.

(10) Johansson, L.; Tilset, M.; Labinger, J. A.; Bercaw, J. E., *J. Am. Chem. Soc.* **2000,** *122*, 10846.

(11) Zhong, H. A.; Labinger, J. A.; Bercaw, J. E., *J. Am. Chem. Soc.* **2002,** *124*, 1378.

(12) Fang, X.-G.; Scott, B. L.; Watkin, J. G.; Kubas, G. J., *Organometallics* **2000,** *19*, 4193.

(13) Binotti, B.; Carfagna, C.; Zuccaccia, C.; Macchioni, A., *Chem. Commun.* **2005**, 92.

(14) Binotti, B.; Bellachioma, G.; Cardaci, G.; Carfagna, C.; Zuccaccia, C.; Macchioni, A., *Chem. Eur. J.* **2007,** *13*, 1570.

(15) Stoffelbach, F.; Poli, R.; Richard, P., *J. Organomet. Chem.* **2002,** *663*, 269.

(16) Matsuo, Y.; Mashima, K.; Tani, K., *Angew. Chem. Int. Ed.* **2001,** *40*, 960.

(17) tom Dieck, H.; Bruder, H., *J. Chem. Soc. Chem. Commun.* **1977**, 24.

(18) tom Dieck, H.; Stamp, L.; Diercks, R.; Muller, C., *New J. Chem.* **1985,** *9*, 289.

(19) Le Floch, P.; Knoch, F.; Kremer, F.; Mathey, F.; Scholz, J.; Scholz, W.; Theile, K.-H.; Zenneck, U., *Eur. J. Inorg. Chem.* **1998**, 119.

(20) Small, B. L.; Rios, R.; Fernandez, E. R.; Carney, M. J., *Organometallics* **2007,** *26*, 1744.

(21) Bart, S. C.; Hawrelak, E. J.; Lobkovsky, E.; Chirik, P. J., *Organometallics* **2005,** *24*, 5518.

(22) Wass, D. F. PhD Thesis, University of London, 1999.

(23) Gibson, V. C.; O'Reilly, R. K.; Reed, W.; Wass, D.; White, A. J. P.; Williams, D. J., *Chem. Commun.* **2002**, 1850.

(24) Gibson, V. C.; O'Reilly, R. K.; Wass, D. F.; White, A. J. P.; Williams, D. J., *Macromolecules* **2003,** *36*, 2591.

(25) O'Reilly, R. K.; Shaver, M. P.; White, A. J. P.; Gibson, V. C., *Macromolecules* **2007,** *40*, 7441.

(26) Kimpe, N. D.; D'Hondt, L.; Stanoeva, E., *Tetrahedron Lett.* **1991,** *32*, 3879.

(27) Helldorfer, M.; Backhaus, J.; Alt, H. G., *Inorg. Chim. Acta* **2003,** *351*, 34.

(28) O'Reilly, R. K.; Gibson, V. C.; White, A. J. P.; Williams, D. J., *Polyhedron* **2004,** *23*, 2921.

(29) Enikolopyan, N. S.; Smirnov, B. R.; Ponomarev, G. V.; Bel'govskii, I. M., *J. Polym. Sci., Polym. Chem. Ed.* **1981,** *19*, 879.

(30) Burczyk, A. F.; O'Driscoll, K. F.; Rempel, G. L., *J. Polym. Sci., Polym. Chem. Ed.* **1984,** *22*, 3255.

(31) Davis, T. P.; Haddleton, D. M.; Richards, S. N., *J. Macromol. Sci., Polym. Rev.* **1994,** *243*, C34.

(32) Suddaby, K. G.; Maloney, D. R.; Haddleton, D. M., *Macromolecules* **1997,** *30*, 702.

(33) Kukulj, D.; Davis, T. P., *Macromol. Chem. Phys.* **1998,** *199*, 1697.

(34) Heuts, J. P. A.; Forster, D. J.; Davis, T. P., *Macromolecules* **1999,** *32*, 3907.

(35) Pierik, B.; Masclee, D.; Herk, A. v., *Macromol. Symp.* **2001,** *165*, 19.

(36) Gridnev, A.; Ittel, D. S., *Chem. Rev.* **2001,** *101*, 3611.

(37) Roberts, G. E.; Heuts, J. P. A.; Davis, T. P., *Macromolecules* **2000,** *33*, 7765.

(38) Gridnev, A. A.; Belgovskii, I. M.; Enikolopyan, N. S., *Dokl. Akad. Nauk.* **1986,** *289*, 1408.

(39) Heuts, J. P. A.; Forster, D. J.; Davis, T. P., *Macromolecules* **1999,** *32*, 2511.

(40) Roberts, G. E.; Heuts, J. P. A.; Davis, T. P., *J. Polym. Sci. A: Polym. Chem.* **2003,** *41*, 752.

Chapter 3

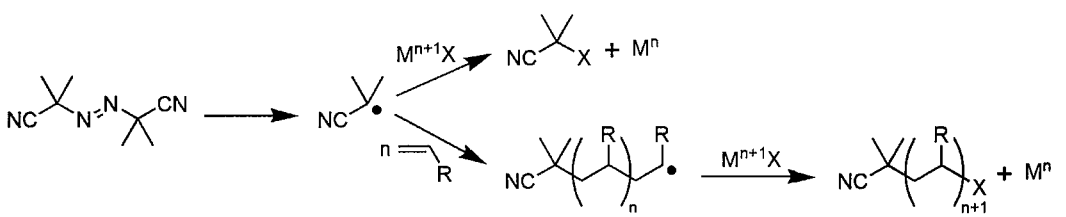
Synthesis and Characterisation of Fe^{III} α-Diimine Complexes: Correlation between Metal Spin-State and Polymerisation Mechanism

3.1 - Introduction

Atom transfer radical polymerisation proceeds through the reversible activation/deactivation of radicals, mediated by a redox-active transition metal species. Deactivation of the radicals occurs through reaction of the propagating chain with the metal complex in its higher oxidation state, and understanding the nature of the oxidised species in the ATRP system is therefore of great importance. Early work reported by Matyjaszewski *et al* used Cu^{II} halides to control the AIBN-initiated living polymerisation of styrene via the 'reverse ATRP' mechanism.[1,2]

Reverse ATRP exploits a metal complex in its higher oxidation state and a conventional radical initiator, such as AIBN, to form polymers with well-controlled molecular weights and narrow molecular weight distributions.[3] Azo-based initiators are the most commonly utilised,[1,3,4] but the use of peroxides[5,6] and sulfur-based thermal iniferters[7,8] has also been reported.

The initiation step involves the thermal decomposition of the initiator (AIBN in Scheme 3.1), and the newly formed radical may then react with the monomer to form a growing radical chain, or with the catalyst to form a reduced metal complex and an alkyl halide species (Scheme 3.1). This combination allows conventional ATRP to take place, with the *in situ* generation of the alkyl halide avoiding problems associated with adding a halide initiator, such as slow or multifunctional initiation, high cost and toxicity. The polymers obtained are α-functionalised by a nitrile group, and ω-functionalised by a halide, and so can be used as the initiating species in subsequent ATRP polymerisations to form block copolymers.



Scheme 3.1 Reverse ATRP mechanism.

Reverse ATRP using Cu^{II} systems has been employed to polymerise a variety of monomers, including MMA,[4,9] BMA,[10] MA[4,11] and styrene.[1,2,5] Simultaneous reverse and normal ATRP using $CuBr_2$/Me_6TREN, in the presence of both AIBN and an alkyl halide, was used for the controlled polymerisation of acrylates which were too reactive to polymerise through ATRP. Decomposition of AIBN was slow at the

reaction temperature of 60°C, resulting in a high concentration of $CuBr_2$ which enabled efficient deactivation of the propagating chains. The contribution of AIBN-initiated chains to the average-number molecular weights was negligible, meaning that the theoretical molecular weights were best calculated through the catalyst to alkyl halide ratio.[9]

The low toxicity and cost of iron has led to significant investigation into reverse ATRP using Fe-based systems. One of the most commonly employed systems is based on $FeCl_3$ and PPh_3, which gave good control over the molecular weights and narrow PDIs in the polymerisation of both styrene[12] and MMA.[3,8] $FeBr_3$ has been used in conjunction with bulky organic counter-ions, such as tetrabutylammonium and tetrabutylphosphonium, for the reverse ATRP of MMA and MA but was unsuccessful for styrene.[13] More complicated systems used $FeCl_3$ and acidic ligands such as pyromellitic or picolinic acids for the polymerisation of MMA.[14,15]

Relevant to the work presented in this thesis, the Fe^{III} complexes of a selection of α-diimine ligands were synthesised and screened as catalysts in the polymerisation of styrene and MMA by reverse ATRP (Figure 3.1).[16] Complexes **I** and **II** were efficient catalysts for reverse ATRP, giving reasonable molecular weight control, moderate PDIs (1.3-1.5) and halogen-terminated polymers. The polymerisation rates were significantly slower than those observed for the Fe^{II} analogues (e.g. $k_{obs.}$ = 0.08 h^{-1} for styrene polymerised by reverse ATRP and **I**, *cf.* 0.25 h^{-1} for normal ATRP) which was attributed to the lower polymerisation temperature of 110°C (*cf.* 120°C in ATRP). However, complexes **III** and **IV** (the *N*-aryl diimines) were poor catalysts for reverse ATRP, with non-linear kinetics and molecular weights which were independent of conversion. The polymer obtained was olefin-terminated and polymerisation was proposed to occur via CCT, in a manner analogous to that observed with the corresponding *N*-aryl Fe^{II} complexes.

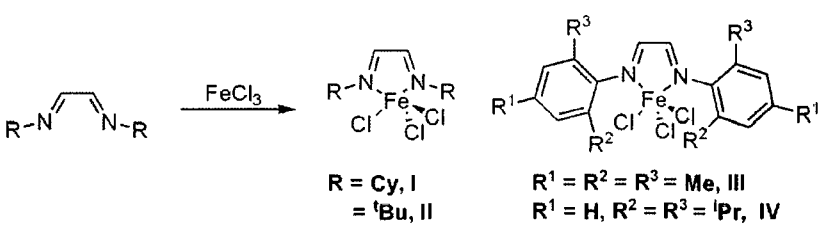


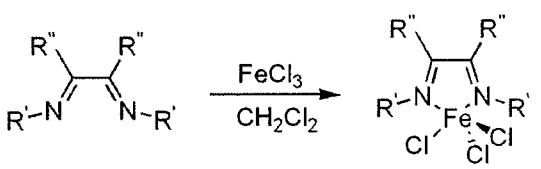
Figure 3.1 α-Diimine Fe^{III} complexes previously synthesised and tested as reverse ATRP catalysts.

The prevalent polymerisation mechanism is not just dependent on the imino *N*-donor atoms, where electron-donating groups favour ATRP and electron-withdrawing groups favour CCT. The previous chapter described the synthesis and polymerisation behaviour of α-diimine Fe^{II} complexes retaining the *N*-alkyl ATRP-directing substituents, but containing electron-withdrawing substituents at the 2,3-positions of the α-diimine ligand backbone. These complexes catalyse styrene polymerisation terminated through CCT, similar to the *N*-aryl complexes. The rest of this chapter details the synthesis and characterisation of the analogous α-diimine Fe^{III} complexes, exploring the effect of substituting electron-withdrawing groups into the 2,3-positions of the diimine backbone.

3.2 - Results and Discussion

3.2.1 - Synthesis of Fe^{III} compounds.

In an effort to characterise all components of the ATRP system, the Fe^{III} analogues of complexes **7-12** were targeted. α-Diimine complexes of the type $^{R',R''}[N,N]FeCl_3$ (where R′ = Cy, ^{t}Bu, Ph and Mes, and R″ = H, Ph or F-Ph) were prepared by treatment of the appropriate α-diimine ligand with $FeCl_3$ (Scheme 3.2). Careful control over the reaction conditions was required to ensure the desired products were obtained in high purity as the resulting complexes were light, air and moisture sensitive, and prone to disproportionation reactions.



	R′	R″
13	Cy	Ph
14	Cy	F-Ph
15	^{t}Bu	H
16	^{t}Bu	Ph
17	^{t}Bu	F-Ph
18	Ph	Ph
19	Mes	F-Ph

Scheme 3.2 Synthesis of Fe^{III} α-diimine complexes.

Complex **15** has been previously reported[16] and is the Fe^{III} analogue of the efficient ATRP catalyst $^{tBu,H}[N,N]FeCl_2$. Synthesis of this complex using the modified procedure adopted for the other Fe^{III} complexes allowed a benchmark to be set, and comparisons made with a known ATRP catalyst. Complexes **13-19** do not give meaningful ^{1}H NMR spectra. The magnetic moments for the 2,3-aryl-substituted derivatives, **13**, **14** and **16-19**, were measured at room temperature in $CDCl_3/CH_2Cl_2$

using the Evans' NMR method,[17] and were found to be in the range 3.9-4.3 B.M., consistent with d^5-intermediate spin Fe^{III} centres. Complex **15**, $^{tBu,H}[N,N]FeCl_3$ had a magnetic moment of 5.9 B.M., consistent with a d^5-high spin Fe^{III} centre (spin only = 5.97 B.M.). This difference in spin-state correlates with the switch in polymerisation mechanism: high spin species catalyse ATRP, whereas intermediate spin species give rise to olefin-terminated polymer via CCT.

In order to confirm that the magnetic moments observed in the room temperature Evans' NMR measurements were consistent with the spin-state present under polymerisation conditions (120°C), variable temperature Evans' NMR experiments were carried out. As shown in Figure 3.2 for $^{Cy,F\text{-}Ph}[N,N]FeCl_3$, **14**, there are only small variations in the measured magnetic moment of a toluene solution (CH_2Cl_2 reference). On closer inspection, there are two transition points which correspond to the changes in phase of the two solvents. At around 50°C there is an increase in the $\mu_{eff.}$ value, from 4.17 to 4.26 B.M., as the CH_2Cl_2 reaches its boiling point and the density of the solution changes. Similarly, the measurement taken at 120°C shows an increase from 4.29 B.M. to 4.37 B.M., correlating to the boiling point of toluene. Thus, the magnetic moment does not alter significantly upon increasing the temperature to that of the polymerisation run.

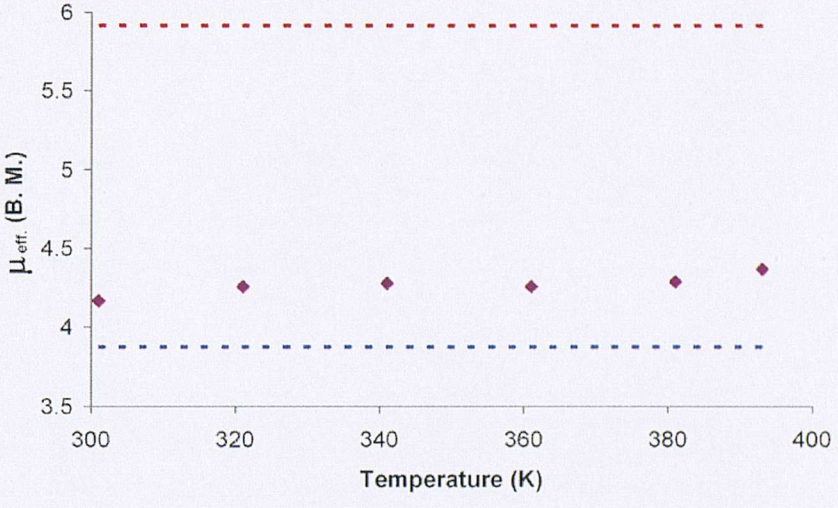


Figure 3.2 Variable temperature Evans' measurements for $^{Cy,F\text{-}Ph}[N,N]FeCl_3$, **14**, showing expected spin-only values for both an intermediate spin and a high spin complex. (Measurements used d_8-toluene and CH_2Cl_2 as the solvent mixture.)

3.2.1.1 - X-ray structure of ^{tBu,H}[N,N]FeCl$_3$, 15.

X-ray structures of L_nFeCl_3 species are surprisingly rare; there are only a few examples of crystallographically characterised 5-coordinate iron trichloride complexes incorporating nitrogen donors.[18,19] Crystals of **15** suitable for X-ray analysis were obtained through slow evaporation of a solution of ^{tBu,H}[*N,N*]FeCl$_3$ in $CDCl_3$ / cyclohexane (95:5 v/v) and comprised two crystallographically independent C_s symmetric molecules; molecule **I** is shown in Figure 3.3. The two molecules have essentially identical geometries (Table 3.1), and the r.m.s. fit of the non-hydrogen atoms is *ca.* 0.05 Å. The only substantial difference between the two molecules lies in the Cl(2)–Fe–Cl(2A) bond angle, which is *ca.* 5° larger in molecule **I**. The mirror plane contains the iron centre, the two imine units and Cl(1). The geometry at the iron is distorted trigonal bipyramidal, with Cl(1) and N(2) in the axial positions; the metal lies *ca.* 0.23 Å out of the equatorial {N(1),Cl(2),Cl(2A)} plane. For both the chlorines and the nitrogens it is noticeable that the axial bonds: Fe–Cl(1) 2.285(3) Å, Fe–N(2) 2.243(7) Å, are longer than their equatorial counterparts: Fe–Cl(2) 2.2053(19) Å, Fe–N(1) 2.145(6) Å.

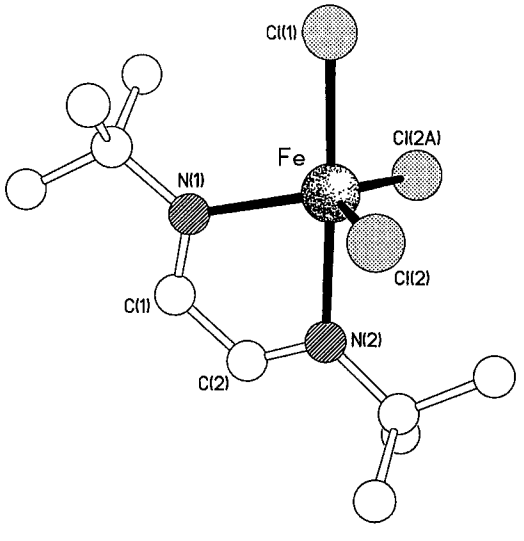


Figure 3.3 The molecular structure of one (**I**) of the two crystallographically independent C_S-symmetric complexes present in the crystals of **15**.

Table 3.1 Selected bond lengths (Å) and angles (°) for the two crystallographically independent C_S-symmetric complexes (**I** and **II**) present in the crystals of **15**.

	Mol I	**Mol II**		**Mol I**	**Mol II**
Fe–Cl(1)	2.285(3)	2.294(3)	Cl(1)–Fe–Cl(2)	94.13(6)	94.68(7)
Fe–Cl(2)	2.2053(19)	2.2109(19)	Cl(1)–Fe–Cl(2A)	94.13(6)	94.68(7)
Fe–Cl(2A)	2.2053(19)	2.2109(19)	Cl(2)–Fe–Cl(2A)	127.08(14)	122.69(13)
Fe–N(1)	2.145(6)	2.141(6)	Cl(1)–Fe–N(1)	100.65(19)	98.7(2)
Fe–N(2)	2.243(7)	2.275(7)	Cl(2)–Fe–N(1)	114.76(7)	117.06(7)
N(1)–C(1)	1.272(10)	1.276(9)	N(1)–Fe–Cl(2A)	114.76(7)	117.06(7)
C(1)–C(2)	1.455(12)	1.456(12)	Cl(1)–Fe–N(2)	177.83(19)	176.4(2)
N(2)–C(2)	1.247(9)	1.265(9)	Cl(2)–Fe–N(2)	86.82(10)	87.03(11)
			N(2)–Fe–Cl(2A)	86.82(10)	87.03(11)
			N(1)–Fe–N(2)	77.2(2)	77.7(2)

3.2.1.2 - Attempted X-ray structure determination of other Fe^{III} derivatives.

The intermediate spin complexes **13**, **14** and **16-19** could not be characterised crystallographically, despite repeated efforts to grow crystals. Attempts to crystallise the dark purple complex $^{tBu,F\text{-}Ph}[N,N]FeCl_3$, **17**, resulted in the formation of red crystals, where two molecules of $^{tBu,F\text{-}Ph}[N,N]FeCl_3$ had disproportionated to form $^{tBu,F\text{-}Ph}[N,N]FeCl_2$, $FeCl_4^-$ and $^{tBu,F\text{-}Ph}[N,N]H^+$, **17a**.

The X-ray structure of crystals of **17a** (Figure 3.4, Table 3.2) revealed the $FeCl_2$ complex, a protonated, cationic free ligand and an $FeCl_4^-$ anion; the picture also shows one orientation of the disordered, 50% occupancy included benzene solvent molecule. The geometry at Fe(1) is distorted tetrahedral with *cis* angles in the range 79.62(17)-121.04(12)°, with the most acute angle associated with the bite of the *N,N'* chelate ligand; this bite angle is in good agreement with that in the previously crystallised complex $^{tBu,F\text{-}Ph}[N,N]FeCl_2$, **10** (79.39(13)°). The Fe(1) centre sits *ca.* 0.31 Å out of the diimine plane (which is coplanar to within *ca.* 0.07 Å), *cf.* 0.62 Å in **10**. The 5-membered chelate ring in **17a** is best described as having an envelope conformation with N(1) lying *ca.* 0.28 Å out of the {Fe(1),N(2),C(1),C(2)} plane, which is coplanar to within *ca.* 0.02 Å. The two fluorophenyl rings are twisted slightly away from orthogonal, the C(1)–Ar and C(2)–Ar torsional angles are *ca.* 83

and 80° respectively. The orientation of these two rings are also considerably affected by the folding of the 5-membered chelate ring such that F(10) lies *ca.* 1.78 Å below, and F(20) *ca.* 0.56 Å above, the {Fe(1),N(2),C(1),C(2)} plane. The C–C bond between the two imine units (1.545(7) Å) is in good agreement with that in **10** (1.521(6) Å). The protonated free ligand also has a similar C–C bond length between the two imines (1.543(7) Å), although the planarity of the diimine units (coplanar to within *ca.* 0.01 Å) means that F(40) and F(50) are both less than *ca.* 0.05 Å out of this plane. The fluorophenyl rings are again oriented almost orthogonally to the diimine plane, with C(31)–Ar and C(32)–Ar torsion angles of *ca.* 87 and 77° respectively.

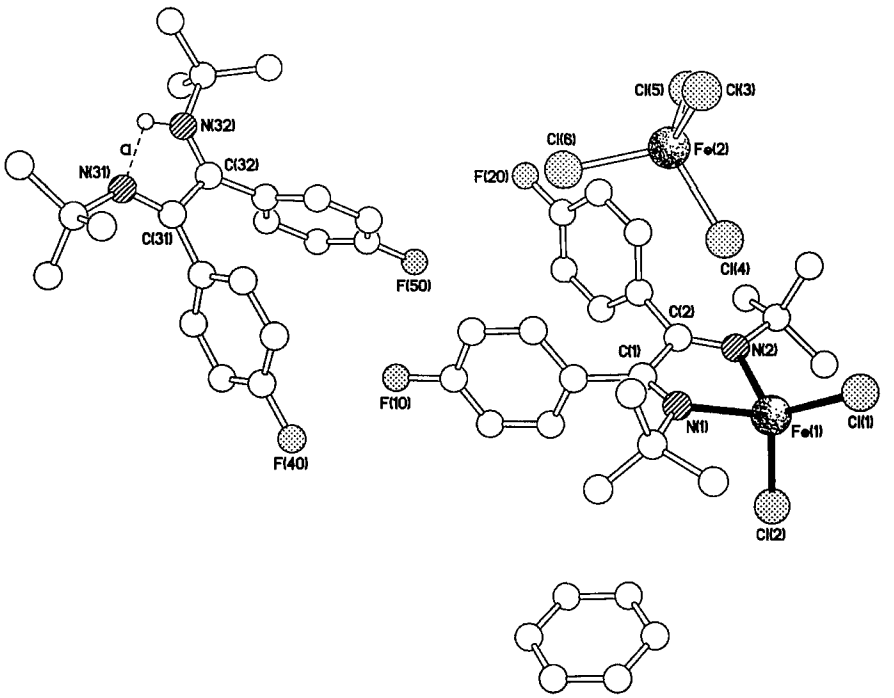


Figure 3.4 The molecular structure of the contents of the asymmetric unit in the crystals of **17a**. The N–H···N hydrogen bond (**a**) has N···N 2.568(6) Å, H···N 2.09 Å and N–H···N 113°.

Table 3.2 Selected bond lengths (Å) and angles (°) for **17a**.

	Fe^{II} complex		**Free ligand**		
Fe(1)–Cl(1)	2.2436(15)			Cl(1)–Fe(1)–Cl(2)	116.35(6)
Fe(1)–Cl(2)	2.2502(16)			Cl(1)–Fe(1)–N(1)	121.04(12)
Fe(1)–N(1)	2.100(4)			Cl(2)–Fe(1)–N(1)	105.43(11)
Fe(1)–N(2)	2.101(4)			Cl(1)–Fe(1)–N(2)	119.16(12)
N(1)–C(1)	1.276(6)	N(31)–C(31)	1.266(5)	Cl(2)–Fe(1)–N(2)	109.36(11)
C(1)–C(2)	1.545(7)	C(31)–C(32)	1.543(7)	N(1)–Fe(1)–N(2)	79.62(17)
N(2)–C(2)	1.273(6)	N(32)–C(32)	1.274(6)	N–H···N	113
		N···N	2.568(6)		
		H···N	2.09		

Attempts to crystallise $^{tBu,Ph}[N,N]FeCl_3$, **16**, from a variety of solvents yielded a yellow-green compound, **16a**, which X-ray structure determination showed to be an ionic compound consisting of the protonated ligand with $FeCl_4^-$ (Figure 3.5, Table 3.3). Red crystals isolated from toluene proved to be the partially decomposed disproportionation product, **16b** (Figure 3.6, Table 3.3), similar to that seen in **17a**.

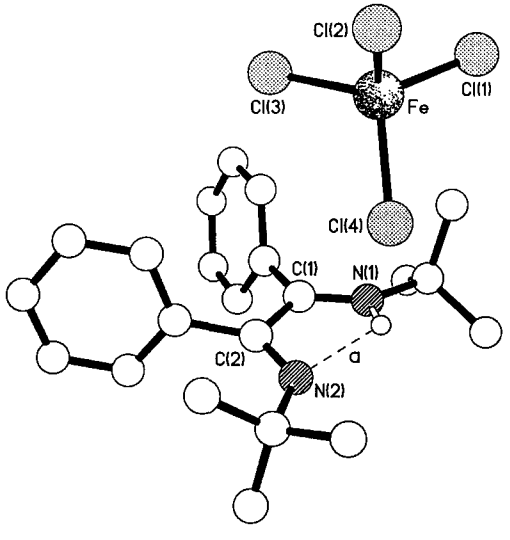


Figure 3.5 The molecular structure of **16a**.

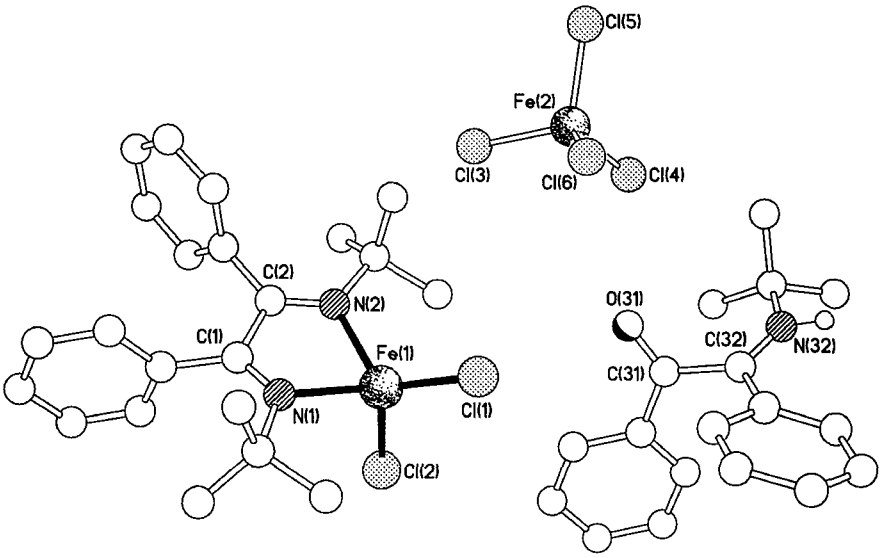


Figure 3.6 The molecular structure of the contents of the asymmetric unit in the crystals of **16b**.

Table 3.3 Selected bond lengths (Å) and angles (°) for **16a** and **16b**.

	16a		**16b**		
		Fe(1)–Cl(1)	2.2348(7)	Cl(1)–Fe(1)–Cl(2)	117.13(3)
		Fe(1)–Cl(2)	2.2971(6)	Cl(1)–Fe(1)–N(2)	122.29(5)
		Fe(1)–N(1)	2.1046(16)	Cl(2)–Fe(1)–N(2)	105.16(5)
		Fe(1)–N(2)	2.0970(18)	Cl(1)–Fe(1)–N(1)	122.29(5)
N(1)–C(1)	1.274(3)	N(1)–C(1)	1.287(3)	Cl(2)–Fe(1)–N(1)	103.64(5)
C(1)–C(2)	1.531(3)	C(1)–C(2)	1.527(2)	N(1)–Fe(1)–N(2)	79.46(6)
N(2)–C(2)	1.261(3)	N(2)–C(2)	1.285(2)		
N···N	2.558(2)	C(31)-C(32)	1.526(3)	N–H···N	116
H···N	2.03	N(32)–C(32)	1.295(3)		
		O(31)–C(31)	1.217(3)		

The geometry at Fe(1) is distorted tetrahedral with *cis* angles in the range 79.46(17)-122.29(5)°, with the most acute angle associated with the bite of the *N,N'* chelate ligand; this bite angle is similar to that seen in **17a** (79.62(17)) and the previously crystallised complex $^{tBu,Ph}[N,N]FeCl_2$, **9** (78.45(12)). Similar to the situation in **9**, the N=C–C=N unit is not planar and there is a torsion angle of *ca.* 16° between the imine units (*cf.* 14° in **9**).

The Cl–Fe–Cl angle is again less distorted away from ideal tetrahedral, when compared to the structure of the previously crystallised $^{tBu,Ph}[N,N]FeCl_2$ as it is 117.13(3)° (*c.f.* 122.11(2)° in **9**). The C–C bond between the two imine units in **16b** (1.527(2) Å) is similar to that seen in **9** (1.532(6) Å) and also in the free ligand **16a** (1.531(3) Å), and is almost identical to the analogous C–C bond length in the ketimine species of **16b** (1.526(3) Å).

All attempts to this date to crystallise the intermediate spin complexes resulted in the isolation of decomposition or disproportionation products. The unstable nature of the Fe^{III} trichloride complexes leads to rapid decomposition, with colour changes in solution notable after just 24 h. The reaction products show evidence for the generation of chlorine radicals, and the lower spin-state is envisaged to facilitate homolytic cleavage of the Fe-Cl bonds in the S = 3/2 Fe^{III} complexes. This would form a chlorine radical plus the corresponding Fe^{II} compound. Abstraction of a hydrogen radical by $Cl^{\bullet}$ would form HCl, which is a likely source of Cl^-. Attack of the chloride anion on another iron trichloride complex would lead to the formation of the $FeCl_4^-$ species. The free H^+ would be attacked by nucleophiles present in the solution, including the basic imino groups of the α-diimine ligand.

There are very few analogous 5-coordinate, *N*-ligated $FeCl_3$ crystal structures in the literature, with $FeCl_4^-$ disproportionation products commonly observed.[20,21] No examples of iron^{III} chloride α-diimine structures have been previously reported in the literature and, excepting the 5-coordinate L_2FeCl_3 complexes mentioned earlier,[18,19] the most closely related structures are octahedral; those of phenanthroline and terpyridine iron trichloride.[22,23] The synthesis of compounds with the empirical formula $Fe(phen)Cl_3$ has been reported several times over the past 40 years but the correct composition of the compounds isolated proved elusive and several formulae were proposed.[24-26] In 1977 the crystal structure of $[Fe(phen)_2Cl_2][FeCl_4]$ was published, with crystals isolated from an acetone/ether mixture.[27] More than 20 years later, the crystal structure of $Fe(phen)Cl_3(H_2O)$, crystallised from a water/MeOH mixture,[22] was published and it is likely that the solvent plays an important role in facilitating the crystallisation of these species.

Good yields were reported for the synthesis of terpyridine $FeCl_3$ complexes and a crystal structure of $Fe(terpy)Cl_3$ was published, with no mention of undesirable side reactions.[23] This may be attributed to the greater stability of 6-coordinate octahedral

complexes of tridentate *N*-donor ligands and $FeCl_3$, further evidenced by the iron trichloride complexes of ligands such as bis(imino)pyridine and bis(benzimidazol)pyridine.[28,29]

3.2.2 - The magnetic behaviour of 14 and 15.

In order to further explore the correlation of Fe^{III} spin-state with polymerisation mechanism, representative high spin and intermediate spin complexes were studied by electron paramagnetic resonance (EPR), superconducting quantum interference device (SQUID) magnetometry and Mössbauer spectroscopy. The good reliability of the synthetic procedure for $^{Cy,F\text{-}Ph}[N,N]FeCl_3$, **14**, and the availability of the crystal structure for $^{tBu,H}[N,N]FeCl_3$, **15**, led us to select these S = 3/2 and S = 5/2 complexes for detailed magnetic characterisation.

3.2.2.1 - Solution and solid state EPR spectroscopy studies.

Electron paramagnetic resonance spectroscopy is used to probe the environment of unpaired electrons within the system and is comparable to the NMR spectroscopy of diamagnetic compounds. Application of a magnetic field splits the ground electronic state into a series of closely spaced levels; the spacing is dependent upon the strength of the applied field. The magnetic moments of the unpaired electrons interact with the applied magnetic field, which causes this splitting of the m_S degeneracy (Zeeman effect). Application of a microwave field can result in an inversion of the electronic spin, which is observed and recorded by the EPR spectrometer. Transitions between states can be observed, according to the EPR spectroscopy selection rule, $\Delta M_S = \pm 1$.

The energy difference between the states is given by $\Delta E = h\nu = g\beta B$, where β is a constant (the electronic Bohr magneton), B is the applied field and g is characteristic of the sample, independent of both ν and B (*cf.* chemical shift in NMR). Energy gaps are typically in the microwave region for typical laboratory magnetic fields, but as microwaves are difficult to tune, the frequency is kept constant and the magnetic field is swept (complementary to NMR spectroscopy where the applied magnetic field is constant but the frequency is variable). Results are recorded as the first derivative of the absorption spectrum (Zeeman modulation) and as sensitivity increases with frequency, the amount of sample required is typically very small.[30,31]

With more than 1 unpaired electron, the quantum number, S, correlates with 2S+1 M_S states, which may be expected to remain degenerate in the absence of a magnetic field (i.e. M_S, M_{S-1},...–M_S are the same energy). However, spin-orbit coupling from electronic excited states can separate these M_S states. This is known as the *zero field splitting* (ZFS) and is dependent on sample specifics, such as the structure of the molecule, the extent of the spin-orbit coupling, etc. Applying a magnetic field removes any remaining degeneracy and transitions between states, obeying the $\Delta M_S = \pm 1$ selection rule, may be observed. In principle there are 2S transitions, with their separations representing the magnitude of the zero field splitting, and it is the electron configuration, the ZFS and the magnetic-field range which determines whether any or all of these transitions will be observed. If the ZFS is very large then systems with an even number of unpaired electrons will have no resonances within the observable range, whereas those with an odd number of unpaired electrons will show only a single resonance, corresponding to the $m_S = -1/2 \rightarrow +1/2$ transition.[30,31]

Samples for EPR were prepared in a glovebox, using freshly synthesised complexes and rigorously dried and degassed solvents. The EPR tubes were loaded under inert atmosphere and sealed into glass tubes for transport to the EPSRC EPR centre in Manchester. Solution samples were transported in liquid nitrogen, to prevent any decomposition. Data were collected by Dr. Joanna Wolowska, on Bruker ESP300E and Bruker Elexsys E600 spectrometers, using a Bruker ER6706KT (K-band) resonator. Magnetic fields and microwave frequencies at K-band were measured with an ER035M NMR gaussmeter and an EIP model 588C microwave pulse counter, respectively.

The K-band, variable temperature, solid state powder spectra of both $^{Cy,F\text{-}Ph}[N,N]FeCl_3$, **14**, and $^{tBu,H}[N,N]FeCl_3$, **15**, had very broad features, typical of solid state Fe. With complex **14**, initially only the g = 2 peak was visible but as the temperature was decreased a broadening of this peak was observed (most noticeably at 10 K). At 5 K, this was resolved into a further peak and the spin-forbidden half-field ($\Delta M_S = \pm 2$) transition was also clearly visible (Figure 3.7). The spectra obtained for complex **15** were also extremely broad, but remained unchanged as the temperature was decreased from room temperature to 5 K (Figure 3.8).

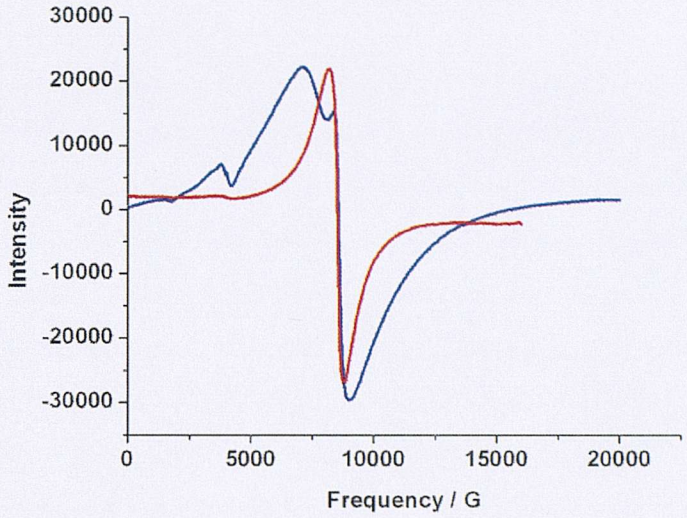


Figure 3.7 Solid state EPR spectra for $^{Cy,F\text{-}Ph}[N,N]FeCl_3$, **14**, 5 K (—) and 293 K (—) at 25 GHz.

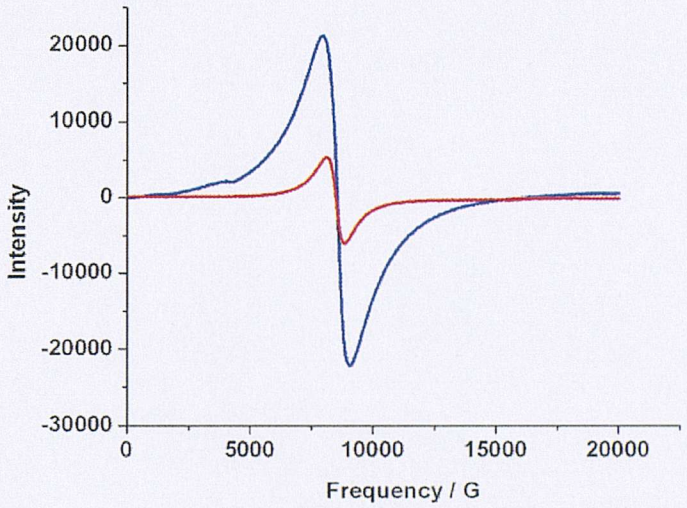


Figure 3.8 Solid state EPR spectra for $^{tBu,H}[N,N]FeCl_3$, **15**, 5 K (—) and 293 K (—) at 25 GHz.

Solution EPR often gives more information about the electronic environment of the molecule. Samples are more dilute, providing a better chance of observing fine structure as the paramagnetic centres are further apart. Cooling the sample is also

advantageous as it can further increase sensitivity by slowing down the relaxation processes, resulting in narrower lines.

The frozen solution EPR spectra of **14** and **15** were run using 5-10 mg of complex dissolved in DCM / toluene (5%). However, there were still 'glassing' problems from the freezing process, resulting in noise and artefacts in the spectra. The frozen solution EPR spectra of **14** at 4 K (where the most features appeared) and 50 K (a typical higher temperature spectrum) are shown in Figure 3.9. There are more features seen than in the powder spectrum, but unfortunately most of them are due to electronic interference and instability. The same is true for the $^{tBu,H}[N,N]FeCl_3$ frozen solution spectra - again there are more features observed than in the powder spectrum, but most are extraneous (Figure 3.10). More dilute samples of each compound were also run but no further fine structure was resolved. Both solid and frozen solution samples of **14** and **15** were also run at W-band (94 GHz) to see whether more detail could be observed at higher frequency, but the spectra were essentially identical in form to those collected at K-band.

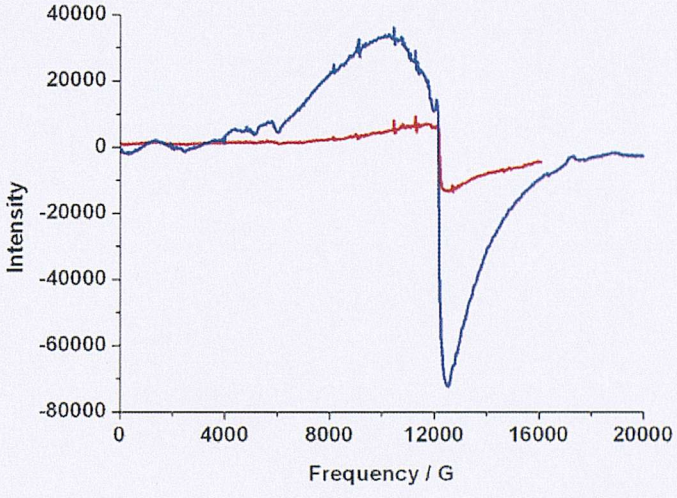


Figure 3.9 Solution state EPR spectra for $^{Cy,F\text{-}Ph}[N,N]FeCl_3$, **14**, 4 K (—) and 50 K (—) at 25 GHz.

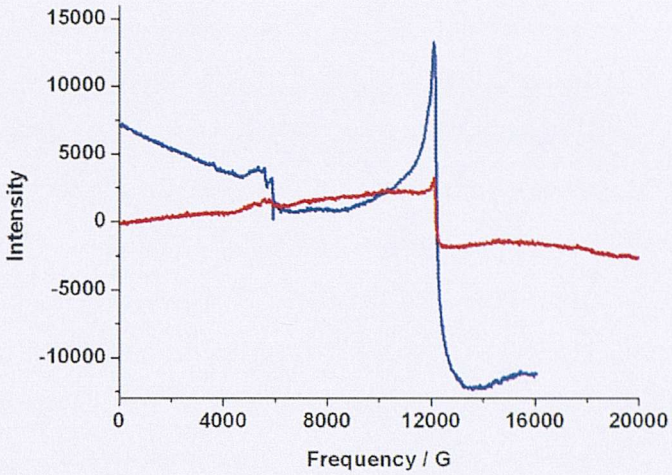


Figure 3.10 Solution state EPR spectra for $^{tBu,H}[N,N]FeCl_3$, **15**, 5 K (—) and 50 K (—) at 25 GHz.

The appearance of the frozen solution spectra for **15** is different to that of **14**, raising hopes that they would be interpretable as different Fe^{III} spin-states. Unfortunately, neither the powder nor the frozen solution spectra could be fitted to a particular spin-state (through simulation programs) due to the poor resolution. It is likely that a large ZFS for complexes **14** and **15** resulted in only the $m_S = -1/2 \rightarrow +1/2$ transition being observed. Therefore, both sets of spectra are indicative of $S > 1/2$, but are not conclusive for either $S = 3/2$ or $S = 5/2$.

3.2.2.2 - SQUID magnetometry studies.

Five-coordinate $iron^{III}$ complexes can exist in the discrete spin-states $S = 5/2$, high spin, $S = 3/2$, intermediate spin, or $S = 1/2$, low spin. There may also be a thermal spin equilibrium between two of these spin-states and/or quantum mechanical mixing of spin-states.[32] In the case of a thermal spin equilibrium system the molecules have two magnetically distinguishable pure spin-states. Some $iron^{III}$ porphyrinates exhibit the spin crossover phenomenon, caused by stimuli such as temperature, pressure or photoirradiation.[33] The most extensively studied spin crossover is that between low ($S = 1/2$) and high ($S = 5/2$) spin-states.[34-37] Spin crossover between low and intermediate ($S = 1/2$, $S = 3/2$) spin-states,[38] and high and intermediate ($S = 5/2$, $S = 3/2$) spin-states[39] are extremely rare.

A spin admixed system contains one single magnetic species whose magnetic properties differ from those corresponding to either of the pure spin-states. Admixing will only occur if the energy separation between the unperturbed, pure spin-states is comparable to, or less than, the spin-orbit coupling constant.[40] Spin admixed systems are of particular interest because of the observation that some bacterial haem proteins display 'anomalous' magnetic and spectral properties, which were interpreted as resulting from spin-mixing (S = 3/2, 5/2), via spin-orbit coupling, between the $^4A_2$ and $^6A_1$ states in a tetragonal d^5 system.[40,41] Spin admixtures have been observed in a number of Fe^{III} porphyrins[33,42-44] and phthalocyanines[45] with square-pyramidal or octahedral geometry, and also in a recently published $[Fe(C_6Cl_5)_4]^-$ square-planar system.[46] The trigonal bipyramidal amidodiphosphino Fe^{III} halide complexes, $FeX_2[N(SiMe_2CH_2PPh_2)_2]$ where X = Br, Cl, were also reported to exhibit unusual magnetic behaviour, consistent with an S = 5/2, S = 3/2 spin admixture.[47]

While high and low spin Fe^{III} complexes are more common, intermediate spin-states (S = 3/2) have been observed in some distorted square-pyramidal[48-50] and trigonal bipyramidal[51,52] Fe^{III} complexes. A number of Fe^{III} porphyrin complexes have also been reported to exist in a relatively pure S = 3/2 spin-state,[38,43,53-55] where weak-field ligands tend to favour the intermediate spin-state whilst stronger field ligands lead to an admixed regime. The occurrence of highly distorted geometries is the common structural feature connecting these systems, which have all been studied using EPR spectroscopy, SQUID magnetometry and Mössbauer spectroscopy.

Variable temperature (2-300 K) DC magnetic susceptibility measurements were carried out by Dr. Floriana Tuna on sealed samples, both polycrystalline and ground-up, of compounds **14** and **15**, using a Quantum Design MPMS-XL SQUID magnetometer equipped with a 7 T magnet. Isothermal magnetization data were collected at 2 and 4 K, with a magnetic field ranging from 1 to 7 T, and zero field cooled (ZFC) and field cooled (FC) magnetic experiments were carried out at different fields ranging from 10 G to 50 kG. Diamagnetic corrections for the compounds were estimated from Pascal's constants and magnetic data were corrected for diamagnetic contributions of the sample holder.

For all of the compounds studied, the sample preparation was extremely important. Using the standard gelatine capsules was unsuccessful, as the Fe^{III} complexes reacted with the SQUID capsule. Polycarbonate capsules were suitable, but unfortunately could not be sealed adequately, resulting in decomposition of the sample as it was

loaded into the magnetometer. A sealed glass tube allowed collection of data without decomposition, but there were concerns about the accuracy of the mass measurements, since a significant amount of the sample adhered to the walls of the tube. Finally, the custom-made, air-tight, teflon capsules designed and loaned by Prof. G. Cloke at Sussex allowed the collection of reliable data. Fresh samples of complexes **14** and **15** were prepared for each measurement and stored under inert atmosphere, away from light sources, before the capsules were loaded. They were then wrapped in tissue paper and sealed into a small round-bottomed flask before being removed from the glovebox and transported to Manchester for the SQUID measurements.

The variable temperature magnetic data for $^{tBu,H}[N,N]FeCl_3$, **15**, showed a smooth decrease in the molar susceptibility, χ_M, with an increase in temperature (Figure 3.11). These data are better represented by the $\chi_M T$ curve, shown in Figure 3.12.

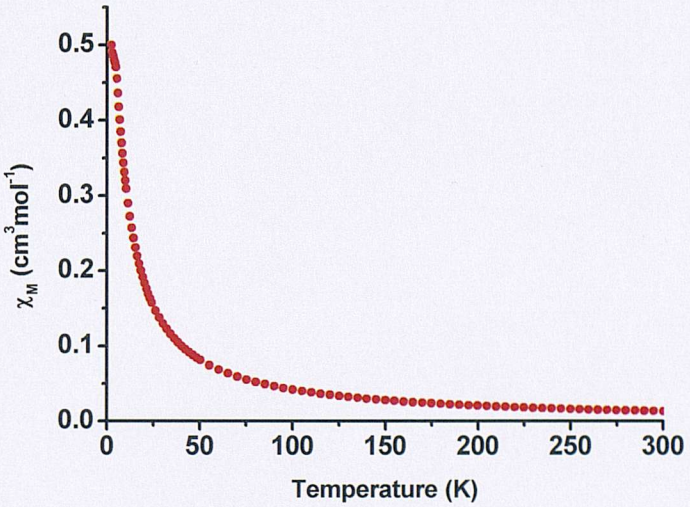


Figure 3.11 χ_M *vs.* temperature for $^{tBu,H}[N,N]FeCl_3$, **15**, at 10 kG.

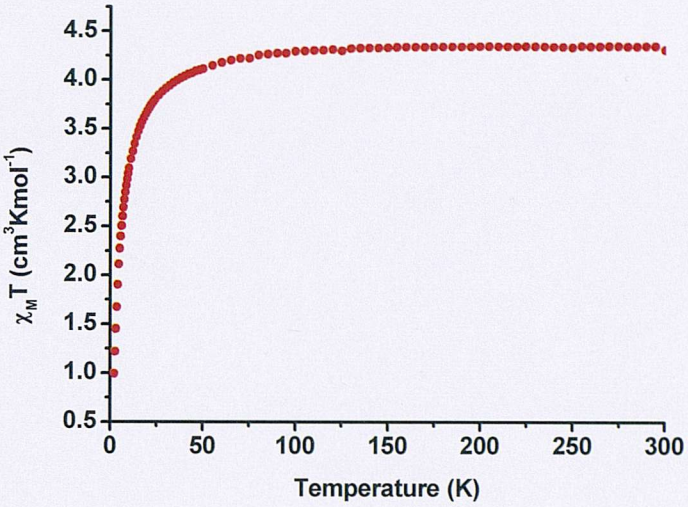


Figure 3.12 $\chi_M T$ *vs.* temperature for $^{tBu,H}[N,N]FeCl_3$, **15**, at 10 kG.

The room temperature $\chi_M T$ values for $^{tBu,H}[N,N]FeCl_3$, **15**, were around 4.35 cm^3Kmol^{-1}, very close to the spin-only value of 4.375 cm^3Kmol^{-1} expected for a high spin, S = 5/2, system (assuming g = 2). Upon cooling, $\chi_M T$ remained almost constant until 80 K and then decreased to 1.06 cm^3Kmol^{-1} at 2 K. This decrease is associated with both intermolecular antiferromagnetic interactions and zero field splitting.

The data were fitted using the Curie-Weiss law (χ = C/(T-θ)), and the Curie constant, C, was found to be 4.4 cm^3 $mol^{-1}K$. θ was found to be -3.25 K at 10 kG (Figure 3.13), and -4.50 K at 1 kG; its negative value suggests the presence of antiferromagnetic interactions.

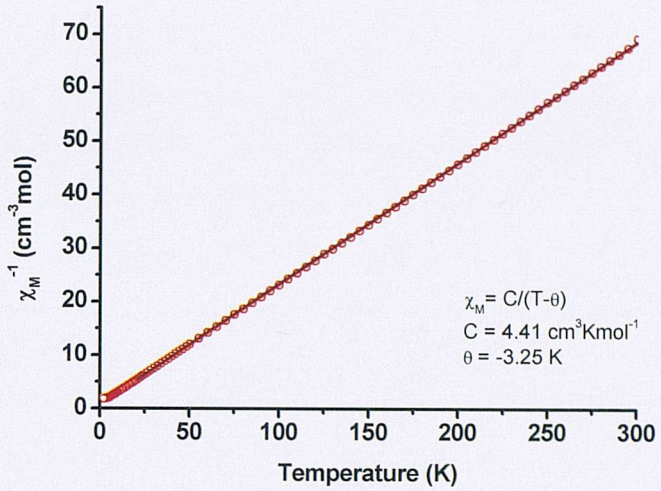


Figure 3.13 χ_M^{-1} *vs.* temperature for ^{tBu,H}[*N,N*]FeCl$_3$, **15**, at 10 kG, with fitting to the Curie-Weiss law.

The magnetic moment of complex **15** is typical of a high spin d^5 Fe^{III} complex, and $\mu_{eff.}$ does not vary significantly until about 100 K (Figure 3.14). The expected spin-only magnetic moment for a complex with 5 unpaired electrons is 5.92 B.M., which agrees very well with the measured $\mu_{eff.}$ for **15** (5.90 B.M. at 300 K).

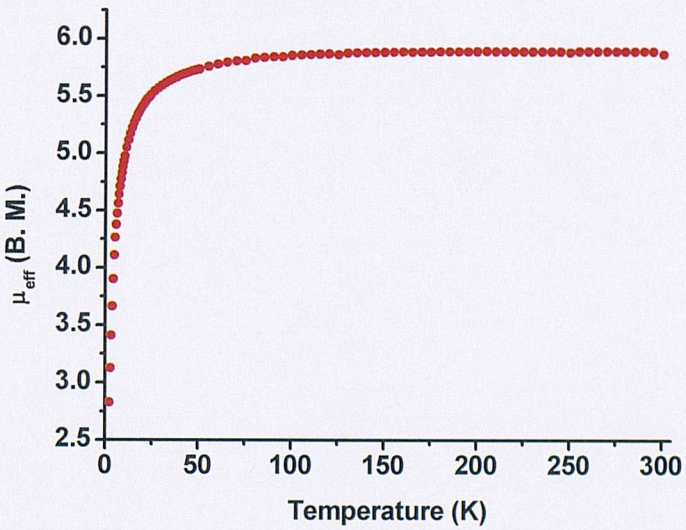


Figure 3.14 $\mu_{eff.}$ *vs.* temperature for ^{tBu,H}[*N,N*]FeCl$_3$, **15**, at 10 kG.

At very low temperatures, unusual magnetic behaviour is observed and a hysteresis curve is present in the χ_M *vs.* T curve. Zero-field cooled magnetism

measurements are different from field cooled measurements, indicating that the sample behaves differently in warming and cooling regimes (Figure 3.15), and suggesting a magnetic phase transition, possibly due to a crystallographic phase transition. As the transition is time dependent, the conversion was monitored by recording data at 2 minute intervals under identical conditions (50 G magnetic field and 2.4 K temperature), Figure 3.16.

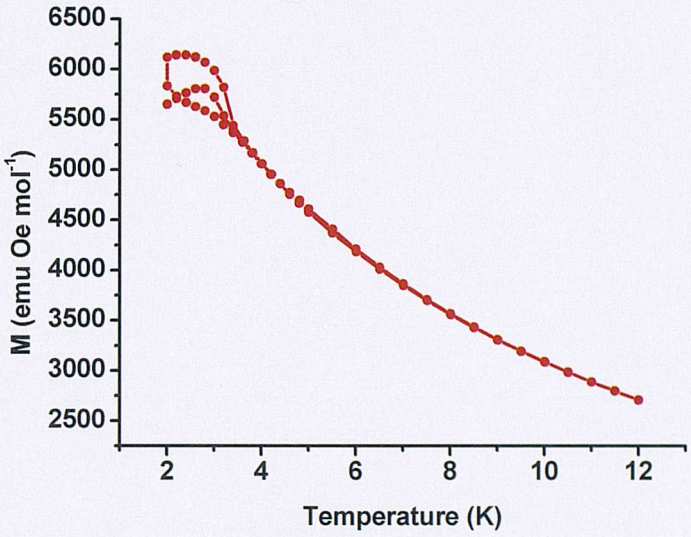


Figure 3.15 Magnetisation *vs.* temperature for $^{tBu,H}[N,N]FeCl_3$, **15**, at 10 kG, FC and ZFC.

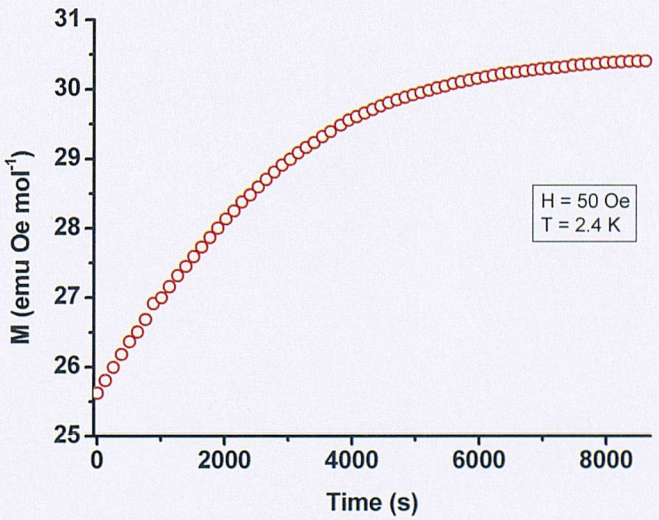


Figure 3.16 Magnetisation *vs.* time for $^{tBu,H}[N,N]FeCl_3$, **15**, at 50 G and 2.4 K.

Similar experiments were carried out on $^{Cy,F\text{-}Ph}[N,N]FeCl_3$, **14**. The room temperature $\chi_M T$ value was 2.95 cm^3Kmol^{-1} which is significantly higher than the 1.875 cm^3Kmol^{-1} expected for an intermediate spin, S = 3/2 complex. However, the orbital contribution can significantly increase this value up to 2.6-2.7 cm^3Kmol^{-1}, and it is appreciably lower than the room temperature $\chi_M T$ product expected for a high spin system (4.35 cm^3Kmol^{-1}, see Figure 3.12). In the cooling regime, $\chi_M T$ remains almost constant until 30 K, before decreasing sharply to 1.21 cm^3Kmol^{-1} at 2 K (Figure 3.18).

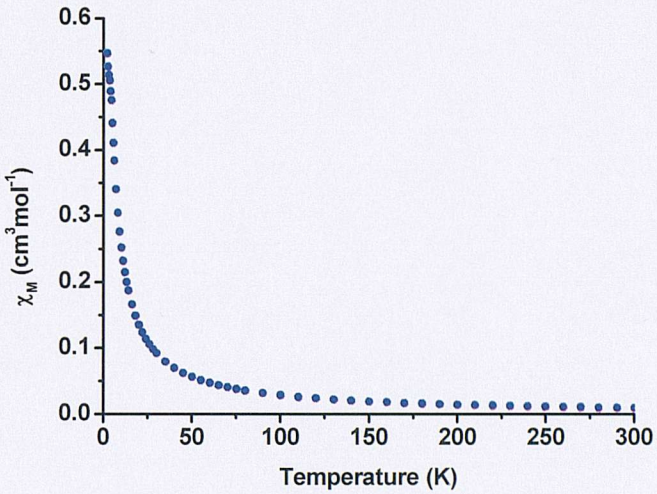


Figure 3.17 χ_M *vs.* temperature for $^{Cy,F\text{-}Ph}[N,N]FeCl_3$, **14**, at 10 kG.

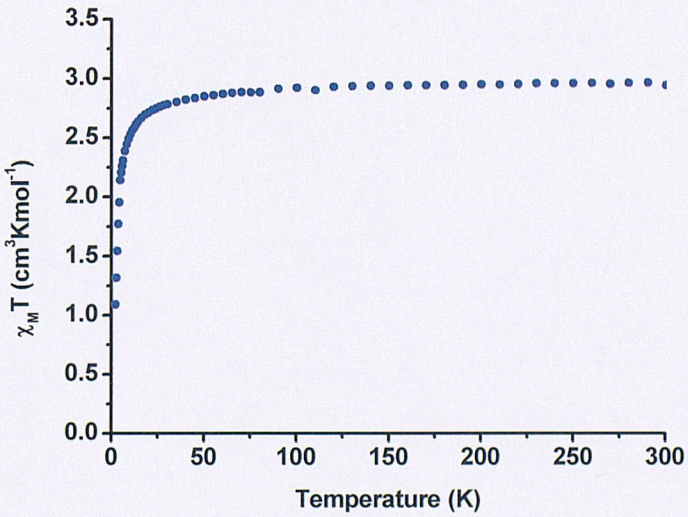


Figure 3.18 $\chi_M T$ *vs.* temperature for $^{Cy,F\text{-}Ph}[N,N]FeCl_3$, **14**, at 10 kG.

Plotting the effective magnetic moment against temperature gives Figure 3.19, where it is clear that the $\mu_{eff.}$ obtained for complex **14** is higher than that expected for a pure intermediate (S = 3/2) spin-state, where the spin only value is 3.87 B.M. However it is also significantly lower than the $\mu_{eff.}$ expected from a pure high (S = 5/2) spin-state, where the spin only value is 5.92 B.M. Figure 3.20 illustrates the difference in the magnetic moments of complexes **14** and **15**.

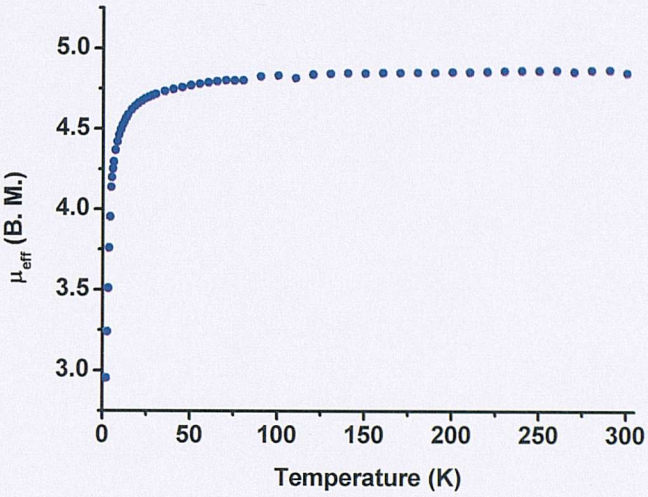


Figure 3.19 $\mu_{eff.}$ *vs.* temperature for $^{Cy,F\text{-}Ph}[N,N]FeCl_3$, **14**, at 10 kG.

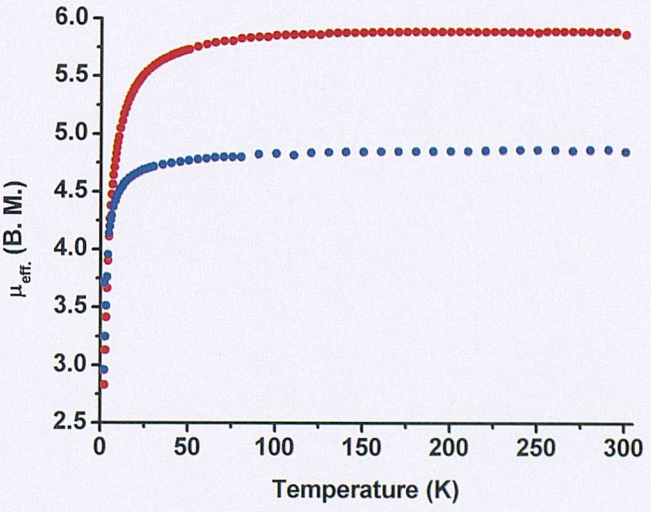


Figure 3.20 $\mu_{eff.}$ *vs.* temperature for $^{tBu,H}[N,N]FeCl_3$, ●, and $^{Cy,F\text{-}Ph}[N,N]FeCl_3$, ●.

Fitting the data for **14** to the Curie-Weiss law (Figure 3.21) ($\chi = C/(T-\theta)$), gave a Curie constant, C, of 2.98 cm^3 $mol^{-1}K$ and a θ of -2.15 K at 10 kG; again the negative value suggests the presence of antiferromagnetic interactions.

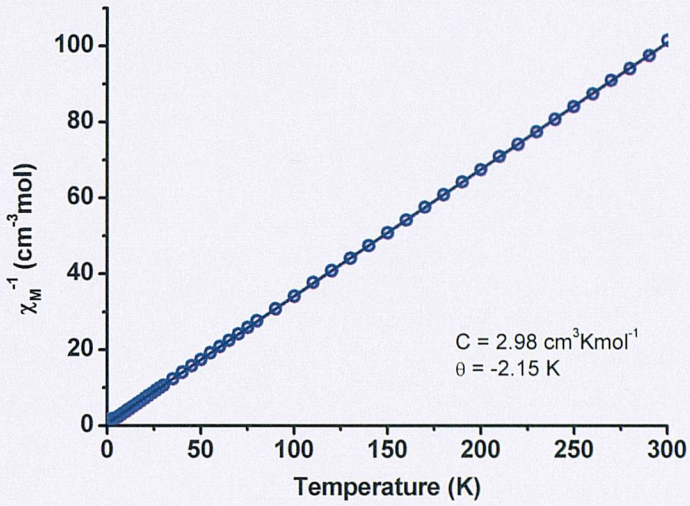


Figure 3.21 χ_M^{-1} *vs.* temperature for $^{Cy,F\text{-}Ph}[N,N]FeCl_3$, **14**, with fitting to the Curie-Weiss law, at 10 kG.

As seen for complex **15**, there is unusual low-temperature behaviour. A hysteresis curve is seen at around 6 K, with the ZFC behaviour clearly differing from that of FC (Figure 3.22). The data obtained are very similar to those acquired with $^{tBu,H}[N,N]FeCl_3$, which is unusual to see in different compounds. Further investigation revealed that these hysteresis curves were only seen in the crushed powder samples, and were not present when data were collected on the microcrystals. Detailed experiments were performed, using different batches of microcrystals and powders, in order to investigate the possibility of a crystallographic phase change. No evidence was found to support this hypothesis and it is more likely that in physically grinding the microcrystals, either an impurity has been introduced, or a chemical transformation / reorganisation has occurred within the sample.

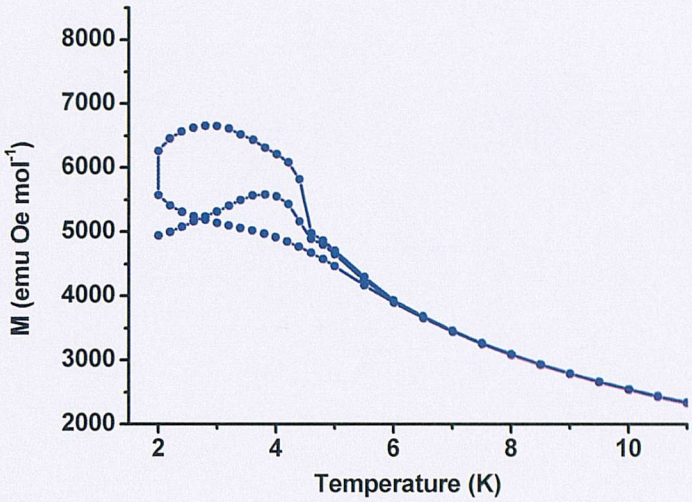


Figure 3.22 χ_M *vs.* temperature for $^{Cy,F\text{-}Ph}[N,N]FeCl_3$, **14**, at 10 kG, FC and ZFC.

It is unsurprising that grinding the samples should cause a change in the magnetic behaviour; the sensitivity of these compounds has been previously discussed and the change in magnetic properties with time was illustrated by a decomposition experiment. The samples were always freshly prepared for SQUID analysis, and loaded into the sealed, teflon capsules inside a glovebox. Rubber O-rings make the capsules airtight; indeed were they not so then the samples would decompose immediately upon being removed from the glovebox. The SQUID data were measured within 24 hours of capsule preparation, but when a sample of **14** was left inside the magnetometer (free of light, O_2 and H_2O) and re-measured after different periods of time, major differences were observed in the magnetic moments (Figure 3.23).

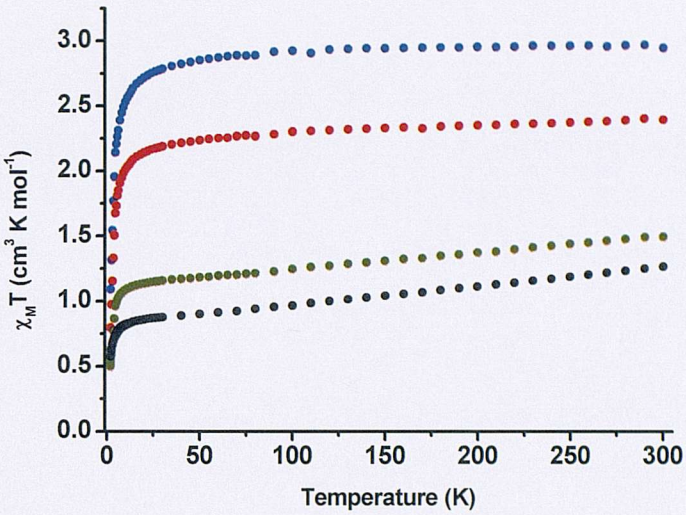


Figure 3.23 $^{Cy,F\text{-}Ph}[N,N]FeCl_3$, **14**, $\chi_M T$ *vs.* temperature plots at 10 kG, after different time periods in the sealed capsule (day 1, ●; day 3, ●; day 6, ●; day 15, ●).

As reported in Figure 3.18, in the first instance the room temperature $\chi_M T$ value for **14** was 2.95 cm^3Kmol^{-1}. After 3 days the room temperature $\chi_M T$ value had decreased to 2.41 cm^3Kmol^{-1}, and a further 3 days later it was 1.49 cm^3Kmol^{-1}. After 2 weeks, further decomposition had decreased the room temperature $\chi_M T$ value to 1.25 cm^3Kmol^{-1}. Interestingly, at this point the hysteresis curve present in the microcrystalline samples had also disappeared, indicating that the likely origin of this behaviour lies within the sample. If it were an external impurity, introduced during the grinding process, it should remain visible even after 2 weeks. These α-diimine Fe^{III} complexes are so unstable that they decompose even in the absence of any external stimuli, forming unknown products with low magnetic moments.

The trigonal bipyramidal compound $Fe(bipy)_2(NCS)_3.(CH_3)_2O$ was reported to have an intermediate, S = 3/2, spin-state.[51] The magnetic moment for this compound was higher than the spin-only value (3.87 B.M.) by comparable amounts to **14**, although the room temperature $\chi_M T$ value of 2.6 cm^3Kmol^{-1} was still lower than that observed for $^{Cy,F\text{-}Ph}[N,N]FeCl_3$. The difference between the spin-only value (1.875 cm^3Kmol^{-1}) and the experimental value (2.6 cm^3Kmol^{-1}) was interpreted by the authors in the terms of a large orbital contribution to the spin-only moment, resulting from Jahn-Teller distortion of the regular trigonal bipyramidal geometry.

Five-coordinate intermediate spin systems are usually characterised by highly distorted coordination geometry. As there is no crystal structure available for complex **14**, it is difficult to predict the spin-state. In compound **15**, the iron^{III} metal ion adopts distorted trigonal-bipyramidal geometry. However, the magnetic behaviour of this compound is typical for a high spin (S = 5/2) system with a minor contribution from the low spin or intermediate spin-state. It is possible that the degree of distortion in the two compounds is different, and/or the ligand field around Fe is different.

For a typical intermediate spin (S = 3/2) system, a magnetic moment of *ca* 3.9 B.M. is expected, which would be independent of temperature except at very low temperatures where zero-field splitting may be operative. The magnetic behaviour of compound **14** is not typical of a pure S = 3/2 system. The large magnetic moment values and the shape of the μ_{eff} *vs.* T curve are very much like those observed for complexes with substantial quantum admixtures of 5/2, 3/2 spin-states. The complex also exhibits Curie-law behaviour, but with a slight reduction in the magnetic moment over a large temperature range, which is another key feature supporting the presence of an admixture.[40,42,45,47] A spin equilibrium system would be expected to show a temperature dependent magnetic moment and a sigmoidal-type curve of the moment versus temperature.[35,39,56] The absence of these features implies that complex **14** is not a spin crossover species. In order to further clarify the spin-state, Mössbauer spectroscopic studies were undertaken.

3.2.2.3 - Mössbauer spectroscopy studies.

Mössbauer spectroscopy is a solid state technique which probes the nucleus using gamma ray radiation and subsequently measures the gamma absorption spectrum.[31,57,58] The energy transitions occur within the absorbing nucleus, but their magnitude depends on the density and distribution of the extranuclear electrons. This gives information on the coordination environment, oxidation state and spin-state of the Mössbauer atom. Only certain isotopes are Mössbauer active; the most commonly studied are ^{57}Fe, ^{99}Ru, ^{119}Sn, ^{121}Sb, ^{127}I, ^{129}I, ^{193}Ir and ^{197}Au.

The spectrum is scanned by Doppler modulation, whereby the gamma source is mounted on a vibrator and a controlled velocity is applied. The spectrometer sweeps through a preset range of velocities and stores the transmitted gamma-counts. The

scan is repeated and accumulated until a satisfactory signal to noise ratio is obtained. It is only the recoil-free fraction (*f*-factor) of the sample which gives rise to the observed absorption spectrum and so the data accumulation can take hours or days. The recoil-free fraction can be increased by lowering the temperature and most molecular materials require cooling to at least liquid nitrogen temperature.

The absorption of gamma radiation involves transitions between the ground state and the first excited state of the nucleus. Excitation requires a rearrangement of the nucleus constituents, resulting in the total spin, I, being different for the two states. Each state may be split into up to 2I+1 sublevels by the presence of, or absence of, electric or magnetic fields. For ^{57}Fe, the first nuclear excited state is split into two sublevels by the presence of an electric field gradient (EFG) across the nucleus. As a result of this, a quadrupole doublet is observed in the ^{57}Fe Mössbauer spectra. Mössbauer spectra are characterised by two main parameters; the isomer shift (i.s.) and quadrupole splitting (q.s.).

The isomer shift governs the overall position of the spectrum on the energy scale (expressed as a velocity in mm s^{-1}) and is measured at the centre of gravity of the doublet, relative to the appropriate standard. For ^{57}Fe, as the electron density at the nucleus increases the isomer shift decreases. The oxidation and spin-states of the Mössbauer atom and the extent of electron donation from the ligand all affect the isomer shift (Figure 3.24). Thus, an Fe^{III} complex will have a smaller isomer shift than the analogous Fe^{II} complex because there are fewer valence electrons to shield the nucleus.

The quadrupole splitting is the separation between the two absorption peaks of the doublet, arising from the presence of the EFG at the Mössbauer nucleus. The magnitude of the quadrupole splitting represents the asymmetry of the electron distribution around the nucleus and relatively large quadrupole splittings are observed with low symmetry complexes. Fe^{III} complexes tend to have smaller quadrupole splittings than their Fe^{II} counterparts (typically 0-1.5 mm s^{-1} for Fe^{III}; 0-4.5 mm s^{-1} for Fe^{II}).

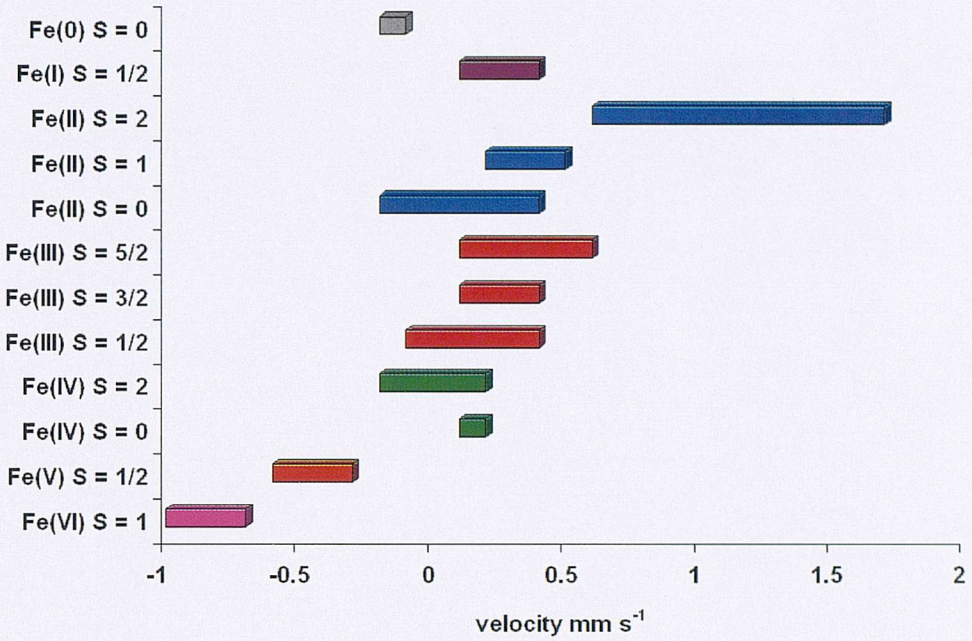


Figure 3.24 Isomer shift ranges for different oxidation and spin-states of ^{57}Fe.[31,57]

If the sample contains the Mössbauer-sensitive atom in more than one distinct environment then the corresponding number of subspectra should be visible. Assuming similar recoil parameters for each environment, the intensities of the subspectra will be proportional to the populations of the various components. In order to further investigate the spin-state of the Fe^{III} complexes studied by EPR and SQUID, Mössbauer studies on the high spin complex $^{tBu,H}[N,N]FeCl_3$ (**15**) and lower spin complex $^{Cy,F\text{-}Ph}[N,N]FeCl_3$ (**14**) were undertaken. The samples were run by Dr. Dave Evans at the John Innes Centre, Norwich, as powdered solids in zero magnetic field using an ES-Technology MS-105 spectrometer, with 125 MBq ^{57}Co source in a Rh matrix. The spectra were referenced to iron foil at 298 K and the spectral parameters were obtained by fitting data with Lorentzian lines. The errors were $\leq \pm 0.01$ unless shown otherwise in parenthesis and used the fitting software ATMOSFIT 4 (written by Dr Ian Morrison, University of Essex).

The Mössbauer spectra obtained for $^{tBu,H}[N,N]FeCl_3$, **15**, were entirely consistent with high spin S = 5/2 Fe^{III}. At 80 K a single doublet was visible, with an isomer shift of 0.41 mms^{-1} and a quadrupole splitting of 0.79 mms^{-1} (Figure 3.25). Upon warming the sample to 173 K, there were no significant changes to the parameters. Cooling the sample back down to 80 K and recollecting the data showed that there were no significant changes during this process (Table 3.4).

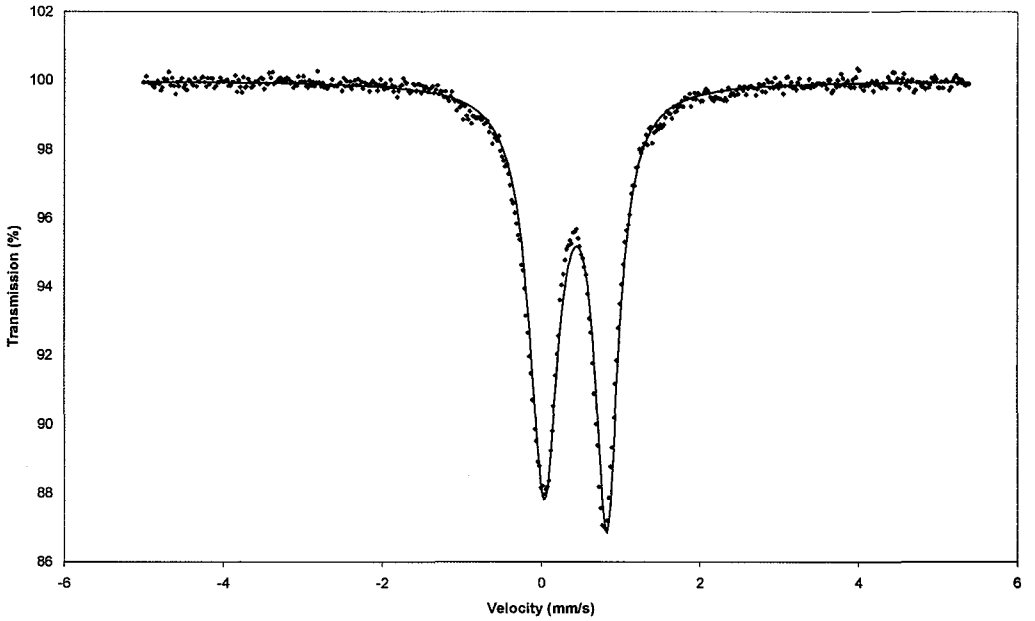


Figure 3.25 Mössbauer spectrum for $^{tBu,H}[N,N]FeCl_3$, complex **15**, at 80 K.

Table 3.4 Mössbauer parameters for complex **15**.

T / K	i.s. / mm s^{-1}	q.s. / mm s^{-1}	h.w.h.m/ mm s^{-1}	%
80	0.41	0.79	0.20	100
173	0.32	0.75	0.18	100
80 (repeat)	0.41	0.79	0.20	100

i.s. = isomer shift; q.s. = quadrupole splitting; h.w.h.m = half-width at half-maximum. Referenced to iron foil at 298 K.

The Mössbauer spectra for $^{Cy,F\text{-}Ph}[N,N]FeCl_3$, **14**, were more complicated than those obtained for **15**. The data were collected at 80 K initially (Figure 3.26), then the sample was warmed to 173 K and the data collected at this temperature. Cooling the sample back down to 80 K and recollecting the data again showed that there were no significant changes during the collection and warming / cooling processes (Table 3.5).

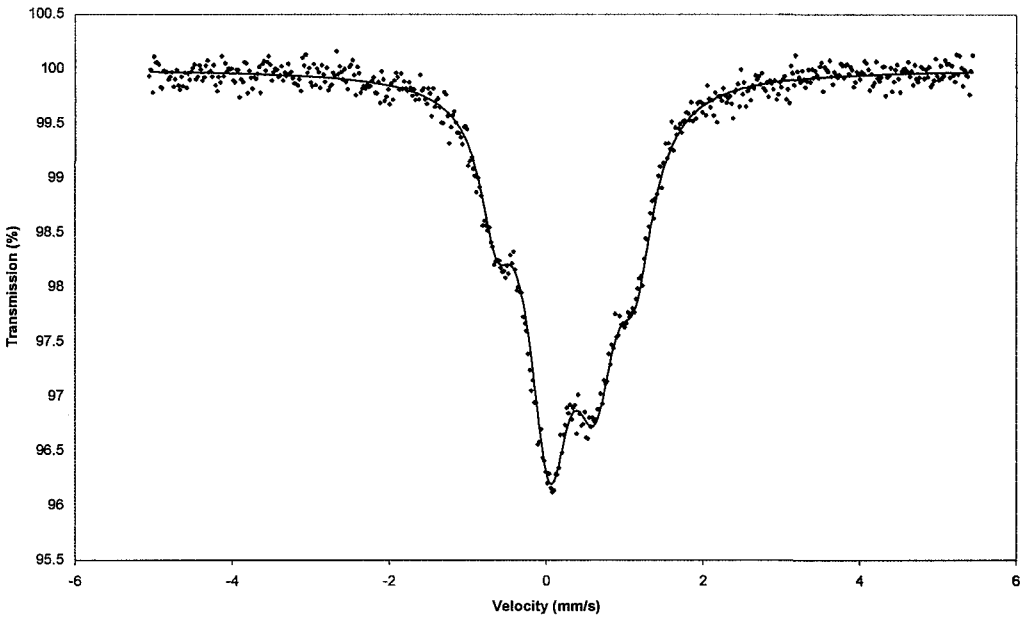


Figure 3.26 Mössbauer spectrum for $^{Cy,F\text{-}Ph}[N,N]FeCl_3$, complex **14**, at 80 K.

Table 3.5 Mössbauer parameters for complex **14**.

T / K	i.s. / mm s^{-1}	q.s. / mm s^{-1}	h.w.h.m/ mm s^{-1}	%
	0.25(1)	1.80(2)	0.24(2)	21
80	0.35(2)	0.56(3)	0.38(2)	71
	-0.04(3)	-	0.23(3)	8
	0.23(1)	1.77(2)	0.22(2)	20
173	0.33(2)	0.57(4)	0.37(3)	72
	-0.05(3)	-	0.18(3)	8
	0.24(1)	1.77(2)	0.23(2)	21
80 (repeat)	0.35(2)	0.58(4)	0.36(2)	70
	-0.02(5)	-	0.24(3)	9

i.s. = isomer shift; q.s. = quadrupole splitting; h.w.h.m = half-width at half-maximum. Referenced to iron foil at 298 K. Errors shown in parentheses.

Although the spectra are broad, data-fitting analysis allowed three distinct signals to be identified: two doublets and a singlet. There is significant overlap between these signals, with the singlet completely obscured by the doublets. This singlet at -0.04(3) mm s^{-1} (at 80 K) is indicative of an S = 1/2 species, since low spin Fe^{III} has either zero or a very small quadrupole splitting. The singlet is the minor component

of the spectrum, accounting for 8% of the total and is likely to be due to unavoidable sample degradation. This is consistent with the data obtained in the SQUID magnetometry experiments, which showed that the magnetic moment of **14** decreased with time (Figure 3.23), suggesting decomposition to a lower spin species.

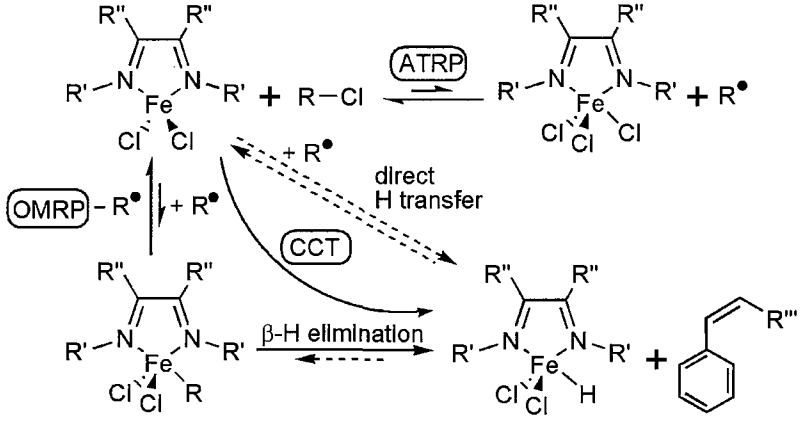
The doublets are consistent with either S = 5/2 or S = 3/2 species, since the isomer shifts are 0.25(1) and 0.35(2) mm s^{-1} (at 80 K) and there is overlap between the isomer shift values for high and intermediate spin Fe^{III} complexes in this region (see Figure 3.24). The doublet at 0.25(1) mm s^{-1} has a quadrupole splitting of 1.80(2) mm s^{-1} and accounts for 21% of the total sample. The broad doublet at 0.35(2) mm s^{-1} is the major component of the sample (71%), and has a smaller quadrupole splitting of 0.56(3) mm s^{-1}. While these signals could be attributed to S = 1/2 species, based on the large isomer shift range for low spin Fe^{III}, these species normally show a strong dependence of the quadrupole splitting on temperature. As Table 3.5 illustrates, this is not observed for either of the doublets in the spectra of **14**. The Mössbauer spectra of intermediate spin, S = 3/2, Fe^{III} in the literature are characterised by large quadrupole splittings, typically 0.97-3.15 mm s^{-1} for the iron 1,2-dithiolate complexes.[57,59] Iron porphyrins in the S = 3/2 spin-state also typically show large quadrupole splittings of *ca.* 3.0-4.0 mm s^{-1},[38,53-55,60] although in the case of spin admixtures of S = 3/2, S = 5/2, there is a gradual decrease in quadrupole splitting as the proportion of S = 5/2 character increases (3.25 to 0.55 mm s^{-1}).[61]

The relatively small quadrupole splittings observed in the Mössbauer spectra of complex **14** suggest that this is not a pure S = 3/2 compound. This is in agreement with the SQUID data, where the observed μ_{eff} of 4.8 B.M. is really too high for an intermediate spin species (spin-only value = 3.9 B.M.). An admixed species would account for the magnetic moments, which are inconsistent with a pure S = 3/2 or S = 5/2 spin-state, and also for the relatively small quadrupole splittings observed in the Mössbauer spectra. However, this does not explain the origin of the two doublets in the spectra; an admixed species would be expected to show a single magnetic environment. It is possible that there are geometric isomers of $^{Cy,F\text{-}Ph}[N,N]FeCl_3$ present in the sample; 5-coordinate Fe^{III} may adopt trigonal bipyramidal or square-based pyramidal geometries and if the barrier to interconversion between the two is too high, the complex may populate both isomers. This was found to be the case for several 5-coordinate Fe^{II} bis(imino)pyridine complexes investigated through

Mössbauer spectroscopy. The presence of two doublets in the spectra led to the proposal that the complexes existed as geometrical isomers in the solid state. Crystallisation of one of these complexes showed that the bulk sample did contain both trigonal bipyramidal and square-based pyramidal complexes.[62]

3.2.3 - Computational studies.

The 2,3 aryl-substituted Fe^{III} complexes **13**, **14**, and **16-19** exhibit lower magnetic moment measurements, which are consistent with a lower spin-state, than the unsubstituted high spin Fe^{III} complex, $^{tBu,H}[N,N]FeCl_3$, **15**. It is likely that this lower spin-state is an admixed species, with both S = 5/2 and S = 3/2 character. This difference in spin-state correlates with the observed differences in polymerisation mechanism, whereby the 2,3 aryl-substituted Fe^{II} complexes **7-12** give rise to CCT behaviour, in contrast to the efficient ATRP catalyst, $^{tBu,H}[N,N]FeCl_2$. This leads to the hypothesis that the observed catalytic activity of the Fe^{II} α-diimine complexes is dependent upon the influence of the metal spin-state in the Fe^{III} species. If we consider the possible reactions of the Fe^{II} complex during a polymerisation as equilibria rather than separate occurrences, the result is as illustrated in Scheme 3.3.



Scheme 3.3 Possible pathways for radical polymerisation of styrene mediated by α-diimine Fe complexes.

The position of the halogen-atom transfer equilibrium established in atom transfer radical polymerisation favours chlorine-capped polymer chains, and minimises the concentration of radicals in solution. The degree of control via ATRP depends upon the propensity of the Fe^{II} species to abstract a halogen atom from an alkyl halide initiator or propagating chain end, which can be viewed as its *halogenophilicity*. The radicals present in solution can also be trapped by the Fe^{II} species to form a new Fe^{III}

organometallic species, establishing an OMRP equilibrium; the analogous idiom for the predilection of the Fe^{II} species to trap a carbon-based radical can be termed *carbophilicity*. Olefin-terminated polymer chains can then be generated via β-hydrogen elimination of this Fe-carbon bond or, alternatively, through direct hydrogen transfer by the original Fe^{II} catalyst. While the term 'halogenophilicity' has been previously used to describe the reaction of a metal complex with a halide ion,[63,64] in this case halogeno- and carbo-philicity are described as the relative predilection for a complex to form metal-halogen and metal-carbon bonds respectively.

Working in collaboration with Professor H. S. Rzepa, the role of metal spin-state in this catalytic system was further investigated through computational analysis of the two competing reactions. A series of Hartree-Fock level all-electron [ROHF/6-31G(3d)] calculations were performed on model systems.[65] Reactions A and B, with R set to either ^{t}Bu or Ph, were computed with the spin-state of the iron complexes specified as either quartet (S = 3/2) or sextet (S = 5/2) for the Fe^{III} species (Figure 3.27).

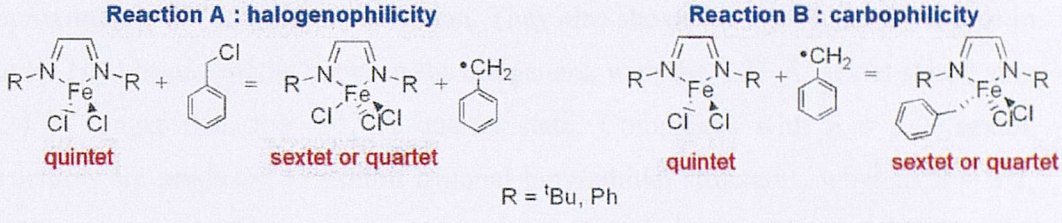


Figure 3.27 Halogenophilic and carbophilic reactions analysed computationally.

The relative preference of the two reactions for a particular spin-state of iron is a determinant of carbo- *vs.* halogeno-philicity. For Fe^{III} sextet systems, halogenophilic behaviour is favoured, as for R = ^{t}Bu and Ph, reaction A is favoured over reaction B by 10.6 and 9.3 kcal/mol respectively. This trend is reversed for intermediate spin quartet systems. For R = ^{t}Bu and Ph, reaction B is now favoured by 0.9 and 4.6 kcal/mol respectively. The calculations thus predict that systems with S = 3/2 spin-states are carbophilic while those with S = 5/2 spin-states are halogenophilic (Figure 3.28). In addition, the calculations show that for R = Ph, the carbophilicity is even more pronounced, supporting the experimental evidence for aryl-imine carbophilicity.

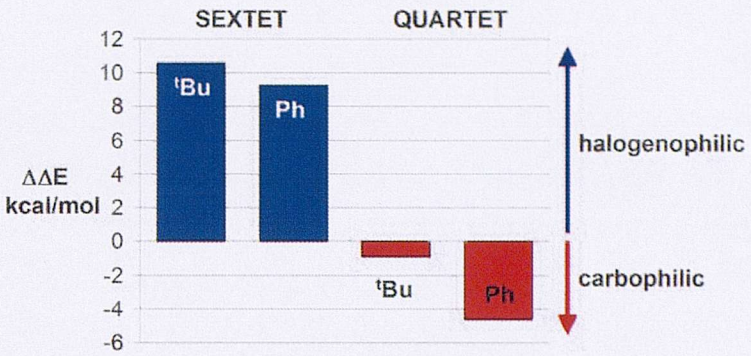


Figure 3.28 Graphical representation of computational results, showing halogenophilic behaviour of sextet Fe^{III} species and carbophilic behaviour of quartet species. ΔΔE is the difference in energy between reaction A and reaction B, corrected for entropy.

The calculations also suggest that a change in spin-state should be visible in the solid state structures of the complexes, due to a distortion of the antiperiplanar nitrogen. The crystal structure of $^{tBu,H}[N,N]FeCl_3$ (Figure 3.3) allowed validation of these calculations, which predict an increase of the Cl(2)-Fe-Cl(2)* angle by approximately 10° in the quartet system. They also showed a significant difference in the Fe-N(2) bond lengths between the congeners, with the 2.31 Å sextet state being 0.24 Å longer than the 2.07 Å quartet state. Complexes with S = 5/2, sextet, structures are predicted to exhibit trigonal bipyramidal structures, whereas S = 3/2, quartet, complexes favour more square pyramidal geometry (Figure 3.29).The Fe-N(2) bond length obtained from the solid state structure of the high spin complex **15** is 2.24 Å, correlating well with the sextet spin-state, and the geometry at the iron centre is best described as trigonal bipyramidal.

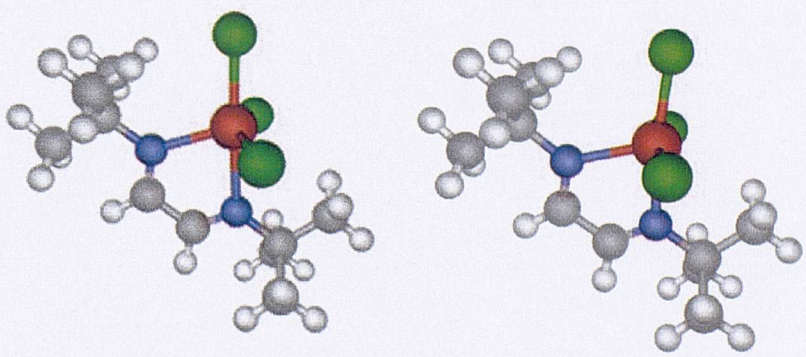


Figure 3.29 Geometry optimised structures for sextet (left) and quartet (right) $^{tBu,H}[N,N]FeCl_3$.

An orbital correlation study between $^{tBu,H}[N,N]FeCl_3$ sextet and quartet spin-states suggested a rationale for the preference of intermediate spin-states for 2,3-substituted complexes. The quartet and sextet states are formally linked by promotion of a single electron, which directly affects the energies of the occupied orbitals and their propensity to mix with other atomic orbitals (AOs). In the sextet state, molecular orbital (MO) 84 is singly occupied and predominately Fe d-AO in character with little other mixing. In the quartet state, this MO becomes doubly occupied with a resulting lower energy (61). This allows mixing of the metal-based d-AO with ligand AOs of similar energy, creating a delocalised MO in which conjugation with the 2,3-positions of the α-diimine ligand backbone is a prominent feature. This coupling suggests that changes to the electronic characteristics of the ligand substituents would have a strong influence on the nature of the molecular orbital (MO 61) derived from the mixing of the doubly occupied d-orbital with the ligand orbitals (Figure 3.30) and hence the quartet/sextet balance. Systematic alteration of the backbone substituents should, therefore, control the metal spin-state and thus catalyst behaviour, without significant alteration of the steric environment at the iron centre.

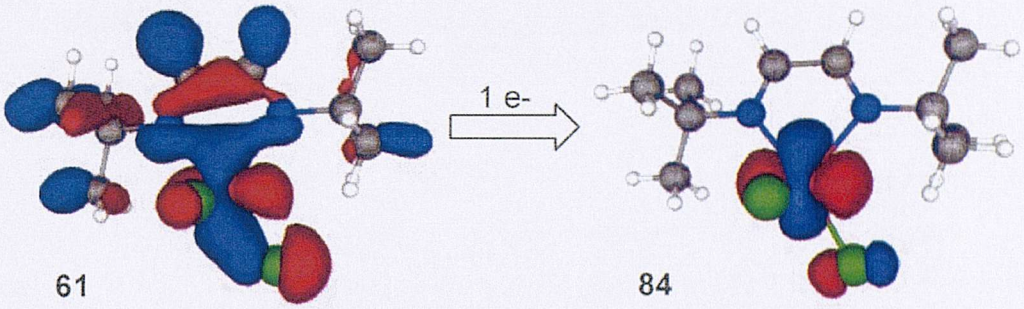


Figure 3.30 Delocalised, doubly occupied MO 61 in quartet state is linked to singly occupied MO 84 through promotion of a single electron.

3.3 - Conclusions

In this chapter, the synthesis of the Fe^{III} complexes of the novel 2,3-aryl substituted α-diimine ligands reported in Chapter 2 has led to the discovery that the behaviour of $^{R',R''}[N,N]FeCl_2$ complexes in catalytic styrene polymerisation can be correlated with the spin-state of the Fe^{III} complex. Complexes which polymerise styrene through a predominantly CCT route are carbophilic, with lower, probably admixed spin-states for the analogous Fe^{III} complexes. High spin, S = 5/2, Fe^{III} complexes can be correlated with controlled ATRP behaviour. The vital role of catalytic polymerisation in this system should be emphasised, as it allows us to monitor the individual events catalysed by the two spin-states. The polymer isolated is a record of these events, with rates, molecular weights and end groups representing the 'signature' of the prevalent mechanism.

Computational analysis has provided a rationale behind the switch in polymerisation mechanism, showing that a quartet spin-state favours the carbophilic reaction of an Fe^{II} complex with a radical over the halogenophilic reaction to form the Fe^{III} trichloride. Conversely, the halogenophilic reaction is favoured for high spin-state systems. Orbital correlation analysis showed that the doubly occupied molecular orbital in the intermediate spin-state is extensively mixed with the ligand atomic orbitals, forming a highly delocalised orbital. This has extensive conjugation, not just at the *N*-substituent, but also into the 2,3-positions of the backbone. The inclusion of electron-withdrawing groups at these positions would therefore be expected to favour the quartet spin-state and polymerisation through CCT, as is observed experimentally.

The α-diimine Fe system appears to be very sensitive to small changes to the ligand framework, and there remains much to investigate within this system. Inclusion of electron-withdrawing groups at the 2,3-positions of the α-diimine backbone has a dramatic impact on the polymerisation mechanism, but the effect of an electron-donating group has not yet been assessed. This will be described in the following chapter, as systematically varying the groups at the 2,3-positions could give valuable mechanistic insights into the relationship between ATRP and CCT events. Furthermore, if the CCT behaviour observed with this system occurs through an M-C bond formation, β-H elimination mechanism, it should be possible to further exploit this organometallic regime. Exploring the reactivity of the Fe^{III} species is one

potential avenue where the lower spin-state complexes may be exploited, whereas control over the OMRP equilibria would also allow access to another method of controlled radical polymerisation (Scheme 3.3).

3.4 - References

(1) Wang, J.-S.; Matyjaszewski, K., *Macromolecules* **1995,** *28*, 7572.

(2) Matyjaszewski, K.; Patten, T. E.; Xia, J. H., *J. Am. Chem. Soc.* **1997,** *119*, 674.

(3) Moineau, G.; Dubois, P.; Jérôme, R.; Senninger, T.; Teyssié, P., *Macromolecules* **1998,** *31*, 545.

(4) Xia, J.; Matyjaszewski, K., *Macromolecules* **1997,** *30*, 7692.

(5) Xia, J.; Matyjaszewski, K., *Macromolecules* **1999,** *32*, 5199.

(6) Zhu, S.; Wang, W.; Tu, W.; Deyue Yan, *Acta Polym.* **1999,** *50*, 267.

(7) Qin, D.-Q.; Qin, S.-H.; Qiu, K.-Y., *Macromolecules* **2000,** *33*, 6987.

(8) Qin, D.-Q.; Qin, S.-H.; Chen, X.-P.; Qiu, K.-Y., *Polymer* **2000,** *41*, 7347.

(9) Gromada, J.; Matyjaszewski, K., *Macromolecules* **2001,** *34*, 7664.

(10) Qiu, J.; Gaynor, S. G.; Matyjaszewski, K., *Macromolecules* **1999,** *32*, 2872.

(11) Wang, W.; Dong, Z.; Xia, P.; Yan, D.; Zhang, Q., *Macromol. Rapid Commun.* **1998,** *19*, 647.

(12) Chen, X.-P.; Kun-Yuan Qiu, *Polym. Int.* **2000,** *49*, 1529.

(13) Teodorescu, M.; Gaynor, S. G.; Matyjaszewski, K., *Macromolecules* **2000,** *33*, 2335.

(14) Wang, G.; Zhu, X.; Cheng, Z.; Zhu, J., *Eur. Polym. J.* **2003,** *39*, 2161.

(15) Wang, G.; Zhu, X.; Cheng, Z.; Zhu, J., *J. Polym. Sci. A: Polym. Chem.* **2006,** *44*, 2912.

(16) O'Reilly, R. K. Synthesis of novel iron complexes and their use in atom transfer radical polymerisation. Ph.D. Thesis, University of London, 2003.

(17) Evans, D. F., *J. Chem. Soc.* **1959**, 2003.

(18) Daran, J.-C.; Jeannin, Y.; Martin, L. M., *Inorg. Chem.* **1980,** *19*, 2935.

(19) Millington, K. R.; Wade, S. R.; Willey, G. R., *Inorg. Chim. Acta* **1984,** *89*, 185.

(20) Witten, E. H.; Reiff, W. M.; Lázár, K.; Sullivan, B. W.; Foxman, B. M., *Inorg. Chem.* **1985,** *24*, 4585.

(21) Sreekanth, A.; Kurup, M. R. P., *Polyhedron* **2004,** *23*, 969.

(22) Kulkarni, P.; Padhye, S.; Sinn, E., *Polyhedron* **1998,** *17*, 2623.

(23) Nakayama, Y.; Baba, Y.; Yasuda, H.; Kawakita, K.; Ueyama, N., *Macromolecules* **2003,** *36*, 7953.

(24) Berrett, R. R.; Fitzsimmons, B. W.; Owusu, A. A., *J. Chem. Soc. (A)* **1968,** 1575.

(25) Harris, C. M.; Lockmeyer, T. N., *Chem. Ind. (London)* **1968**, 1231.

(26) Ghosh, S. N., *Ind. J. Chem.* **1975,** *13*, 66.

(27) Goodwin, H. J.; McPartlin, M.; Goodwin, H. A., *Inorg. Chim. Acta* **1977,** *25*, L74.

(28) Wang, X.; Wang, S.; Li, L.; Sundberg, E. B.; Gacho, G. P., *Inorg. Chem.* **2003,** *42*, 7799.

(29) Ionkin, A. S.; Marshall, W. J.; Adelman, D. J.; Fones, B. B.; Fish, B. M.; Schiffhauer, M. F., *Organometallics* **2006,** *25*, 2978.

(30) McInnes, E. J. L.; Collison, D.; Wolowska, J.; Kowalczyk, R. In 4th Workshop on the Theory and Practice of EPR Spectroscopy, Manchester, 2005.

(31) Parish, R. V., *NMR, NQR, EPR, and Mössbauer Spectroscopy in Inorganic Chemistry*. First ed.; Ellis Horwood: London, 1990.

(32) Mitra, S., *Iron porphyrins*, Eds. Lever, A. B. P.; Gray, H. B., Addison-Wesley: Reading, 1982.

(33) Nakamura, M., *Coord. Chem. Rev.* **2006,** *250*, 2271.

(34) Scheidt, W. R.; Geiger, D. K.; Haller, K. J., *J. Am. Chem. Soc.* **1982,** *104*, 495.

(35) Ellison, M. K.; Nasri, H.; Xia, Y.-M.; Marchon, J.-C.; Schulz, C. E.; Debrunner, P. G.; Scheidt, W. R., *Inorg. Chem.* **1997,** *36*, 4804.

(36) Neya, S.; Tsubaki, M.; Hori, H.; Yonetani, T.; Funasaki, N., *Inorg. Chem.* **2001,** *40*, 1220.

(37) Neya, S.; Chang, C. K.; Okuno, D.; Hoshino, T.; Hata, M.; Funasaki, N., *Inorg. Chem.* **2005,** *44*, 1193.

(38) Ikeue, T.; Ohgo, Y.; Yamaguchi, T.; Takahashi, M.; Takeda, M.; Nakamura, M., *Angew. Chem.* **2001,** *113*, 2687.

(39) Ohgo, Y.; Chiba, Y.; Hashizume, D.; Uekusa, H.; Ozekie, T.; Nakamura, M., *Chem. Commun.* **2006**, 1935.

(40) Maltempo, M. M., *J. Chem. Phys.* **1974,** *61*, 2540.

(41) Maltempo, M. M.; Moss, T. H., *Quart. Rev. Biophys.* **1976,** *9*, 2.

(42) Reed, C. A.; Mashiko, T.; Bentley, S. P.; Kastner, M. E.; Scheidt, W. R.; Spartalian, K.; Lang, G., *J. Am. Chem. Soc.* **1979,** *101*, 2948.

(43) Nakamura, M.; Ikeue, T.; Ohgo, Y.; Takahashi, M.; Takeda, M., *Chem. Commun.* **2002**, 1198.

(44) Reed, C. A.; Guiset, F., *J. Am. Chem. Soc.* **1996,** *118*, 3281.

(45) Kennedy, B. J.; Murray, K. S.; Homborg, H.; Kalz, W., *Inorg. Chem.* **1986,** *25*, 2539.

(46) Alonso, P. J.; Arauza, A. B.; Fornies, J.; Garcia-Monforte, M. A.; Martin, A.; Martinez, J. I.; Menjon, B.; Rillo, C.; Saiz-Garitaonandia, J. J., *Angew. Chem. Int. Ed.* **2006,** *45*, 6707.

(47) Fryzuk, M. D.; Leznoff, D. B.; Ma, E. S. F.; Rettig, S. J.; Victor G. Young, J., *Organometallics* **1998,** *17*, 2313.

(48) Carlin, R. L., *Science* **1985,** *227*, 1291.

(49) Keutel, H.; Käpplinger, I.; Jäger, E.-G.; Grodzicki, M.; Schünemann, V.; Trautwein, A. X., *Inorg. Chem.* **1999,** *38*, 2320.

(50) Ghosh, P.; Bill, E.; Weyhermüller, T.; Neese, F.; Wieghardt, K., *J. Am. Chem. Soc.* **2003,** *125*, 1293.

(51) Moliner, N.; Real, J. A.; Munoz, M. C.; Martinez-Manez, R.; Juan, J. M. C., *Dalton Trans.* **1999**, 1375.

(52) Ray, M.; Golombek, A. P.; Hendrich, M. P.; Yap, G. P. A.; Liable-Sands, L. M.; Rheingold, A. L.; Borovik, A. S., *Inorg. Chem.* **1999,** *38*, 3110.

(53) Toney, G. E.; terHaar, L. W.; Savrin, J. E.; Gold, A.; Hatfield, W. E.; Sangaiah, R., *Inorg. Chem.* **1984,** *23*, 2561.

(54) Ikeue, T.; Saitoh, T.; Yamaguchi, T.; Ohgo, Y.; Nakamura, M.; Takahashi, M.; Takedac, M., *Chem. Commun.* **2000**, 1989.

(55) Ikeue, T.; Ohgo, Y.; Takahashi, M.; Takeda, M.; Neya, S.; Funasaki, N.; Nakamura, M., *Inorg. Chem.* **2001,** *40*, 3650.

(56) Walker, J. D.; Poli, R., *Inorg. Chem.* **1989,** *28*, 1793.

(57) Gibb, T. C.; Greenwood, N. N., *Mössbauer Spectroscopy*. First ed.; Chapman and Hall: London, 1971.

(58) Banwell, C. N.; McCash, E. M., *Fundamentals of Molecular Spectroscopy*. Fourth ed.; McGraw-Hill: Maidenhead, 1994.

(59) Birchall, T.; Greenwood, N. N., *J. Chem. Soc. (A)* **1969**, 286.

(60) Simonato, J.-P.; Pecaut, J.; Le Pape, L.; Oddou, J.-L.; Jeandey, C.; Shang, M.; Scheidt, W. R.; Wojaczynski, J.; Wolowiec, S.; Latos-Grazynski, L.; Marchon, J.-C., *Inorg. Chem.* **2000,** *39*, 3978.

(61) Ohgo, Y.; Neya, S.; Ikeue, T.; Takahashi, M.; Takeda, M.; Funasaki, N.; Nakamura, M., *Inorg. Chem.* **2002,** *41*, 4627.

(62) McTavish, S. J. Ethylene polymerisation catalysts based on bisiminopyridine complexes of iron: synthesis, polymerisation and activity studies. PhD Thesis, University of London, 2001.

(63) Gillies, M. B.; Matyjaszewski, K.; Norrby, P.-O.; Pintauer, T.; Poli, R.; Richard, P., *Macromolecules* **2003,** *36*, 8551.

(64) Tsarevsky, N. V.; Pintauer, T.; Matyjaszewski, K., *Macromolecules* **2004,** *37*, 9768.

(65) Shaver, M. P.; Allan, L. E. N.; Rzepa, H. S.; Gibson, V. C., *Angew. Chem. Int. Ed.* **2006,** *45*, 1241.

Chapter 4

Structure-Activity Relationships for α-Diimine Iron Catalysts

4.1 - Introduction

In Chapters 2 and 3 the catalytic reactivity of the α-diimine Fe^{II} dichloride complexes was shown to differ depending upon the spin-state of the Fe^{III} trichloride species generated in the ATRP/OMRP equilibria. High spin (S = 5/2) metal centres gave typical ATRP behaviour, whereas lower spin systems (with S = 3/2 character) resulted in CCT. The fundamental role which metal spin-state can play is exemplified in the reactivity of life-supporting biomolecules such as the haem-based metallo-proteins.[1-4] In non-biological systems the connection between metal spin-state and reactivity, especially in catalysis, has remained largely undeveloped. This α-diimine iron system, where closely related iron complexes with differing metal spin-states afford starkly contrasting mechanistic outcomes in catalytic polymerisation, represents the first time such distinct catalytic reaction pathways have been delineated for metal spin-state isomers outside a biological manifold.

Catalytic reactivity can often be modified by changing the substituents at strategic positions on the catalyst. Hammett relationships have been investigated in anionic,[5] cationic[6] and radical[7,8] polymerisation reactions, although these studies introduced the *para* substituent to the monomer rather than the catalyst. Typically, substituted aryl monomers were used, and the effect of substituent on the reactivity was assessed.

The chiral porphyrins, **I**, used with FeBr and PhIO as epoxidation catalysts for olefins were investigated with a range of *para* substituents on the aromatic ring of the R-group (Figure 4.1), and it was found that there was a linear relationship between the Hammett substituent, σ, and the enantioselectivity.[9] Electron-donating groups gave increased enantioselectivities because the lower reactivity led to a later transition state, with improved selectivity.

A similar conclusion was drawn from the data obtained from the Jacobsen Mn-salen epoxidation catalyst, **II**. Inclusion of an electron-donating group at the *para* position of the aryl ring led to higher levels of asymmetric induction.[10,11] It was proposed that the ligand substituents influenced the enantioselectivity by moderating the reactivity of the high valent salen-Mn oxo intermediate. Electron-withdrawing groups gave more reactive intermediates which added to the olefin in an early transition state, leading to lower enantioselectivity. The presence of an electron-

withdrawing group destabilises the Mn^{IV} oxo species, making it a more reactive oxidant, and a linear correlation between σ and $E_{1/2}$ was discovered.[11]

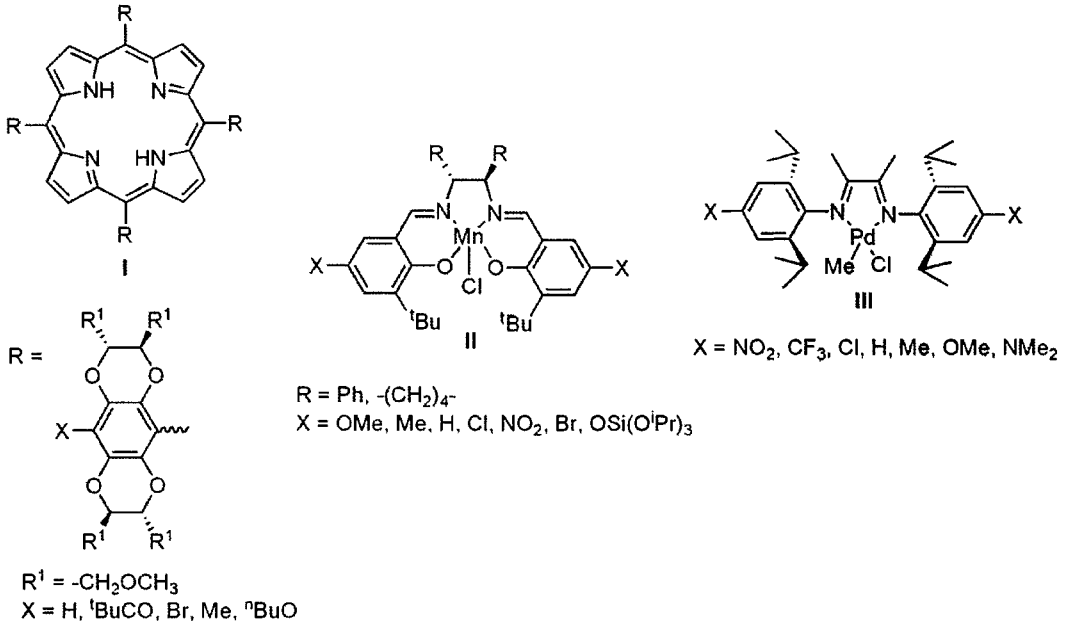


Figure 4.1 Examples of catalytic systems where the *para* substituent significantly affects the catalytic reactivity.

A study of a variety of α-diimine complexes of Pd, $^{Me,p\text{-}X\text{-}DiPP}$[*N,N*]Pd(CO)Me, where the *N*-aryl substituent was a *para*-substituted di*iso*propylphenyl group (X = NO_2, CF_3, Cl, H, Me, OMe, NMe_2), **III**, showed that σ could be correlated with both the ^{1}H chemical shift of the Pd-Me group and ν_{CO} of the carbonyl.[12] Despite the remote position of the *para* group and the large dihedral angle between the backbone and the aromatic ring, the substituents still significantly affect the electronic properties of the ligands and complexes. There was also a correlation between the activity of the $^{Me,p\text{-}X\text{-}DiPP}$[*N,N*]PdClMe complexes in ethylene polymerisation and the *para* substituent, with electron-donating groups generally giving higher turnover frequencies and higher molecular weight polymer. However, the 'original' unsubstituted catalyst ^{Me,DiPP}[*N,N*]PdClMe remained the most active catalyst, although this point was overlooked by the authors. Copolymerisation of ethylene and methyl acrylate was investigated and the incorporation ratio of MA was found to be dependent on the *para* substituent. Catalysts with electron-donating groups had a higher incorporation ratio than those with electron-withdrawing groups, and this was linked to the decreased electrophilicity of the metal centre resulting in an increased binding of the electron deficient olefin (MA) relative to ethylene.

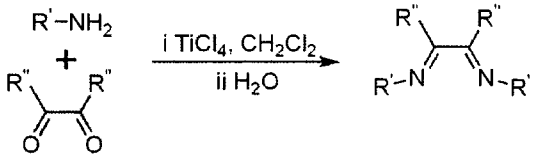
Structure-activity relationships in atom transfer radical polymerisation have been limited to investigation of the effect of the *para* substituent on styrenyl monomers. Matyjaszewski's CuBr/bipy system was used in conjunction with a range of substituted styrenes, including *p*-CF_3, *p*-Br, *p*-Cl, *p*-Me, *p*-CMe_3 and *p*-OMe.[7] Monomers containing an electron-withdrawing group resulted in faster polymerisation and lower PDIs than those containing electron-donating groups. This was attributed to the electron-withdrawing groups destabilising the partial positive charge of the C-X bonds, and decreasing the bond dissociation energy. Similar findings were reported using a Ru(cymene)Cl_2PPh_3 catalyst,[8] and both papers noted that *p*-MeO-styrene gave only low molecular weight products, indicative of chain transfer reactions.

Whilst the effects of *N*-substitution on the polymerisation behaviour of the α-diimine Fe^{II} catalysts have been previously studied in detail,[13,14] the computational studies described in Chapter 3 suggested the importance of investigating the substituents at the 2,3-positions of the backbone. The 2,3-aryl substituted α-diimine ligand is set up for facile derivatisation, allowing investigation into the effects which electron-withdrawing and electron-donating groups on the α-diimine backbone have on the polymerisation behaviour of the Fe^{II} complexes under ATRP conditions. This chapter details the synthesis, characterisation and polymerisation behaviour of a range of 2,3-aryl substituted α-diimine Fe complexes, with different *para* substituents.

4.2 - Results and Discussion

4.2.1 - Synthesis of Fe^{II} compounds.

The α-diimine ligands, $^{R',R''}[N,N]$, (where $^{R',R''}[N,N]$ = R′-N=CR″-CR″=N-R′, R′ = *tert*-butyl (^{t}Bu), cyclohexyl (Cy), and R″ = *para*-bromophenyl (Br-Ph), *para*-methylphenyl (Me-Ph), *para*-methoxyphenyl (MeO-Ph), *para*-dimethylaminophenyl (Me_2N-Ph)) were prepared through modification of a literature procedure,[15] using $TiCl_4$ as an activating agent (Scheme 4.1). After aqueous workup, the crude residues were recrystallised from hot alcohol to give the desired products in good yield (65-85%).

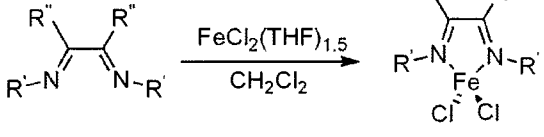


	R'	R"
20	Cy	Br-Ph
21	Cy	Me-Ph
22	Cy	MeO-Ph
23	Cy	Me_2N-Ph

	R'	R"
24	^{t}Bu	Br-Ph
25	^{t}Bu	Me-Ph
26	^{t}Bu	MeO-Ph
27	^{t}Bu	Me_2N-Ph

Scheme 4.1 Synthesis of *para*-phenyl substituted 2,3-aryl α-diimine ligands.

The Fe^{II} chloride complexes, **28-35**, were formed using $FeCl_2(THF)_{1.5}$ (Scheme 4.2) and isolated in good yields (64-77%). Addition of CH_2Cl_2 to an intimate mixture of ligand and metal precursor produced a deep blue solution, except in the case of **31** and **35** which were red-brown. After stirring overnight the solution was filtered and concentrated, before the desired product was obtained as a purple or red-brown solid after precipitation with pentane.



	R'	R"
28	Cy	Br-Ph
29	Cy	Me-Ph
30	Cy	MeO-Ph
31	Cy	Me_2N-Ph

	R'	R"
32	^{t}Bu	Br-Ph
33	^{t}Bu	Me-Ph
34	^{t}Bu	MeO-Ph
35	^{t}Bu	Me_2N-Ph

Scheme 4.2 Synthesis of *para*-phenyl substituted 2,3-aryl α-diimine Fe^{II} complexes.

Despite the paramagnetism of the complexes, contact-shifted ^{1}H NMR spectra could be obtained for each compound and assigned on the basis of integrated signal intensities and chemical shifts. As an example, the spectra obtained for complexes **31** and **35** are shown in Figures 4.2 and 4.3 and are extremely similar to those discussed in Chapter 2 for $^{Cy,Ph}[N,N]FeCl_2$, **7**, and $^{Cy,F\text{-}Ph}[N,N]FeCl_2$, **8**. In the case of $^{Cy,Me2N\text{-}Ph}[N,N]FeCl_2$, **31**, the highly deshielded resonance, H_d, appears at 193 ppm (*cf.* 192 ppm for $^{Cy,Ph}[N,N]FeCl_2$). The most shielded resonances are again the methylene ring protons, which appear between 4 and -58 ppm (*cf.* δ -6 to -48 for $^{Cy,Ph}[N,N]FeCl_2$). The increased shielding in complex **31** may be attributed to the increased electron density at the metal centre; with the electron-donating NMe_2 group on the aryl ring, the iron centre is more electron rich. The aromatic protons, H_a, H_b and H_c appear between 2 and 16 ppm, very similar to the shifts seen for $^{Cy,Ph}[N,N]FeCl_2$ (6.5-16 ppm). This is a general trend within the *para*-substituted complexes; while there is little difference in the position of H_d (193-195 ppm for complexes with *p*-Br, *p*-F, *p*-H, *p*-Me, *p*-MeO and *p*-Me_2N groups) or the aromatic ring protons, as the *para* substituent becomes more electron-donating the effect on

the most shielded resonance increases. Thus $^{Cy,Br\text{-}Ph}[N,N]FeCl_2$, **28**, has the least amount of shielding, with the methylene resonance appearing at -46 ppm and $^{Cy,Me2N\text{-}Ph}[N,N]FeCl_2$, **31**, has the largest amount of shielding (-58 ppm).

FAB-MS of **28-35** showed the expected $[M+H]^+$ peaks as well as common fragments, such as $[M\text{-}Cl]^+$, and the imine $\nu_{C=N}$ stretches for **28-35** were visible between 1590-1610 cm^{-1}. In each case, the stretch for the Fe^{II} complex appeared at a lower frequency than that of the free ligand, with the exception of **31** and **35**. In the case of the *p*-Me_2N-substituted complexes, the imine stretch increased in frequency when compared to the free ligands (from 1596 to 1606 cm^{-1} for **31**, and from 1599 to 1610 cm^{-1} for **35**). This indicates that the C=N imine bond is stronger in the metal complex than the ligand, potentially due to the strongly electron-donating nature of the dimethylamino groups installed on the backbone. Crystals suitable for X-ray structure analysis of complexes **31** and **35** were obtained through slow cooling of a saturated solution of **31** or **35** in toluene. The complexes had similar, monomeric solid-state structures with 4-coordinate metal centres, analogous to those discussed in Chapter 2 for the phenyl and fluorophenyl-substituted derivatives, **7-10**.

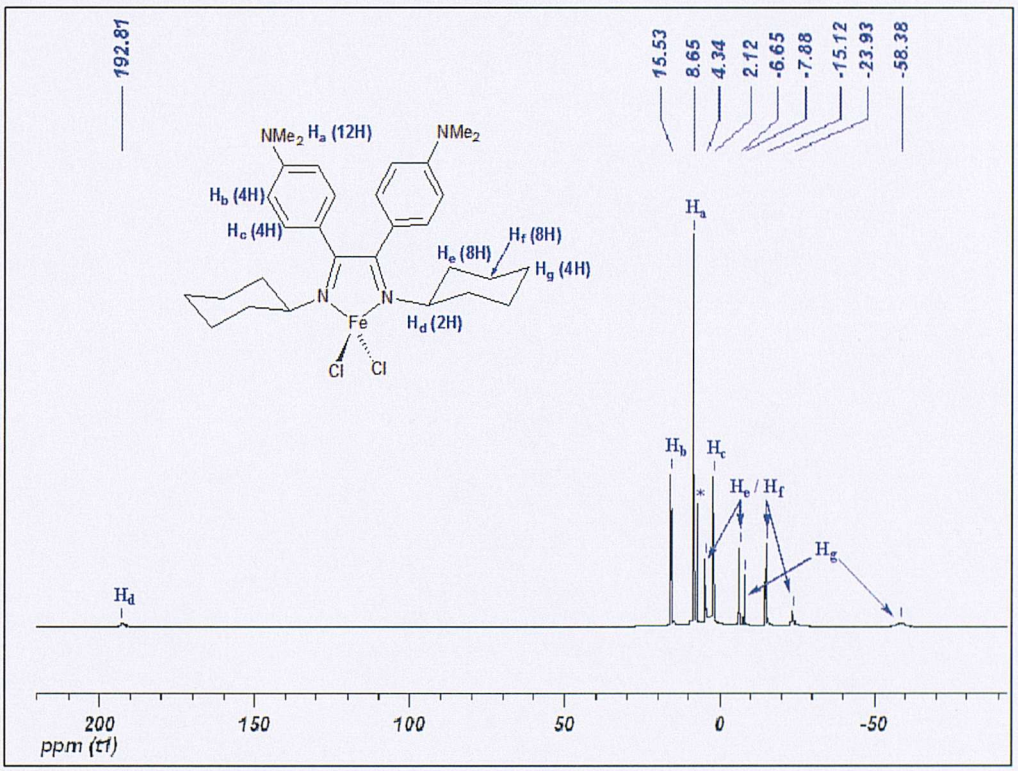


Figure 4.2 ^1H NMR spectrum for $^{Cy,Me2N}[N,N]FeCl_2$, complex **31** (* indicates residual proton signal in $CDCl_3$).

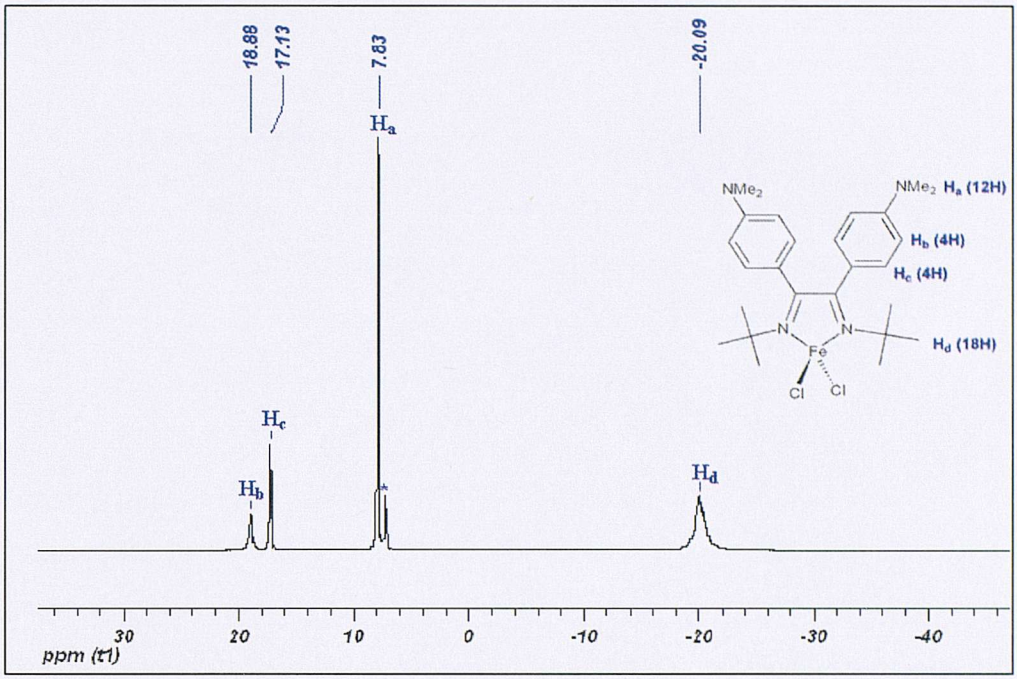


Figure 4.3 ^{1}H NMR spectrum for $^{tBu,Me2N}[N,N]FeCl_2$, complex **35** (* indicates residual proton signal in $CDCl_3$).

The X-ray crystal structure of **31** revealed a C_2-symmetric complex with a highly distorted tetrahedral iron centre, with *cis* angles in the range 78.37(5)-122.06(2)°, and where the most acute angle is the bite angle of the chelating *N,N'* ligand (Figure 4.4, Table 4.1). There is a distortion to the N=C-C=N plane, which in most previous crystal structures has been planar with the Fe atom sitting *ca.* 10-15° above the plane. In the case of $^{Cy,Me2N-Ph}[N,N]FeCl_2$, **31**, the imine is puckered and so there is no plane, as seen in the example of $^{tBu,Ph}[N,N]FeCl_2$, **9**, reported in Chapter 2.

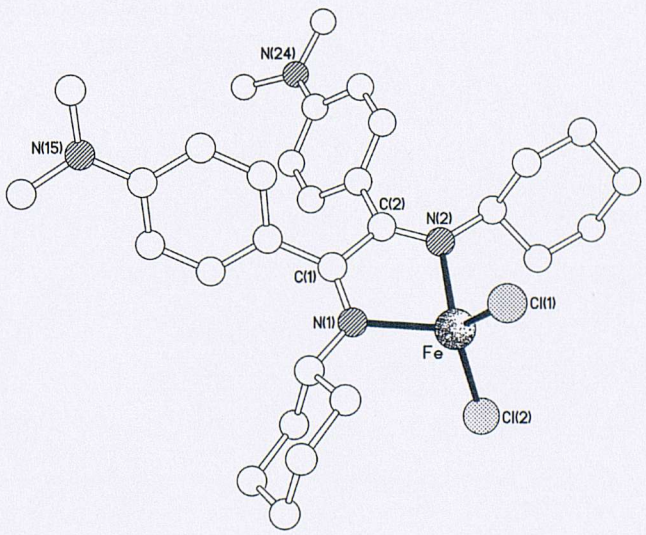


Figure 4.4 The molecular structure of **31.**

Table 4.1 Selected bond lengths (Å) and angles (°) for **31**.

Fe–Cl(1)	2.2438(6)	Cl(1)–Fe–Cl(2)	122.06(2)
Fe–Cl(2)	2.2548(6)	Cl(1)–Fe–N(1)	115.42(4)
Fe–N(1)	2.1040(14)	Cl(1)–Fe–N(2)	105.81(4)
Fe–N(2)	2.1050(13)	Cl(2)–Fe–N(1)	107.39(4)
N(1)–C(1)	1.2890(19)	Cl(2)–Fe–N(2)	119.93(4)
C(1)–C(2)	1.535(2)	N(1)–Fe–N(2)	78.37(5)
C(2)–N(2)	1.2911(19)		

The C=N bonds in **31** are 1.2890(19)-1.2911(19) Å in length; significantly longer than in the aldimine derivative, $^{Cy,H}[N,N]FeCl_2$ (1.239(6) Å) and the methyl ketimine derivative, $^{Cy,Me}[N,N]FeCl_2$ (1.277(3) Å). They are most similar in length to **7**, the 2,3-phenyl substituted complex $^{Cy,Ph}[N,N]FeCl_2$ (1.284(4) Å) and although appear to be significantly shorter than **8**, the electron deficient complex $^{Cy,F\text{-}Ph}[N,N]FeCl_2$ (1.280(15)-1.302(12) Å), the error on these measurements makes an accurate comparison impossible. This implies that both the sterics and electronics of the ligand affect the C=N bond length; **31** has extremely electron-donating groups on the backbone, yet is most similar to a complex with an electron-withdrawing group on the backbone. The Fe–N bond lengths, however, appear to be dependent almost solely on electronics. In **31**, the Fe–N bond lengths of 2.1040(14)-2.1050(13) Å are significantly shorter than the 2.125(4) Å bond length in $^{Cy,H}[N,N]FeCl_2$ and are similar to the 2.102(2) Å Fe–N bond length in $^{Cy,Me}[N,N]FeCl_2$. They are noticeably longer than the Fe–N bond lengths in the electron deficient complexes **7** and **8**, which are 2.077(3) and 2.064(8)-2.094(11) Å, respectively.

The solid state structure of compound **35** (Figure 4.5) contains two independent molecules, both of which were significantly disordered. In each molecule two orientations were identified for the $FeCl_2$, both of the ^tBu, and one of the $Me_2N\text{-}C_6H_4$ moieties. For molecule **I** the occupancies of the major and minor occupancy orientations for the $FeCl_2$, N(1)-^tBu, $Me_2N\text{-}C_6H_4$ and N(2)-^tBu moieties were *ca.* 53:47, 54:46, 58:42 and 51:49% respectively (Figure 4.6, Table 4.2). For molecule **II** the equivalent occupancies were *ca.* 52:48, 60:40, 70:30 and 51:49% respectively. The similarity between the disorder of the two independent molecules means that the

possibility that the crystal studied was a twin cannot be discounted. The data reported here are still sufficient to confirm the chemical nature of the compound.

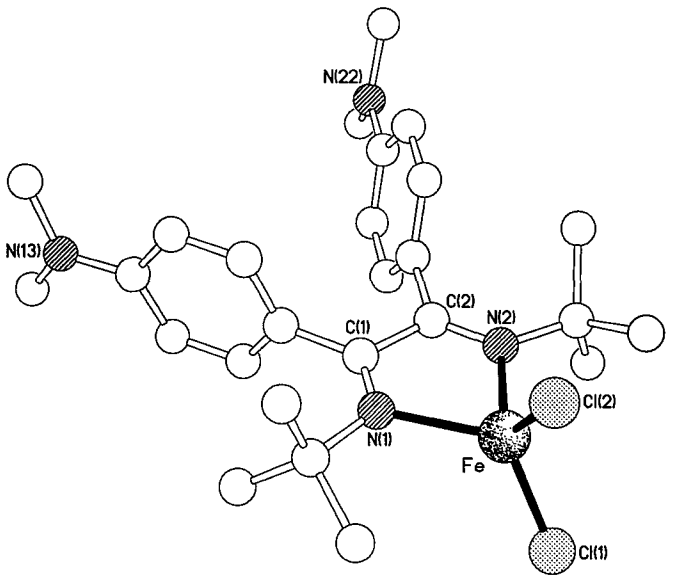


Figure 4.5 The molecular structure of one (**I**) of the two crystallographically independent complexes present in the crystals of **35**.

The crystal structure revealed that in the solid state structure of $^{tBu,Me2N\text{-}Ph}[N,N]FeCl_2$, **35**, N=C-C=N is planar, although in this structure the Fe atom sits *in* the plane, reminiscent of the crystal structures reported for the efficient ATRP catalysts $^{R',H}[N,N]FeCl_2$ where R′ = Cy, ^{t}Bu, $C_{10}H_{23}$.[13,16,17] The same general trends as discussed above for the $^{Cy,R''}[N,N]FeCl_2$ complexes are observed, although the presence of 2 or 3 independent molecules in the unit cells makes the differences less pronounced. The C=N bonds in **35** are 1.271(4)-1.291(5) Å long, which appear longer than the 2,3-aryl substituted complexes **9** and **10**. The C=N bond lengths in $^{tBu,Ph}[N,N]FeCl_2$, **9**, are 1.269(5)-1.285(5) Å, while in $^{tBu,F\text{-}Ph}[N,N]FeCl_2$, **10**, they are 1.280(4)-1.285(4) Å. However, these differences are within the errors on the measurements and so cannot be used to prove conclusive differences between the complexes. The Fe–N bond lengths in **35** are 2.109(3)-2.125(3) Å, which are slightly longer but not significantly different to the Fe–N bond lengths in **9** and **10** (2.112(3)-2.130(3) and 2.100(2)-2.103(2) Å, respectively).

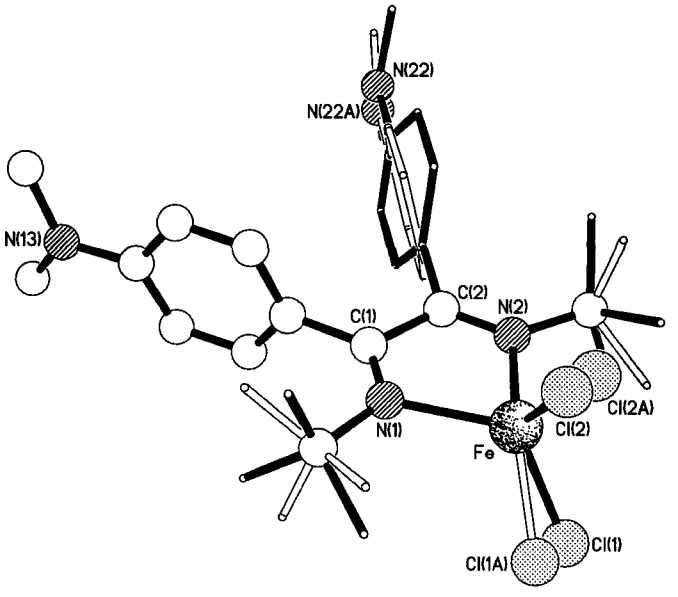


Figure 4.6 The molecular structure of one (**I**) of the two crystallographically independent complexes present in the crystals of **35** showing the disorder in the $FeCl_2$, both of the ^tBu and one of the Me_2N-Ph moieties. In each case the major occupancy orientations are shown with dark bonds, and the minor occupancy orientations with open bonds.

Table 4.2 Selected bond lengths (Å) and angles (°) for the two crystallographically independent complexes (**I** and **II**) present in the crystals of **35** (major occupancy orientations).

	Mol I	**Mol II**		**Mol I**	**Mol II**
Fe–Cl(1)	2.263(3)	2.290(3)	Cl(1)–Fe–Cl(2)	118.40(13)	118.13(16)
Fe–N(1)	2.123(3)	2.125(3)	Cl(1)–Fe–N(2)	107.2(2)	106.9(2)
C(1)–N(1)	1.284(4)	1.291(5)	Cl(2)–Fe–N(2)	119.1(2)	118.1(2)
C(2)–N(2)	1.285(4)	1.271(4)	Cl(1)–Fe–N(1)	118.6(2)	121.8(2)
Fe–Cl(2)	2.275(4)	2.245(4)	Cl(2)–Fe–N(1)	109.1(2)	107.5(2)
Fe–N(2)	2.112(3)	2.109(3)	N(1)–Fe–N(2)	78.29(11)	78.57(12)
C(1)–C(2)	1.537(5)	1.549(5)			

4.2.2 - Polymerisation data.

4.2.1.1 - Styrene polymerisation.

Compounds **28-35** were tested for the ATRP of styrene (200 equiv., bulk), under inert atmosphere at 120°C, using 1-phenylethyl chloride (1-PECl) as the initiator. As seen previously with the fluorophenyl and phenyl derivatives, complexes with electron-withdrawing groups in the *para* position of the phenyl ring (**28**, **29**, **32** and **33**) resulted in polymerisations which proceeded relatively slowly. They required *ca.* 50 hours to reach 90% conversion, with pseudo-first order rate constants of 0.01-0.10 h^{-1}. This is significantly slower than the aldimine derivatives, which reached high conversions in 24 hours, with significantly greater rate constants (0.25-0.27 h^{-1}).[16] Figure 4.7 illustrates this, showing data for complexes **28** and **29** as well as the reported rate for $^{Cy,H}[N,N]FeCl_2$ as a comparison.

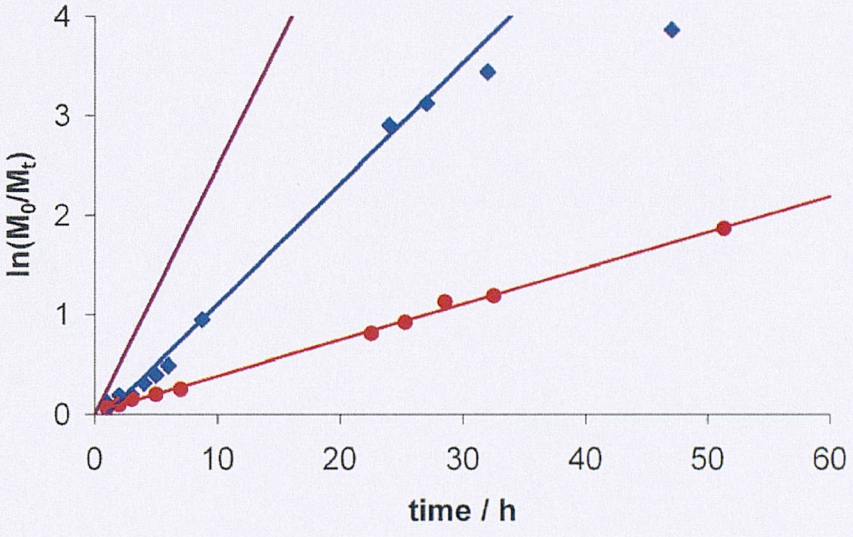


Figure 4.7 Rates for the bulk polymerisation of styrene (200 eq., 1-PECl, 120°C) by $^{Cy,R''}[N,N]FeCl_2$ complexes **28** and **29** (R''= *p*-Me-Ph, ●; R'' = *p*-Br-Ph, ◆). $^{Cy,H}[N,N]FeCl_2$ rate (—) included for reference.[16]

The molecular weight data obtained for these catalysts (**28-29**) showed that the predominant mechanism of polymerisation was not ATRP; molecular weights did not increase linearly with conversion (Figure 4.8). Low molecular weight polymer was isolated, with molecular weights independent of conversion, consistent with the operation of a CCT mechanism. End group analysis by multinuclear NMR spectroscopy revealed the presence of olefinic end-groups at 6.1-6.4 (2H, **) ppm

(Figure 4.9), which correlate to a methine proton at 3.2 (1H, *) ppm. There is no evidence for the chlorine-terminated chains expected from an ATRP mechanism (δ = 4.6) and PDIs are broad, typically ranging from 1.4-2.3 throughout the polymerisation.

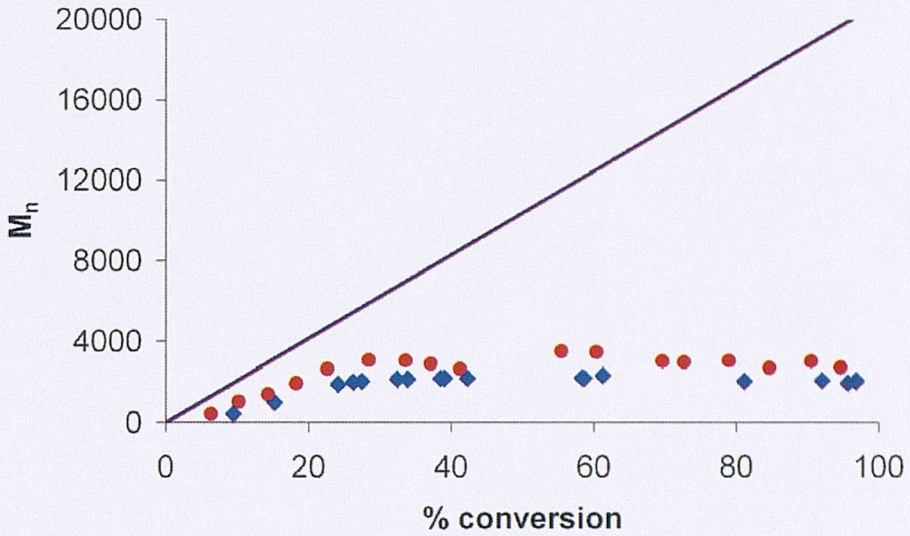


Figure 4.8 Molecular weight *versus* conversion for the bulk polymerisation of styrene (200 eq., 1-PECl, 120°C) by $^{Cy,R''}[N,N]FeCl_2$ complexes **28** and **29** (R″ = *p*-Me-Ph, ●; R″ = *p*-Br-Ph, ◆; $M_{n,th}$ = —).

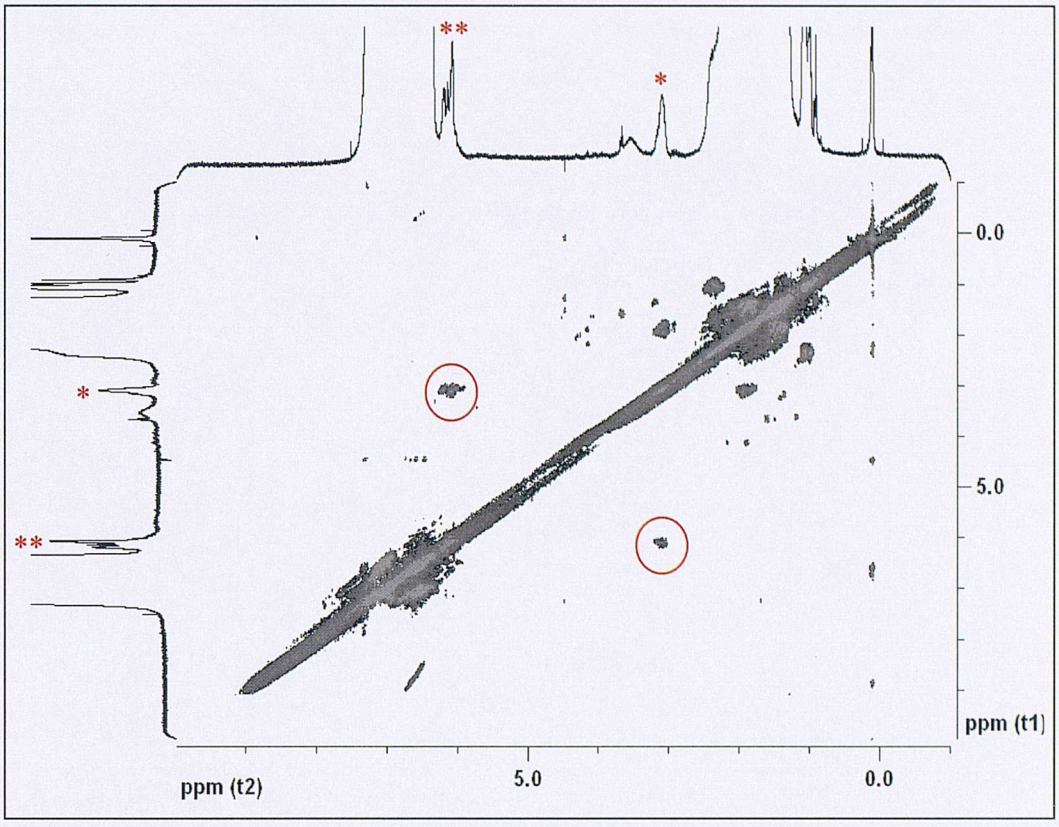


Figure 4.9 COSY spectrum of olefin end groups from a styrene polymerisation using **29**.

Polymerisation of styrene using complexes containing a more electron-donating group at the *para* position of the phenyl ring resulted in a trend in reactivity back towards typical ATRP behaviour (as illustrated by Figures 4.10 and 4.11 for complexes **30** and **31**). In the case of *p*-Me-Ph substituted complexes, **29** and **33**, rates were still relatively slow (0.04-0.06 h^{-1}) and the molecular weight data did not increase linearly with conversion. End group analysis confirmed termination through CCT at 33 monomer units (M_n ~ 3500 Da), a value higher than that obtained for the Ph substituted complexes. A methoxy group in the *para* position, as in complexes **30** and **34**, increased the rate to 0.07-0.10 h^{-1}, and molecular weights showed an initial linear increase with conversion. A limit is reached, at around 8000 Da, and the polymer shows only olefin end groups, with no signals in the ^1H NMR spectrum which can be attributed to halogen end-groups (Figure 4.12). The most electron-donating substituent studied in this series, *p*-Me_2N-Ph, resulted in catalysts which were extremely efficient. Styrene polymerisation rates were extremely fast (0.36-0.72 h^{-1} for **31** and **35**) and the molecular weight was found to increase linearly with

conversion, up until around 85% conversion. End-group analysis showed that the polymer was halogen terminated, with no visible olefin peaks (Figure 4.13).

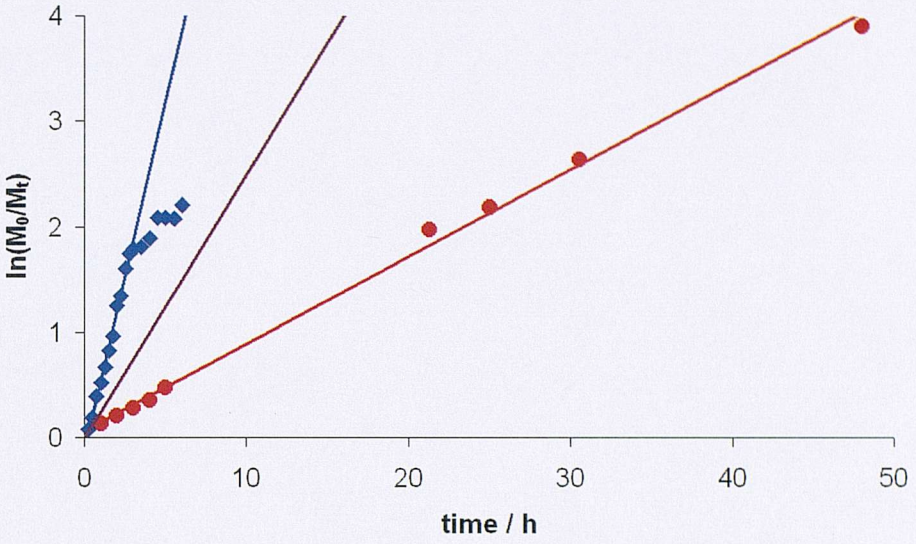


Figure 4.10 Rates for the bulk polymerisation of styrene (200 eq., 1-PECl, 120°C) by $^{Cy,R''}[N,N]FeCl_2$ complexes **30** and **31** (R″ = *p*-MeO-Ph, ●; R″ = *p*-Me_2N-Ph, ◆). $^{Cy,H}[N,N]FeCl_2$ rate (—) included for reference.[16]

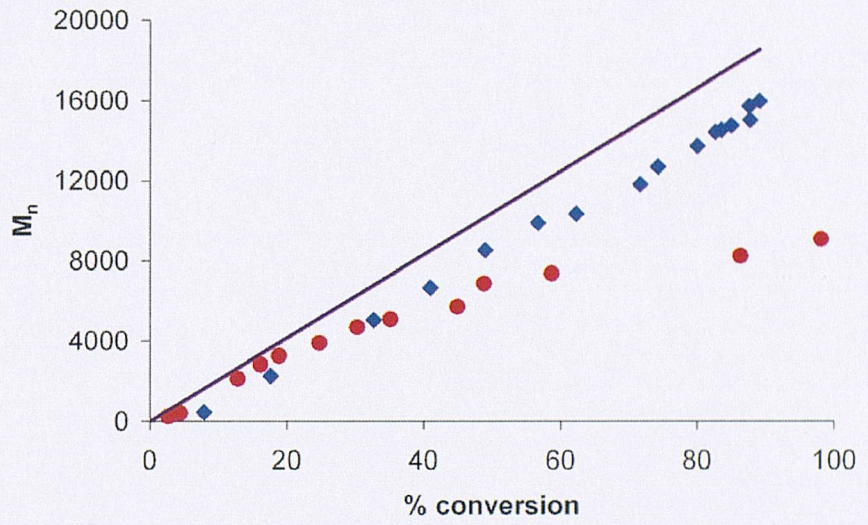


Figure 4.11 Molecular weight *versus* conversion for the bulk polymerisation of styrene (200 eq., 1-PECl, 120°C) by $^{Cy,R''}[N,N]FeCl_2$ complexes **30** and **31** (R″ = *p*-MeO-Ph, ●; R″ = *p*-Me_2N-Ph, ◆; $M_{n,th}$ = —).

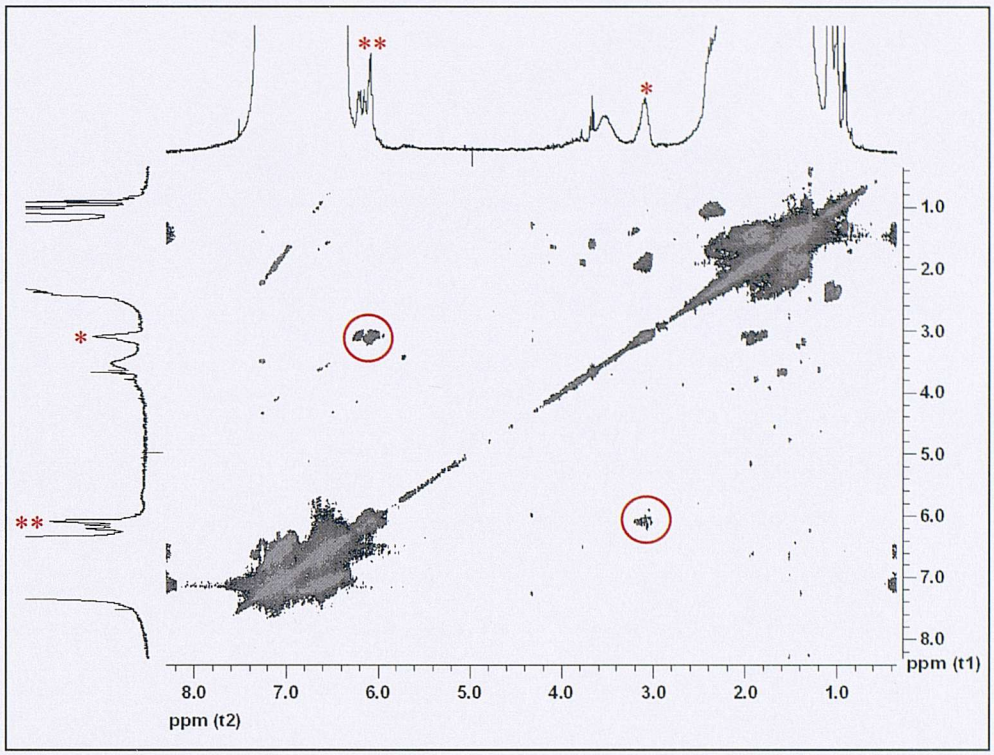


Figure 4.12 COSY spectrum of olefin end groups from a styrene polymerisation using **30**.

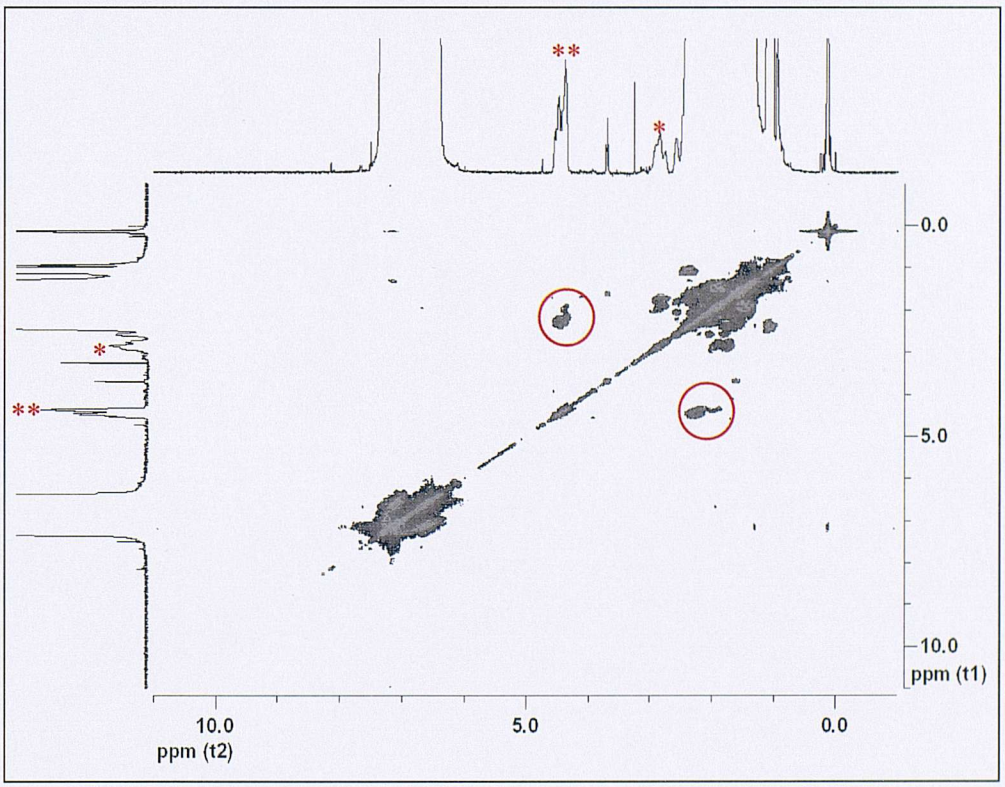


Figure 4.13 COSY spectrum of chlorine end groups from a styrene polymerisation using **31**.

Complex **31** is the fastest ever reported iron-based ATRP catalyst, reaching 85% conversion in 3 hours, and is almost 3 times faster than the aldimine α-diimine catalyst, $^{Cy,H}[N,N]FeCl_2$ (0.72 h^{-1} *versus* 0.25 h^{-1}). It is also 32-46% faster than the salicylaldiminato catalysts, which incorporated tridentate ligands with nitrogen-based donor arms ($k_{obs.}$ = 0.39-0.49 h^{-1}).[18] However, molecular weights for **31** do not correspond perfectly with theoretical values, and are slightly lower than expected. This is attributed to a small amount of termination through CCT, giving olefin-terminated oligomers which can not be reincorporated into the polymer. The PDIs range from 1.2-1.3 until around 75% conversion, where they broaden to 1.4, and it is notable that the GPC traces show an asymmetry, tailing towards low molecular weight and supporting the occurrence of a small amount of chain transfer (Figure 4.14). GC-MS and ^1H NMR spectroscopy (Figure 4.15) confirmed the presence of small amounts of olefin terminated products, isolated from the hydrocarbon-soluble fraction of a polymerisation reaction.

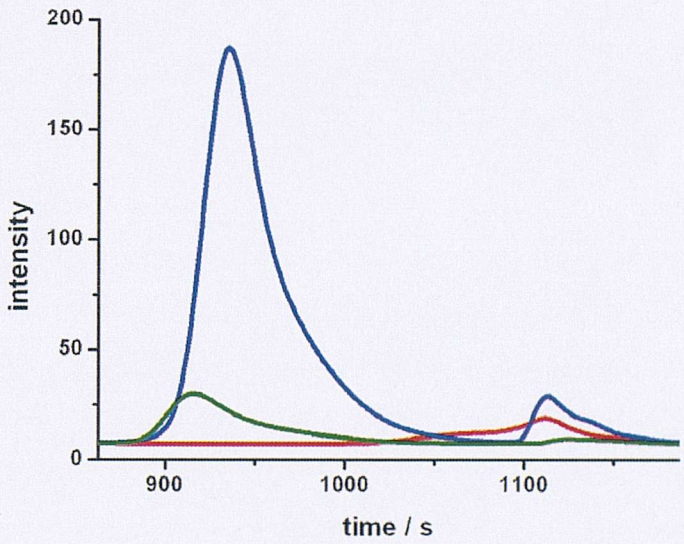


Figure 4.14 Partial GPC traces for $^{Cy,Me2N}[N,N]FeCl_2$, **31**, showing the tailing towards low molecular weight (0.25 h, —; 1.75 h, —; 2.5 h, —).

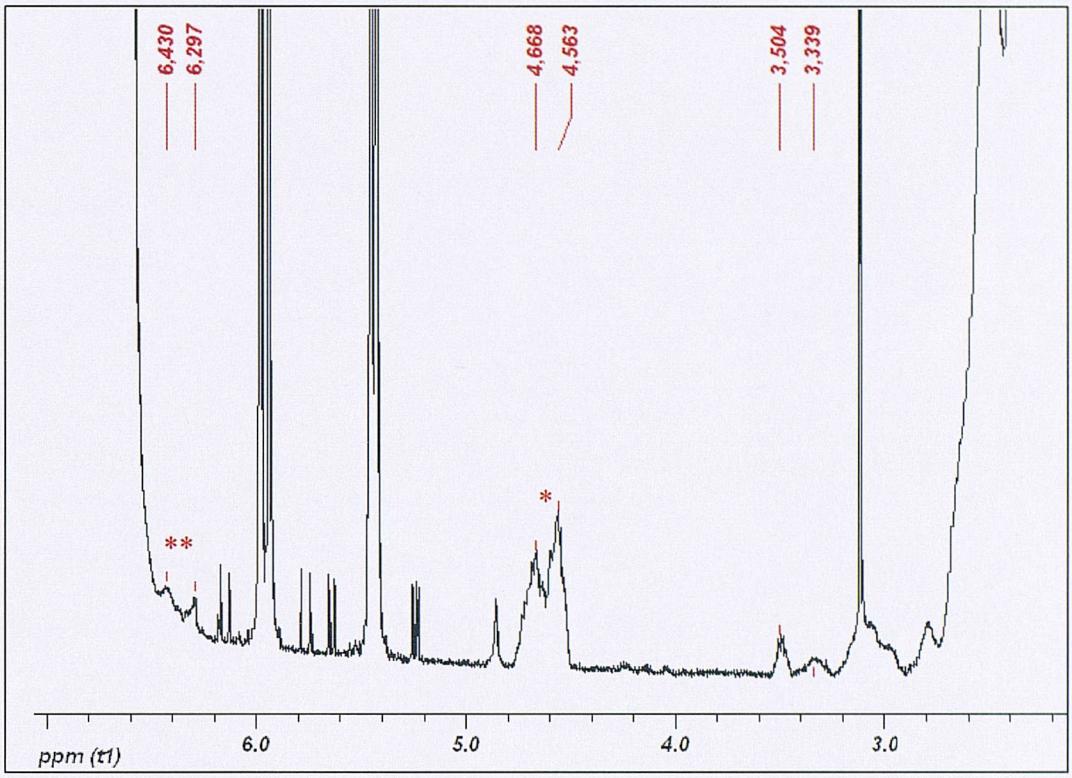


Figure 4.15 ^{1}H NMR spectrum of oligomers isolated from the hydrocarbon-soluble fraction of a polymerisation reaction using **31**, showing both chloro (*) and olefin (**) end-groups.

Similar trends to those described above are seen in the rates and molecular weight data for the ^{t}Bu derivatives, **32-35**. Addition of electron-withdrawing groups to the backbone of the catalysts resulted in the production of low molecular weight, alkene-terminated polymer, whereas electron-donating groups shifted back towards ATRP behaviour. However, due to the greater sensitivity of the ^{t}Bu-substituted complexes, the catalysts had a tendency to decompose with time, often resulting in a sudden increase in rate of polymerisation. As the catalyst dies, thermal polymerisation predominates, leading to an increase in molecular weight. This is illustrated in Figures 4.16 and 4.17 for complex **32**.

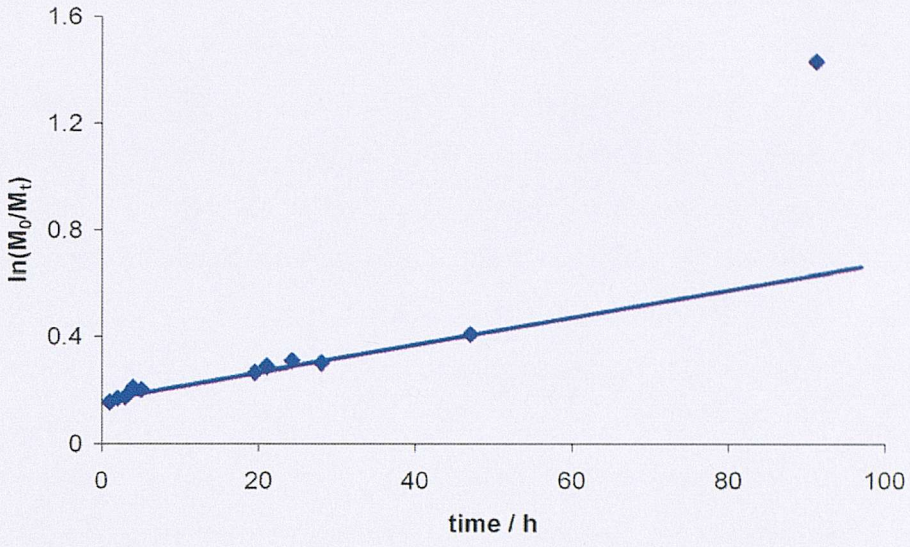


Figure 4.16 Rate for the bulk polymerisation of styrene (200 eq., 1-PECl, 120°C) by $^{tBu,Br\text{-}Ph}[N,N]FeCl_2$, **32**.

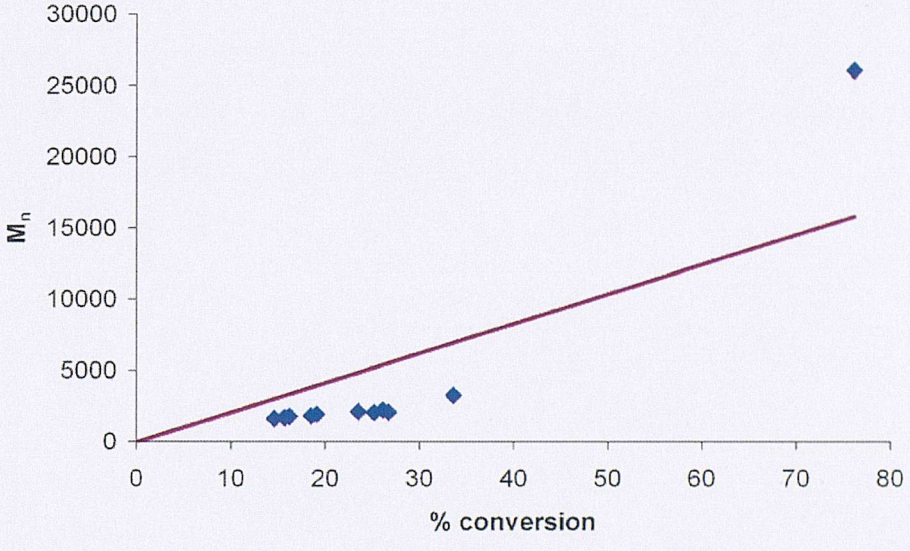


Figure 4.17 Molecular weight *versus* conversion for the bulk polymerisation of styrene (200 eq., 1-PECl, 120°C) by $^{tBu,Br\text{-}Ph}[N,N]FeCl_2$, **32**. ($M_{n,th}$ = —).

The observed rate of styrene polymerisation for $^{tBu,Br\text{-}Ph}[N,N]FeCl_2$, **32**, is 0.02 h^{-1}, which is significantly slower than that observed for the analogous Cy-substituted complex, **28** ($k_{obs.}$ = 0.11 h^{-1}). This may be due to the increased steric bulk around the metal centre; in the case of the ATRP catalysts with H-substituted backbones, the ^{t}Bu-substituted catalyst is slower than the Cy-substituted catalyst ($k_{obs.}$ = 0.19 h^{-1} *cf.* 0.25 h^{-1}).[16] In the case of the catalysts which undergo termination through CCT,

increased steric crowding is likely to play an even bigger role, as it will hinder formation of a bond between the growing polystyrene oligomer and the metal complex. The trapping of the polystyryl radical by the Fe^{II} complex will be more difficult with ^{t}Bu substituents than with Cy substituents, as the metal centre is more sterically crowded by the bulky groups. With formation of the 5-coordinate organometallic species disfavoured, the radicals are likely to undergo bimolecular termination reactions or to react at other sites of the catalyst. This would account for the slow rates of polymerisation, higher than expected molecular weight polymer and observed decomposition of the catalyst.

This trend is continued in the other ^{t}Bu-substituted catalysts. Complex **33**, $^{tBu,Me-Ph}[N,N]FeCl_2$, polymerised styrene with a $k_{obs.}$ of 0.035 h^{-1}, which was significantly slower than the analogous Cy-substituted complex (Figure 4.18). However, there was only a small difference in the molecular weights of polymers produced using complexes **29** and **33**, although this became more noticeable towards the end of the polymerisation, where the ^{t}Bu-substituted complexes were more prone to decomposition (Figure 4.19). Above 60% conversion, the molecular weights for **33** increased from *ca.* 3800 Da to 5000 Da, whereas the molecular weights for **29** remained at around 3000-3500 Da throughout the polymerisation.

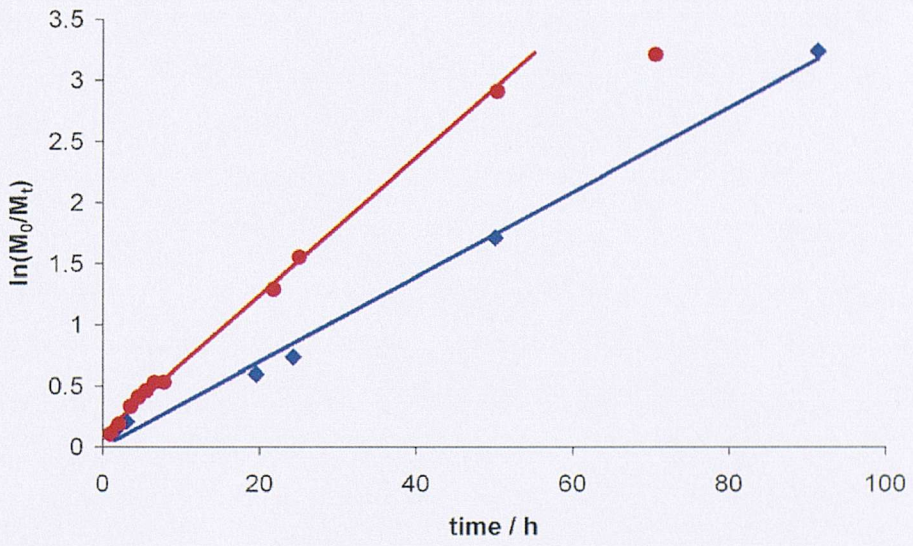


Figure 4.18 Rates for the bulk polymerisation of styrene (200 eq., 1-PECl, 120°C) by $^{R',Me-Ph}[N,N]FeCl_2$ complexes (R′ = Cy, ●; ^{t}Bu, ◆), **29** and **33**.

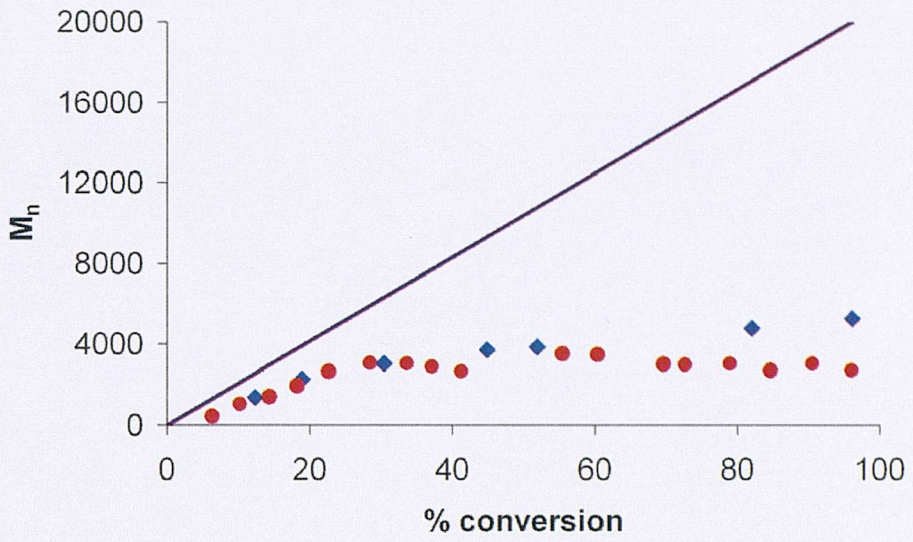


Figure 4.19 Molecular weight *versus* conversion for the bulk polymerisation of styrene (200 eq., 1-PECl, 120°C) by $^{R',Me\text{-}Ph}[N,N]FeCl_2$ complexes (R′ = Cy, ●; ^{t}Bu, ◆; $M_{n,th}$ = —), **29** and **33**.

Inclusion of a more electron-donating methoxy group at the *para* positions of the 2,3-aryl substituted ligand further increased the polymerisation rate of styrene. The rate of reaction for the ^{t}Bu-substituted complex was again slower than the Cy analogue (Figure 4.20). $k_{obs.}$ for **34** was 0.07 h^{-1}, whereas $k_{obs.}$ for **30** was 0.10 h^{-1}, with **34** reaching 75% conversion in 24 h *vs.* 85% conversion for **30**. Molecular weights for the ^{t}Bu-substituted complex were slightly lower than the corresponding Cy derivative in the case of $^{R',MeO\text{-}Ph}[N,N]FeCl_2$ complexes, which may be attributed to the increased prevalence of an ATRP mechanism (Figure 4.21). The initial linear increase of molecular weight with conversion suggests that the ATRP equilibrium is playing a greater role in polymerisations mediated by **30** and **34**; a faster polymerisation will result in the polymer chains reaching higher molecular weights before terminating. The final step is termination via CCT, as the polymer is solely olefin-terminated.

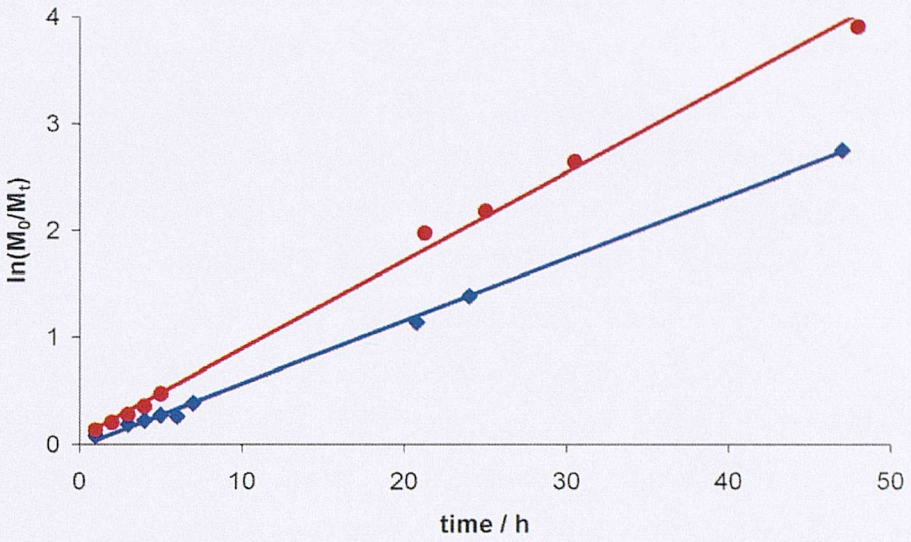


Figure 4.20 Rates for the bulk polymerisation of styrene (200 eq., 1-PECl, 120°C) by $^{R',MeO\text{-}Ph}[N,N]FeCl_2$ complexes (R′ = Cy, ●; ^{t}Bu, ◆), **30** and **34**.

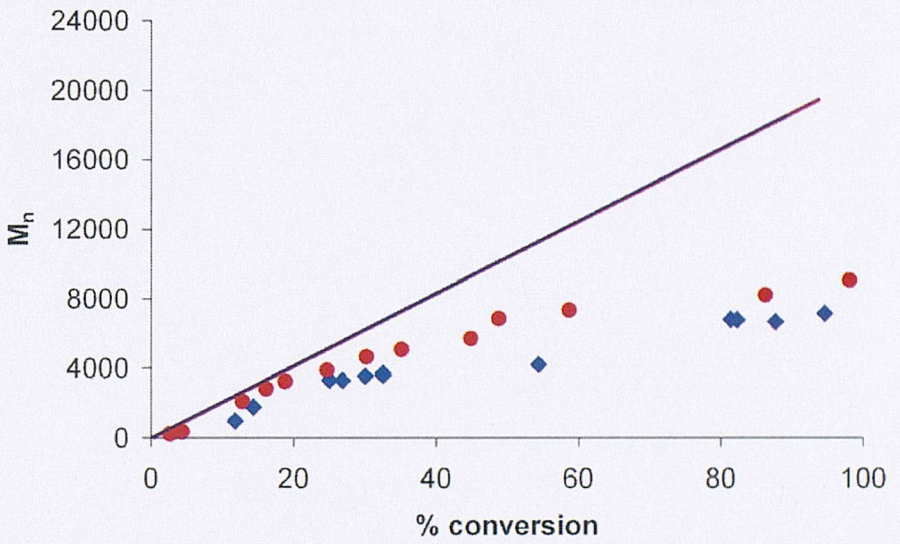


Figure 4.21 Molecular weight *versus* conversion for the bulk polymerisation of styrene (200 eq., 1-PECl, 120°C) by $^{R',MeO\text{-}Ph}[N,N]FeCl_2$ complexes (R′ = Cy, ●; ^{t}Bu, ◆; $M_{n,th}$ = —), **30** and **34**.

Upon moving to the most electron-donating substituent studied in this series, Me_2N-Ph which displays ATRP behaviour, the ^{t}Bu-substituted derivative was again slower than the Cy analogue ($k_{obs.}$ = 0.36 h^{-1}, *cf.* 0.72 h^{-1}) (Figure 4.22). Both complex **31** and complex **35** were actually faster than the previous best α-diimine iron catalyst, $^{Cy,H}[N,N]FeCl_2$, ($k_{obs.}$ = 0.25 h^{-1}). Both $^{R',Me2N\text{-}Ph}[N,N]FeCl_2$ complexes

catalysed the formation of polymer with molecular weights which were slightly lower than theoretical. Molecular weights obtained using $^{tBu,Me2N\text{-}Ph}[N,N]FeCl_2$, **35**, were consistently lower than those obtained using the Cy derivative, **31** (Figure 4.23). It is likely that the slower polymerisation rate seen for **35** results in more of the growing oligomer chains terminating via CCT, meaning that the overall molecular weights are reduced. Reinitiation following the formation of an olefin terminated chain means that there are more growing chains present than are derived solely from the initiator. An increased number of growing chains means that there are fewer equivalents of styrene available to each chain, which will thus not be able to incorporate the full 200 equivalents of monomer. Therefore, even though the majority of the deactivation steps are through ATRP, the polymer samples obtained throughout the polymerisation have molecular weights which are lower than the theoretical values.

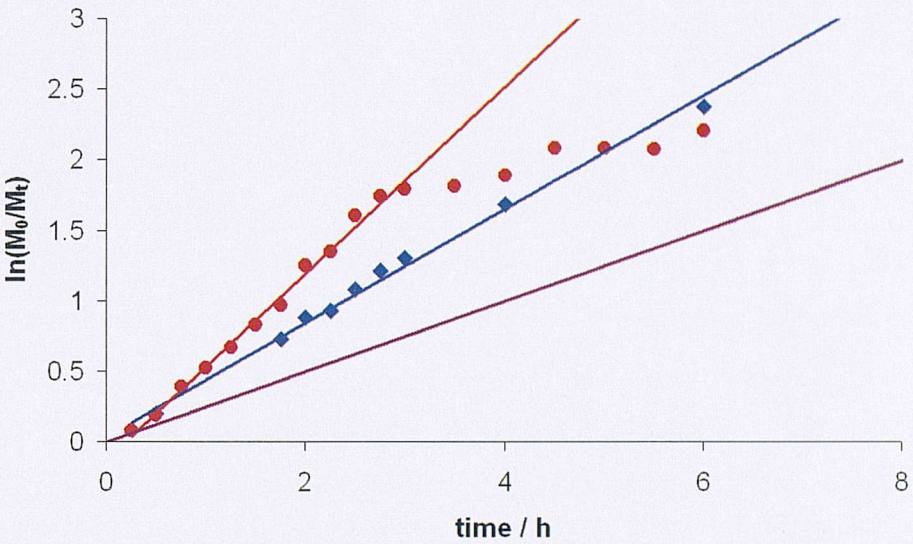


Figure 4.22 Rates for the bulk polymerisation of styrene (200 eq., 1-PECl, 120°C) by $^{R',Me2N\text{-}Ph}[N,N]FeCl_2$ complexes (R′ = Cy, ●; ^{t}Bu, ◆), **31** and **35**. $^{Cy,H}[N,N]FeCl_2$ rate (—) included for reference.[16]

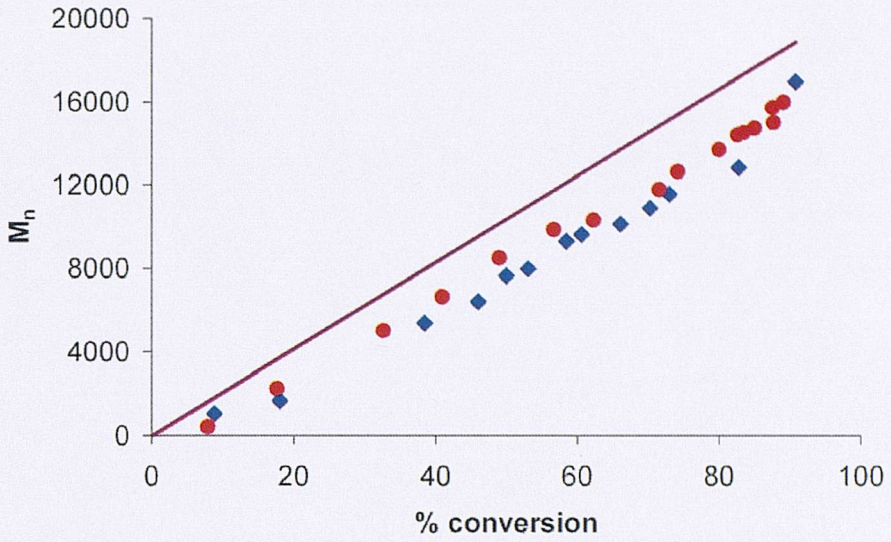


Figure 4.23 Molecular weight *versus* conversion for the bulk polymerisation of styrene (200 eq., 1-PECl, 120°C) by $^{R',Me2N\text{-}Ph}[N,N]FeCl_2$ complexes (R′ = Cy, ●; ^{t}Bu, ◆; $M_{n,th}$ = —), **31** and **35**.

4.2.2.2 - MMA polymerisation.

The complexes which polymerise styrene through CCT (**28-30** and **32-34**) were unsuitable catalysts for the polymerisation of MMA. Similar to the data reported in Chapter 2, molecular weights were significantly higher than theoretical molecular weights and PDIs were broad. However, screening reactions showed that complexes **31** and **35** polymerised MMA by ATRP, as evidenced by molecular weights in good agreement with the theoretical values and narrow PDIs of *ca.* 1.3. Complex **31** was investigated further to assess its suitability as an MMA ATRP catalyst. Although the polymerisation was rapid, molecular weights increased linearly with conversion and PDIs were relatively narrow (Figure 4.25). Figure 4.24 shows the semilogarithmic plot for complex **31**, $^{Cy,Me2N\text{-}Ph}[N,N]FeCl_2$, along with the literature rate for the unsubstituted complex, $^{Cy,H}[N,N]FeCl_2$, as a comparison.

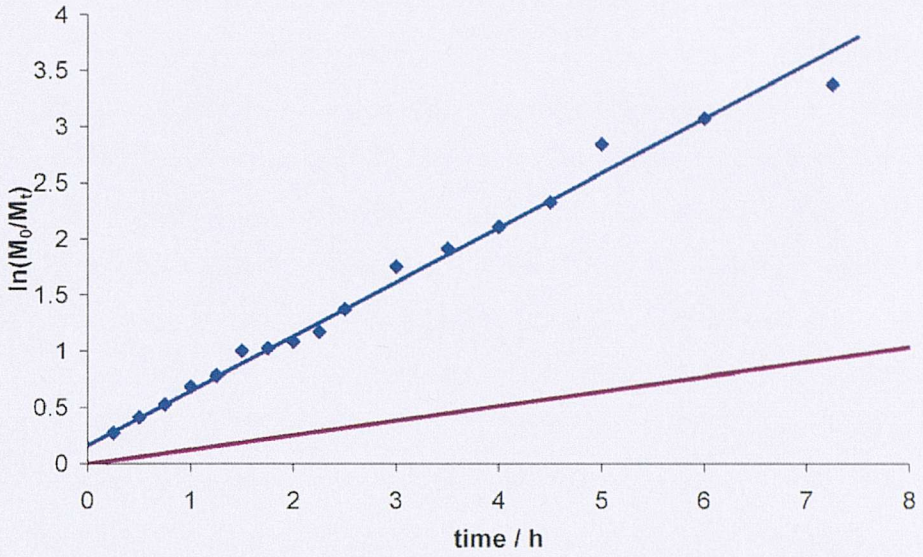


Figure 4.24 Rate for the polymerisation of MMA (100 eq., 33% w/w tol., EBrB, 80°C) by $^{Cy,Me2N\text{-}Ph}[N,N]FeCl_2$, **31**. $^{Cy,H}[N,N]FeCl_2$ rate (—) included for reference.[17]

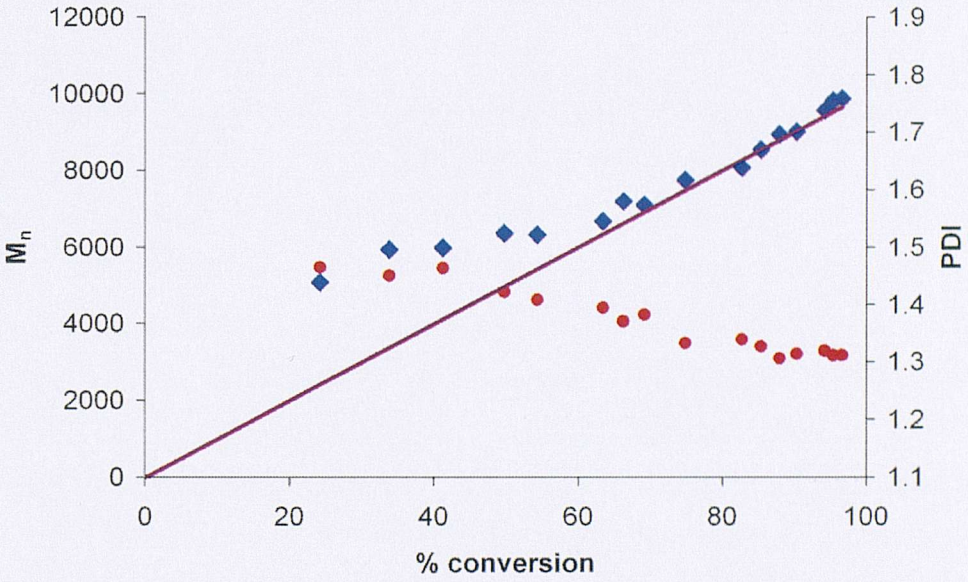


Figure 4.25 Molecular weight and PDI *versus* conversion for the polymerisation of MMA (100 eq., 33% w/w tol., EBrB, 80°C) by $^{Cy,Me2N\text{-}Ph}[N,N]FeCl_2$, **31**, ($M_n$, ◆; PDI, ●; $M_{n,th}$, —).

The rate of polymerisation was extremely rapid ($k_{obs.}$ = 0.49 h^{-1}), with the linear semilogarithmic plot confirming that the radical concentration was constant throughout the reaction. The literature rate of MMA polymerisation using $^{Cy,H}[N,N]FeCl_2$ under similar conditions (100 eq., 10% w/w tol., EBrB, 80°C) is 0.13

h^{-1}, and so complex **31** is extremely efficient, even at a lower concentration. However, the molecular weight control was not as good as the data reported for $^{Cy,H}[N,N]FeCl_2$ as molecular weights were significantly higher than the theoretical values until around 60% conversion. The molecular weight *versus* conversion plot (Figure 4.25) resembles those where the initiator efficiency is low due to a slow rate of activation relative to propagation. Only a fraction of the initiator molecules are activated at a particular time and these chains grow at a regular rate, while another fraction of the initiator remains unchanged. This behaviour results in a broadened PDI, although as the reaction progresses all of the initiator becomes activated and the efficiency factor (*f*) tends to 1 as the PDIs decrease.[19] However, the PDIs were relatively narrow throughout the polymerisation (Figure 4.25) although, as in a typical ATRP reaction, they did decrease slightly as the monomer conversion increased. The dramatic decrease in PDI typically associated with low initiator efficiency due to slow initiation is not observed in MMA polymerisations using **31**, although it is possible that the fast rate of polymerisation did not allow full observation of this trend.

Matching the reactivity of the catalyst and monomer is an important facet of designing a successful ATRP system. MMA is a more reactive monomer than styrene, and catalysts which are effective for one monomer are not necessarily efficient catalysts for the other. Complex **31** is an extremely efficient catalyst for styrene, but this catalyst may be too reactive to allow good control over MMA polymerisation. Figure 4.25 clearly shows that the initial control is poor, and one possible explanation for this is that complex **31** was suitably reactive as to initiate polymerisation at room temperature. If some poorly controlled polymerisation was occurring after preparation of the ampoules inside the glovebox, but before the reactions reached the required experimental temperature (where the atom transfer equilibrium functions efficiently), it would increase the molecular weights and PDIs of those initial points.

This proved to be the case; when the solution containing the monomer, initiator, catalyst and solvent was stirred at room temperature (25°C) for 30 minutes before a sample was removed, the reaction had reached 8% conversion. The molecular weight was extremely high (*ca.* 12,400 Da) and the PDI was broad (1.89). However, a repeat polymerisation, adding the monomer, catalyst and solvent to the ampoule and then allowing it to reach 80°C before addition of the initiator showed only a partial

mitigation of the problem, as it exhibited similar trends in molecular weight and PDI data (Figure 4.26).

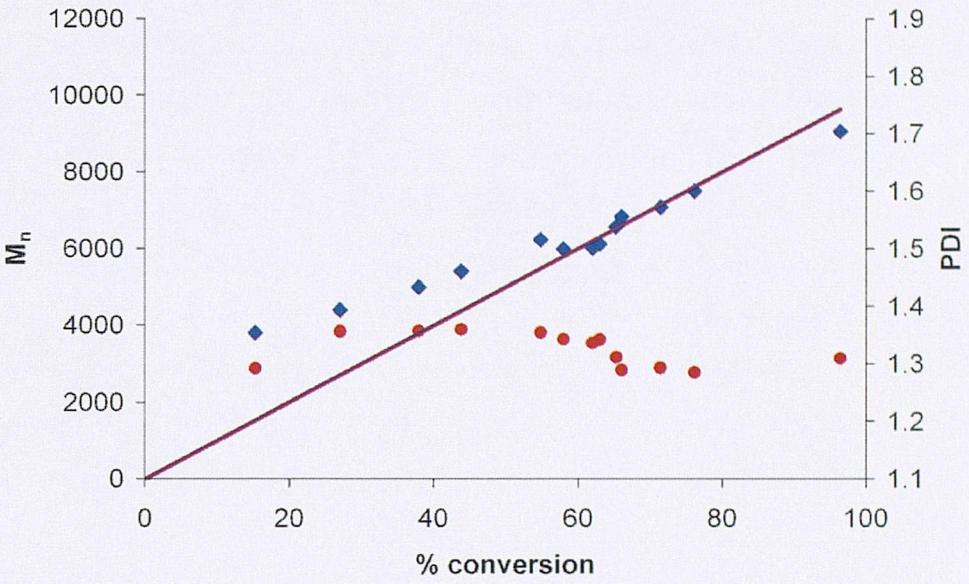


Figure 4.26 Molecular weight and PDI *versus* conversion for the polymerisation of MMA (100 eq., 33% w/w tol., EBrB, 80°C) by $^{Cy,Me2N\text{-}Ph}[N,N]FeCl_2$, **31**, ($M_n$, ◆; PDI, ●; $M_{n,th}$, —).

Again, molecular weights are higher than theoretical although as the polymerisation progresses the molecular weights correspond better to the theoretical values, indicating that there is some delay before the atom transfer equilibrium is functioning efficiently. This could be due to halogen redistribution; using a chloro catalyst and a bromo initiator can cause deviations from the expected behaviour.[20,21] The weaker C-Br bonds, coupled with the higher reactivity of the monomer (MMA is approximately 6 times as reactive as styrene) result in a higher radical concentration, making the polymerisation more difficult to control.

It is obvious that EBrB is not a particularly efficient initiator for the ATRP of MMA using $^{Cy,Me2N\text{-}Ph}[N,N]FeCl_2$. A room temperature halogen abstraction is possible, and the overall initiator efficiency appears to be low. These factors result in molecular weights which are higher than theoretical until around 60% conversion. TosCl was therefore tested for the ATRP of MMA using **31**, with the hypothesis that a less reactive chloro initiator would provide better control over the polymerisation. TosCl should not initiate at room temperature, and also eliminates the bromo / chloro redistribution reactions.

The polymerisation of MMA by $^{Cy,Me2N\text{-}Ph}[N,N]FeCl_2$ under identical conditions (100 eq., 33% w/w tol., 80°C), using TosCl instead of EBrB, proceeded much more slowly, with a $k_{obs.}$ of 0.15 h^{-1}. There was a notable induction period of 2.5 h during which time only limited polymerisation occurred (Figure 4.27), but after that time the semilogarithmic plot of $\ln[M]_0/[M]_t$ *versus* time was linear. Molecular weights were again higher than theoretical, but remained higher throughout the polymerisation (Figure 4.28). This may indicate inefficient initiation due to a slow deactivation rate, whereby the concentration of propagating radicals is high, and so termination through bimolecular reactions occurs.[19] However, the PDIs were fairly narrow throughout the polymerisation (1.38 initially, decreasing to 1.21 at high conversions, see Figure 4.28), indicating that the overall control over the reaction is good. TosCl is an initiator better suited to this system, but is still not ideal.

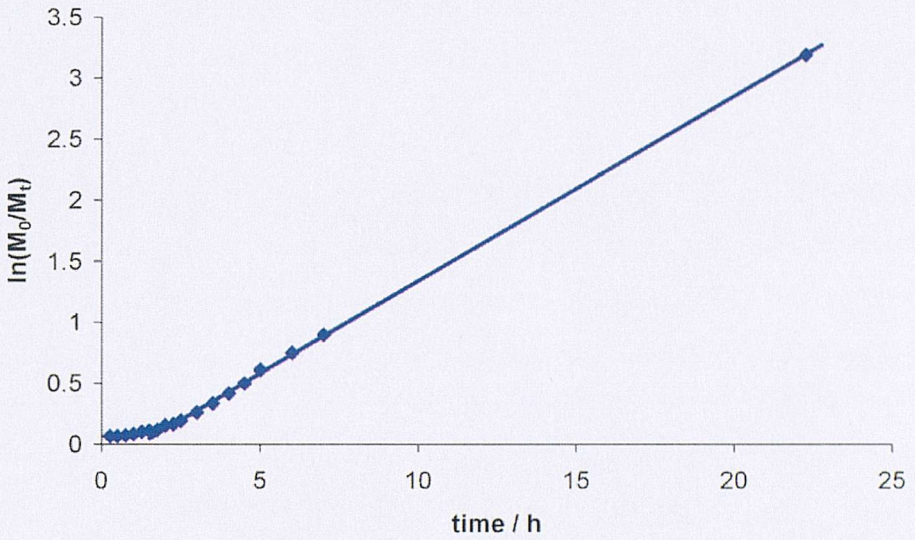


Figure 4.27 Rate for the polymerisation of MMA (100 eq., 33% w/w tol., TosCl, 80°C) by $^{Cy,Me2N\text{-}Ph}[N,N]FeCl_2$, **31**.

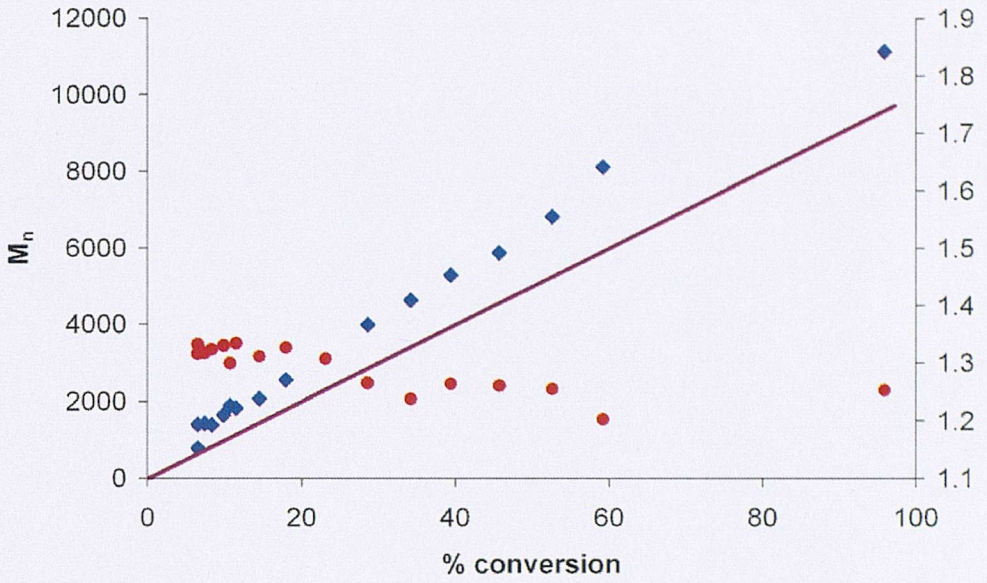


Figure 4.28 Molecular weight and PDI *versus* conversion for the polymerisation of MMA (100 eq., 33% w/w tol., TosCl, 80°C) by $^{Cy,Me2N\text{-}Ph}[N,N]FeCl_2$, **31**, ($M_n$, ◆; PDI, ●; $M_{n,th}$, —).

In order to increase the rate of polymerisation, the amount of toluene in the reaction was decreased. The induction period was still evident, but was shortened to 2 hours, after which the polymerisation proceeded with a constant concentration of radicals (Figure 4.29). $k_{obs.}$ under these conditions was 0.43 h^{-1}; approaching the rate observed with the bromo initiator, EBrB. The faster polymerisation rate had little effect on the molecular weights, which were still consistently higher than the theoretical values (Figure 4.30). The relatively constant deviation from the theoretical values supports the proposal that the initiator efficiency is low. Irreversible loss of some initiator molecules through bimolecular termination reactions would result in fewer propagating chains. These chains would therefore have more than 100 equivalents of monomer available to them, resulting in molecular weights which were always slightly higher than theoretical.

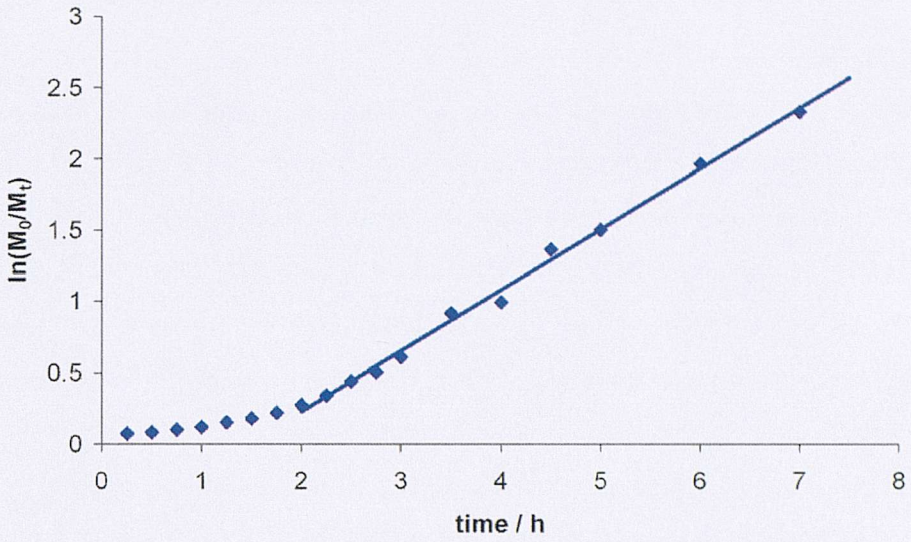


Figure 4.29 Rate for the polymerisation of MMA (100 eq., 10% w/w tol., TosCl, 80°C) by $^{Cy,Me2N\text{-}Ph}[N,N]FeCl_2$, **31**.

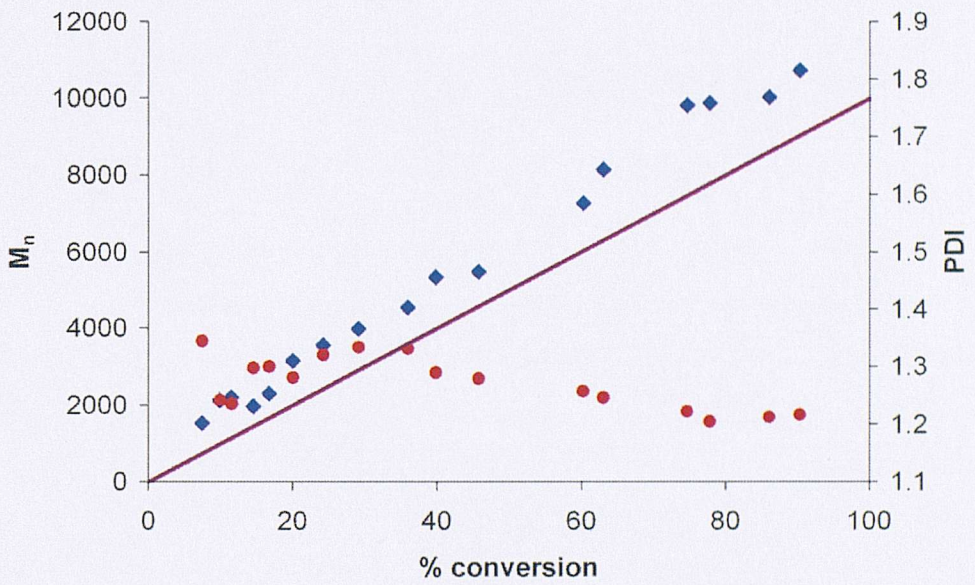
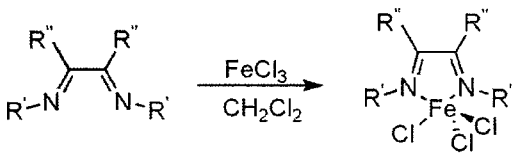


Figure 4.30 Molecular weight and PDI *versus* conversion for the polymerisation of MMA (100 eq., 10% w/w tol., TosCl, 80°C) by $^{Cy,Me2N\text{-}Ph}[N,N]FeCl_2$, **31**, ($M_n$, ◆; PDI, ●; $M_{n,th}$, —).

4.2.3 - Synthesis of Fe^{III} compounds.

The polymerisation data obtained from the range of α-diimine Fe^{II} catalysts studied in this chapter showed that the change in prevalent polymerisation mechanism was continuous rather than discrete. As more electron-withdrawing groups were included, more catalytic chain transfer was observed. Similarly, as more electron-donating groups were included, atom transfer radical polymerisation became more dominant. However, there was not a 'switch' in the mechanism but rather a progression and it appears as if styrene polymerisation using even the extremely electron-donating Me_2N-Ph group results in some chain transfer.

In order to assess whether the origin of the differing polymerisation mechanisms observed with the α-diimine iron catalysts, could still be correlated with spin-state, complexes of the type $^{R',R''}[N,N]FeCl_3$ (where R′ = ^{t}Bu, Cy, and R″ = Br-Ph, Me-Ph, MeO-Ph and Me_2N-Ph) were prepared (Scheme 4.4).



	R′	R″
36	Cy	Br-Ph
37	Cy	Me-Ph
38	Cy	MeO-Ph
39	Cy	Me_2N-Ph

	R′	R″
40	^{t}Bu	Br-Ph
41	^{t}Bu	Me-Ph
42	^{t}Bu	MeO-Ph
43	^{t}Bu	Me_2N-Ph

Scheme 4.4 Synthesis of *para* substituted 2,3-aryl α-diimine Fe^{III} complexes.

Complexes **36-43** did not give meaningful ^{1}H NMR spectra, but the magnetic moment measurements using the Evans' NMR method confirmed the presence of Fe^{III}. The solution magnetic moments for the majority of the 2,3-aryl substituted derivatives, **36-38**, and **40-42** were found in the range 3.9-4.3 B.M., consistent with d^5-intermediate spin Fe^{III} centres. Interestingly, the *para*-dimethylamino substituted complexes, **39** and **43**, exhibited solution magnetic moments approaching high spin (5.6-5.8 B.M.). This difference in spin-state correlates with the switch in polymerisation mechanism displayed by the analogous Fe^{II} complexes and continues the trend exhibited by the $^{R',Ph}[N,N]FeCl_2$ and $^{R',F\text{-}Ph}[N,N]FeCl_2$ complexes, **7-10**, discussed previously: high-spin species catalyse ATRP, whereas lower-spin species give rise to olefin-terminated polymer via CCT.

Despite many efforts, the new Fe^{III} complexes **36-43** could not be characterised crystallographically due to their instability in both solid and solution states and only decomposition or hydrolysis products were obtained. As discussed previously for

$^{R',R''}[N,N]FeCl_3$ complexes where R′ = ^{t}Bu, Cy, and R″ = Ph, F-Ph, disproportionation and decomposition reactions are common in these complexes, which are sensitive to light as well as to air and moisture. Control over the concentration, time and temperature of a reaction was necessary in order to isolate pure complexes.

4.2.4 - SQUID Magnetometry.

In order to further investigate the magnetic properties of the Fe^{III} complexes, and to assess the relationship between catalytic reactivity and spin-state, the Cy-substituted complexes were studied by SQUID magnetometry. The $^{Cy,R''}[N,N]FeCl_3$ derivatives were more stable than their $^{tBu,R''}[N,N]FeCl_3$ counterparts, and this also allowed comparison with the data obtained in Chapter 3.

Variable temperature (2-300 K) DC magnetic susceptibility measurements were carried out by Dr. Floriana Tuna on sealed polycrystalline samples of compounds **36-39**, using a Quantum Design MPMS-XL SQUID magnetometer equipped with a 7 T magnet. Isothermal magnetisation data were collected at 2 and 4 K, with a magnetic field ranging from 1 to 7 T, and zero field cooled (ZFC) magnetic experiments were carried out at different fields ranging from 10 G to 50kG. Diamagnetic corrections for the compounds were estimated from Pascal's constants, and magnetic data were corrected for diamagnetic contributions of the sample holder.

The effective magnetic moments for complexes **36-39** all fell in the region between high and intermediate spin-states (Figure 4.31). The magnetic moment *versus* temperature plots for each of the complexes **36-39** showed a slow, smooth reduction in moment as the temperature was decreased from 300 K down to around 20 K. Below this point, sharper reductions in magnetic moment were observed and the moments tended to decrease rapidly down to 2 K. At these low temperatures, factors such as zero field splitting become more important and it is often the case that the magnetic moments decrease faster. However, there are no sharp transitions, as in a sigmoidal curve, which would be expected for spin crossover systems. Complexes **36-39** are consistent with admixed spin species, incorporating different proportions of the S = 5/2 and S = 3/2 spin-states as the *para* substituent of the phenyl groups at the 2,3-positions of the backbone is changed.

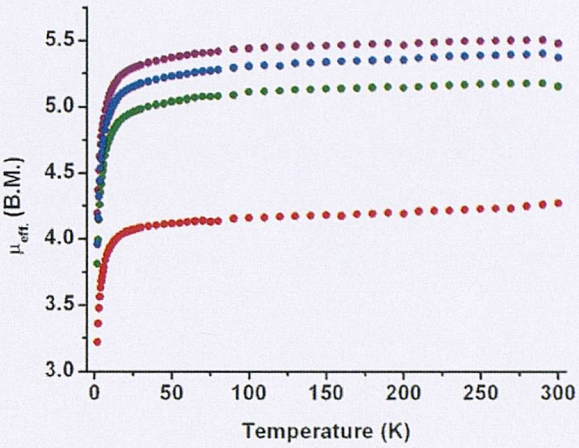


Figure 4.31 $\mu_{eff.}$ *vs.* temperature for $^{Cy,R''}[N,N]FeCl_3$ complexes **36-39** at 10 kG. (R″ = *p*-Me_2N-Ph, ●; R″ = *p*-MeO-Ph, ●; R″= *p*-Me-Ph, ●; R″ = *p*-Br-Ph, ●).

Complex **36**, $^{Cy,Br-Ph}[N,N]FeCl_3$, had a room temperature magnetic moment of 4.28 B.M. This is close to the spin only value expected for an intermediate spin system (3.87 B.M.) and it is likely that complex **36** exhibits a fairly pure S = 3/2 spin-state. The orbital contribution to the magnetic moment can increase the observed $\mu_{eff.}$ up to 4.6 B.M.[22] Due to the nature of these α-diimine iron complexes, and their observed magnetic properties, it is likely that complex **36** also exists in an admixed state, but with a low proportion of S = 5/2 character.

Complex **37**, $^{Cy,Me-Ph}[N,N]FeCl_3$, had a room temperature magnetic moment of 5.37 B.M., somewhat higher than expected, when compared to the other complexes in the series. Complex **38**, $^{Cy,MeO-Ph}[N,N]FeCl_3$, has a lower room temperature $\mu_{eff.}$ of 5.15 B.M. The polymerisation behaviour of the Fe^{II} analogues appears to be sensitive to the spin-state of the complexes, with ATRP equilibrium predominating as the proportion of high spin character increases. Complex **37** is a less efficient ATRP catalyst than complex **38**, with slower polymerisation rates and lower molecular weights. Yet the magnetic moment obtained with **37** is higher than that of **38** (Figure 4.31), which implies that the accuracy limits of the experiments have been reached. With the handling difficulties and sample degradation problems, it is possible that these small differences are within experimental error. Both complexes exhibit magnetic moments which are too high for a pure intermediate spin-state but which are too low for a pure high spin-state, implying the presence of spin admixed states.

Complex **39**, $^{Cy,Me2N\text{-}Ph}[N,N]FeCl_3$, had a room temperature magnetic moment of 5.48 B.M. This is approaching the spin-only value expected for a high spin, S = 5/2, complex (5.91 B.M.) but is significantly lower than the value expected for a pure spin-state. Incorporation of some percentage of the S = 3/2 spin-state, to form an admixed spin-state would explain the lower magnetic moment. This also correlates well with the observation that styrene polymerisation using the Fe^{II} analogue, **31**, is predominantly ATRP but with some CCT.

The polymerisation behaviour of the Fe^{II} complexes studied showed that there is a fine balance between the ATRP and CCT equilibria, and that small changes to the electron-donating ability of the ligand result in incremental changes to the polymerisation. The presence of an admixed spin-state for each of these complexes, incorporating variable proportions of the S = 5/2 and S = 3/2 spin-states, explains why the polymerisation behaviour is continuous rather than discrete. More electron-donating groups at the *para* position result in a higher proportion of S = 5/2 character in the admixture. As the effective magnetic moment increases, with increased electron-donating ability of the *para* substituent, so too does the ATRP behaviour of the Fe^{II} species. The temperature dependent magnetic moments of $^{Cy,R''}[N,N]FeCl_3$ complexes, along with the 'true' high spin complex $^{tBu,H}[N,N]FeCl_3$, are shown in Figure 4.32, and make a compelling case for the presence of admixed species.

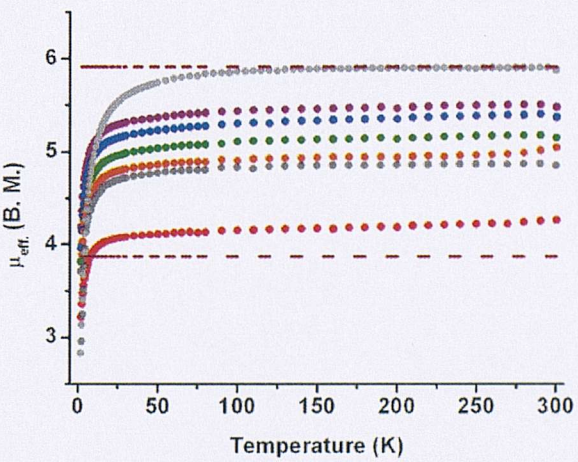


Figure 4.32 $\mu_{eff.}$ *vs.* temperature for $^{Cy,R''}[N,N]FeCl_3$ complexes **13**, **14**, **36-39** and $^{tBu,H}[N,N]FeCl_3$, **15**, (●) at 10 kG. (R″ = *p*-Me_2N-Ph, ●; R″ = *p*-MeO-Ph, ●; R″= *p*-Me-Ph, ●; R″= Ph, ●; R″= *p*-F-Ph, ●; R″ = *p*-Br-Ph, ●). Dashed lines represent spin-only values for high spin (5.91 B.M.) and intermediate spin (3.87 B.M.).

The magnetic behaviour of the complexes offers more evidence for spin admixtures. There is no major dependence of the magnetic moments on temperature, and all complexes obey the Curie-Weiss law. Table 4.3 shows the changes in $\mu_{eff.}$ at selected temperatures, illustrating the relatively small decreases in magnetic moment from 300 K to 20 K and larger decrease in moment from 20 K to 2 K.

Table 4.3. Magnetic moments at selected temperatures for complexes **13-15, 36-39.**

complex	$\mu_{eff.}$ / B.M.		
	300 K	20 K	2 K
$^{Cy,Br-Ph}[N,N]FeCl_3$, **36**	4.28	4.05	3.22
$^{Cy,F-Ph}[N,N]FeCl_3$, **14**	4.86	4.66	2.96
$^{Cy,Ph}[N,N]FeCl_3$, **13**	5.05	4.77	3.71
$^{Cy,Me-Ph}[N,N]FeCl_3$, **37**	5.37	5.12	3.96
$^{Cy,MeO-Ph}[N,N]FeCl_3$, **38**	5.15	4.93	3.81
$^{Cy,Me2N-Ph}[N,N]FeCl_3$, **39**	5.48	5.26	4.20
$^{tBu,H}[N,N]FeCl_3$, **15**	5.90	5.43	2.83

4.2.5 - Correlation of para substituent with reactivity for $^{R',R''}$[N,N]FeCl$_2$ catalysts.

Addition of the electron-withdrawing phenyl groups to the α-diimine backbone results in a switch of the polymerisation mechanism from ATRP towards CCT, despite the presence of the ATRP-directing *N*-alkyl group. When the more electron-withdrawing *para*-fluorophenyl substituents are incorporated, there is a greater prevalence of CCT, the rate is decreased and the polymer obtained is of even lower molecular weight. $M_n \approx 1800$ Da for $^{Cy,F-Ph}[N,N]FeCl_2$, *cf.* $M_n \approx 3400$ Da for $^{Cy,Ph}[N,N]FeCl_2$, which corresponds to approximately 17 insertions of the monomer rather than 33. Similarly, addition of an electron-donating group in the *para* position of the phenyl ring results in an increase both in rate and in the molecular weight of the polymer obtained. The "top-out" molecular weight is ≈ 3500 Da for $^{Cy,Me-Ph}[N,N]FeCl_2$, *cf.* $M_n \approx 7000$ Da for $^{Cy,MeO-Ph}[N,N]FeCl_2$, which corresponds to approximately 34 insertions of the monomer rather than 67. When a strongly electron-donating group is installed in the *para* position, as in the case of $^{Cy,Me2N-}$

$^{Ph}[N,N]FeCl_2$, the mechanism switches back to ATRP and the rate is further increased. The equilibria between the two competing mechanisms are very finely balanced; small changes to the electronics of the ligand backbone dramatically affect the prevalence of ATRP *versus* CCT.

There is a clear correlation between the nature of the *para* substituent of the phenyl ring in the 2,3-aryl substituted complexes and both the rate of styrene polymerisation and molecular weight of polystyrene obtained. As the *para* substituent becomes more electron-donating, the rate of polymerisation increases and the "top-out" molecular weight for the complexes terminating through CCT is higher. A Hammett plot of substituent constant[23] *versus* both $\log(k_X/k_H)$ and the molecular weight at 50% conversion shows a strong linear relationship between 5 of the 6 points, as illustrated by Figures 4.33 and 4.34 (R^2 = 0.996 and 0.994, respectively) for the $^{Cy,R''}[N,N]FeCl_2$ catalysts, **7**, **8**, **28-31**.

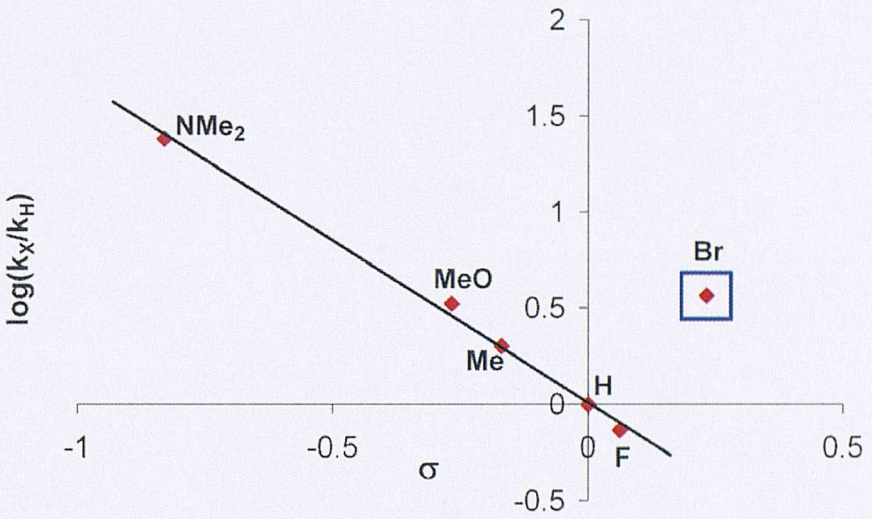


Figure 4.33 Hammett plot showing correlation between substituent constant and rate of styrene polymerisation for $^{Cy,R''}[N,N]FeCl_2$ catalysts.

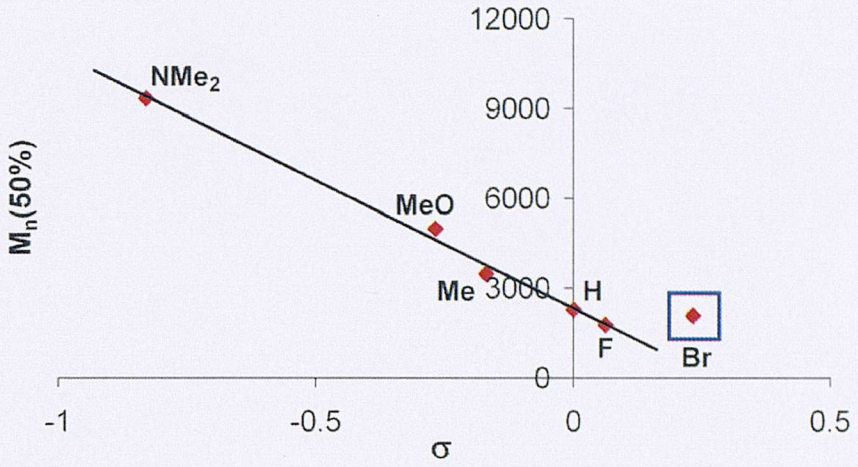


Figure 4.34 Hammett plot showing correlation between substituent constant and molecular weight of polystyrene at 50% conversion for $^{Cy,R''}[N,N]FeCl_2$ catalysts.

The Hammett plots of substituent constant *versus* both $\log(k_X/k_H)$ and molecular weight at 50% conversion also show reasonably good linearity for $^{tBu,R''}[N,N]FeCl_2$ catalysts, **9**, **10**, **32-35** (Figures 4.35 and 4.36; R^2 = 0.963 and 0.982 respectively). The agreement is not as good as for the cyclohexyl-substituted catalysts because there is greater variability in the polymerisation reactions for the more sensitive ^{t}Bu-substituted complexes and the data obtained is not as consistent as for the Cy-substituted complexes.

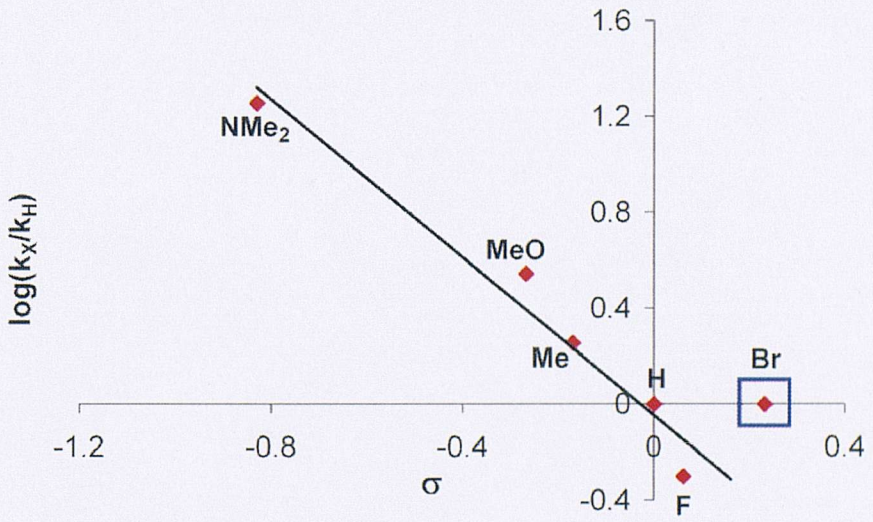


Figure 4.35 Hammett plot showing correlation between substituent constant and rate of styrene polymerisation for $^{tBu,R''}[N,N]FeCl_2$ catalysts.

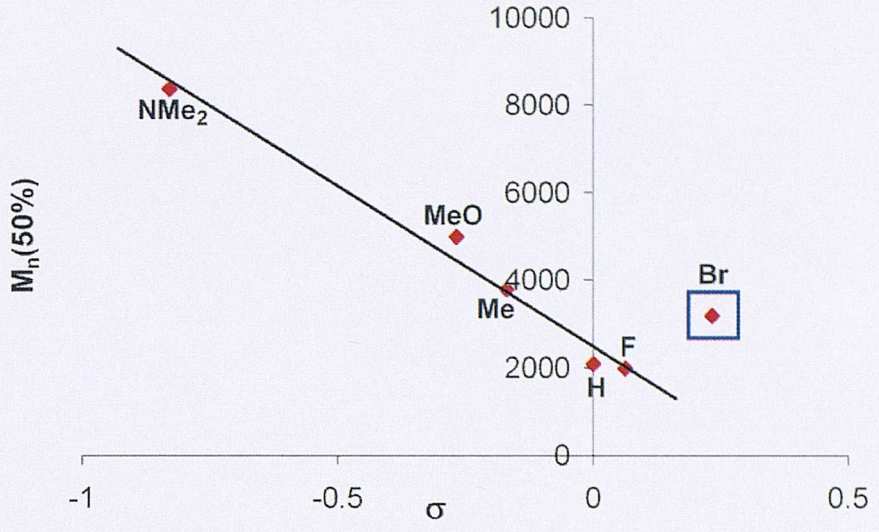


Figure 4.36 Hammett plot showing correlation between substituent constant and molecular weight of polystyrene at 50% conversion for $^{tBu,R''}[N,N]FeCl_2$ catalysts.

The outliers in the Hammett plots are the *p*-Br-Ph substituted complexes, **28** and **32**, which are not consistent with the trends predicted by the other complexes in the series. $^{R',Ph\text{-}Br}[N,N]FeCl_2$ catalysts polymerise styrene at a faster rate than expected and give polymers of higher molecular weights. In order to assess whether this was due to halogen redistribution between the backbone and the iron centre, or the initiator, experiments were carried out using bromobenzene as an additive. $^{Cy,Ph}[N,N]FeCl_2$ and 1-PECl were reacted with 200 equivalents of styrene, at 120°C, in the presence and absence of 2 equivalents of bromobenzene. In the presence of bromobenzene, the rate of polymerisation is increased, although the effect on the molecular weight is minimal (Figures 4.37 and 4.38).

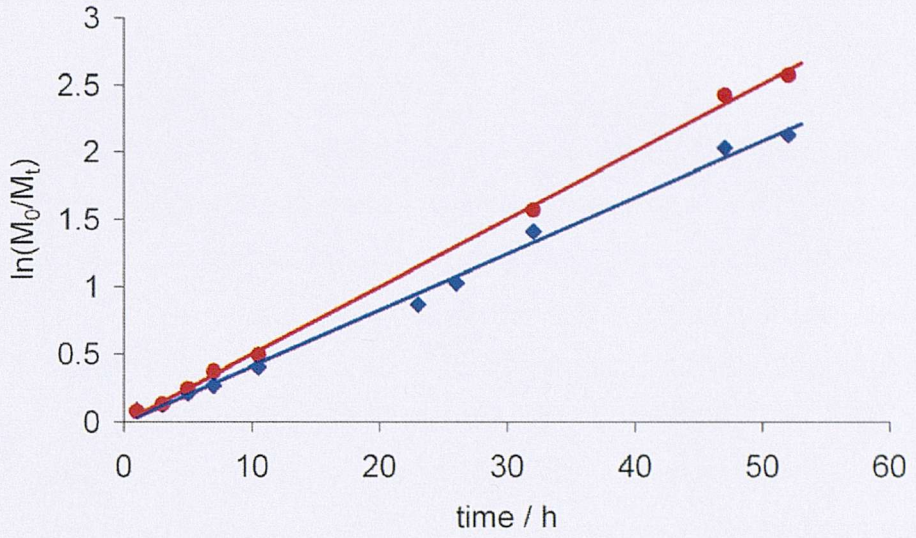


Figure 4.37 Rates for the bulk polymerisation of styrene (200 eq., 1-PECl, 120°C) by $^{Cy,Ph}[N,N]FeCl_2$ (2 equiv. bromobenzene, ●; 0 equiv. bromobenzene, ◆).

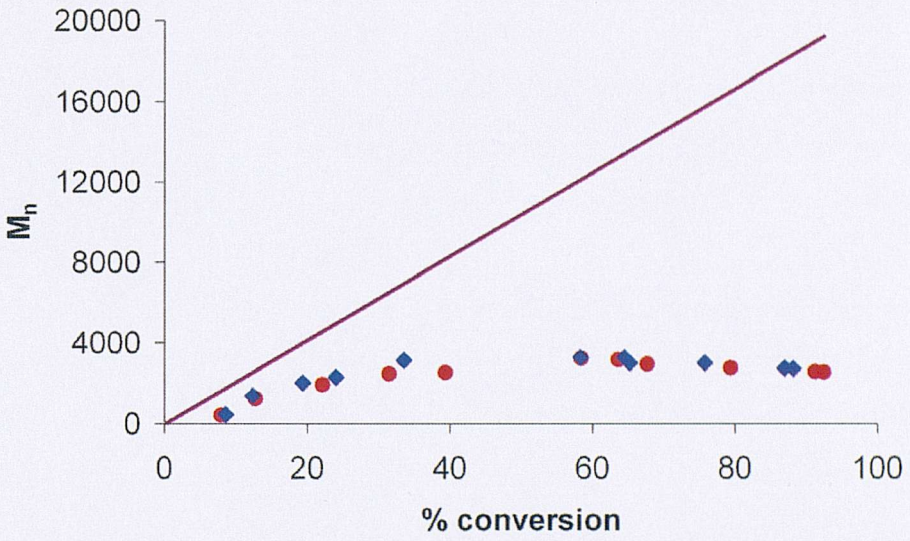


Figure 4.38 Molecular weight *versus* conversion for the bulk polymerisation of styrene (200 eq., 1-PECl, 120°C) by $^{Cy,Ph}[N,N]FeCl_2$ (2 equiv. bromobenzene, ●; 0 equiv. bromobenzene, ◆; $M_{n,th}$, —).

This halogen exchange results in two distinct effects on the catalyst, which have complementary effects on the polymerisation rate. $^{Cy,Br\text{-}Ph}[N,N]FeCl_2$ catalyses faster styrene polymerisation than $^{Cy,Ph}[N,N]FeCl_2$ ($k_{obs.}$ = 0.11 h^{-1} compared with 0.03 h^{-1}). There are two positions in which the bromo group may have an effect- at the *para*

position of the aryl ring, and on the metal centre. The addition of an electron-withdrawing Br group at the *para* position of the aryl ring would be expected to decrease the polymerisation rate. The unexpected increase in rate could be due to loss of the bromine from the *para* position, forming $^{Cy,Ph}[N,N]FeCl_2$ which, according to the Hammett plot, should catalyse faster styrene polymerisation. The other effect involves the behaviour of the free Br group, which is likely to replace the Cl ligands at the metal centre. When bromobenzene is added to a reaction using $^{Cy,Ph}[N,N]FeCl_2$ the polymerisation rate is increased, although the rate is not as rapid as 0.11 h^{-1}. This may be the result of formation of $^{Cy,Ph}[N,N]FeBrX$, as Fe-Br bonds are weaker than Fe-Cl bonds, and polymerisations generally occur faster with a bromo species. Polymerisations using $^{Cy,Br\text{-}Ph}[N,N]FeBrX$ may be even faster and the rapid rate of styrene polymerisation when using the $^{R',Br\text{-}Ph}[N,N]$ ligands may be due to the formation of various mixed species, all of which participate in the reaction.

4.3 - Conclusions

The α-diimine iron complexes $^{R',R''}[N,N]FeCl_2$ are efficient catalysts for the atom transfer radical polymerisation (ATRP) of styrene when R′ and R″ are electron-donating substituents and favour catalytic chain transfer (CCT) when electron-withdrawing substituents are used.

The catalytic reactivity of the Fe^{II} dichloride complexes has been investigated through styrene polymerisation studies and the prevalent polymerisation mechanism has been shown to correlate with the spin-state of the analogous Fe^{III} trichloride complexes. Inclusion of electron-withdrawing groups, such as Ph or F-Ph, at the 2,3-positions of the ligand backbone switches the prevalent polymerisation mechanism from ATRP to CCT and results in lower $\mu_{eff.}$ values. Substituting the *para* position of the aryl groups at the 2,3-positions of the ligand backbone with electron-donating substituents of increasing strength incrementally switches the polymerisation mechanism back towards ATRP, culminating in the $^{Cy,Me2N\text{-}Ph}[N,N]FeCl_2$ catalyst which is the fastest iron-based ATRP catalyst reported to date. The effective magnetic moments of the analogous $^{R',R''}[N,N]FeCl_3$ complexes also increase as the more electron-donating substituents are incorporated, consistent with admixtures of S = 5/2, S = 3/2 where the amount of S = 5/2 character increases with electron donation from the ligand. Detailed Mössbauer spectroscopic analysis is required in

order to fully investigate this issue and conclusively resolve whether the $^{R',R''}[N,N]FeCl_3$ complexes exist as spin admixture isomers or in spin equilibrium.

The Hammett substituent constant, σ, correlates well with both the rate of styrene polymerisation and the "top-out" molecular weight of the polymer obtained, illustrating a structure-activity relationship which can be used to design catalysts to give a specific rate of polymerisation or target molecular weight. The outliers in the Hammett plots, $^{R',Ph\text{-}Br}[N,N]FeCl_2$, **28** and **32**, were investigated through experiments with bromobenzene and $^{Cy,Ph}[N,N]FeCl_2$, which supported the presence of a halogen redistribution effect. Further investigation of this unusual reactivity, through synthesis of the analogous $^{R',R''}[N,N]FeBr_2$ complexes was not pursued. Investigation of the polymerisation behaviour of bromo complexes, both alone and in a mixed system with $^{R',R''}[N,N]FeCl_2$ species, would be a topic for future investigations.

As discussed earlier, the potential link between the ATRP and CCT mechanisms is the OMRP equilibrium. Circumstantial evidence suggests that the CCT events with the α-diimine Fe system occur through a bond-formation β-H elimination mechanism, rather than direct H-transfer. However, this issue has not yet been fully explored or resolved. Chapter 5 will discuss the role of organometallic intermediates in the ATRP and CCT equilibria through a series of experiments designed to further elucidate the mechanistic subtleties.

4.4 - References

(1) Williams, R. J. P., *Fed. Proc. Fed. Am. Soc. Exp. Biol.* **1961,** *20*, 5.

(2) Hoard, J. L.; Hoard, M. J.; Hamor, T. A.; Caughey, W. S., *J. Am. Chem. Soc.* **1965,** *87*, 2312.

(3) Meunier, B.; deVisser, S. P.; Shaik, S., *Chem. Rev.* **2004,** *104*, 3947.

(4) Scheidt, W. R.; Reed, C. A., *Chem. Rev.* **1981,** *81*, 543.

(5) Busson, R.; Beylen, M. V., *Macromolecules* **1977,** *10*, 1320.

(6) Kobayashi, S.; Tokuzawa, T.; Saegusa, T., *Macromolecules* **1982,** *15*, 707.

(7) Qiu, J.; Matyjaszewski, K., *Macromolecules* **1997,** *30*, 5643.

(8) Simal, F.; Jan, D.; Delaude, L.; Demonceau, A.; Spirlet, M.-R.; Noels, A. F., *Can. J. Chem.* **2001,** *79*, 529.

(9) Nakagawa, H.; Sei, Y.; Yamaguchi, K.; Naganoa, T.; Higuchi, T., *Tetrahedron: Asymmetry* **2004,** *15*, 3861.

(10) Jacobsen, E. N.; Zhang, W.; Guler, M. L., *J. Am. Chem. Soc.* **1991,** *113*, 6703.

(11) Palucki, M.; Finney, N. S.; Pospisil, P. J.; Guler, M. L.; Ishida, T.; Jacobsen, E. N., *J. Am. Chem. Soc.* **1998,** *120*, 948.

(12) Popeney, C.; Guan, Z., *Organometallics* **2005,** *24*, 1145.

(13) O'Reilly, R. K. Synthesis of novel iron complexes and their use in atom transfer radical polymerisation. Ph.D. Thesis, University of London, 2003.

(14) O'Reilly, R. K.; Shaver, M. P.; White, A. J. P.; Gibson, V. C., *Macromolecules* **2007,** *40*, 7441.

(15) Kimpe, N. D.; D'Hondt, L.; Stanoeva, E., *Tetrahedron Lett.* **1991,** *32*, 3879.

(16) Gibson, V. C.; O'Reilly, R. K.; Reed, W.; Wass, D.; White, A. J. P.; Williams, D. J., *Chem. Commun.* **2002**, 1850.

(17) Gibson, V. C.; O'Reilly, R. K.; Wass, D. F.; White, A. J. P.; Williams, D. J., *Macromolecules* **2003,** *36*, 2591.

(18) Gibson, V. C.; O'Reilly, R. K.; White, A. J. P.; Williams, D. J., *J. Am. Chem. Soc.* **2003,** *125*, 8450.

(19) Poli, R., *Angew. Chem. Int. Ed.* **2006,** *45*, 5058.

(20) O'Reilly, R. K.; Shaver, M. P.; Gibson, V. C., *Inorg. Chim. Acta* **2006,** *359*, 4417.

(21) Matyjaszewski, K.; Wang, J.-L.; Grimaud, T.; Shipp, D., *Macromolecules* **1998,** *31*, 1527.

(22) Moliner, N.; Real, J. A.; Munoz, M. C.; Martinez-Manez, R.; Juan, J. M. C., *Dalton Trans.* **1999**, 1375.

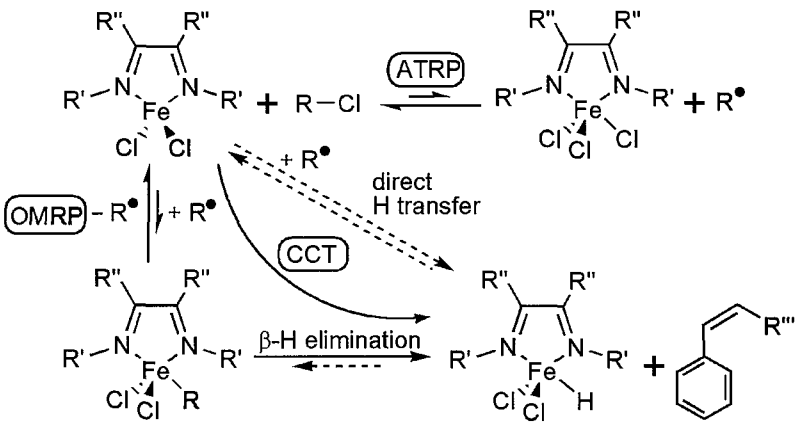
(23) Gordon, A. J.; Ford, R. A. T., *The Chemist's Companion: A Handbook of Practical Data, Techniques, and References.* First ed.; Wiley: New York, 1972.

Chapter 5

Investigating the Polymerisation Mechanism of α-Diimine Iron Catalysts

5.1 - Introduction

In Chapters 2, 3 and 4 the correlation between the spin-state of the α-diimine Fe^{III} trichloride complexes and the observed polymerisation mechanism of styrene using the analogous Fe^{II} dichloride catalysts was discussed. The experimental results led to the hypothesis that all mechanisms are possible and occur simultaneously during the polymerisation. The balance between these equilibria is what determines the prevalent termination mechanism and defines the polymer characteristics (Scheme 5.1). For high spin Fe^{III} complexes the ATRP equilibrium predominates and so the polymerisation proceeds in a typically controlled ATRP manner, to give halogen-terminated polymer chains. For lower spin Fe^{III} complexes the OMRP/CCT equilibria play a greater role and termination through CCT gives low molecular weight, olefin-terminated polymer chains with broad PDIs. The interplay of these various one-electron processes has been recently reviewed.[1]



Scheme 5.1 Possible pathways for radical polymerisation of styrene mediated by α-diimine Fe complexes.

This scheme raises several points for discussion. There are two routes through which the olefin-terminated polymer chains characteristic of a CCT mechanism may be formed. Direct H-transfer is widely believed to be the prevalent mechanism by which the Co porphyrin and cobaloxime systems catalyse chain transfer.[2-5] Thus, CCT is generally regarded as a 2-step process consisting of hydrogen abstraction by the Co^{II} complex, followed by a subsequent reinitiation reaction between the Co^{III} hydride complex and a molecule of monomer. In each case, a direct H-transfer reaction is regarded as most likely mechanistically, although β-elimination of a hydrogen atom from a coordinated radical species is also a noted possibility.[5] In the case of the coordinated radical, bond formation would occur, followed by β-H

elimination to give the vinyl-terminated oligomer. These types of β-H elimination reactions are well-documented in the organometallic literature, often occurring after bond formation between an organic radical and a transition metal complex.[6] Stable organocobalt species have been reported[3,7] and observed through MALDI mass spectrometry[8] and ^{1}H NMR spectroscopy.[9] Reversible cobalt-carbon bond formation has been postulated to have no significant effect in the polymerisation of MMA by CCT, although it does affect the polymerisation behaviour of styrene in this system.[10]

If this latter β-H elimination mechanism is possible, then what of the organometallic Fe^{III} species formed with this system? Potentially, this equilibrium could be used to control a radical polymerisation, in the same manner as has been reported for OMRP using Co,[11] Mo[12] and Os[13] catalysts. Fe^{III} alkyl complexes are relatively rare and often difficult to isolate.[14,15] Many of the reported compounds are porphyrin-based (Figure 5.1, **I**) and are usually synthesised through the reaction of a suitable halide precursor with a Grignard reagent.[16,17] Reaction with super-hydride ($LiHBEt_3$), which unusually transferred an alkyl group,[18] and also with sodium borohydride plus an alkene,[19] are other routes to porphyrin Fe^{III} alkyl complexes. They have also been synthesised through the electrochemical oxidation of the corresponding Fe^{II} complex.[20] The Fe^{III} alkyl porphyrin complexes have been studied in terms of O_2,[18,21] SO_2,[22] CO[23] and CO_2[23] insertion reactions, and one report was particularly interesting as it detailed the effects of spin-state.[24] This study used ^{1}H NMR, EPR and Mössbauer spectroscopies and SQUID magnetometry, and found that for the iron-carbon σ-bonded porphyrins, the Fe atom may be in either a high spin (S = 5/2) state, a low spin (S = 1/2) state, or a mixture of the two. Several factors affected the spin-state, the main one being the nature of the axial and equatorial ligands, although solvent, temperature and sample preparation methods also had an effect. Pure high spin behaviour was observed with perfluoroaryl axial groups (C_6F_4H and C_6F_5), with more electron-donating groups giving predominantly low spin behaviour with some high spin contribution.[24]

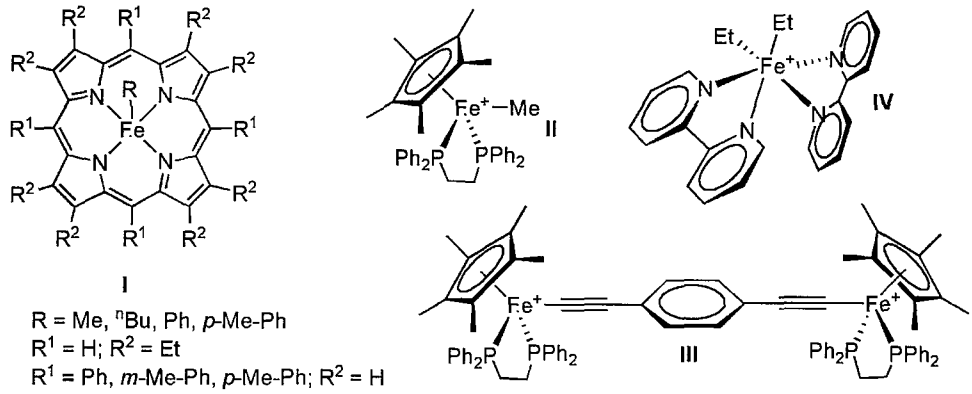
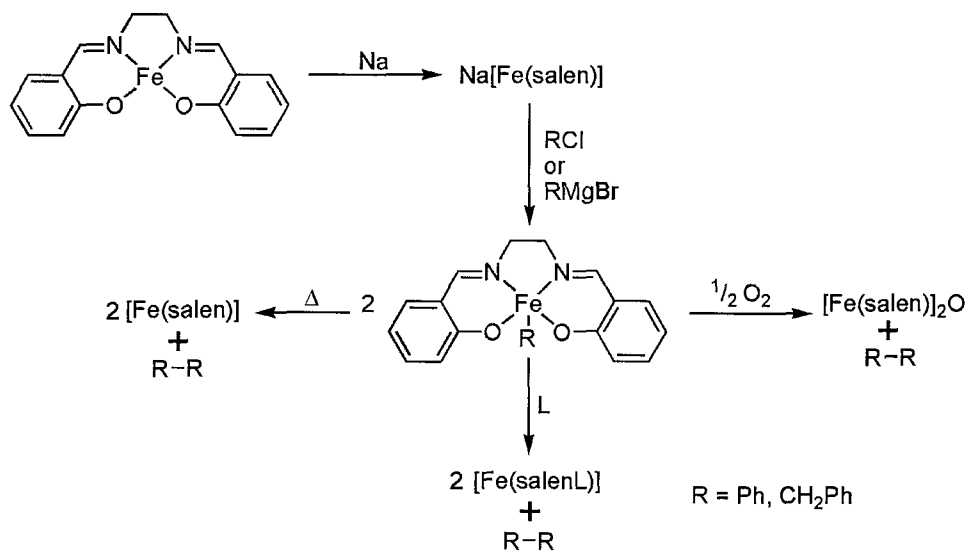


Figure 5.1 Literature Fe^{III} alkyl species.

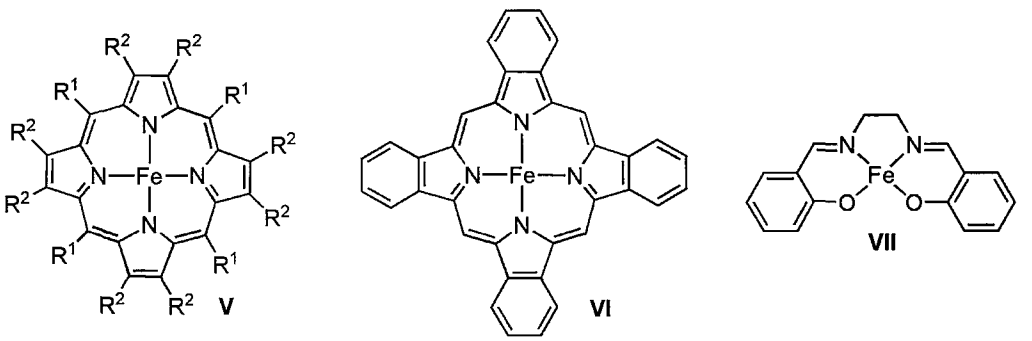
Non-porphyrin Fe^{III} alkyls include the cationic complexes $[Cp^*Fe(dppe)R]^+$,[25-27] and the related dimeric complexes $[\{Fe(\eta^5\text{-}C_5H_5)(\eta^2\text{-dppe})\}_2\text{-}\mu\text{-}(R)][PF_6]_2$.[28,29] These compounds (Figure 5.1, **II** and **III**) have been studied using ^1H NMR, EPR, Mössbauer and IR spectroscopies and X-ray crystallography. More similar to the α-diimine system under investigation in this thesis are those complexes incorporating nitrogen donors, such as the salen Fe^{III} alkyls[30] and $Et_2Fe(bipy)_2^+$ (Figure 5.1, **IV**), which was formed from the electrochemical oxidation of $Et_2Fe(bipy)_2$.[31] The reactivity studies of the salen Fe^{III} alkyls showed that these were unusual high spin organometallic species, which reacted with O_2, N_2 and Lewis bases such as pyridine to give the Fe(salen)L complex and coupled alkyl species (Scheme 5.2).[32]



Scheme 5.2 Synthesis and reactivity of salen Fe^{III} alkyl complexes.

The $^{R',R''}[N,N]FeCl_2$ complexes are established catalysts for ATRP and CCT, but the role of the organometallic equilibria and OMRP in controlling the polymerisation

of styrene in this system is rather less well understood. Relevant to our studies, alkyl iron porphyrin, **V**, phthalocyanine, **VI**, and salen, **VII**, complexes prepared *in situ* have been used to control styrene polymerisation through OMRP (Figure 5.2). The alkyl iron porphyrins undergo facile alkyl group exchange reactions through thermal homolysis of the Fe-C bond.[33,34] This means that they provide a steady state source of radicals at ambient temperature, and are suitable as OMRP catalysts. The analogous halide complexes were active for ATRP, and the author also invoked a 'double protection' scheme whereby both OMRP and ATRP mechanisms were used simultaneously to control the polymerisation.[35] However, the presence of termination reactions such as free radical coupling or disproportionation and β-H abstraction by the Fe^{II} species, resulted in a limited conversion of only 40% under OMRP conditions.



R^1 = Ph; R^2 = H
R^1 = C_6F_5; R^2 = H
R^1 = *p*-$MeOC_6H_4$; R^2 = H
R^1 = H; R^2 = Et

Figure 5.2 Tetradentate iron complexes used in OMRP.

In this chapter, the ability of the $^{R',R''}[N,N]FeCl_2$ catalysts to participate in the OMRP equilibrium and the factors which influence the mechanistic pathways (ATRP *vs.* OMRP) followed in the reactions are explored. The work described in this section was carried out collaboratively with Dr. M. P. Shaver, working in this laboratory. Whilst the relative halogenophilicity *vs.* carbophilicity determines the observed polymerisation mechanism, both halogenophilic and carbophilic reactions assist in controlling the reaction through lowering the radical concentration. Radical concentrations are therefore a useful tool to use in extending the mechanistic understanding from the relative halogenophilicity or carbophilicity of a particular catalyst to the effect of catalyst choice on the absolute halogenophilicity and carbophilicity for styrene polymerisations.

5.2 - Results and Discussion

5.2.1 - β-H elimination versus direct H-transfer.

Reactivity of Fe^{III} compounds

The reactivity of the Fe^{III} α-diimine complexes (synthesised in Chapter 3) was explored to further investigate the effects of the metal spin-state, and to correlate behaviour with the observed polymerisation mechanisms dominant for the analogous Fe^{II} species. While the halogenophilicity of the complexes is exemplified by the clean reaction of $^{R',R''}[N,N]FeCl_2$ species with R-Cl compounds under polymerisation conditions, yielding the coupled product and the corresponding $^{R',R''}[N,N]FeCl_3$ complex, probing the carbophilicity of these systems allowed the differences between the high spin and lower spin admixed complexes to be illustrated.

5.2.1.1 - Alkylation experiments.

Working in collaboration with Dr. M. P. Shaver, alkylation studies were carried out using the lower spin (S = 3/2, S = 5/2) admixed complexes $^{Cy,Ph}[N,N]FeCl_3$, **13**, $^{Cy,F\text{-}Ph}[N,N]FeCl_3$, **14**, $^{tBu,Ph}[N,N]FeCl_3$, **16** and $^{tBu,F\text{-}Ph}[N,N]FeCl_3$, **17**. In order to have a direct comparison of how the relative carbophilicities of the Fe^{II} polymerisation catalysts were affected by the spin-state of the parent Fe^{III} complexes, the reactions were also performed with the high spin (S = 5/2) complexes $^{tBu,H}[N,N]FeCl_3$, **15**, and $^{Cy,H}[N,N]FeCl_3$.

The high spin $^{R',R''}[N,N]FeBnCl_2$ complexes were thermally unstable and decomposed immediately at -78°C to give bibenzyl as the major product through reductive alkylation. However, the lower spin $^{R',R''}[N,N]FeBnCl_2$ complexes produced very different results with the GC analysis showing that toluene rather than bibenzyl was the major product. As the solutions were warmed to –30°C, a colour change coincided with a switch to Bn_2 becoming the major decomposition product. The radical coupling occurred at a much higher temperature than for high spin complexes, implying that the alkyl complexes had improved stability (Figure 5.3).

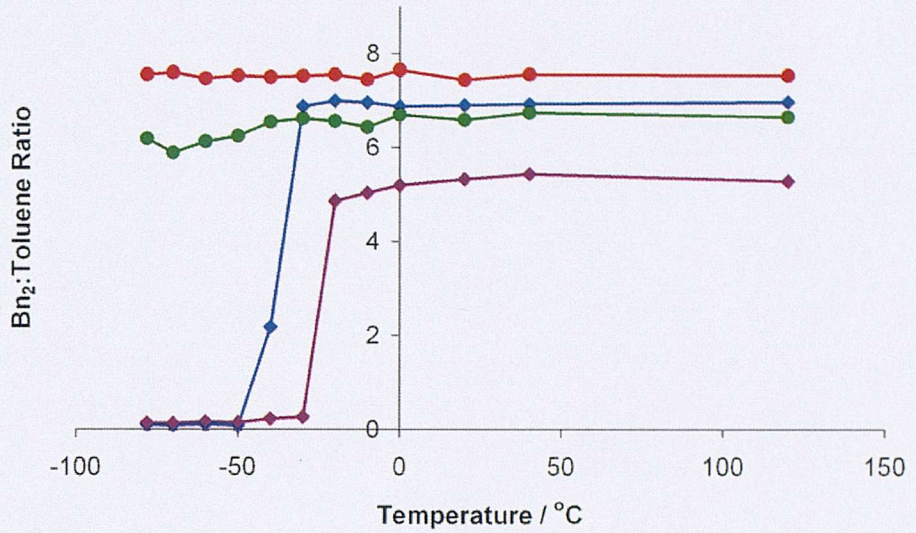
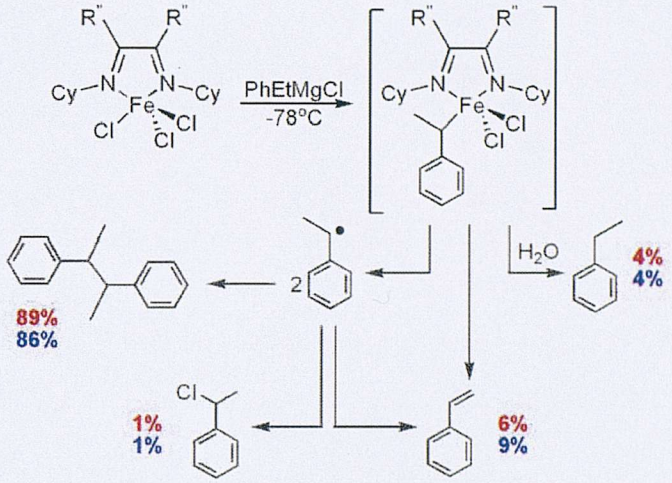


Figure 5.3 Ratio of integrated GC peaks for the formation of bibenzyl and toluene *vs.* temperature arising from the decomposition of $^{R',R''}[N,N]FeCl_2(CH_2Ph)$ complexes (R′ = Cy, R″ = H, ●; R′ = Cy, R″ = F-Ph, ◆; R′ = ^{t}Bu, R″ = H, ●; R′ = ^{t}Bu, R″ = F-Ph, ◆).

The stability of the Fe^{III} alkyl complexes clearly demonstrates a correlation between iron-carbon bond strength and the spin-state of the parent Fe^{III} trichloride complex. High spin (S = 5/2) Fe^{III} complexes show minimal carbophilicity, while substitution of electron-withdrawing aryl groups at the 2,3-positions gives improved thermal stability to the alkyl species, and correlates to a change in the Fe^{III} spin-state to the lower spin admixed species. These admixed spin-state complexes, with intermediate spin character, are more efficient alkyl radical traps and correlate with the switch to catalytic chain transfer as the observed chain termination mechanism. The formation of the organometallic species from the trichloride and a Grignard reagent lends credence to the hypothesis that the catalytic chain transfer route may be β-H elimination rather than direct H-abstraction.

The benzylation reactions do not reproduce the formation of olefinic end-groups in catalytic chain transfer because the $^{R',R''}[N,N]FeCl_2Bn$ intermediates lack β-hydrogens. In order to more accurately reproduce the chemical environment within a polymerisation reaction, Dr. Shaver targeted 1-phenylethyl iron complexes. With the presence of β-hydrogens, a much greater product distribution was observed (Scheme 5.3). For both R″ = H and F-Ph, the major product (accounting for almost 90% of the

organic product formed) was 2,3-diphenylbutane. Styrene (6% for $^{Cy,H}[N,N]FeCl_2(CHMePh)$; 9% for $^{Cy,F\text{-}Ph}[N,N]FeCl_2(CHMePh)$), ethylbenzene (4%), 1-chloro-phenylethane (1%) and other minor products were also observed. The increased stability of the secondary radical promotes longer radical lifetimes and increases the propensity for two radicals to couple. Although the more carbophilic complex may be expected to generate styrene as the major product, if β-hydrogen elimination predominated in these reactions, it would prevent the formation of the oligomers isolated from the polymerisation reactions, with $M_n \approx 2000$ Da.



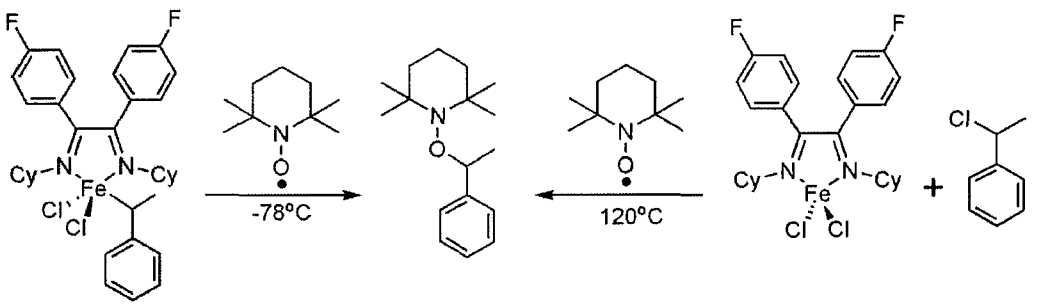
Scheme 5.3 Decomposition pathways for $^{Cy,R''}[N,N]FeCl_2(CHMePh)$ complexes. Yields of products shown for R'' = H (red) and R'' = F-Ph (blue).

While β-hydrogen elimination would directly generate styrene from the alkyl complex, a direct hydride transfer to the Fe^{II} species from the persistent radical would result in the same product. Although styrene is only produced in small quantities, the electron-withdrawing, carbophilic complex, $^{Cy,F\text{-}Ph}[N,N]FeCl_3$, formed 50% more of the olefin product than the halogenophilic complex, $^{Cy,H}[N,N]FeCl_3$. The increased carbophilicity of the complexes containing electron-withdrawing groups means that $^{R',F\text{-}Ph}[N,N]FeCl_2R$ complexes have longer lifetimes, and therefore decomposition through β-H elimination would be expected to generate more styrene. Conversely, a direct hydride transfer mechanism would depend on the concentration of the Fe^{II} complex, rather than on the Fe-R stability. A higher concentration of the Fe^{II} complex would result in a greater probability of phenylethyl radicals reacting with the Fe^{II} species and undergoing H-abstraction to form styrene. However, addition of $^{Cy,F\text{-}Ph}[N,N]FeCl_2$ to the reaction mixture prior to decomposition of the

alkyl complex did not affect the amount of styrene formed. These observations together support the presence of a β-hydrogen elimination mechanism.

5.2.1.2 - Radical trapping experiments.

The major product formed during the decomposition of 1-phenylethyl iron complexes was 2,3-diphenylbutane, which is formed through the coupling of two phenylethyl radicals in solution. Work carried out in collaboration with Dr. Shaver showed that these phenylethyl radicals can also be trapped to form other organic species, and illustrate the efficiency of the α-diimine iron complexes as promoters of halogen atom transfer. Decomposition of the $^{Cy,F\text{-}Ph}[N,N]FeCl_2(CHMePh)$ complex in the presence of TEMPO gave the coupled product shown in Scheme 5.4. The same product can be generated through reaction of the Fe^{II} complex with 1-phenylethyl chloride in the presence of TEMPO (Scheme 5.4), mimicking the ATRP initiation step. The initiation reaction generates phenylethyl radicals, with which the persistent TEMPO radical reacts, coupling to form a new carbon-oxygen bond. The instability of the Fe^{III} species at temperatures above -78°C makes an extensive study of the inorganic products from this reaction impractical and so a full comparison of this system with the copper amide systems investigated by Patten *et al* cannot yet be made.[36,37] While UV-vis studies of these systems indicated that there were no organometallic intermediates present in ATRP using Cu^I, the same conclusions cannot be drawn here.



Scheme 5.4 Trapping of alkyl radicals using TEMPO, from decomposition of $^{Cy,F\text{-}Ph}[N,N]FeCl_2(CHMePh)$ and ATRP initiation reaction using $^{Cy,F\text{-}Ph}[N,N]FeCl_2$.

5.2.1.3 - Catalyst loading.

In the classic Co-based CCT systems, doubling the concentration of catalyst maintains a similar rate of polymerisation but decreases the molecular weight of the short-chain oligomers formed.[2,3,38] As the H-abstraction step is dependent on the availability of the reduced metal complex, the concentration of the catalyst determines how rapidly chain transfer occurs. Having more catalyst present means that the chain transfer events occur faster, and the molecular weights of the oligomers formed are therefore reduced.

Doubling the concentration of $^{Cy,F\text{-}Ph}[N,N]FeCl_2$, **8**, in the α-diimine Fe system from 1 equivalent to 2 equivalents of catalyst doubled the rate of reaction ($k_{obs.}$ = 0.02 h^{-1}, compared with $k_{obs.}$ = 0.04 h^{-1}) but did not significantly change the molecular weight of the polymer obtained. Further increasing the concentration of **8** in the polymerisation reaction to 4 equivalents again doubled the rate ($k_{obs.}$ = 0.08 h^{-1}), but had only a minimal effect on the molecular weights (Figures 5.4 and 5.5), which actually increased slightly with 4 equivalents of catalyst.

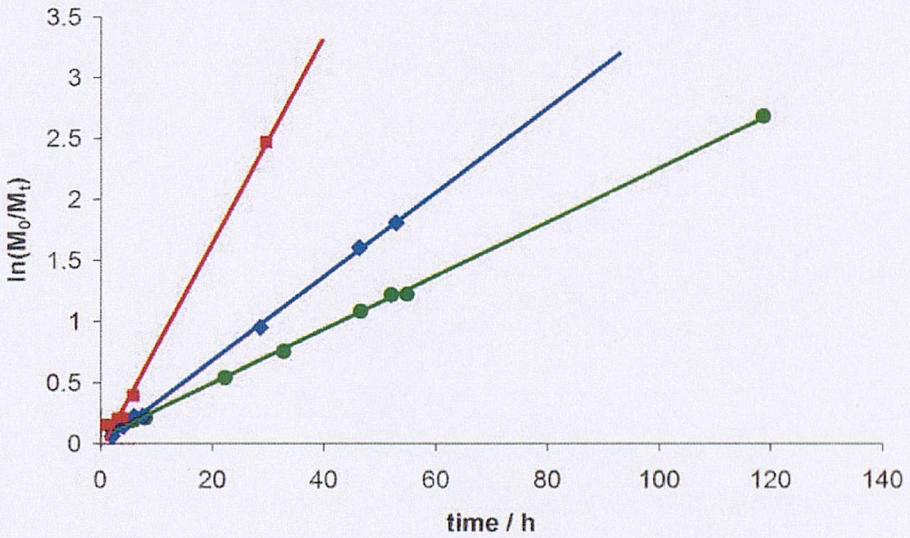


Figure 5.4 Rates for the bulk polymerisation of styrene (200 eq., 1-PECl, 120°C) by different concentrations of $^{Cy,F\text{-}Ph}[N,N]FeCl_2$ (1 equivalent, ●; 2 equivalents, ◆; 4 equivalents, ■).

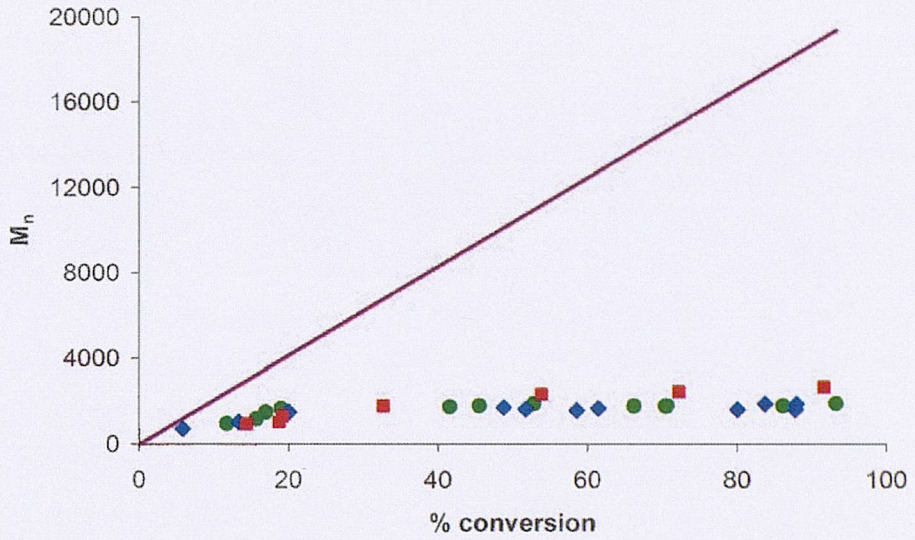


Figure 5.5 Molecular weight *versus* conversion for the bulk polymerisation of styrene (200 eq., 1-PECl, 120°C) by different concentrations of $^{Cy,F\text{-}Ph}[N,N]FeCl_2$ (1 equivalent, ●; 2 equivalents, ◆; 4 equivalents, ■; $M_{n,th}$, —).

This suggests that the α-diimine Fe system does not operate under a traditional direct H-transfer CCT mechanism, but instead undergoes the proposed bond formation followed by β-H elimination mechanism. In this case, the rate of reaction would increase due to a shift in the ATRP equilibrium and an increase in radicals in solution, whilst the organometallic complexes formed would also double in concentration. As both monomer consumption and termination rates are doubled, the observed molecular weight remains the same.

5.2.2 - Radical concentrations and the role of OMRP for $^{R',R''}[N,N]FeCl_2$ catalysts.

If the mechanism by which the CCT products are formed is via a β-H elimination step from an organometallic intermediate, and $^{R',R''}[N,N]FeCl_2$ complexes are able to form $^{R',R''}[N,N]FeCl_2P$ species under ATRP conditions, then it should be possible to enter the OMRP regime and induce polymerisation through an entirely organometallic route. Recent work in our laboratory by Dr. M. P. Shaver has focused on the organometallic pathway illustrated in Scheme 5.1, through both the alkylation studies with the Fe^{III} complexes and OMRP reactions with the Fe^{II} catalysts.[39]

Initial investigations used $^{Cy,H}[N,N]FeCl_2$ and $^{DiPP,H}[N,N]FeCl_2$ complexes with AIBN and 300 equivalents of styrene at 120°C. The polymer products generated

using the high spin, halogenophilic complex, $^{Cy,H}[N,N]FeCl_2$, were bimodal, with broad PDIs. The lower molecular weight peak appeared as a shoulder when 1, 2 and 8 equivalents of catalyst were used, but could be resolved from the higher molecular weight peak when 4.0 equivalents were used. Analysis of the M_p values revealed that bimolecular coupling was the likely source of the two molecular weight components; the lower M_p value of 21,000 Da being almost half the value of the higher M_p value (50,000 Da). As the catalyst loading was increased relative to the AIBN concentration, the lower molecular weight fraction of the polymer increased proportionately, due to the more efficient radical trapping by the Fe^{II} species. With 8 equivalents of catalyst in the polymerisation reaction, the lower molecular weight peak was dominant. $^{DiPP,H}[N,N]FeCl_2$, the lower spin, more carbophilic complex, was a more efficient OMRP catalyst and gave polymers with monomodal distributions. Increasing the catalyst loading decreased the PDIs, and moderate control over the polymerisation was observed with 8 equivalents of catalyst (M_n = 2190, $M_{n,th}$ = 2333, PDI = 1.4). At these high temperatures the Fe-C bonds are extremely unstable and so a high catalyst loading is required in order to obtain moderate control. However, the high catalyst loading means that these polymerisations are extremely slow, reaching only 10% conversion in 48 h.

Using V70 (2,2'-azobis(4-methoxy-2,4-dimethyl valeronitrile)), an initiator which operates efficiently at lower temperatures, gave better control over the polymerisations which were monomodal for both $^{Cy,H}[N,N]FeCl_2$ and $^{DiPP,H}[N,N]FeCl_2$ catalysts, with $M_n \approx M_{n,th}$. PDIs were still somewhat broad (1.5-2.5) except in the case of 2 equivalents of $^{DiPP,H}[N,N]FeCl_2$ (12% conversion, M_n = 3586, $M_{n,th}$ = 3749, PDI = 1.3) However, only low conversions were reached, and kinetic studies showed that irreversible termination occurred at around 25% conversion. Only saturated end groups were observed in the polymer and it was proposed that the acidic protons on the α-diimine backbone could facilitate protonolysis of the growing polymer chain.

Investigation of the 2,3-aryl substituted α-diimine complexes $^{Cy,F\text{-}Ph}[N,N]FeCl_2$, **8**, and $^{tBu,F\text{-}Ph}[N,N]FeCl_2$, **10**, under the same conditions resulted in polymerisations which reached high conversions. However, these complexes did not give good control over the polymerisations as the PDIs were broad (2.0-3.0) and the molecular weight distribution bimodal. End group analysis showed predominantly saturated chain ends, consistent with the OMRP mechanism, although olefin-terminated

groups were also visible. It was hypothesised that these complexes may be too bulky to allow efficient and reversible transfer of the growing polymer chain. The equilibrium would therefore be shifted too far towards the active species, resulting in poor control and multiple termination reactions.

The $^{R',R''}[N,N]FeCl_2$ catalysts exert only modest control over styrene polymerisations under OMRP conditions, but the experiments do support the presence of trapped alkyl radicals in the ATRP equilibria. Control of the polymerisation through the carbophilic regime is mediocre, regardless of the catalyst used. In many ways this is expected since, regardless of the backbone substituent, the Fe^{III} alkyl complexes decompose at low temperatures (-30°C). This means that they will have a short half-life at the polymerisation temperature (120°C). With the OMRP equilibrium shifted towards the Fe^{II} species, the concentration of radicals remains high and control is lost, unless the catalyst loading is increased and the reaction temperature decreased. The broad polydispersities of the polymers obtained indicates that the high radical concentrations are causing side reactions, such as bimolecular termination. But if poor carbophilicity persists across the substitution patterns studied, why is such a drastic switch in polymerisation mechanism observed?

Halogen- and olefin-terminated polymer products are formed in an ATRP reaction because of differences in the *relative* halogeno- and carbophilicities of α-diimine iron catalysts. The efficiency of the Fe^{II} complexes in OMRP can be considered a measure of the *absolute* carbophilicity of the catalysts. Under ATRP conditions, both halogenophilic and carbophilic reactions assist in lowering the radical concentration and thus controlling the reaction. Radical concentrations are an important tool in illustrating how changes in the *absolute* halogenophilicity and carbophilicity of a particular catalyst affect the *relative* halogenophilicity *vs.* carbophilicity and thus the characteristics of the polymer formed. The concentration of radicals is related to the apparent rate constant by Equation 1, where $k_{app.}$ is the apparent rate constant for the polymerisation, and k_p is the propagation rate constant for styrene at a temperature T.[40,41] Values for $[R^\bullet]$ with different α-diimines under ATRP and OMRP conditions are tabulated in Table 5.1.

$$k_{app} = k_p [R^\bullet] \text{ where } k_p = 10^{7.63} \cdot e^{(-32510/RT)} \text{ Lmol}^{-1}\text{s}^{-1} \qquad (1)$$

Table 5.1 Radical concentrations for ATRP and OMRP of styrene using $^{R',R''}[N,N]FeCl_2$.

Entry	R′	R″	k_{app} (s^{-1})	[$R^{\bullet}$] (mol L^{-1})	Mechanism
1	Cy	Me_2N-Ph	2.00×10^{-4}	9.78×10^{-8}	ATRP
2	Cy	H	6.83×10^{-5}	3.34×10^{-8}	ATRP
3	Cy	Me	4.67×10^{-5}	2.28×10^{-8}	ATRP/CCT
4	Cy	MeO-Ph	2.83×10^{-5}	1.38×10^{-8}	ATRP/CCT
5	Mes	F-Ph	1.67×10^{-5}	8.15×10^{-9}	CCT
6	DiPP	H	1.39×10^{-5}	6.80×10^{-9}	CCT
7	Cy	Me-Ph	1.17×10^{-5}	5.72×10^{-9}	CCT
8	Cy	Ph	9.44×10^{-6}	4.62×10^{-9}	CCT
9	Ph	Ph	7.50×10^{-6}	3.67×10^{-9}	CCT
10	Cy	F-Ph	6.11×10^{-6}	2.99×10^{-9}	CCT
11	Cy	H	1.67×10^{-6}	3.47×10^{-9}	OMRP
12	DiPP	H	1.53×10^{-6}	3.19×10^{-9}	OMRP

k_p = 2045 $Lmol^{-1}s^{-1}$ for styrene under ATRP conditions (120°C) and k_p = 480 $Lmol^{-1}s^{-1}$ for styrene under OMRP conditions (70°C).

Entries 1-10 refer to kinetic runs carried out under ATRP conditions and described in either Chapters 2 and 4, or papers detailing these catalysts.[42-44] Entries 11 and 12 refer to kinetic runs carried out under OMRP conditions and reported in a recent paper.[39] A correlation between the radical concentration and polymerisation mechanism is readily apparent. Increased electron donation from the α-diimine ligand leads to higher radical concentrations and substantially faster polymerisation rates. In entries 1 and 2, for $^{Cy,\ Me2N\text{-}Ph}[N,N]FeCl_2$ and $^{Cy,H}[N,N]FeCl_2$, classic ATRP behaviour is observed because the consumption of monomer is fast relative to chain transfer reactions. With complexes such as $^{Cy,Me}[N,N]FeCl_2$ and $^{Cy,MeO\text{-}Ph}[N,N]FeCl_2$, a decrease in [$R^{\bullet}$] and k_{app} slows monomer consumption. In these cases, catalytic chain transfer events become kinetically relevant, and evidence for both mechanisms is observed in the molecular weight data and polymer characteristics. When the polymerisation rates are slowed even further, as with $^{Cy,R''}[N,N]FeCl_2$ when R″ = Ph, Me-Ph and F-Ph, catalytic chain transfer events dominate and short-chain, olefin-terminated polymers are observed.

A comparison of the ATRP and OMRP regimes in the context of radical concentration is also informative. OMRP radical concentrations are lower than those observed under ATRP conditions; [R•] for $^{Cy,H}[N,N]FeCl_2$ under ATRP conditions is 3.34×10^{-8} mol L^{-1}, whereas under OMRP conditions it is 3.47×10^{-9} mol L^{-1}. This indicates that the poor OMRP control is not due to higher radical concentrations, but must result from inefficient exchange between growing polymer chains and dormant species. The difference between the radical concentrations for $^{DiPP,H}[N,N]FeCl_2$ and $^{Cy,H}[N,N]FeCl_2$ under OMRP conditions is relatively minor (entries 11, 12), but under ATRP conditions there is an 8 fold increase in [R•] for these catalysts (entries 2 and 6). The difference in *carbophilicity* between these two catalysts is measurable, but not particularly significant. This leads to the suggestion that the spin-state of the parent Fe^{III} complexes induces a more drastic change in the *halogenophilicity* of the complexes, resulting in the observed change in mechanism.

A lower radical concentration would also have a marked effect on the rate of catalytic chain transfer. A low [R•] would lead to a higher [Fe^{II}] which would favour the formation of the alkyl species and increase the rate of chain transfer. Alternatively, a higher [Fe^{II}] would also increase the rate of direct hydrogen transfer, as both mechanisms are dependent on the concentration of the Fe^{II} species. This agrees quite well with the observed "top-out" molecular weights for various CCT catalysts, discussed in Chapter 4. The lower the radical concentration, the lower the maximum molecular weight observed. For example, $^{Cy,F\text{-}Ph}[N,N]FeCl_2$ has the lowest [R•], the slowest $k_{obs.}$ (0.02 h^{-1}), and the molecular weights top-out at around 2000 Da. $^{Cy,MeO\text{-}Ph}[N,N]FeCl_2$ has a significantly higher radical concentration, a $k_{obs.}$ of 0.10 h^{-1}, and a "top-out" molecular weight of 10,000 Da. $^{Cy,Ph}[N,N]FeCl_2$ is in between those two examples in terms of the [R•], and similarly has an intermediate rate constant ($k_{obs.}$ = 0.03 h^{-1}), and "top-out" molecular weight (3200 Da). These trends are not limited to the Cy-substituted complexes; entries 5 and 9 represent the aryl-substituted catalysts $^{Ph,Ph}[N,N]FeCl_2$, **11**, and $^{Mes,F\text{-}Ph}[N,N]FeCl_2$, **12**. Complex **12** is the faster catalyst, with a $k_{obs.}$ of 0.06 h^{-1} (*cf.* 0.03 h^{-1} for **11**), a [R•] of 8.15×10^{-9} mol L^{-1} (*cf.* 3.67×10^{-9} mol L^{-1} for **11**) and a "top-out" molecular weight of 3300 Da (*cf.* 1700 Da for **11**).

The limited success of OMRP using these catalysts can be attributed to the inability of the organometallic pathway to control the polymerisation alone, because most of the control is actually derived from the atom transfer equilibrium. As shown

in Scheme 5.1, the radical trapping equilibrium disfavours the formation of the unstable Fe^{III} alkyl complex, keeping the radical concentration high unless excessive catalyst loadings are used. This organometallic pathway, whilst not dominant, still provides a route to catalytic chain transfer. Decreased halogenophilicity is provided by electron-withdrawing groups on the catalyst backbone and signified by a decrease in spin-state of the parent Fe^{III} complexes. Under ATRP conditions, the polymerisation slows and causes the termination events to be kinetically relevant, generating CCT products. The α-diimine iron catalysts can effectively control the polymerisation through the ATRP equilibrium, whilst the OMRP equilibrium provides some control and, more importantly, provides a link between halogen-terminated and olefin-terminated polymer products.

The organometallic mediated radical polymerisation studies support the presence of $^{R',R''}[N,N]FeCl_2(P)$ species during the ATRP of styrene catalysed by $^{R',R''}[N,N]FeCl_2$ complexes. Although the complexes studied are inefficient catalysts for the OMRP of styrene, the results clearly show that the atom transfer radical polymerisation equilibria are not necessarily independent from the formation of organometallic species. As in the model studies (section 5.2.1.1), a spin-state effect is observed, with systems which favour lower spin Fe^{III} parent complexes acting as superior catalysts.

5.2.2.1 - Mixed catalyst systems.

Analysis of the radical concentrations in the polymerisation reactions demonstrated that the change from ATRP to CCT behaviour with the α-diimine Fe catalysts is not sudden; rather it occurs as a consequence of a gradual decrease in $k_{app.}$ relative to the chain-transfer reactions. This is consistent with the discussion in Chapter 4 that the rates and "top out" molecular weights of polymers obtained using the *para*-phenyl substituted $^{R',R''}[N,N]FeCl_2$ catalysts decrease as the electron-withdrawing ability of the *para* group increases. This gradual switch in mechanism should be reproduced through mixing an efficient ATRP catalyst with a catalyst which gives termination through CCT. Varying the relative amounts of the ATRP and CCT catalyst was anticipated to allow control over the rate of polymerisation and molecular weight of the polymer obtained. Indeed, it should be possible to mimic the polymerisation behaviour of all the *para*-phenyl substituted catalysts simply by increasing or decreasing the CCT component.

Styrene polymerisations were conducted using a mixed catalyst system comprising the halogenophilic catalyst $^{Cy,H}[N,N]FeCl_2$ and a catalyst with decreased halogenophilicity and increased carbophilicity, $^{Cy,F\text{-}Ph}[N,N]FeCl_2$, **8**, in ratios of 9:1, 3:1 and 1:1. These reactions showed that, despite an overall loss in control, an increased concentration of **8** both decreased the rate (Figure 5.6) and lowered the molecular weight (Figure 5.7) of the resultant polymer. The polymerisation rate using 10% $^{Cy,F\text{-}Ph}[N,N]FeCl_2$ was 0.20 h^{-1} but decreased significantly to 0.09 h^{-1} when 25% of **8** was present and 0.06 h^{-1} with 50% of **8**. As the concentration of the CCT catalyst was increased, the radical concentration decreased and the chain termination reactions increased. This resulted in a decrease in molecular weights and asymmetrical molecular weight distributions; a pronounced tailing towards lower molecular weights is observed and can be attributed to the increase in the proportion of chain transfer events (Figure 5.8).

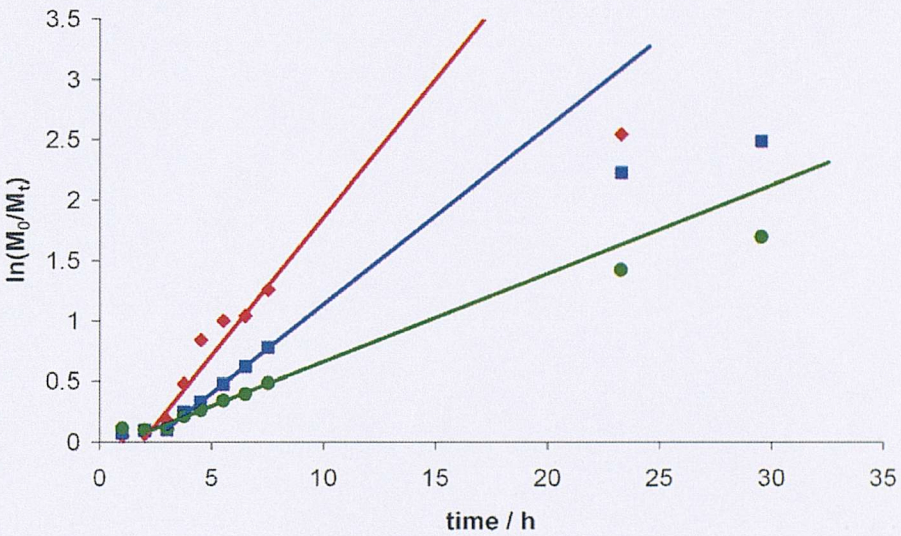


Figure 5.6 Rates for the bulk polymerisation of styrene (200 eq., 1-PECl, 120°C) by mixed catalyst systems containing different ratios of $^{Cy,H}[N,N]FeCl_2$ and $^{Cy,F\text{-}Ph}[N,N]FeCl_2$ complexes (9:1, ◆; 3:1, ■; 1:1, ●).

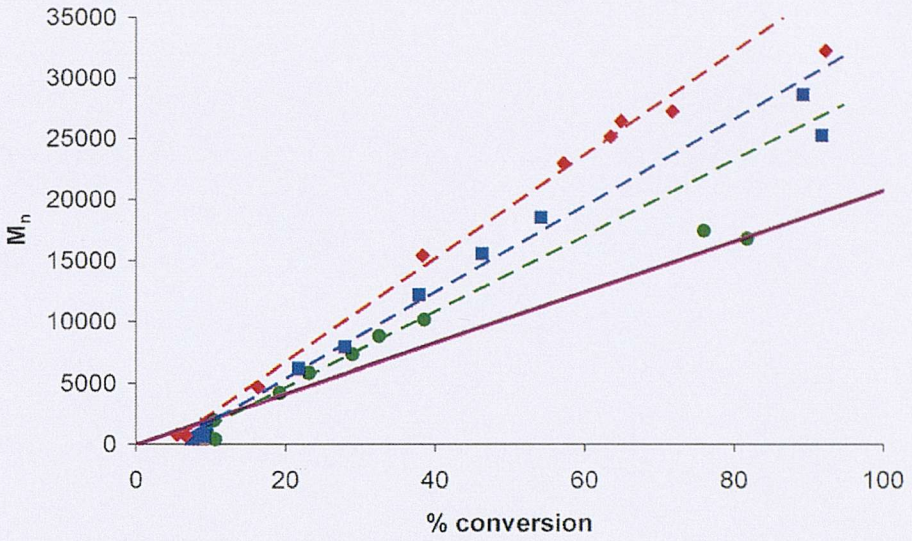


Figure 5.7 Molecular weight *versus* conversion for the bulk polymerisation of styrene (200 eq., 1-PECl, 120°C) by mixed catalyst systems containing different ratios of $^{Cy,H}[N,N]FeCl_2$ and $^{Cy,F\text{-}Ph}[N,N]FeCl_2$ complexes (9:1, ◆; 3:1, ■; 1:1, ●). Dashed lines illustrate linear increase of molecular weight with conversion.

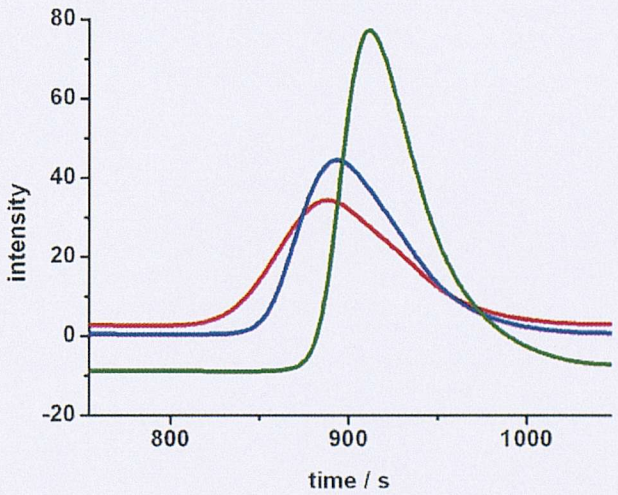


Figure 5.8 Partial GPC traces of 23 h samples for the bulk polymerisation of styrene (200 eq., 1-PECl, 120°C) by mixed catalyst systems containing different ratios of $^{Cy,H}[N,N]FeCl_2$ and $^{Cy,F\text{-}Ph}[N,N]FeCl_2$ complexes (9:1, —; 3:1, —; 1:1, —).

To attempt to overcome the loss in control using the $^{Cy,H}[N,N]FeCl_2$ catalyst, the experiments were repeated using different ratios of $^{Cy,Me2N\text{-}Ph}[N,N]FeCl_2$, **31**, and $^{Cy,F\text{-}Ph}[N,N]FeCl_2$, **8**, both complexes whose polymerisation behaviour had been

extensively studied in Chapters 2 and 4. The same trend in terms of the rates was observed; as the proportion of **8** was increased, the rate decreased. The plots of $\ln[M]_0/[M]_t$ remained linear up until high conversions, indicating that the radical concentration remained constant during the reaction (Figure 5.9). At high conversions there is some deviation from linearity, as observed with the styrene polymerisation catalysed by **31** reported in Chapter 4, due to the high viscosity of the polymerisation medium which results in inefficient stirring.

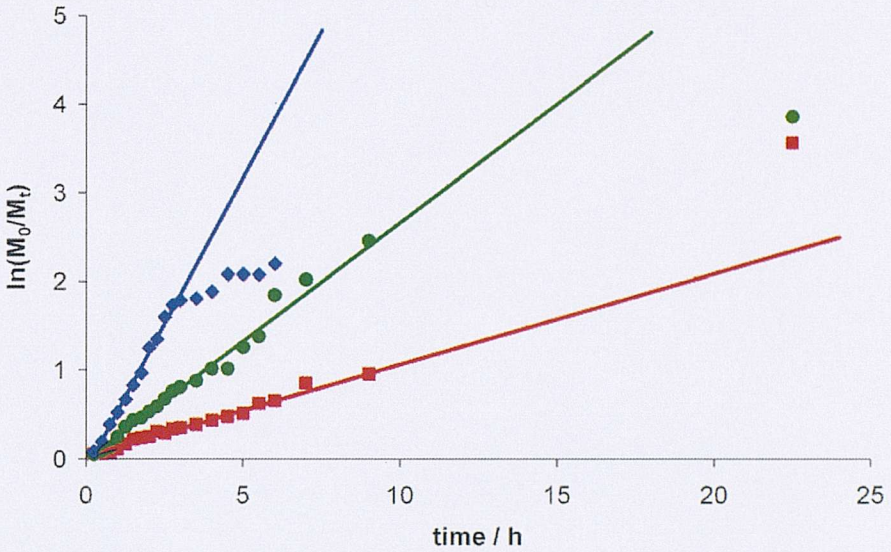


Figure 5.9 Rates for the bulk polymerisation of styrene (200 eq., 1-PECl, 120°C) by mixed catalyst systems containing different ratios of $^{Cy,Me2N\text{-}Ph}[N,N]FeCl_2$ and $^{Cy,F\text{-}Ph}[N,N]FeCl_2$ complexes (1:0, ◆; 9:1, ●; 1:1, ■).

However, the effect of mixing the $^{Cy,Me2N\text{-}Ph}[N,N]FeCl_2$ and $^{Cy,F\text{-}Ph}[N,N]FeCl_2$ catalysts on the molecular weights of the polymer obtained was less than anticipated. As illustrated by Figure 5.10, there is only a limited effect observed, and while the polymerisations conducted with more of the CCT catalyst do appear to have slightly lower molecular weights, it is not a large difference. Interestingly, there is also an effect on the polydispersities of the polymer obtained during the reactions. With an increased proportion of catalytic chain transfer, the low molecular weight 'tails' observed in the GPC traces of polymerisations mediated by $^{Cy,Me2N\text{-}Ph}[N,N]FeCl_2$ (discussed in Chapter 4) increase (Figure 5.11). This would be expected to broaden the PDIs, and at high conversions this is the case. However, while the PDIs for a catalyst ratio of 9:1 are generally broader than for a 1:0 ratio, the presence of 50% of $^{Cy,F\text{-}Ph}[N,N]FeCl_2$ does not significantly broaden the PDIs until high conversions are

reached. At 60% conversion, the relative PDIs for catalyst systems containing 0, 10 and 50% of **8** are 1.20, 1.29 and 1.21 respectively. By 80% conversion, the PDIs in each reaction have broadened, more significantly in the cases of the mixed systems: 1.27 for 0% **8**, 1.44 for 10% **8** and 1.36 for 50% **8**.

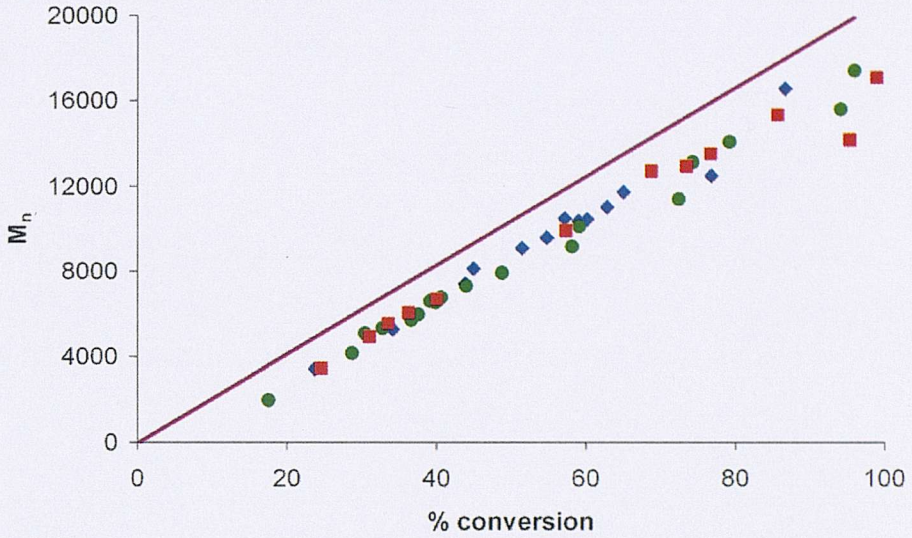


Figure 5.10 Molecular weight *versus* conversion for the bulk polymerisation of styrene (200 eq., 1-PECl, 120°C) by mixed catalyst systems containing different ratios of $^{Cy,Me2N-Ph}[N,N]FeCl_2$ and $^{Cy,F-Ph}[N,N]FeCl_2$ complexes (1:0, ◆; 9:1, ●; 1:1, ■).

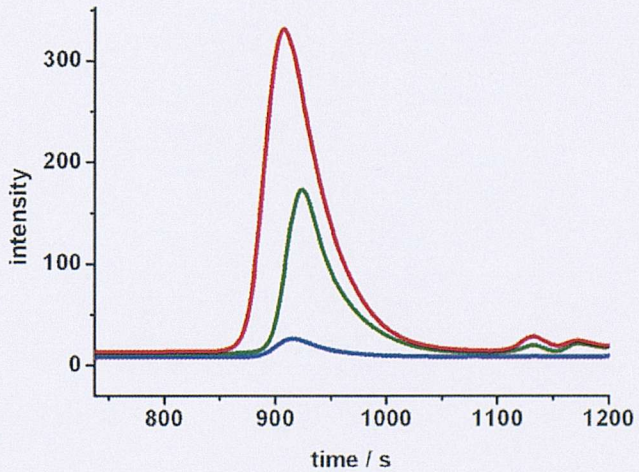


Figure 5.11 GPC traces for the bulk polymerisation of styrene (200 eq., 1-PECl, 120°C) by mixed catalyst systems containing different ratios of $^{Cy,Me2N-Ph}[N,N]FeCl_2$ and $^{Cy,F-Ph}[N,N]FeCl_2$ complexes (1:0, —; 9:1, —; 1:1, —).

Although the effect of mixing the catalysts on the rates of polymerisation was as predicted, there was an unexpected lack of significant variation in the molecular weights of the polymer samples obtained. This could be due to the efficiency of the ATRP catalyst - $^{Cy,Me2N-Ph}[N,N]FeCl_2$ is an extremely rapid and effective catalyst for the polymerisation of styrene. In contrast, $^{Cy,F-Ph}[N,N]FeCl_2$ is an extremely slow and ineffective catalyst for styrene polymerisation, and by mixing the two complexes we actually see a 'normal' ATRP polymerisation but with only half (or 90%) of the usual amount of catalyst. The ATRP equilibrium is robust enough to cope with this, and although the rates are compromised, the control is almost as good as when 100% of the ATRP catalyst is present. Obviously, once higher conversions are reached, the slow CCT processes become more significant and an increase in PDI and 'tailing' in the GPC traces are observed. In terms of the halogenophilicity of the system, in the case of $^{Cy,Me2N-Ph}[N,N]FeCl_2$, **31**, it is extremely high, which makes it such an efficient ATRP catalyst. In contrast, the halogenophilicity of $^{Cy,F-Ph}[N,N]FeCl_2$, **8**, is low, and this catalyst does not want to participate in the ATRP equilibrium. The growing, halogen-terminated polymer chains initiated by **31** do not interact with **8**, and $^{Cy,F-Ph}[N,N]FeCl_2$ is effectively a spectator in the reaction.

5.3 - Conclusions

The work presented in Chapters 2-4 resulted in the conclusion that the contrasting ATRP versus CCT behaviour of $^{R',R''}[N,N]FeCl_2$ catalysts correlates strongly with the spin-state of the oxidised Fe^{III} species and is dependent upon the electronic properties of the R′ and R″ substituents. This chapter concentrated on addressing the prevailing question of whether the CCT mechanism operates via a bond formation followed by β-H elimination route, or via direct H-transfer, and the role played by the OMRP equilibrium in the α-diimine Fe system.

The alkylation studies carried out in collaboration with Dr. Shaver illustrated the differences in carbophilicity of the $^{R',R''}[N,N]FeCl_3$ complexes. Lower spin, carbophilic complexes containing electron-withdrawing groups on the α-diimine ligand gave rise to $^{R',R''}[N,N]FeCl_2R$ complexes with stronger Fe-C bonds than the high spin, halogenophilic complexes. The presence of alkyl radicals derived from the decomposition of $^{R',R''}[N,N]FeCl_2R$ species was further demonstrated through trapping reactions with TEMPO, but attempts to further exploit the reactivity of either the $^{R',R''}[N,N]FeCl_2R$ or $^{R',R''}[N,N]FeCl_3$ complexes resulted in decomposition.

The evidence reported in this chapter suggests that the CCT mechanism is likely to occur via the bond formation followed by β-H elimination route. The increased styrene generation of lower spin catalysts during decomposition of 1-phenylethyliron complexes, the ineffectiveness of "spiking" the reaction mixture with the Fe^{II} complex, and the behaviour of the system under polymerisation conditions using different catalyst concentrations all support this route over direct H-abstraction. Furthermore, the ability of the $^{R',R''}[N,N]FeCl_2$ complexes to participate in the OMRP equilibrium lends additional support to this conclusion.

The $^{R',R''}[N,N]FeCl_2$ complexes are inefficient OMRP catalysts for styrene, giving only moderate control at best, because the Fe-R bonds are unstable. However, the results of OMRP experiments demonstrate the existence of the OMRP equilibrium with these catalysts and support the participation of this equilibrium under ATRP conditions. The universally poor absolute carbophilicity exhibited by the $^{R',R''}[N,N]FeCl_2$ complexes consequently led to the conclusion that it is the relative halogenophilicity of the catalysts which determines the prevalent polymerisation mechanism. The halogenophilicity of the Fe^{II} complexes is determined by the electronic properties of the ligand substituents and manifests as a gradual switch in polymerisation mechanism, controlled through the spin-state of the analogous Fe^{III} complex. By including electron-withdrawing groups, CCT can be favoured; addition of electron-donating groups results in ATRP behaviour.

Under ATRP conditions, the radical concentrations in polymerisations mediated by the α-diimine Fe catalysts are regulated by both the atom transfer reaction and the trapping of radicals by the Fe^{II} species. The observed polymerisation mechanism (ATRP *vs.* CCT) strongly correlates to the radical concentration. Halogenophilic catalysts with electron-donating substituents provide increased ATRP control, increased rates of monomer consumption and the chain transfer reaction is not kinetically competitive; in these cases, predominantly halogen-terminated polymers are observed. Conversely, catalysts with electron-withdrawing groups have decreased halogenophilicity, resulting in slower rates of monomer consumption and the observation of olefin-terminated polymer chains arising from chain transfer.

The mechanistic understanding of the α-diimine Fe system reported in this chapter is valuable because a comprehensive understanding of the system is necessary before the behaviour of the catalysts be confidently predicted. New catalysts can be designed to maximise the involvement of the ATRP or OMRP/CCT equilibria;

including extremely electron-donating groups should lead to an extremely efficient, halogenophilic ATRP catalyst (Figure 5.12). Similarly, including highly electron-withdrawing groups would be expected to give a lower spin, carbophilic catalyst which would give a slow polymerisation and olefin-terminated polymer of low molecular weights (Figure 5.12). Industrially, being able to synthesise polymers of known molecular weights and controlled PDIs at a specified rate would be extremely useful, as the properties of the polymer could be tailored as desired.

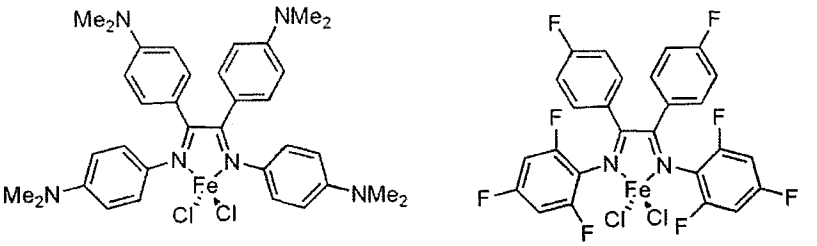


Figure 5.12 Potential catalysts for ATRP and CCT, bearing α-diimine ligands containing highly electron-donating and highly electron-withdrawing groups.

5.4 - References

(1) Poli, R., *Angew. Chem. Int. Ed.* **2006,** *45*, 5058.

(2) Burczyk, A. F.; O'Driscoll, K. F.; Rempel, G. L., *J. Polym. Sci., Polym. Chem. Ed* **1984,** *22*, 3255.

(3) Gridnev, A. A.; Ittel, S. D.; Fryd, M.; Wayland, B. B., *Organometallics* **1993,** *12*, 4871.

(4) Gridnev, A. A.; Ittel, S. D.; Fryd, M.; Wayland, B. B., *Organometallics* **1996,** *15*, 222.

(5) Gridnev, A. A.; Ittel, S. D.; Wayland, B. B.; Fryd, M., *Organometallics* **1996,** *15*, 5116.

(6) Brookhart, M.; Green, M. L. H.; Wong, L.-L., *Progr. Inorg. Chem.* **1988,** *36*, 1.

(7) Gridnev, A.; Ittel, S. D.; Fryd, M.; Wayland, B. B., *J. Chem. Soc. Chem. Commun.* **1993**, 1010.

(8) Roberts, G. E.; Heuts, J. P. A.; Davis, T. P., *Macromolecules* **2000,** *33*, 7765.

(9) Morrison, D. A.; Davies, T. P.; Heuts, J. P. A.; Messerle, B.; Gridnev, A. A., *J. Polym. Sci. Part A: Polym. Chem.* **2006,** *44*, 6171.

(10) Heuts, J. P. A.; Forster, D. J.; Davis, T. P., *Macromolecules* **1999,** *32*, 2511.

(11) Wayland, B. B.; Poszmik, G.; Mukerjee, S. L.; Fryd, M., *J. Am. Chem. Soc.* **1994,** *116*, 7943.

(12) Grognec, E. L.; Claverie, J.; Poli, R., *J. Am. Chem. Soc.* **2001,** *123*, 9513.

(13) Braunecker, W. A.; Itami, Y.; Matyjaszewski, K., *Macromolecules* **2005,** *38*, 9402.

(14) Kobrich, G.; Buttner, H., *J. Organomet. Chem.* **1969,** *18*, 117.

(15) Evans, D. J.; Henderson, R. A.; Hills, A.; Hughes, D. L.; Oglieve, K. E., *J. Chem. Soc. Dalton Trans.* **1992**, 1259.

(16) Clarke, D. A.; Dolphin, D.; Grigg, R.; Johnson, A. W.; Pinnock, H. A., *J. Chem. Soc. (C)* **1968**, 881.

(17) Cocolios, P.; Lagrange, G.; Guilard, R., *J. Organomet. Chem.* **1983,** *253*, 65.

(18) Balch, A. L.; Cornman, C. R.; Safari, N.; Latos-Grazinsky, L., *Organometallics* **1990,** *9*, 2420.

(19) Setsune, J.; Ishimaru, Y.; Sera, A., *Chem. Lett.* **1992,** *21*, 377.

(20) Lexa, D.; Mispelter, J.; Savéant, J.-M., *J. Am. Chem. Soc.* **1981,** *103*, 6806.

(21) Arasasingham, R. D.; Balch, A. L.; Cornman, C. R.; Latos-Grazynski, L., *J. Am. Chem. Soc.* **1989,** *111*, 4357.

(22) Cocolios, P.; Laviron, E.; Guilard, R., *J. Organomet. Chem.* **1982,** *228*, C39.

(23) Arafa, I. M.; Shin, K.; Goff, H. M., *J. Am. Chem. Soc.* **1988,** *110*, 5228.

(24) Tabard, A.; Cocolios, P.; Lagrange, G.; Gerardin, R.; Hubsch, J.; Lecomte, C.; Zarembowitch, J.; Guilard, R., *Inorg. Chem.* **1988,** *27*, 110.

(25) Guillaume, V.; Thominot, P.; Coat, F.; Mari, A.; Lapinte, C., *J. Organomet. Chem.* **1998,** *565*, 75.

(26) Roger, C.; Toupet, L.; Lapinte, C., *J. Chem. Soc. Chem. Commun.* **1988**, 713.

(27) Roger, C.; Hamon, P.; Toupet, L.; Raba, H.; Saillard, J.-Y.; Hamon, J.-R.; Lapinte, C., *Organometallics* **1991,** *10*, 1045.

(28) Narvor, N. L.; Lapinte, C., *Organometallics* **1995,** *14*, 634.

(29) Narvor, N. L.; Toupet, L.; Lapinte, C., *J. Am. Chem. Soc.* **1995,** *117*, 7129.

(30) Floriani, C.; Calderazzo, F., *J. Chem. Soc. Chem. Commun.* **1968**, 417.

(31) Lau, W.; Huffman, J. C.; Kochi, J. K., *Organometallics* **1982,** *1*, 155.

(32) Floriani, C.; Calderazzo, F., *J. Chem. Soc. (A)* **1971**, 3665.

(33) Li, Z.; Goff, H. M., *Inorg. Chem.* **1992,** *31*, 1547.

(34) Song, B.; Goff, H. M., *Inorg. Chem.* **1994,** *33*, 5979.

(35) Claverie, J. P., *Res. Discl.* **1998,** *416*, 1595.

(36) Goodwin, J. M.; Olmstead, M. M.; Patten, T. E., *J. Am. Chem. Soc.* **2004,** *126*, 14352.

(37) Patten, T. E.; Troeltzsch, C.; Olmstead, M. M., *Inorg. Chem.* **2005,** *44*, 9197.

(38) Enikolopyan, N. S.; Smirnov, B. R.; Ponomarev, G. V.; Bel'govskii, I. M., *J. Polym. Sci., Polym. Chem. Ed.* **1981,** *19*, 879.

(39) Shaver, M. P.; Allan, L. E. N.; Gibson, V. C., *Organometallics* **2007,** *26*, 2252.

(40) Herk, A. M. v., *J. Macromol. Sci., Rev. Macromol. Chem. Phys.* **1997,** *C37*, 633.

(41) Maria, S.; Stoffelbach, F.; Mata, J.; Daran, J.-C.; Richard, P.; Poli, R., *J. Am. Chem. Soc.* **2005,** *127*, 2537.

(42) Allan, L. E. N.; Shaver, M. P.; White, A. J. P.; Gibson, V. C., *Inorg. Chem.* **2007,** *46*, 8963.

(43) O'Reilly, R. K. Synthesis of novel iron complexes and their use in atom transfer radical polymerisation. Ph.D. Thesis, University of London, 2003.

(44) Gibson, V. C.; O'Reilly, R. K.; Reed, W.; Wass, D.; White, A. J. P.; Williams, D. J., *Chem. Commun.* **2002**, 1850.

Chapter 6

Towards ATRP in Aqueous Media Using New α-Diimine Iron Complexes

6.1 - Introduction

The synthesis of catalysts which are soluble in polar or protic media, such as alcohols and water, has become an area of extensive interest as a result of the growing concern over the impact of industrial processes and protection of the environment. The use of water-soluble organometallic transition metal complexes has been realised in aqueous biphasic systems, where charged or polar groups such as $-SO_3Na$, $-PO_3Na_2$, $-CO_2H$ and -OH have been used to impart aqueous solubility.[1,2] More recent work has recognised the possibility of complexing transition metals with hydrophilic nitrogen donor ligands, as an alternative to their well-studied phosphine counterparts. This has provided new alternatives to processes commonly carried out in organic solvents such as alcohol oxidations,[3] coordination polymerisations,[4,5] ring opening metathesis polymerisations[6] and other chemical transformations.[7,8]

Industrially, the use of atom transfer radical polymerisation in aqueous media is attractive, not just because of the environmental impact but also because of the increasing importance of water-soluble polymers. These are used for a variety of applications, including drug delivery systems, sensors, stabilisers, coatings and other biomaterials.[9-11] Sawamoto was the first to introduce water into an ATRP reaction, reporting that the addition of a small amount of water midway through MMA polymerisation (10 equivalents, relative to the initiator) had no effect on the reaction, which continued in a controlled and living manner.[12] The first aqueous polymerisation was reported by Matyjaszewski *et al* in 1998, who used their CuBr/bipy system to polymerise 2-hydroxyethyl acrylate in water (50% v/v) at 90°C. This polymerisation reached almost 90% conversion in 12 h, with a final molecular weight in good agreement with the theoretical value, and a PDI of 1.34.[10]

Over the last 10 years, a variety of hydrophilic, functionalised monomers have been polymerised through ATRP, using copper or ruthenium catalysts. The tolerance of ATRP towards functional groups is illustrated by this wide range of monomers, several of which are shown in Figure 6.1.

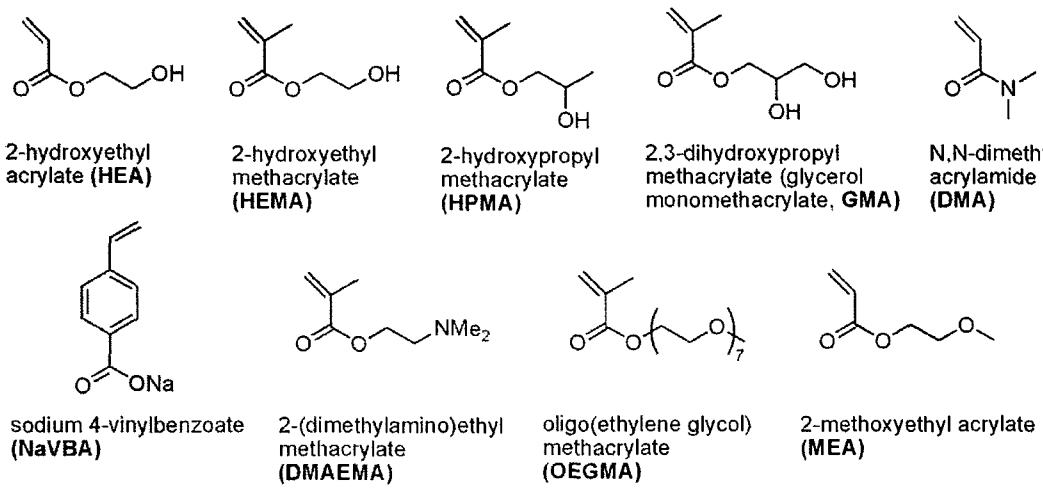


Figure 6.1 Selected ATRP monomers containing hydrophilic functional groups.

Copper halides, with multidentate nitrogen-donor ligands, have been most frequently studied as ATRP catalysts under aqueous conditions. They have successfully been used to polymerise monomers containing pendant hydroxyl groups such as 2-hydroxyethyl acrylate (HEA),[10] 2-hydroxyethyl methacrylate (HEMA),[13] 2-hydroxypropyl methacrylate (HPMA)[14] and glycerol monomethacrylate (GMA)[14] with good control over molecular weights and low PDIs. Closely related monomers containing terminal methoxy-groups, such as 2-methoxyethyl acrylate (MEA)[15] and oligo(ethylene glycol) methacrylate (OEGMA)[16-19] have also been successfully polymerised using Cu-mediated ATRP. Polymerisations of OEGMA were typically carried out at ambient temperature (25°C), since the copper complexes were unstable in aqueous solution at higher temperatures.[17]

Polymerisation of *N,N*-dimethyl acrylamide (DMA) proved difficult to control and led to the conclusion that ATRP was an unsuitable polymerisation method for acrylamides because the Cu salts complexed to the amide chain ends, stabilising the radicals and retarding the deactivation step.[20,21] However, polymerisation of the amino-containing monomer 2-(dimethylamino)ethyl methacrylate (DMAEMA) was achieved using CuBr with a variety of bi- and tetra-dentate amine ligands, giving excellent control over molecular weights and PDIs.[9] Monomers such as sodium methacrylate[22] and sodium 4-vinylbenzoate (NaVBA)[23] have also been successfully polymerised using the CuBr/bipy ATRP system, again illustrating the wide monomer scope afforded by ATRP.

The approach to aqueous ATRP using ruthenium catalysts has developed in a different manner to the copper systems. Although the first ATRP polymerisation

containing water was carried out using $RuCl_2(PPh_3)_3$,[12] ruthenium has received much less attention and, as a result, more specialised catalysts have been developed. Figure 6.2 shows some of the Ru complexes used in aqueous ATRP.

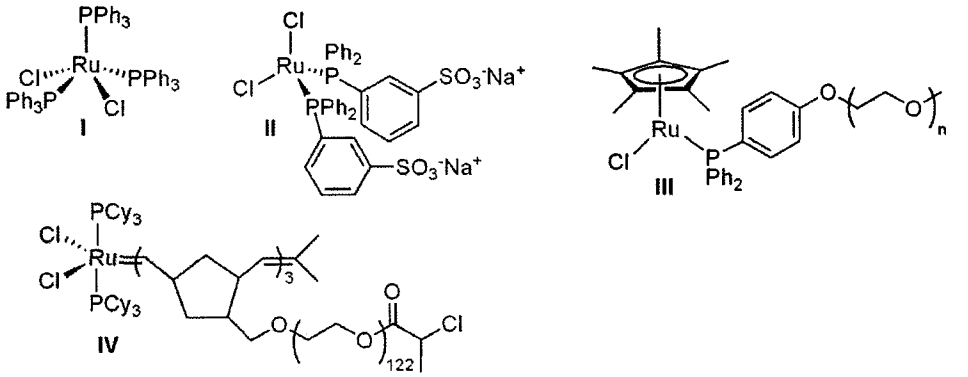


Figure 6.2 Selected ruthenium-based catalysts used in aqueous ATRP.

The polymerisation of MMA using $RuCl_2(PPh_3)_3$, **I**, and various initiators in alcohols and water was studied. These systems gave living suspension polymerisations, with molecular weights in good agreement with theoretical values and narrow PDIs (1.1-1.3).[24] This complex was also investigated for the ATRP of HEMA in MeOH, but although molecular weights increased linearly with conversion, the PDIs were relatively broad (1.7).[25] This was attributed in part to the heterogeneous nature of the reaction and so a more hydrophilic Ru complex with ionic phosphine ligands, **II**, was prepared. This system allowed the homogeneous living radical polymerisation of HEMA in MeOH, with PDIs as low as 1.4.[26]

A ruthenium complex with a hydrophilic and thermoresponsive polyethylene glycol (PEG) ligand, **III**, allowed facile catalyst recycling in the suspension polymerisation of MMA. The hydrophilic complex was soluble in water at room temperature, but addition of monomer and initiator in toluene resulted in a 2-phase mixture. However, the amphiphilic nature of the complex, with the hydrophilic PEG segment and the hydrophobic Cp* and PPh_3 ligands, meant that an emulsion was formed when the reaction was stirred. The PMMA obtained during ATRP with this system was well-controlled, with PDIs of 1.1, and the ease of separating out organic and aqueous components meant that the polymer was essentially metal-free, whilst the catalyst could be re-used.[27,28]

The modified Grubbs' catalyst, **IV**, is significant as it is an example of a ruthenium complex successfully designed to be active in the concurrent tandem catalysis (CTC) of norbornene ROMP and MMA ATRP.[29] Simultaneous ROMP and ATRP reactions

were carried out in aqueous dispersed medium, allowing successful homo- and co-polymerisations of norbornene and MMA under mini-emulsion conditions. This allowed the 1-pot synthesis of three different types of polymer architecture; nanoscale blends of homopolymers and graft and star-like copolymers.

Although aqueous ATRP has been a notable success using Ru-based complexes, there has been very little reported about the Fe analogues. The main drawbacks of the copper and ruthenium systems are their toxicity and the need to remove all traces of metal residue from the polymer before use in catering or biomedical applications. Using iron would negate this requirement and also be more cost-effective for use in industry, but iron complexes are often unstable in water. An obvious exception to this rule is ferrocene, and the first reported iron-catalysed suspension ATRP was carried out using the half-metallocene iron complexes **V-VII** (Figure 6.3).[30] These water-stable complexes (discussed in Chapter 1) were efficient catalysts for the polymerisation of *n*-butyl acrylate, *t*-butyl acrylate, methyl acrylate and styrene in 1:1 water/toluene mixtures. Block and random copolymers could also be obtained, and in both homo- and co-polymers controlled molecular weights were obtained, with PDIs of 1.2-1.3.

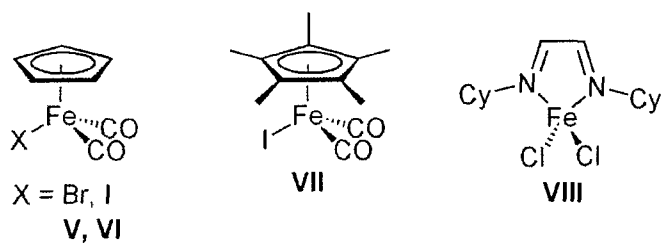


Figure 6.3 Iron-based catalysts used in aqueous ATRP

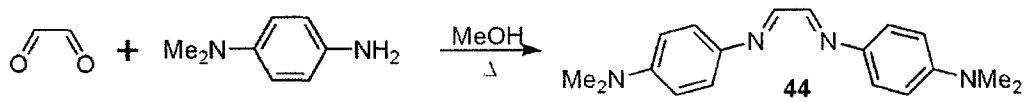
The α-diimine iron system is relatively robust and $^{Cy,H}[N,N]FeCl_2$, **VIII**, has been tested for the ATRP of hydrophilic monomers including HEA, HEMA, HPMA and DMAEA in MeOH and MeOH / water mixtures.[31,32] Promising results were obtained, particularly for the polymerisation of HPMA in MeOH, which proceeded with controlled molecular weights and narrow PDIs (1.1-1.4) at both ambient temperature and 60°C. However, the α-diimine iron complexes were found to be unstable towards high concentrations of MeOH and the presence of water. In this chapter, new α-diimine ligands which incorporate hydrophilic amine and hydroxy groups for aqueous solubility will be targeted, with the resulting Fe^{II} complexes screened for ATRP activity in MeOH and water using hydrophilic monomers.

6.2 - Results and Discussion

6.2.1 - Synthesis and polymerisation behaviour of amino-functionalised Fe^{II} complexes.

6.2.1.1 - Aryl amino substituents.

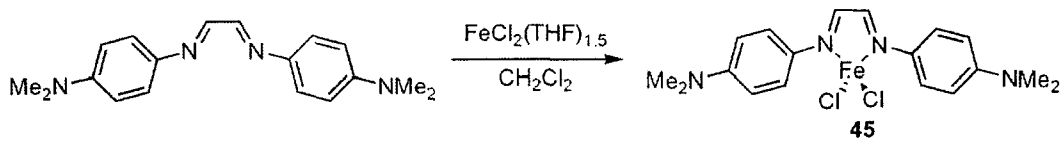
In order to synthesise a ligand containing a tertiary amine group, the condensation reaction between dimethyl-*p*-phenylenediamine and glyoxal (Scheme 6.1) was carried out, through modification of literature procedures. The dark brown crude product was recrystallised from $CHCl_3$ / pentane to give ligand **44** as an orange solid in good yield (65%), with spectroscopic characterising data in good agreement with the literature.[33]



Scheme 6.1 Synthesis of amino-functionalised ligand, **44**.

In order to make the ligand more soluble in polar media, attempts were made to quaternise the tertiary amino groups. However, reaction of $^{Me2N\text{-}Ph,H}[N,N]$, **44**, with MeI, Me_2SO_4 and HCl was unsuccessful under various conditions. It is likely that extended conjugation exists within this ligand, making it unreactive in nucleophilic addition reactions. Donation of the lone pair of the tertiary amine into the aromatic ring would mean that it was not available for quaternisation.

The Fe^{II} chloride complex of ligand **44** was prepared through dropwise addition of a solution of **44** in CH_2Cl_2 to a suspension of $FeCl_2(THF)_{1.5}$ in CH_2Cl_2. A colour change to dark green was observed and, after stirring overnight, the complex was isolated through filtration, washed with CH_2Cl_2 and dried under vacuum to give $^{Me2N\text{-}Ph,H}[N,N]FeCl_2$, **45**, in excellent yield (85%, Scheme 6.2).



Scheme 6.2 Synthesis of amino-functionalised Fe^{II} chloride complex, **45**.

The IR spectrum of $^{Me2N\text{-}Ph,H}[N,N]FeCl_2$, **45**, showed that the $\nu_{C=N}$ stretch had shifted only slightly upon coordination, from 1605 cm^{-1} in the ligand (**44**) to 1603 cm^{-1} in the complex (**45**). FAB-MS showed the expected $[M+H]^+$ peak at 422 a.m.u., and also common fragments such as $[M\text{-}Cl]^+$ and $[L+H]^+$. Although a meaningful ^1H

NMR spectrum could not be acquired, crystals suitable for X-ray analysis of **45** were obtained through slow cooling of a saturated solution of acetonitrile (Figure 6.4, Table 6.1), in order to confirm the identity of the complex.

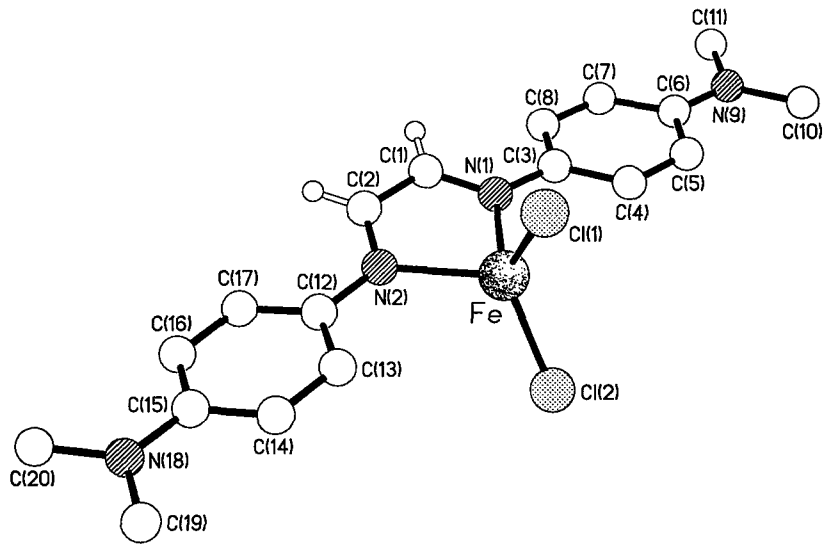


Figure 6.4 The molecular structure of the C_{2v}-symmetric complex, **45**.

Table 6.1 Selected bond lengths (Å) and angles (°) for complex **45**.

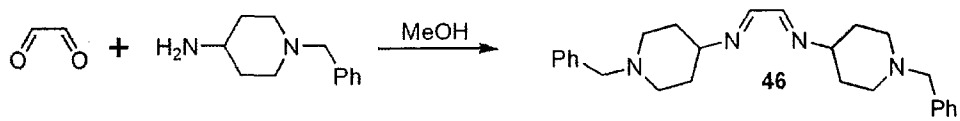
Fe–Cl(1)	2.214(2)	Cl(1)–Fe–Cl(2)	123.25(9)
Fe–Cl(2)	2.233(2)	Cl(1)–Fe–N(1)	110.4(2)
Fe–N(1)	2.143(8)	Cl(1)–Fe–N(2)	109.6(2)
Fe–N(2)	2.111(7)	Cl(2)–Fe–N(1)	112.4(2)
N(1)–C(1)	1.294(14)	Cl(2)–Fe–N(2)	113.4(2)
C(1)–C(2)	1.447(11)	N(1)–Fe–N(2)	79.5(2)

The complex exhibits crystallographic C_{2v} symmetry and the geometry at the iron centre is distorted tetrahedral. The inter-bond angles are in the range 79.5(2)-123.25(9)°, with the acute angle associated with the bite of the *N,N'* chelate ligand. The ligand is arranged in an unusually planar conformation around the metal centre, with an angle between the dimethylamine nitrogen atoms and the metal centre of approximately 178°. This suggests widespread π-delocalisation within the ligand, where the nitrogen lone pairs of the NMe_2 group are donated into the π-system of the aromatic ring and imine double bonds, to give a conjugated system. Donation of the

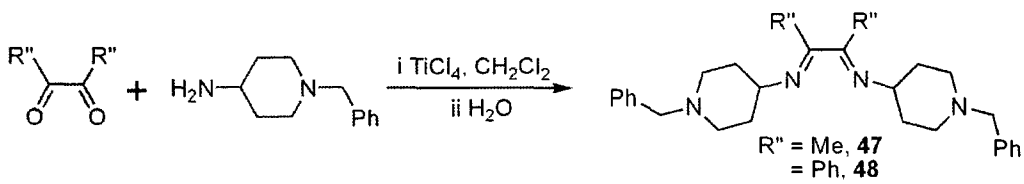
amino nitrogen lone pairs into the π-system would result in a decreased reactivity of the amine group, due to the unavailability of these lone pairs for nucleophilic attack. This is one potential explanation for the lack of reactivity of ligand **44** towards electrophiles such as MeI.

6.2.1.2 - Alkyl amino substituents.

In order to break the conjugation between the tertiary amine group and the imine groups, aliphatic amine-containing ligands were targeted. These were initially based on the commercially available 4-aminobenzyl piperidine moiety, with a range of R groups at the 2,3-positions of the ligand backbone. This ligand family was designed to retain the *N*-alkyl group which favours ATRP, and also to keep the steric properties similar to the efficient ATRP catalyst $^{Cy,H}[N,N]FeCl_2$.[34,35] The electronic properties of the piperidine ring were also anticipated to be similar to $^{Cy,H}[N,N]FeCl_2$, although the effects of having a nitrogen atom within the 6-membered ring were unknown. The aldimine ligand, with H at the 2,3-positions, was prepared through a simple bulk condensation reaction between the amine and glyoxal (Scheme 6.3), but the Me- and Ph-substituted ketones required activation with $TiCl_4$ (Scheme 6.4).



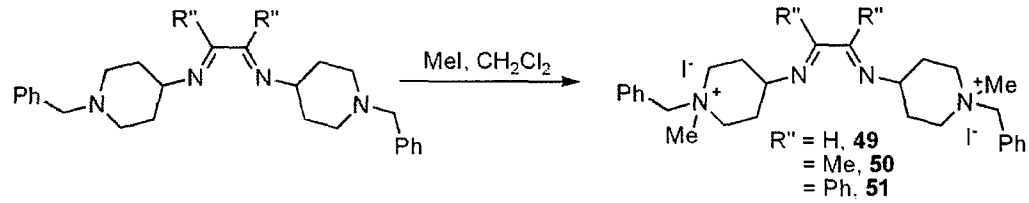
Scheme 6.3 Synthesis of aliphatic, amine-containing ligand **46**.



Scheme 6.4 Synthesis of aliphatic, 2,3-substituted amine-containing ligands **47-48**.

Ligands **46-48** were obtained in fairly good yields (50-65%) after recrystallisation from MeOH. Two-dimensional COSY and HETCOR spectra were used to assign the proton and carbon environments, with the only ambiguous assignments being that of the diastereotopic axial and equatorial protons on the piperidine ring. The imine $\nu_{C=N}$ stretches were clearly visible in the IR spectra of the ligands, between 1616-1634 cm^{-1}, and CI-MS showed the expected $[M+H]^+$ peaks. Reaction of ligands **46-48**

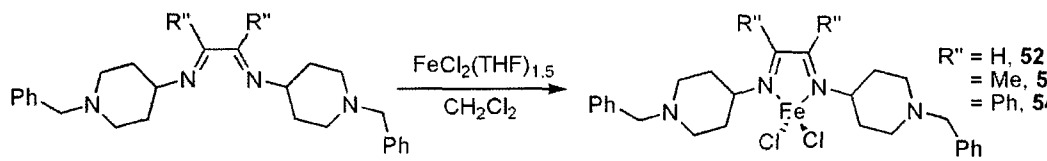
with MeI gave essentially quantitative conversion to the quaternised derivatives, ligands **49-51** (Scheme 6.5).



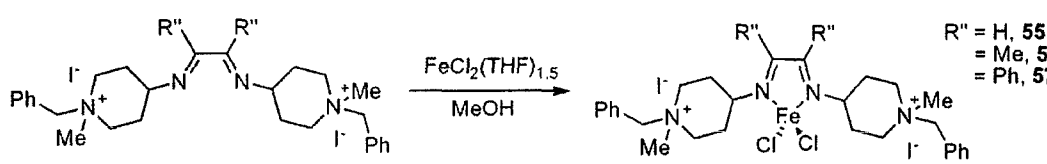
Scheme 6.5 Synthesis of piperidinium ligands **49-51**.

The ^{1}H NMR spectra of **49-51** were indicative of the desired products, with new methyl environments visible at around 3.0 ppm, although the spectra were somewhat broadened in d_6-dmso. The ^{13}C NMR also showed the new methyl environment, with an aliphatic signal occurring at around 26.4 ppm. FAB-MS gave the expected mass peaks of $[M\text{-}I]^+$ at 559, 587 and 711 a.m.u. for **49-51** respectively. The $\nu_{C=N}$ stretch shifted to slightly higher frequencies in the salts (1622-1643 cm^{-1} for **49-51**, *cf.* 1616-1634 cm^{-1} for **46-48**), indicating that the imine bond is strengthened by the increased amine substitution.

Synthesis of the Fe^{II} chloride complexes of ligands **46-51** was accomplished by stirring a solution of $FeCl_2(THF)_{1.5}$ and ligand at room temperature in CH_2Cl_2 (Scheme 6.6) or MeOH (Scheme 6.7). Complexes **52-54** were obtained in good yields of 74-88% after filtration, concentration and precipitation using pentane. Complexes **55-57** were obtained in yields of 64-78% after filtration, concentration and precipitation using CH_2Cl_2.



Scheme 6.6 Synthesis of Fe^{II} complexes **52-54**.



Scheme 6.7 Synthesis of Fe^{II} complexes **55-57**.

Complexes **52-54** were extremely air-sensitive and only the FAB-MS of **53** showed the $[M\text{-}Cl]^+$ signal from the metal complex. Ligand signals were observed for complexes **52** and **54**, although solutions for FAB-MS of all complexes were prepared with the exclusion of air and moisture, using dried and degassed solvents. The $[M\text{-}I]^+$ signal was visible in the FAB-MS spectra of complexes **55** and **56**, although **57** showed only ligand peaks. No meaningful ^1H NMR spectra could be obtained for complexes **52-57** and the Evans' measurements of 4.76-5.12 B.M. confirmed the presence of 4 unpaired electrons in the complexes, consistent with high spin Fe^{II}. The IR spectra of complexes **52-54** showed an increase in the stretching frequency of $\nu_{C=N}$ upon coordination to the metal centre, indicating a stronger imine bond. However, the quaternised complexes **55-57** showed a decrease in $\nu_{C=N}$ when compared to the free ligand stretches. The force constants within the complexes are clearly affected by the presence of the quaternary nitrogen group, which results in a weakening of the imine C=N bond. The ligand salts will be less electron-donating than the non-quaternised ligands which is in agreement with the IR data reported in Chapters 2 and 4. The $\nu_{C=N}$ stretches of very electron-donating ligands, such as $^{R',Me2N\text{-}Ph}[N,N]$, increased in frequency upon coordination to the metal, whereas the less electron-donating ligands resulted in a decrease in $\nu_{C=N}$ frequency when the Fe^{II} complex was compared to the free ligand.

Crystals of $^{pip,H}[N,N]FeCl_2$, **52**, suitable for X-ray structure determination were obtained by layering an equal volume of dichloromethane and pentane and allowing slow diffusion to occur (Figure 6.5, Table 6.2).

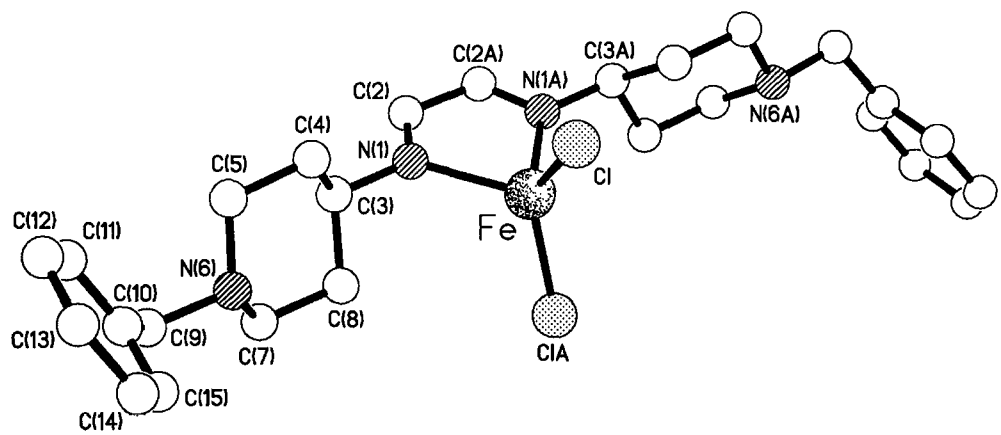


Figure 6.5 The molecular structure of the C_2-symmetric complex, **52**.

Table 6.2 Selected bond lengths (Å) and angles (°) for complex **52**.

Fe–Cl	2.2258(12)	Cl–Fe–Cl(A)	123.72(8)
Fe–Cl(A)	2.2258(12)	Cl–Fe–N(1)	111.11(8)
Fe–N(1)	2.130(3)	Cl–Fe–N(1A)	111.71(9)
Fe–N(1A)	2.130(3)	Cl(A)–Fe–N(1)	111.71(9)
N(1)–C(2)	1.2750(5)	Cl(A)–Fe–N(1A)	111.11(8)
C(2)–C(2A)	1.489(7)	N(1)–Fe–N(1A)	78.59(16)

$^{pip,H}[N,N]FeCl_2$, complex **52**, has crystallographic C_2 symmetry, about an axis which passes through the Fe centre and bisects the C(2)–C(2A) bond. The geometry at the iron centre is distorted tetrahedral with inter-bond angles in the range 78.59(16)-123.72(8)°. The bonding within the essentially planar five-membered chelate ring shows a distinct pattern of bond ordering. The C=N linkages are shorter than the C–C bond (1.270(5) Å compared with 1.489(7) Å) which indicates an absence of bond delocalisation.

X-ray diffraction quality crystals of $^{pip,Me}[N,N]FeCl_2$, complex **53**, were also obtained by layering a saturated dichloromethane solution with pentane and allowing slow diffusion to occur (Figure 6.6, Table 6.3).

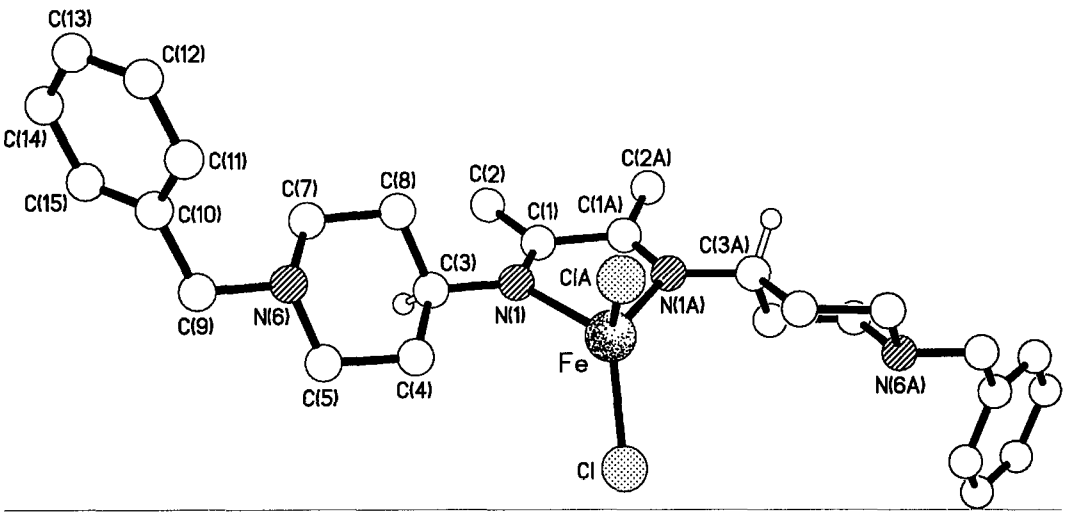


Figure 6.6 The molecular structure of the C_2-symmetric complex, **53**.

Table 6.3 Selected bond lengths (Å) and angles (°) for complex **53**.

Fe–Cl	2.2500(4)	Cl–Fe–Cl(A)	122.17(2)
Fe–Cl(A)	2.2491(4)	Cl–Fe–N(1)	115.00(3)
Fe–N(1)	2.1051(11)	Cl–Fe–N(1A)	109.32(3
Fe–N(1A)	2.1058(11)	Cl(A)–Fe–N(1)	109.28(3)
N(1)–C(1)	1.2846(16)	Cl(A)–Fe–N(1A)	114.97(3)
C(1)–C(1A)	1.5240(2)	N(1)–Fe–N(1A)	77.76(6)

The structure obtained is very closely related to that of complex **52**. Complex **53** also exhibits crystallographic C_2 symmetry about an axis which passes through the Fe centre and bisects the C(1)–C(1A) bond. The geometry at the iron centre is also distorted tetrahedral with inter-bond angles in the range 77.76(6)-122.17(2)°, and the bonding within the essentially planar five-membered chelate ring again shows the distinct pattern of bond ordering indicative of an absence of bond delocalisation. The C=N linkages of 1.2846(16) Å are shorter than the C–C bond (1.5240(2) Å). The Fe–N bond lengths are significantly shorter in the ketimine derivative, **53**, than in the aldimine derivative, **52** (2.105(11) Å compared with 2.130(3) Å). However, there are no significant differences in the C=N bond lengths, which are 1.2846(16) Å for **53** and 1.270(5) Å for **52**.

6.2.1.3 - Polymerisation studies using the amino-substituted complexes.

The Fe^{II} chloride complexes **45** and **52-57** were tested for the ATRP of styrene (200 equiv., bulk), under inert atmosphere at 120°C, using 1-PECl as the initiator. The complexes were also tested for the ATRP of MMA (100 equiv., 80°C, EBrB) in toluene and methanol solutions. The complexes of the quaternised salts, **54-57**, were additionally screened for ATRP using a more hydrophilic monomer, 2-hydroxypropyl methacrylate (HPMA).

Styrene polymerisation using $^{Me2N\text{-}Ph,H}[N,N]FeCl_2$, complex **45**, proceeded rapidly and reached 75% conversion in just 3 hours, with a pseudo-first order rate constant ($k_{obs.}$) of 0.36 h^{-1}. Molecular weights were significantly higher than theoretical and it was proposed that the low solubility of the complex in the monomer was decreasing the effective concentration of the catalyst, causing an increase in the polymerisation

rate and molecular weights. The polymerisation was repeated using diphenyl ether as a solvent (50% v/v), under otherwise identical conditions, resulting in a decrease in rate ($k_{obs.}$ = 0.15 h^{-1}, Figure 6.7). However, the molecular weights were still significantly higher than theoretical (Figure 6.8) and the PDIs remained broad.

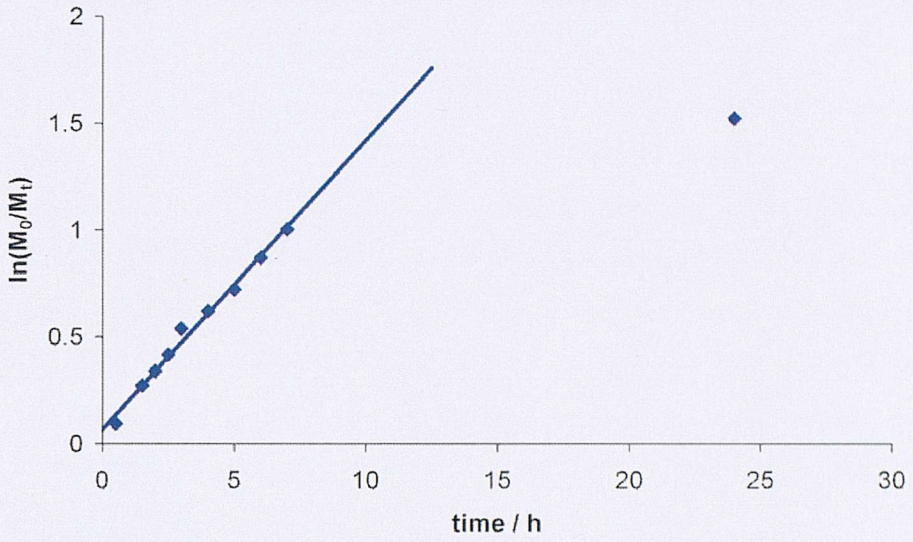


Figure 6.7 Rate for the solution polymerisation of styrene (200 eq., 50% v/v Ph_2O, 1-PECl, 120°C) by $^{Me2N\text{-}Ph,H}$[*N,N*]$FeCl_2$, **45**.

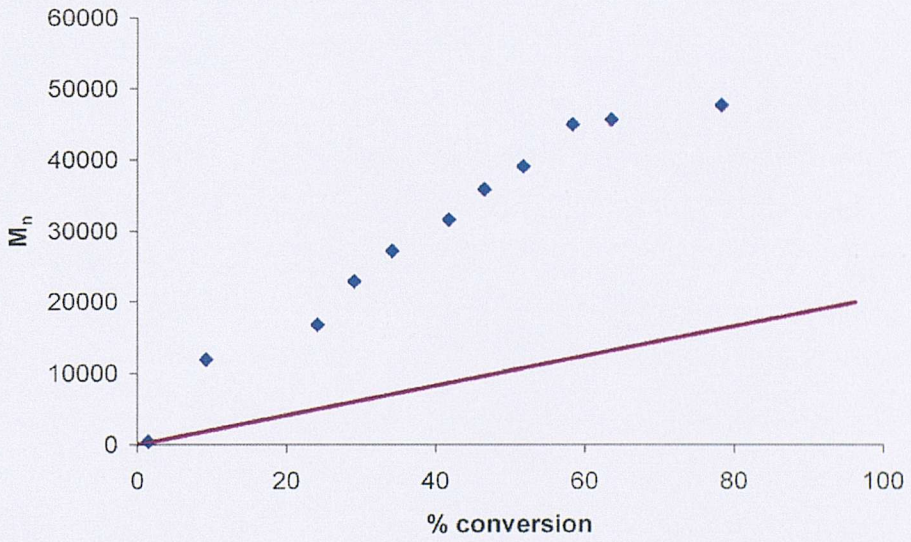


Figure 6.8 Molecular weight *versus* conversion for the solution polymerisation of styrene (200 eq., 50% v/v Ph_2O, 1-PECl, 120°C) by $^{Me2N\text{-}Ph,H}$[*N,N*]$FeCl_2$, **45**. ($M_{n,th}$ = —).

Although the complex was partially soluble in diphenyl ether, the reaction was not homogeneous, and it is likely that the effective concentration of **45** was still lower than calculated. With less of the catalyst in solution, there would be fewer propagating radicals and so a smaller number of propagating chains. However, the average molecular weight of these chains would be higher; a trend which is supported by the molecular weight data (Figure 6.8). Although the molecular weight increases with conversion, it does not do so in a perfectly linear manner and the molecular weights correlate poorly with theoretical values. PDIs are relatively broad, typically *ca.* 1.7-2.1 for polymerisations carried out bulk and *ca.* 1.4-1.8 for the slower solution polymerisations. This implies that polymerisation is not occurring solely through ATRP. Although higher than theoretical molecular weights are often obtained in ATRP reactions, this is usually attributed to low initiator efficiency. A slow deactivation rate causes a high concentration of propagating radicals, which results in a significant amount of bimolecular termination. This type of inefficient initiation is accompanied by PDIs which are broad initially but which decrease significantly during the reaction. Although a significant amount of the initiator is lost irreversibly, and the initiator efficiency factor remains low throughout the reaction, the persistent radical effect brings the polymerisation back under control and the PDIs decrease as the conversion increases.[36] This is not the case for polymerisations using **45**, where the PDIs broaden as the conversion increases. End group analysis of the polystyrene obtained from polymerisations using complex **45** showed neither olefin nor chloro end groups. It is possible that the high molecular weight of the polymer meant that the concentration of end groups was too low to observe by ^{1}H NMR. Another possibility is that the polymer does not contain many chloro end groups; termination through bimolecular coupling would result in alkyl chain ends.

The polymerisation of MMA using $^{Me2N\text{-}Ph,H}[N,N]FeCl_2$, **45**, was carried out in solution (20% v/v toluene) and proceeded relatively slowly, reaching only 55% conversion in 24 h. However, the molecular weights did not correspond with the theoretical values nor increase in a linear manner, indicating that this complex is an unsuitable catalyst for the ATRP of MMA. Molecular weights were extremely high at the beginning of the polymerisation and decreased with conversion, in the manner typical of an uncontrolled thermal polymerisation. PDIs were extremely broad throughout the polymerisation (1.7-2.8), again typical of a thermal polymerisation.

Complexes **52-54** were tested for the ATRP of styrene (200 equiv., bulk) initiated with 1-PECl at 120°C, under inert atmosphere. For complex **52**, $^{pip,H}[N,N]FeCl_2$, the polymerisation proceeded very rapidly, reaching 98% conversion in just 3.5 hours, with a pseudo-first order rate constant ($k_{obs.}$) of 0.72 h^{-1}. However, the molecular weights obtained were much higher than theoretical, with broad polydispersities. The polymerisation was repeated using diphenyl ether as a solvent (1:1 w/w with respect to monomer), under otherwise identical conditions, and the rate was found to decrease ($k_{obs.}$ = 0.36 h^{-1}, Figure 6.9). Although there was a slight decrease in the M_n (40,700 Da, compared to 46,100 Da), the polymerisation was still uncontrolled (Figure 6.10). Molecular weights were much higher than theoretical and the polydispersities remained high (*ca.* 1.9).

Similar trends were observed with complex **53**, as molecular weights were again much higher than theoretical and decreased with conversion. At just 8% conversion, the molecular weight was almost 18,000 Da with a PDI of 1.72, indicating that it was likely that termination was occurring through the bimolecular coupling of the propagating radicals. This hypothesis was supported by the ^1H NMR spectra of polymer samples obtained using complexes **52** and **53**, which did not show signals for either chloro or olefin end groups. Bimolecular coupling reactions from an uncontrolled polymerisation would give alkyl chain ends which would not be distinguishable in the ^1H NMR spectra from the bulk polymer signals. However, the data obtained for complex **54** showed a noticeably more controlled polymerisation (Figure 6.10). A summary of the data collected using the $^{pip,R''}[N,N]FeCl_2$ complexes is shown in Table 6.4.

Table 6.4 Selected data for styrene polymerisation using complexes **52-54**.

Complex	Conditions (200 equiv., 120°C, 1-PECl)	$k_{obs.}$ / h^{-1}	M_n / Da	$M_{n,th}$ / Da	PDI
52	Bulk	0.72	46109	20518	1.92
	Solution (1:1)	0.36	40695	19997	1.93
	Solution (10:1)	ND	23139	19726	1.82
53	Bulk	0.31	33459	20163	2.03
	Solution (1:1)	0.15	24366	20018	2.38
54	Bulk	0.25	14880	18122	1.63
	Solution (1:1)	0.12	19731	19559	1.27

ND = not determined

The semilogarithmic plots of $\ln([M]_0/[M]_t)$ versus time were linear for the solution polymerisation of styrene using **52-54**, as illustrated by Figure 6.9. The bulk reactions tended to deviate from linearity, possibly due to the cessation of stirring after about 90 minutes, but more likely because of the non-constant concentration of radicals as a result of increased bimolecular termination reactions. The polymerisation rates decreased as the steric bulk of the backbone was increased. Complex **52** had an initial rate of 0.36 h^{-1}, while complex **53** had a much slower rate of 0.15 h^{-1}. Adding the bulkier, electron-withdrawing phenyl groups to the backbone, **54**, further decreased the rate to 0.12 h^{-1}.

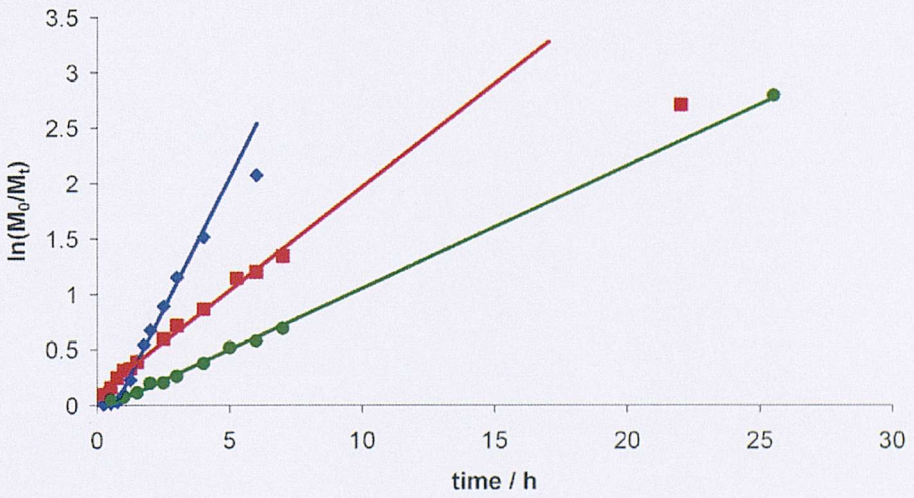


Figure 6.9 Rates for the solution polymerisation of styrene (200 eq., 50% w/w Ph_2O, 1-PECl, 120°C) by $^{pip,R''}[N,N]FeCl_2$ complexes **52-54** (R″ = H, ◆; R″ = Me, ■; R″ = Ph, ●).

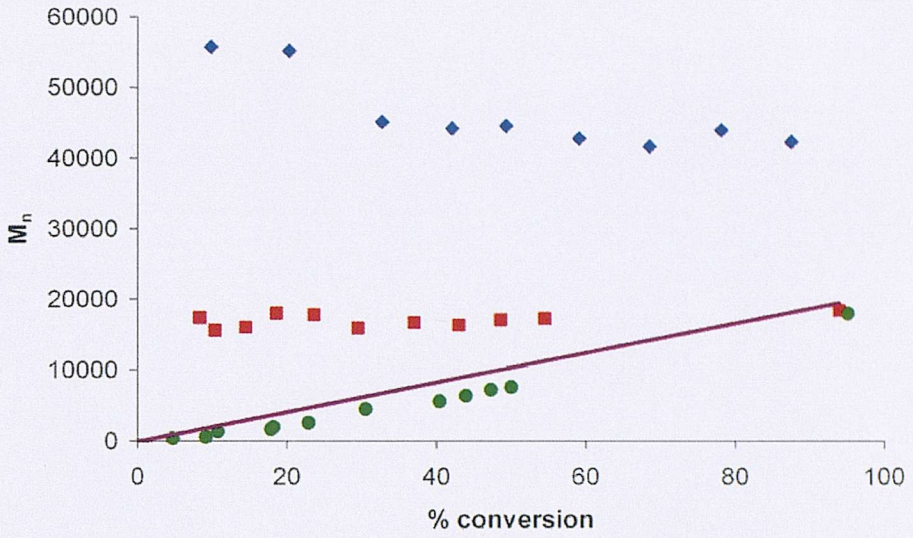


Figure 6.10 Molecular weights *vs.* conversion for the solution polymerisation of styrene (200 eq., 50% w/w Ph_2O, 1-PECl, 120°C) by $^{pip,R''}[N,N]FeCl_2$ complexes **52-54** (R″ = H, ◆; R″ = Me, ■; R″ = Ph, ●; $M_{n,th}$ = —).

The molecular weight data obtained in styrene polymerisations using complexes **52** and **53** showed that these polymerisations were uncontrolled. However, the plot of molecular weight *vs.* conversion for complex **54**, $^{pip,Ph}[N,N]FeCl_2$, showed molecular weights which increased linearly with conversion and were in relatively good agreement with the theoretical molecular weights (Figure 6.10), consistent with an ATRP mechanism. The PDIs for this polymerisation were also significantly lower than for complexes **52** and **53**, typically ranging between 1.59-1.27, which indicates a reasonable level of control. The molecular weights are, however, noticeably lower than the theoretical values and the plots resemble those reported in Chapter 4 for $^{R',Me2N-Ph}[N,N]FeCl_2$ complexes. It was hypothesised that CCT was occurring within the predominantly ATRP reaction in those cases, supported by the isolation of olefin-terminated polymer from the crude reaction mixture. End-group analysis of the polystyrene obtained using complex **54** showed mainly chloro end groups at 4.6 ppm (**, Figure 6.11), but there was evidence of some olefin-terminated polymer at 6.2 ppm (**, Figure 6.11). The presence of the 'dead' olefin-terminated polymer chains causes a decrease in the effective concentration of monomer. The reinitiation step, following β-H transfer to form the olefin-terminated oligomer, generates a new propagating radical. As there are more propagating chains than those initiated by 1-

PECl, there are fewer than 200 equivalents of monomer available to each chain. This means that the molecular weights will be lower than the theoretical values, while the presence of 'dead' chains and chains propagating at different molecular weights means that the PDIs are broadened.

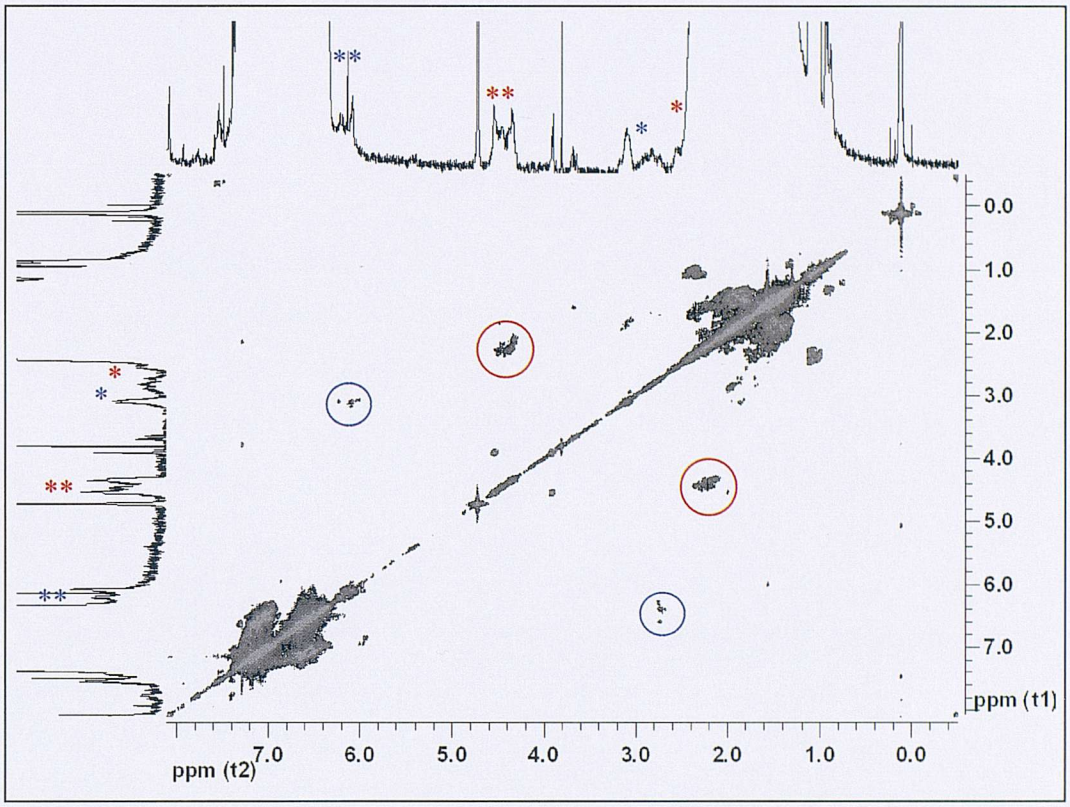


Figure 6.11 COSY spectrum of chloro (**) and olefin (**) end groups from a styrene polymerisation using $^{pip,Ph}[N,N]FeCl_2$, **54**.

The styrene polymerisations using $^{pip,R''}[N,N]FeCl_2$ complexes showed that when R″ = H or Me, there is almost no control. A rapid initiation is followed by an essentially uncontrolled thermal polymerisation, characterised by high molecular weights which decrease with conversion and broad PDIs. A kinetic experiment using styrene and 1-PECl characterised the non-catalysed reaction; after 1 h the conversion was 10%, the M_n = 87,980 Da and PDI = 1.83. After 24 h, the conversion was 77% with M_n = 36,100 Da and PDI = 2.59. The role played by the complex is in facilitating the initiation - it has little effect on the atom transfer equilibrium after propagation has begun. The piperidine complexes **52** and **53** appear to form the oxidised species readily but in an essentially irreversible step, rendering them unsuitable as catalysts for ATRP. The atom transfer equilibrium lies too far to the

right, towards the Fe^{III} species and propagating radical. This means that radical concentrations are high and propagation is rapid, while the deactivation step is inefficient.

Complex **54** behaves differently and allows some control over the polymerisation. The radical concentration for the bulk polymerisation of styrene using **54** is almost identical to that for the literature ATRP complex $^{Cy,H}[N,N]FeCl_2$. This may be because the presence of the electron withdrawing phenyl groups at the 2,3-positions of the backbone destabilises the Fe^{III} species. This complex has less affinity for being in the oxidised state and thus an equilibrium exists between the Fe^{II} and Fe^{III} complexes, allowing ATRP to proceed. Catalytic chain transfer events play a small role in the polymerisation of styrene using **54**, as evidenced by the lower than theoretical molecular weights and the olefin-terminated polymer.

Complexes **52-54** were also tested for the ATRP of MMA (100 equiv., 20% toluene, EBrB, 80°C) with the data obtained showing similar trends to the styrene polymerisation results. Using $^{H,pip}[N,N]FeCl_2$, **52**, the polymerisation was extremely rapid, reaching 93% conversion in 2.5 hours. However, this seemed to be an essentially thermal polymerisation, with broad PDIs (1.59-2.51), molecular weights which decreased with time (Figure 6.12) and non-linear kinetics. $^{Me,pip}[N,N]FeCl_2$, **53**, showed essentially the same trends, although the polymerisation was not as rapid. After 8 h the conversion was 53%, but the reaction solution was extremely viscous, indicating extremely high molecular weights. Again, the PDIs were broad (1.65-2.23), the molecular weights decreased with time (Figure 6.12) and the kinetics were non-linear.

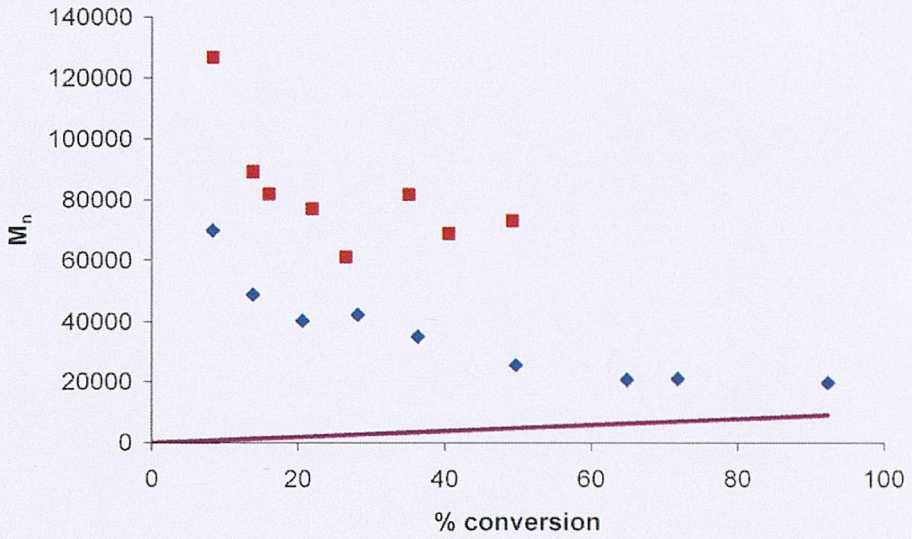


Figure 6.12 Molecular weights *vs.* conversion for the solution polymerisation of MMA (100 eq., 20% w/w toluene, EBrB, 80°C) by $^{pip,R''}[N,N]FeCl_2$ complexes **52** and **53** (R″ = H, ◆; R″ = Me, ■; $M_{n,th}$ = —).

Using $^{Ph,pip}[N,N]FeCl_2$, **54**, the polymerisation reached 90% conversion in 6 h. Molecular weights were still much higher than theoretical (Figure 6.13), but not as high as for the H and Me-substituted analogues, **52** and **53**. The kinetics were still non-linear and the PDIs were extremely broad (1.49-6.98) because the GPC traces showed bimodal and trimodal polymer signals (Figure 6.14). Clearly, the polymerisation is not controlled ATRP although the complex is exerting some influence over the polymerisation. It is likely that there is some ATRP occurring, but that the monomer is too reactive to be effectively controlled by this inefficient catalyst. Termination through side reactions including bimolecular coupling and catalytic chain transfer would result in a broad polydispersity index as there would be a wide range of polymer chain lengths.

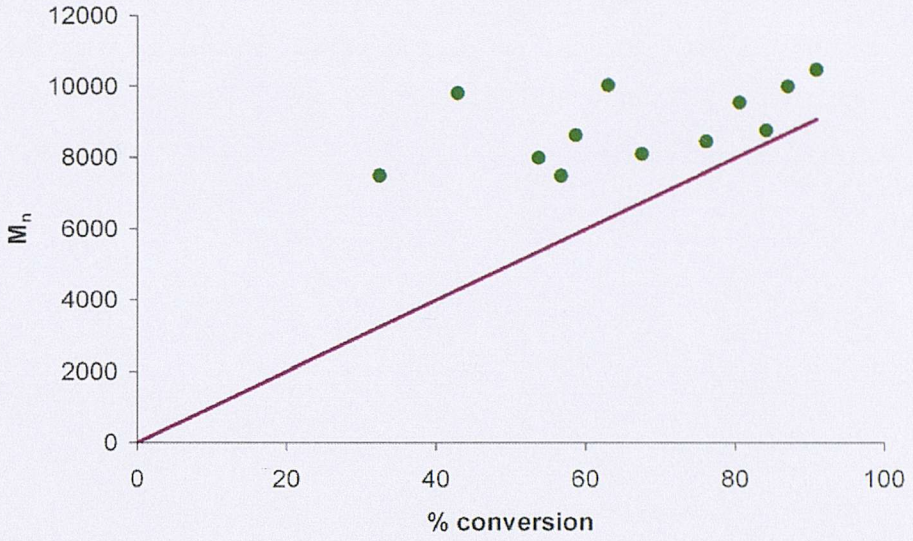


Figure 6.13 Molecular weights *versus* conversion for the solution polymerisation of MMA (100 eq., 20% w/w toluene, EBrB, 80°C) by $^{pip,Ph}[N,N]FeCl_2$, **54**. ($M_{n,th}$ = —).

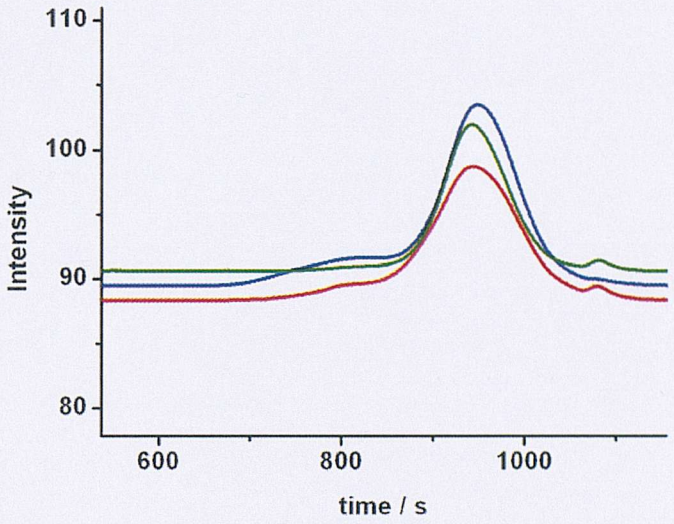


Figure 6.14 Selected partial GPC traces for the solution polymerisation of MMA (100 eq., 20% w/w toluene, EBrB, 80°C) by $^{pip,Ph}[N,N]FeCl_2$, **54**. (t = 0.5 h, —; t = 3 h, —; t = 6 h, —).

MMA is a more reactive monomer than styrene, and so it is not surprising that the piperidine complexes **52-54** are ineffective catalysts for the ATRP of MMA. Again, with complexes **52** and **53** there seems to be a very rapid initiation step but no control over the propagation. This leads to a polymerisation which mimics a thermal

polymerisation in terms of molecular weights and PDIs, but which occurs much more rapidly due to the quick halogen abstraction from the initiator by the complex.

The quaternised complexes **55-57** were screened for the ATRP of styrene, MMA and 2-HPMA. Data obtained in the styrene polymerisation experiments is collected in Table 6.5.

Table 6.5 Selected data for styrene polymerisation using complexes **55-57**.

Complex	Conditions (200 equiv., 120°C, 1-PECl)	$k_{obs.}$ / h^{-1}	M_n / Da	$M_{n,th}$ / Da	PDI
55	Bulk	ND	28037	19789	1.84
	Ph_2O solution (1:1)	0.18	32982	19601	1.67
56	Bulk	ND	29546	20205	1.82
	Ph_2O solution (1:1)	ND	30983	19997	1.76
57	Bulk	ND	27024	19372	1.74
	Ph_2O solution (1:1)	ND	24458	19580	1.68

ND = not determined

Unfortunately the quaternised complexes **55-57** behaved in a similar manner to complexes **52-54** and were not efficient catalysts for styrene polymerisation. Molecular weights were higher than theoretical values and the PDIs were broad. The poor solubility of the catalysts in this monomer is likely to contribute to the uncontrolled nature of the polymerisations. Screening reactions with styrene and **55-57** in MeOH resulted in no polymerisation, most likely due to the immiscibility of the solvent and monomer solutions.

The semilogarithmic plot for complex **55** showed a linear relationship between $\ln([M]_0/[M]_t)$ and time up until 70% conversion, with a pseudo-first order rate constant, $k_{obs.}$, of 0.18 h^{-1} (Figure 6.15). However, the plot of molecular weight *versus* conversion for **55** showed that the molecular weights did not increase linearly with conversion, nor correlate well with the theoretical molecular weights (Figure 6.16). Interestingly, the molecular weights obtained using $^{pip\text{-}I,H}[N,N]FeCl_2$, **55**, were lower than with the non-quaternised complex $^{pip,H}[N,N]FeCl_2$, **52**. Molecular weight values for **55** ranged between 45,000-30,000 Da and were typically around 35,000 Da, significantly lower than the M_n values for **52**. The decreased rate of

polymerisation using **55** (0.18 h^{-1}, *cf.* 0.36 h^{-1} for **52**) is likely to contribute to these lower molecular weights. Polydispersities were typically broad, in both cases around 1.7.

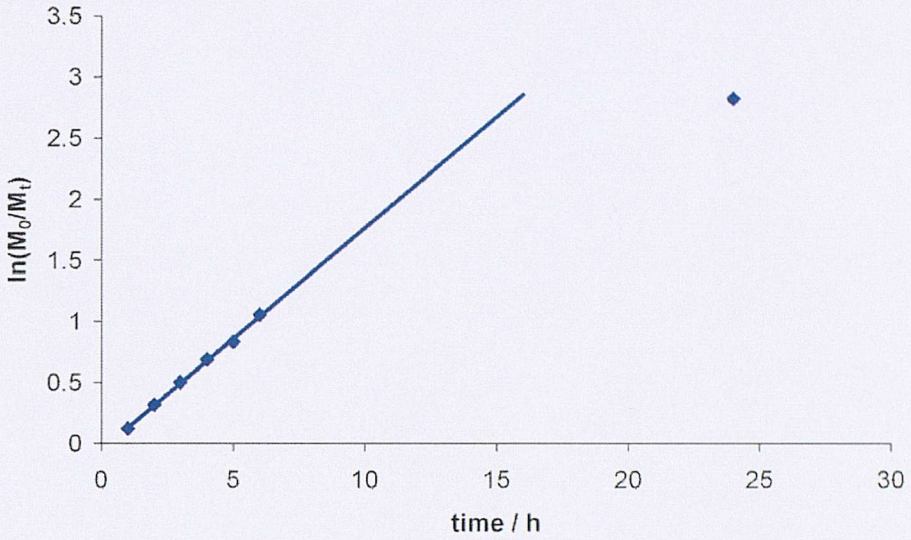


Figure 6.15 Rate for the solution polymerisation of styrene (200 eq., 50% w/w Ph_2O, 1-PECl, 120°C) by $^{pip\text{-}I,H}[N,N]FeCl_2$, **55**.

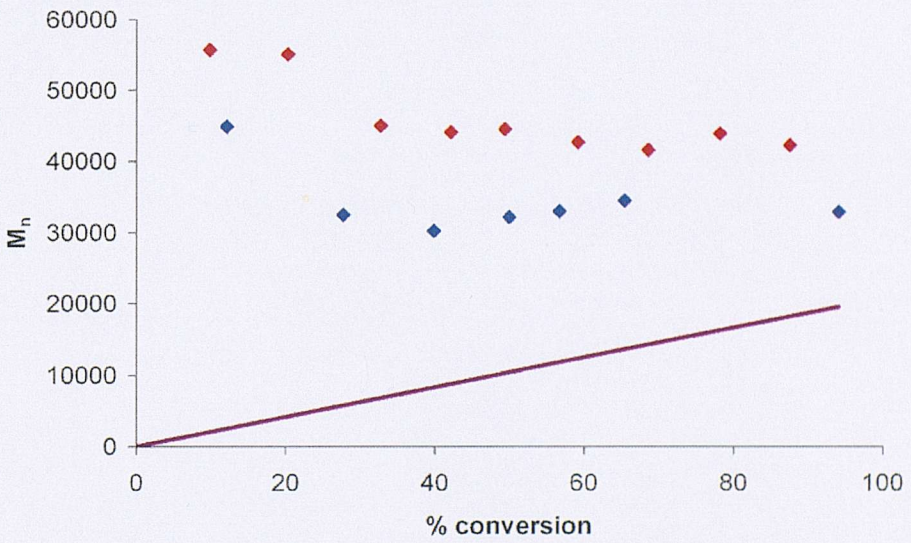


Figure 6.16 Molecular weights *versus* conversion for the solution polymerisation of styrene (200 eq., 50% w/w Ph_2O, 1-PECl, 120°C) by $^{pip,H}[N,N]FeCl_2$ complexes **52** and **55** ($^{pip,H}[N,N]FeCl_2$, ◆; $^{pip\text{-}I,H}[N,N]FeCl_2$, ◆; $M_{n,th}$ = —).

With the more polar monomers, MMA and 2-HPMA, the polymerisations were screened both in bulk and MeOH solution. Selected results are collected in Table

6.6. It was noticeable that solutions of **55-57** were not stable in MeOH under polymerisation conditions. Without MeOH, the complexes were not completely soluble in the monomer, but the presence of the polar, protic solvent under the polymerisation conditions led to decomposition of the complex, as evidenced by a colour change and precipitation of ligand and metal residue. The molecular weights were therefore much higher than theoretical and the PDIs were broad, indicating that the complexes exerted little or no control over these polymerisations.

Table 6.6 Selected data for MMA and 2-HPMA polymerisation using complexes **55-57**.

Complex	Monomer[a,b] and conditions	M_n / Da	$M_{n,th}$ / Da	PDI
-	MMA	239345	7710	2.07
-	2-HPMA, MeOH solution (1:1)	47358	1010	1.47
55	MMA, MeOH solution (1:1)	38319	6908	1.68
	2-HPMA, bulk	12556	4690	1.63
	2-HPMA, MeOH solution (1:1)	11798	7210	1.38
	2-HPMA, MeOH solution (1:1), rt[c]	10414	7060	1.47
56	MMA, MeOH solution (1:1)	36245	6538	1.76
	2-HPMA, bulk	10812	4470	1.72
	2-HPMA, MeOH solution (1:1)	9247	5620	1.39
57	MMA, MeOH solution (1:1)	28746	4910	1.63
	2-HPMA, bulk	3088	1730	1.14
	2-HPMA, MeOH solution (1:1)	39317, 1898	510	1.48, 1.12

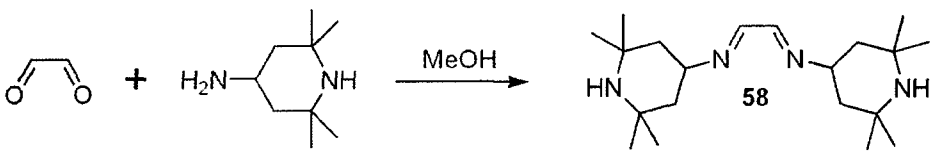
[a] MMA conditions were 100 equiv., 80°C, EBrB, 8 h. [b] 2-HPMA conditions were 50 equiv., 60°C, MBPA, 24 h. [c] rt = room temperature (25°C).

There were promising results with complex **57**, $^{pipI,Ph}[N,N]FeCl_2$, and bulk 2-HPMA, although the observed molecular weight was much higher than the theoretical value.

The conversion only reached 24% in 24 h, and the M_n of 3088 Da was significantly higher than the $M_{n,th}$ of 1730 Da. However, the extremely narrow PDI of 1.14 indicated good control over the polymerisation and it is possible that inefficient initiation, due either to slow initiation or slow deactivation, increased the observed molecular weight. It is also interesting to note that in the methanol solution polymerisation the GPC trace was bimodal. The separation between the peaks was such that individual M_p values could be calculated, and both a high molecular weight peak with broad PDI, presumably from a thermal polymerisation pathway, and a lower molecular weight peak with a narrow PDI, potentially from a controlled process, could be observed. Difficulty in processing the polymer samples did not allow further experiments to be conducted, but this complex would be a potential starting point for further investigations using polar monomers.

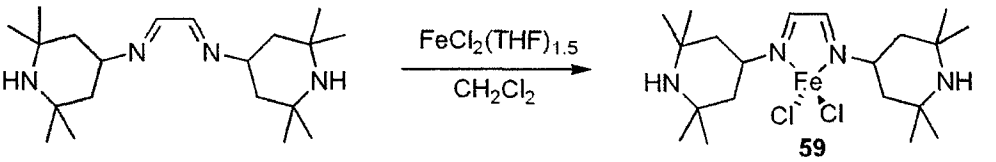
6.2.1.4 - Next generation amino substituents.

One possible explanation for the poor performance of the piperidine-based catalysts **52-55** in ATRP is the presence of an available lone pair on the benzyl-substituted amine group. Although the solid state structures of **52** and **53** did not show coordination of this nitrogen to the metal centre, the behaviour of the complexes at high temperatures in solution, under polymerisation conditions, may be different. In order to investigate this, a ligand with substitution at the positions *ortho* to the piperidine amine group was synthesised (Scheme 6.8). $^{TEMP,H}[N,N]$ was prepared in bulk and recrystallised from a solution of Et_2O/MeOH to give **58** in 66% yield. Unfortunately, attempts to prepare a more soluble *N*-methylated version of **58** were unsuccessful.



Scheme 6.8 Synthesis of ligand **58**.

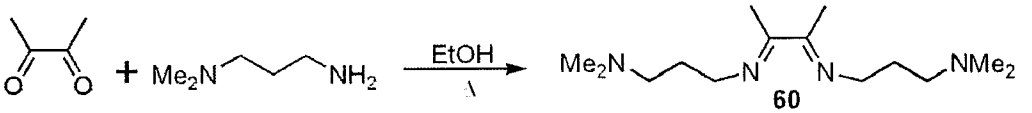
Reaction of **58** with $FeCl_2(THF)_{1.5}$ in CH_2Cl_2 (Scheme 6.9) resulted in an immediate colour change to dark blue, and $^{TEMP,H}[N,N]FeCl_2$, **59**, was obtained as a purple solid, in 75% yield, after extraction in CH_2Cl_2, concentration and precipitation with pentane.



Scheme 6.9 Synthesis of Fe^{II} complex **59**.

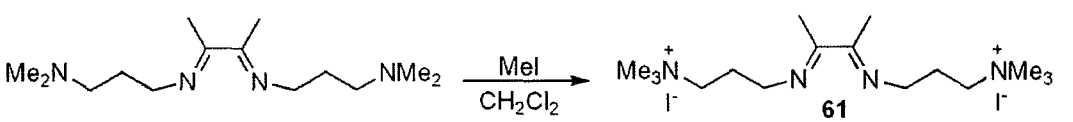
As with the related piperidine complexes **52-57**, no meaningful ^1H NMR spectra could be obtained for complex **59**. However, the imine $\nu_{C=N}$ stretch was clearly visible at 1637 cm^{-1}, a slight increase in frequency from the free ligand (1630 cm^{-1}). This is consistent with the observations for complexes **52-54**, where coordination to the metal increases the strength of the C=N bond, probably due to the electron donating properties of the *N*-substituent. The FAB-MS of **59** showed only ligand signals, but Evans' NMR magnetic susceptibility measurements confirmed that the Fe^{II} complex was d^6 high spin (μ_{eff} = 4.90 B. M.).

A further tertiary-amine functionalised ligand was prepared through the condensation of 2,3-butanedione with *N,N*-dimethylaminopropylamine, following a literature procedure (Scheme 6.10).[37] After refluxing the reactants in EtOH, the solvent was removed and the dark brown crude product distilled under reduced pressure to give $^{Me2N\text{-}nPr,Me}[N,N]$, **60**, as an air-sensitive, pale yellow oil in 31% yield.



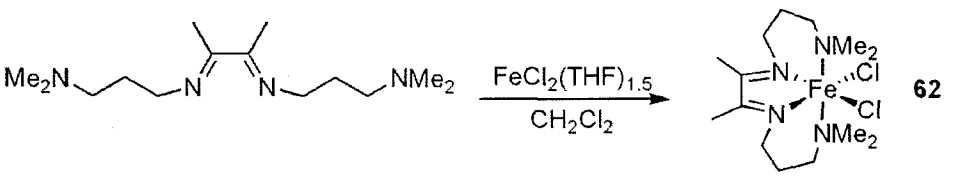
Scheme 6.10 Literature synthesis of ligand **60**.

Ligand **60** was readily quaternised through reaction of $^{Me2N\text{-}nPr,Me}[N,N]$ with MeI in CH_2Cl_2 to give the methyl iodide salt, **61**, in essentially quantitative yield (Scheme 6.11). As with the piperidinium ligands **55-57**, the $[M\text{-}I]^+$ peak was observed in the FAB-MS of **61**. The new methyl environment was visible in the ^1H and ^{13}C NMR, at δ 3.12 and 52.8 ppm, respectively. The absence of the free nitrogen lone pair means that these signals are shifted significantly upfield from the NMe_2 ^1H and ^{13}C signals of ligand **60**, at δ 2.19 and 45.5 ppm.



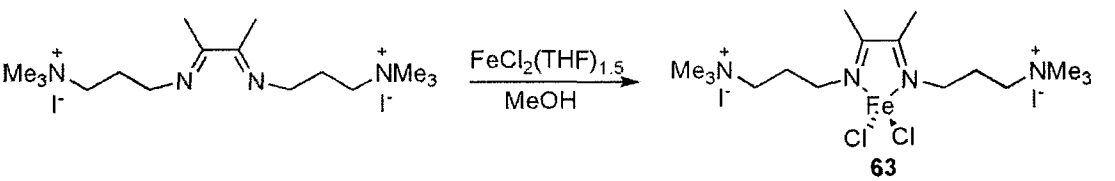
Scheme 6.11 Synthesis of ligand **61**.

The Fe^{II} chloride complex of **60** was also reported in the literature, and was synthesised using a modified procedure (Scheme 6.12). Extraction in CH_2Cl_2, concentration and precipitation with pentane gave $^{Me2N\text{-}nPr,Me}[N,N]FeCl_2$ as a dark blue solid in 61% yield. The characterising data was in good agreement with the data in the literature,[37] which reported the complex to be octahedral through coordination of the tertiary amine groups to the iron centre. This is likely to result in an ineffective catalyst for ATRP, as the metal centre is crowded and oxidation to the Fe^{III} species will be hindered, unless the 'arms' of the ligand dissociate.



Scheme 6.12 Synthesis of Fe^{II} complex **62**.

The quaternised ligand, **61**, will be prevented from acting as a tetradentate ligand by the unavailability of the amine nitrogen lone pair. Thus, efficient ATRP should be possible using this complex, which was prepared through the reaction of $FeCl_2(THF)_{1.5}$ and **61** in MeOH (Scheme 6.13). Concentration and precipitation using Et_2O gave **63** as a dark blue solid in 65% yield.



Scheme 6.13 Synthesis of Fe^{II} complex **63**.

The IR spectrum of **63** showed the imine stretch, $\nu_{C=N}$, at 1634 cm^{-1} which is significantly higher frequency than the $\nu_{C=N}$ of the free ligand, **61**, which was at 1621 cm^{-1}. FAB-MS showed both the $[M\text{-}Cl]^+$ peak, at 629 a.m.u. and the $[M\text{-}I]^+$ signal, common to all the quaternised salts, at 537 a.m.u. No meaningful ^1H NMR spectrum could be obtained for complex **63** but the Evans' NMR method gave a solution magnetic moment of 5.14 B.M., consistent with the postulated Fe^{II} complex.

6.2.1.5 - Polymerisation studies using the new amino complexes.

The polymerisation of styrene (200 equiv., bulk, 120°C, 1-PECl) using $^{TEMP,H}[N,N]FeCl_2$, **59**, was poorly controlled. The reaction proceeded rapidly, with

$k_{obs.}$ = 0.78 h^{-1}, and a linear semilogarithmic plot up until 70% conversion (Figure 6.17). However, molecular weights were higher than theoretical and did not increase linearly with conversion (Figure 6.18). The molecular weights were typically around 45,000 Da, independent of conversion. This is very similar to the data obtained for ^{pip,H}[*N,N*]$FeCl_2$, **52**, where molecular weights decreased from *ca.* 55,000 Da initially to 42,000 Da. PDIs were broad, typically between 1.7-2.0 throughout the polymerisation, consistent with the data obtained with complex **52**.

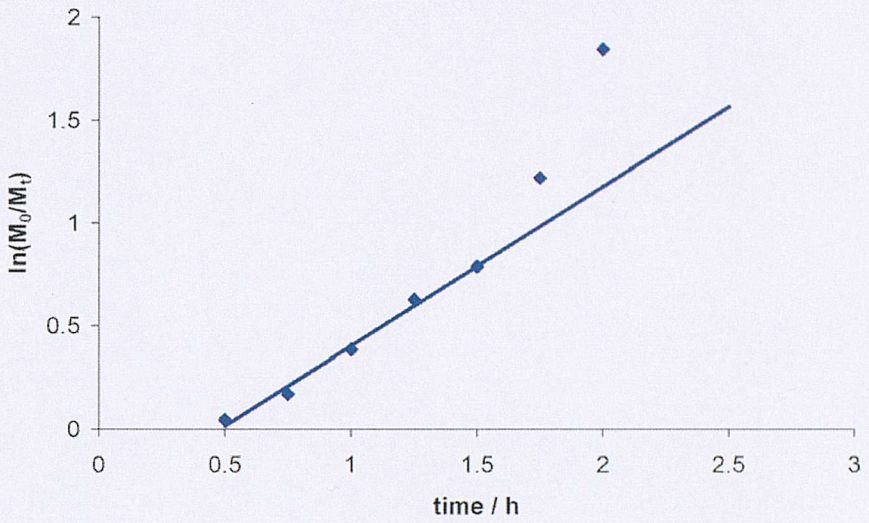


Figure 6.17 Rate for the polymerisation of styrene (200 eq., 1-PECl, 120°C) by ^{TEMP,H}[*N,N*]$FeCl_2$, **59**.

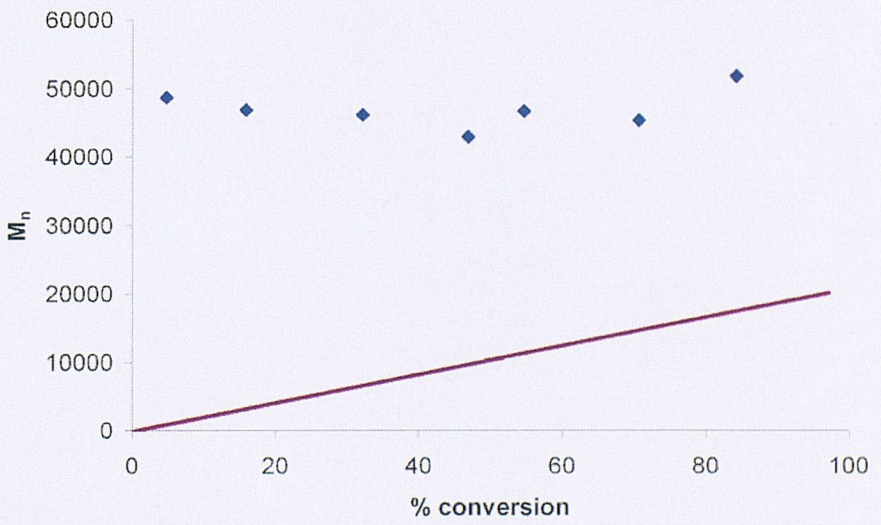


Figure 6.18 Molecular weights *versus* conversion for the polymerisation of styrene (200 eq., 1-PECl, 120°C) by ^{TEMP,H}[*N,N*]$FeCl_2$, **59**. ($M_{n,th}$ = —).

Polymerisation of MMA using **59** also proceeded in a manner very similar to **52**. Although the semilogarithmic plot was linear (Figure 6.19), with a $k_{obs.}$ of 0.68 h^{-1}, molecular weights were independent of conversion and decreased from *ca.* 100,000 Da at 12% conversion to 60,000 Da at 68% conversion (Figure 6.20). The PDIs were broad throughout the polymerisation, typically *ca.* 1.9.

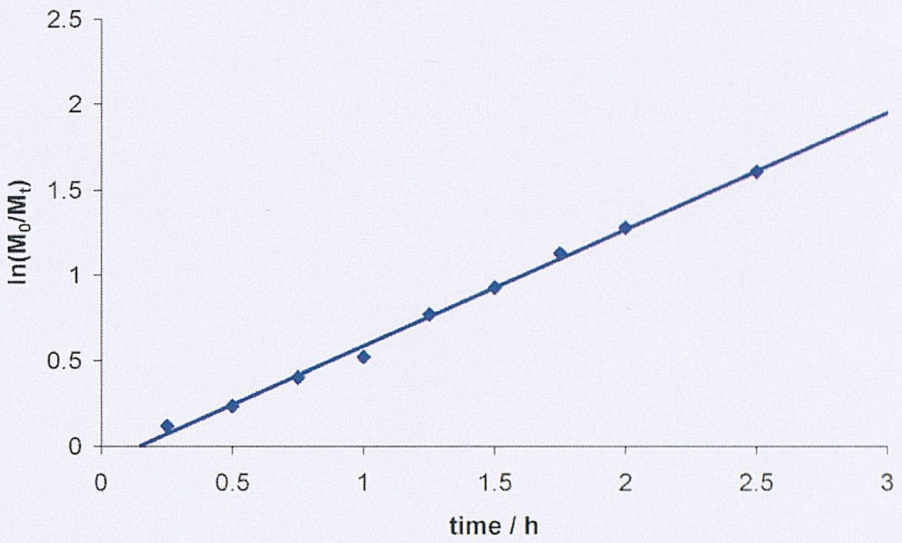


Figure 6.19 Rate for the polymerisation of MMA (100 eq., 20% toluene, EBrB, 80°C) by $^{TEMP,H}[N,N]FeCl_2$, **59**.

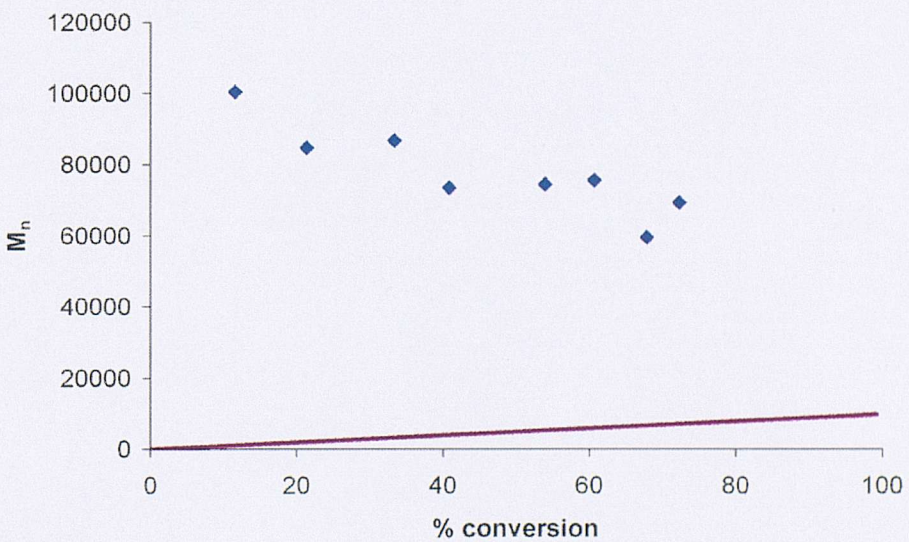


Figure 6.20 Molecular weights *versus* conversion for the solution polymerisation of styrene (200 eq., 1-PECl, 120°C) by $^{TEMP,H}[N,N]FeCl_2$, **59**. ($M_{n,th}$ = —).

The similarity in the data obtained for styrene and MMA polymerisations using complexes **52** and **59** indicates that the ineffectiveness of the $^{pip,R''}[N,N]FeCl_2$ complexes as catalysts for ATRP is not due to the coordination of the amine group. This is supported by the behaviour of the quaternised complexes **55-57**, which also possess non-coordinating amine groups but are ineffective catalysts for styrene and MMA ATRP.

There are several factors which may play a role in contributing to the inefficiency of this family of complexes as ATRP catalysts. The general poor solubility of the piperidine complexes in the monomers studied is likely to reduce their efficiency, through the presence of a lower effective concentration of catalyst. The electronic characteristics of the ligand are extremely important in mediating the polymerisation, as Chapters 2-5 illustrated, and it may be that the nitrogen-containing ring is too electron donating. The halogenophilicity of the metal centre would be extremely high, potentially leading to irreversible formation of the oxidised metal complex. This would result in a rapid initiation step, but without the ready availability of a halogen atom from the Fe^{III} complex to form the dormant species, the propagation would be uncontrolled.

The final family of amino complexes studied for ATRP in aqueous media were those based on the literature synthesis of $^{Me2N\text{-}nPr,Me}[N,N]FeCl_2$. As expected, complex **62** was a poor catalyst for the ATRP of styrene and MMA due to the tetradentate nature of the ligand. Polymerisations were rapid, reaching 100% conversion in under 4 h, and molecular weights were much higher than theoretical with broad PDIs. Complex **63**, with the quaternised amino groups, was a slightly better catalyst than **62**, although molecular weights for styrene and MMA polymerisations were still significantly higher than the theoretical values and the PDIs were broad. Selected polymerisation data obtained using complexes **62** and **63** are shown in Table 6.7.

Table 6.7 Selected data for polymerisation using complexes **62** and **63**.

Complex	Monomer[a,b,c] and conditions	M_n / Da	$M_{n,th}$ / Da	PDI
62	Styrene, bulk	87677	20413	1.71
	MMA, bulk	55487	9712	1.89
63	Styrene, MeOH solution (1:1)	59953	20830	2.05
	MMA, MeOH solution (1:1)	26426	10012	1.85
	MMA, MeOH solution (2:1)	40462	10012	2.11
	2-HPMA, bulk	13158	3820	2.31
	2-HPMA, MeOH solution (1:1)	5887	3320	1.45

[a] Styrene conditions were 200 equiv., 120°C, 1-PECl, 6 h. [b] MMA conditions were 100 equiv, 80°C, EBrB, 6 h. [c] 2-HPMA conditions were 50 equiv., 60°C, MBPA, 24 h.

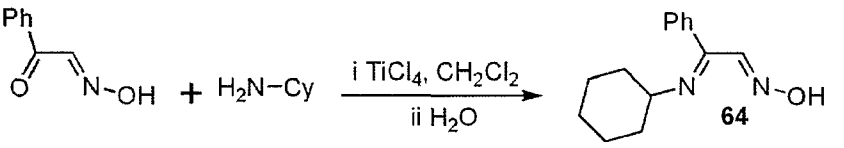
Complex **63** is potentially a useful catalyst for the polymerisation of 2-HPMA in MeOH. Although the PDIs for the reaction were relatively broad (1.45), the complex appeared to be stable under the polymerisation conditions and the polymer molecular weights were not too much higher than the theoretical values (M_n = 5887, $M_{n,th}$ = 3320). In contrast to the piperidine catalysts, there was a noticeable improvement in control when the polymerisation was carried out in MeOH solution. The bulk reaction using **63** was extremely fast (solid in 5 h) and uncontrolled, with molecular weights much higher than theoretical values (M_n = 13158, $M_{n,th}$ = 3820) and broad PDIs (2.31). Kinetic experiments using **63** with 2-HPMA and other polar monomers in MeOH and other polar protic solvents would be a starting point for further work into this system.

6.2.2 - Synthesis and polymerisation behaviour of hydroxy-substituted Fe^{II} complexes.

The other functional group targeted as likely to impart solubility in polar and protic media was hydroxyl groups. There are α-diimine ligands containing hydroxyl groups commercially available, in the form of oximes, and $^{OH,Ph}[N,N]$ and $^{OH,Me}[N,N]$ were used as ligands. The cobalt complexes of oximes are extremely effective CCT catalysts,[38] as discussed in Chapter 1, and so asymmetric ligands with *N*-alkyl substituents were also targeted in order to increase the electron donation and favour ATRP.

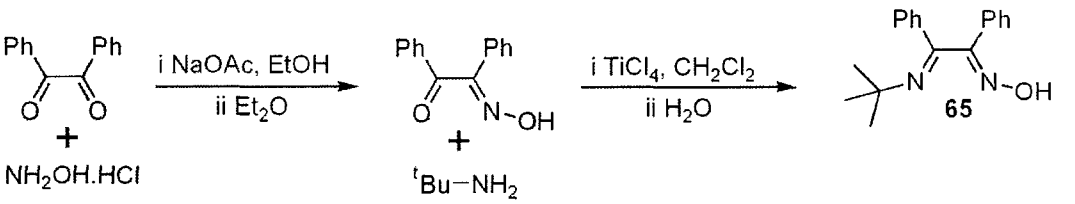
6.2.2.1 - Synthesis of Fe^{II} oxime complexes.

The synthesis of an oxime ligand containing an *N*-cyclohexyl group was accomplished though the condensation of 2-*iso*nitrosoacetophenone with $CyNH_2$, using $TiCl_4$ as an activating agent (Scheme 6.14). After recrystallisation of the crude material from hot MeOH, the desired ligand, **64**, was obtained in moderate yield of 40%.



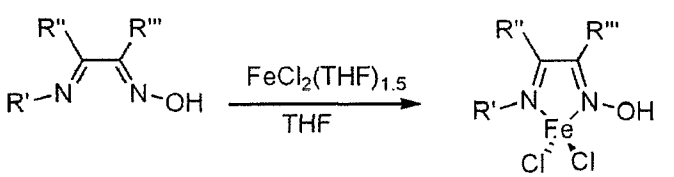
Scheme 6.14 Synthesis of asymmetric monoxime ligand **64**.

To eliminate the proton on the backbone, a potential site for side reactions during a radical polymerisation, another route to asymmetric *N*-alkyl oximes was developed. Reaction of benzil with 1 equivalent of hydroxylamine yielded the benzil monoxime compound in excellent yield (83%) after recrystallisation. The benzil monoxime can be condensed with a variety of amines to give a range of ligands. However, for the purposes of the initial investigation, the monoxime and $^tBuNH_2$ were reacted using the $TiCl_4$ method. Formation of ^{tBu,Ph}[*N,NOH*], **65**, was achieved in good yields of 64% after recrystallisation from EtOH (Scheme 6.15).



Scheme 6.15 Synthesis of asymmetric monoxime ligand **65**.

The Fe^{II} chloride complexes of ligands **64** and **65** and the commercially available oximes ^{OH,Ph}[*N,N*] and ^{OH,Me}[*N,N*] were prepared through the reaction of the ligand with $FeCl_2(THF)_{1.5}$ in THF (Scheme 6.16).



	R'	R''	R'''
66	OH	Me	Me
67	OH	Ph	Ph
68	Cy	Ph	H
69	^{t}Bu	Ph	Ph

Scheme 6.16 Synthesis of Fe^{II} oxime complexes **66-69**.

Complexes **66-69** were prepared in good yields (51-88%) but unfortunately did not give meaningful ^{1}H NMR spectra. The complexes were insoluble in most organic solvents, fairly soluble in THF and readily dissolved in MeOH. The IR spectra of the complexes showed that $\nu_{C=N}$ increased in frequency upon coordination, from 1593-1614 cm^{-1} in the free ligands to 1605-1643 cm^{-1} in the complexes. This implies that the C=N bonds are stronger in the complexes than in the free ligands. The ν_{O-H} stretches decreased in frequency, from 3111-3280 cm^{-1} in the free ligands to 3025-3197cm^{-1} in the complexes. Both FAB-MS and CI-MS proved to be unsuitable for identifying the $[M+H]^+$ signals, and in each case, only the $[L+H]^+$ peaks were observed. Crystals of **66** (Figure 6.21, Table 6.8) and **67** (Figure 6.22, Table 6.9) suitable for X-ray structure analysis were obtained through layering a saturated THF solution with pentane, and allowing slow diffusion to occur.

Complex **66** is a C_i-symmetric, dimeric molecule with the Fe centres bridged through two shared chlorine atoms. The geometry at the metal centres is distorted octahedral, with inter-bond angles of 71.00(5)°-111.482(15)°. The most acute angle represents the bite of the *N,N'* chelate ligand and is much narrower than other complexes reported in this thesis, illustrating the flexibility of the α-diimine ligands in coordination chemistry. The bond lengths are similar to those seen in previous complexes, with the distinct pattern of bond ordering indicating an absence of bond delocalisation. The C=N linkages at 1.2899(18) and 1.2877(18) Å are shorter than the 1.476(2) Å C–C bond. Interestingly, the N=C–C=N unit is not planar and the chelate ring is puckered, with a torsion angle of *ca.* 5° between the imine units.

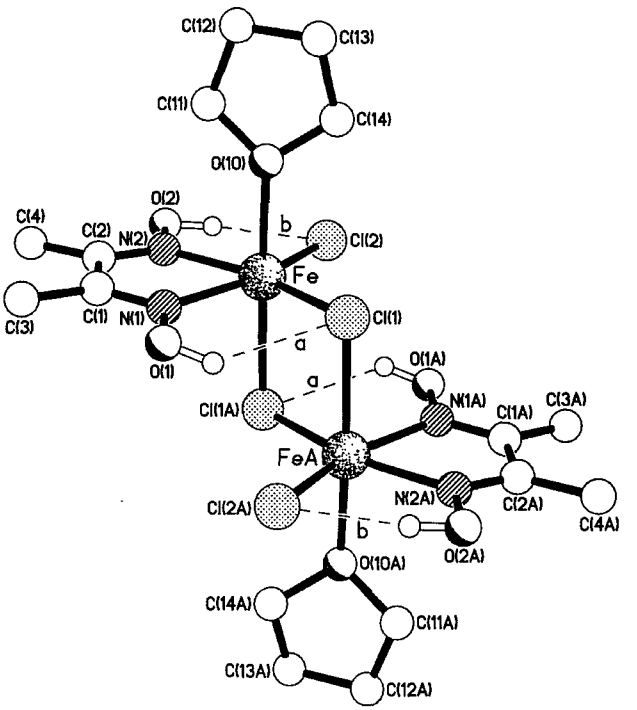


Figure 6.21 The molecular structure of complex **66**. The hydrogen bonds have the following geometries: (a) [O...Cl] 3.2376(13) Å, [H...Cl] 2.54 Å, [N-H...Cl] 135°. (b) [O...Cl] 3.1149(13) Å, [H...Cl] 2.25 Å, [N-H...Cl] 162°. [O-H fixed at 0.900 Å]

Table 6.8 Selected bond lengths (Å) and angles (°) for complex **66**.

Fe–Cl(1)	2.4072(4)	Cl(1)–Fe–Cl(1A)	86.943(12)
Fe–Cl(2)	2.3735(4)	Cl(1)–Fe–Cl(2)	111.482(15)
Fe–Cl(1A)	2.5430(4)	Cl(1)–Fe–N(1)	88.64(3)
Fe(A)–Cl(1)	2.5430(4)	Cl(1A)–Fe–N(1)	87.04(3)
Fe–N(1)	2.1991(11)	Cl(1)–Fe–N(2)	159.46(3)
Fe–N(2)	2.1497(12)	N(1)–Fe–N(2)	71.00(5)
N(1)–C(1)	1.2899(18)	Fe–Cl(1)–Fe(A)	93.057(12)
N(2)–C(2)	1.2877(18)	O(1)-H...Cl(1)	135
C(1)–C(2)	1.476(2)	O(2)-H...Cl(2)	162
O(1)...Cl(1)	3.2376(12)		
H...Cl(1)	2.54		
O(2)...Cl(2)	3.1149(13)		
H...Cl(2)	2.25		

The final coordination site at the metal centre is occupied by a molecule of THF, which explains the observed colour changes from orange to red when $^{OH,Me}[N,N]FeCl_2$ or $^{OH,Ph}[N,N]FeCl_2$ are dissolved in coordinating solvents. There are hydrogen bonds between the hydroxyl proton of the oxime and the geometrically accessible chlorine atoms. The length of these hydrogen bonds (2.25-2.54 Å) is similar to that seen in an asymmetric amine-oxime copper complex, which had an intermolecular hydrogen bond between the OH group of the oxime and the chlorine atom of 2.42 Å.[39] The structure obtained for complex **66** is unusual in that the oxime is neutral; most similar reports in the literature detail the reaction of Fe^{II} with the diphenylglyoximato anion and various ancillary ligands.[40,41] There are many examples of structurally characterised metal oximes, but these again tend to be deprotonated and either have ancillary ligands such as PR_3, CO or py, or are bridged with species such as BF_2.[42-47]

Complex **67** exhibits very similar geometry to **66** (Figure 6.22, Table 6.9) and crystallised with 2 independent C_i-symmetric molecules in the unit cell. Again, the complex is dimeric and bridged through 2 chlorine atoms. Hydrogen bonds link the hydroxyl protons with the chlorine atoms; the hydrogen bonds are between 2.20-2.45 Å in length, slightly shorter than those in **66**. There is more of a twist to the N=C–C=N unit, with a torsion angle of *ca.* 19° between the two imines, presumably as a result of the bulkier Ph groups on the 2,3-positions of the ligand backbone.

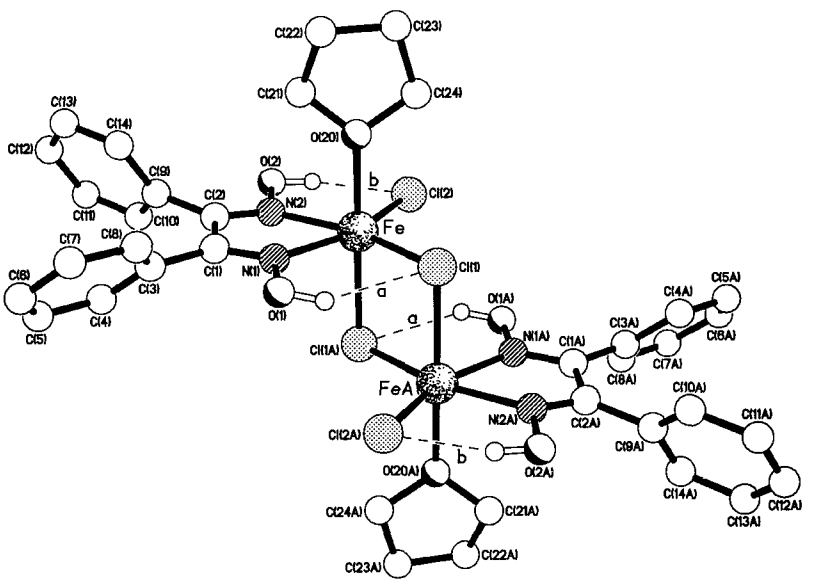


Figure 6.22 The molecular structure of the C_i-symmetric complex, **67**. The hydrogen bonds have the following geometries; (a) [O...Cl] 3.2474(13) Å, [H...Cl] 2.45 Å, [N-

H...Cl] 148°. (b) [O...Cl] 3.0253(15) Å, [H...Cl] 2.20 Å, [N-H...Cl] 153°. [O-H fixed at 0.900 Å].

Table 6.9 Selected bond lengths (Å) and angles (°) for complex **67**.

	Mol. I	**Mol. II**		**Mol. I**	**Mol. II**
Fe–Cl(1)	2.4044(7)	2.3884(6)	Cl(1)–Fe–Cl(1A)	87.13(2)	89.16(2)
Fe–Cl(2)	2.3490(7)	2.3519(7)	Cl(1)–Fe–Cl(2)	110.53(2)	109.15(2)
Fe–Cl(1A)	2.5509(6)	2.5419(6)	Cl(1)–Fe–N(1)	90.90(4)	90.66(4)
Fe(A)–Cl(1)	2.5509(6)	2.5419(6)	Cl(1A)–Fe–N(1)	88.75(4)	90.04(4)
Fe–N(1)	2.1726(14)	2.1865(14)	Cl(1)–Fe–N(2)	161.87(4)	161.87(4)
Fe–N(2)	2.1464(15)	2.1479(14)	N(1)–Fe–N(2)	70.97(6)	71.21(5)
N(1)–C(1)	1.297(2)	1.292(2)	Fe–Cl(1)–Fe(A)	92.87(2)	90.84(2)
N(2)–C(2)	1.291(2)	1.2932(19)	O(1)-H...Cl(1)	148	143
C(1)–C(2)	1.490(2)	1.487(2)	O(2)-H...Cl(2)	153	150
O(1)...Cl(1)	3.2474(13)	3.2164(14)			
H...Cl(1)	2.45	2.45			
O(2)...Cl(2)	3.0253(15)	3.0694(14)			
H...Cl(2)	2.20	2.26			

6.2.2.2 - Polymerisation studies using Fe^{II} oxime complexes.

The oxime-containing complexes **66-69** were inefficient catalysts for the ATRP of styrene. However, some control over MMA ATRP was observed for the *N*-alkyl substituted asymmetrical oxime complexes, **68** and **69**. Selected polymerisation results are given in Table 6.10.

Table 6.10 Selected data for polymerisation using complexes **66-69**.

Complex	Monomer[a,b] and conditions	M_n / Da	$M_{n,th}$ / Da	PDI
66	Styrene, bulk	2499	20413	1.89
	MMA, bulk	nr[c]	-	-
	MMA, MeOH solution (2:1)	nr	-	-
67	Styrene, bulk	1460	20830	1.52
	MMA, bulk	nr	-	-
	MMA, toluene solution (10:1)	nr	-	-
	MMA, MeOH solution (2:1)	nr	-	-
68	Styrene, MeOH solution (1:1)	51651	15018	1.79
	MMA, bulk	6375	6258	1.32
	MMA, MeOH solution (1:1)	7683	6508	1.53
69	Styrene, MeOH solution (1:1)	76893	16872	1.87
	MMA, bulk	6042	5006	1.41
	MMA, MeOH solution (1:1)	22241	7008	2.80

[a] Styrene conditions were 200 equiv., 120°C, 1-PECl. [b] MMA conditions were 100 equiv., 80°C, EBrB. [c] nr = no reaction

Complexes **66** and **67** appear to be extremely efficient Fe-based CCT catalysts, reaching 100% conversion in under 3 h, but with molecular weights independent of conversion. The semilogarithmic plots of $\ln([M]_0/[M]_t)$ *vs.* time were non-linear, molecular weights were typically less than 2500 Da (Figure 6.23) and PDIs were broad (1.5-2.0). End group analysis showed the presence of both chloro and olefin end groups (Figure 6.24). Complexes **66** and **67** catalyse much more rapid styrene polymerisation than the CCT catalysts such as $^{R',F\text{-}Ph}[N,N]FeCl_2$, reported in Chapters 2 and 4, and the faster rate of polymerisation means that the chloro end groups are observed. Interestingly, these complexes were ineffective for the polymerisation of

MMA, both under bulk and solution conditions. A colour change indicated probable coordination of the monomer, and no polymer could be isolated even after extended reaction times.

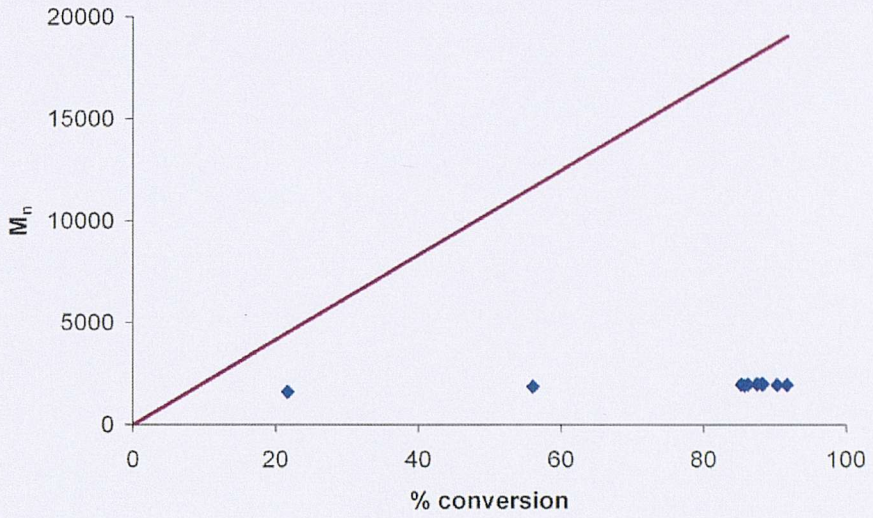


Figure 6.23 Molecular weights *versus* conversion for the bulk polymerisation of styrene (200 eq., 1-PECl, 120°C) by ^{OH,Ph}[*N,N*]$FeCl_2$, **67**. ($M_{n,th}$ = —).

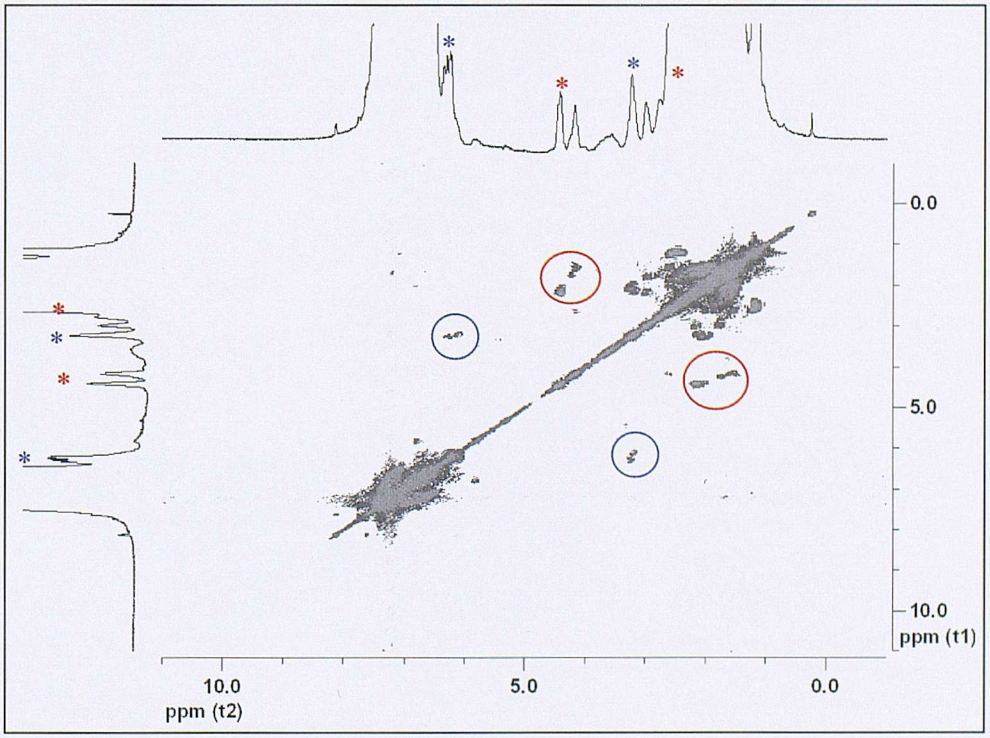


Figure 6.24 Cosy spectrum of polystyrene formed using ^{OH,Ph}[*N,N*]$FeCl_2$, **67**, showing the presence of chloro (**) and olefin (**) end groups.

Complexes **68** and **69** were tested for the ATRP of styrene in MeOH solution, in an attempt to dissolve the complexes. However, molecular weights were much higher than the theoretical values and the PDIs were broad, indicating that there was very little control over the polymerisation. Complexes **68** and **69** were reasonable catalysts for the ATRP of MMA, both in bulk and MeOH solution. However, the inclusion of MeOH both increased the rate and decreased the control over the polymerisation, as evidenced by molecular weights significantly higher than theoretical values and broad PDIs (Table 6.10).

For complex **68**, the bulk polymerisation of MMA proceeded with $k_{obs.} = 0.03\ h^{-1}$, reaching 60% conversion in 24 h. The linear semilogarithmic plot of $\ln([M]_0/[M]_t)$ *vs.* time (Figure 6.25) indicated that the radical concentration remained constant during this time. Molecular weights increased linearly with conversion, although were noticeably higher than theoretical at the beginning of the polymerisation (Figure 6.26).

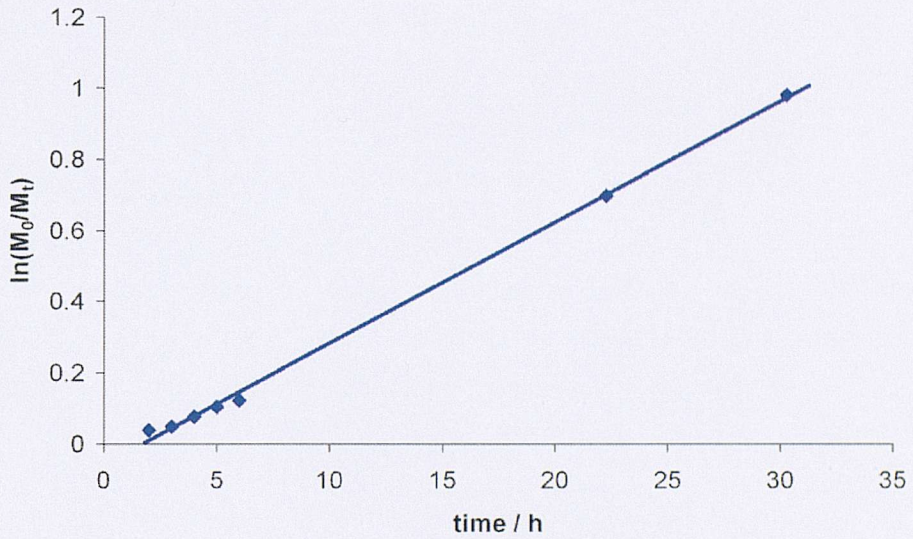


Figure 6.25 Rate for the bulk polymerisation of MMA (100 eq., EBrB, 80°C) by $^{Cy,OH,Ph,H}[N,N]FeCl_2$, **68**.

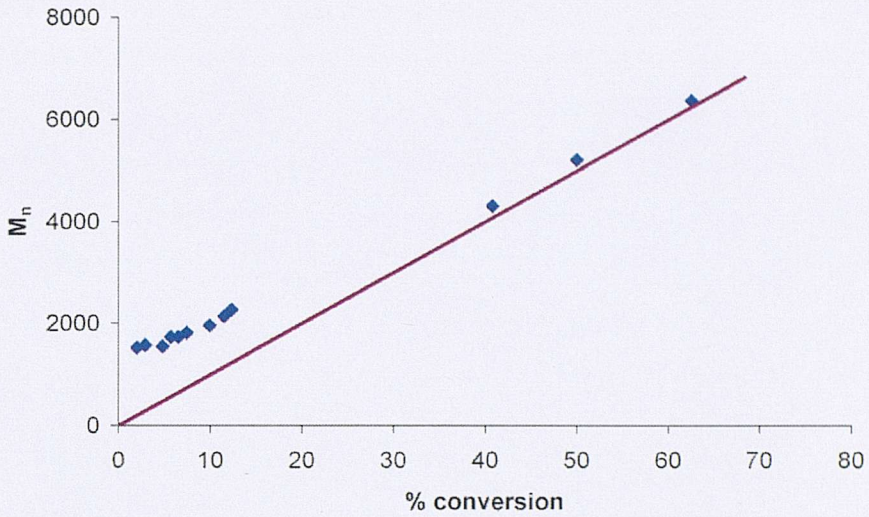


Figure 6.26 Molecular weights *versus* conversion for the bulk polymerisation of MMA (100 eq., EBrB, 80°C) by $^{Cy,OH,Ph,H}[N,N]FeCl_2$, **68**. ($M_{n,th}$ = ▬).

This loss in molecular weight control indicates inefficient initiation, most likely due to a slow initiation process where only a fraction of the initiator molecules are activated at a particular time. However, this would be expected to lead to broadened PDIs at the beginning of the polymerisation, which would decrease as the polymerisation progressed.[36] As this is not the case (PDIs are 1.2-1.3 throughout the polymerisation, with no noticeable decrease with increasing conversion, Figure 6.27), it is more likely that the presence of a mixed-halogen system resulted in an initial loss of control as redistribution occurred. This is similar to the results reported in Chapter 4 for the polymerisation of MMA using $^{Cy,Me2N\text{-}Ph}[N,N]FeCl_2$.

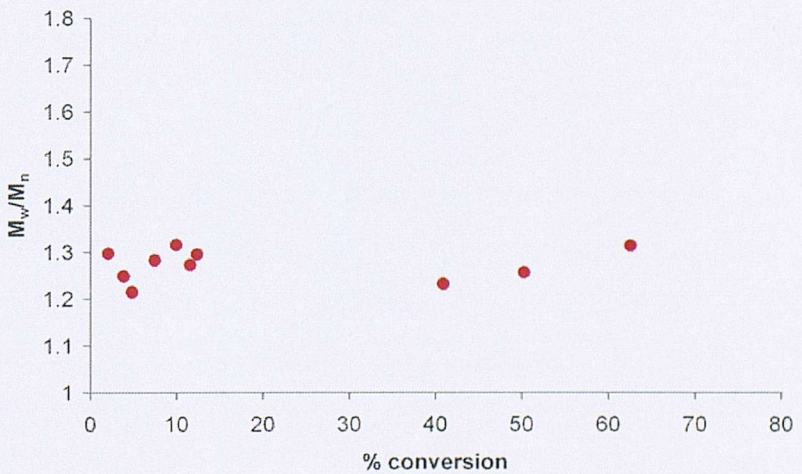


Figure 6.27 PDIs *versus* conversion for the bulk polymerisation of MMA (100 eq., EBrB, 80°C) by $^{Cy,OH,Ph,H}[N,N]FeCl_2$, **68**.

The polymerisation of MMA by complex **69** was not as well controlled as **68**. This is likely to be due to the poor solubility of **69** in the monomer. The semilogarithmic plot of $\ln([M]_0/[M]_t)$ *vs.* time was non-linear, and although the molecular weights did increase with conversion, they were significantly higher than theoretical for most of the polymerisation (Figure 6.28). PDIs were extremely broad throughout the reaction (2.1-2.4), indicating that the inefficient initiation was coupled with significant termination through side reactions such as bimolecular coupling.

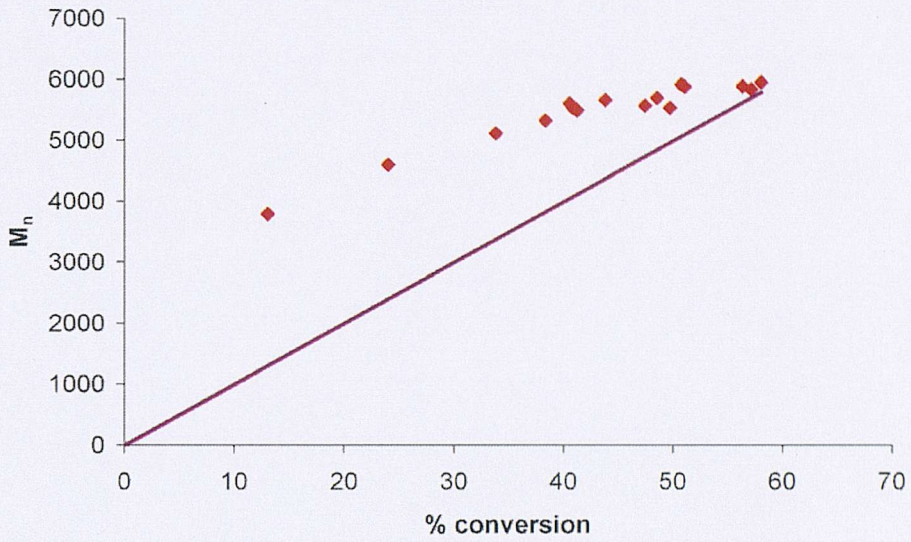
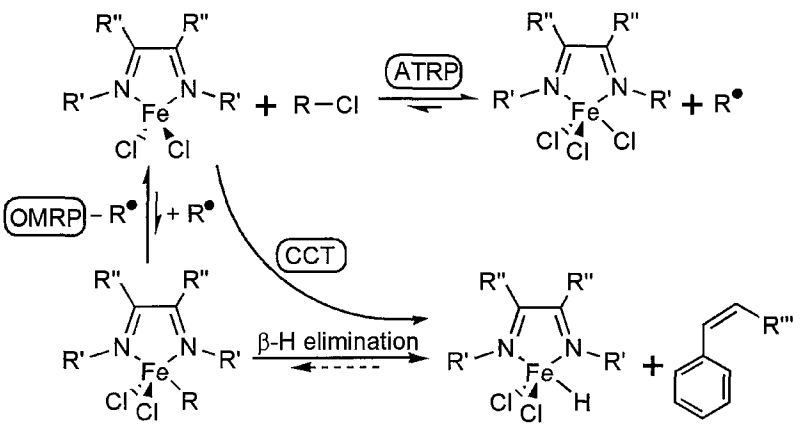


Figure 6.28 Molecular weights *versus* conversion for the bulk polymerisation of MMA (100 eq., EBrB, 80°C) by $^{tBu,OH,Ph}[N,N]FeCl_2$, **69**. ($M_{n,th}$ = ▬).

6.3 - Conclusions and Further Work

Despite the synthesis of a range of amino- and hydroxyl-substituted ligands and complexes, the polymerisation testing in this chapter was largely unsuccessful. Attempts to synthesise a complex with an *N*-aryl group containing an ammonium group were unsuccessful, and this was attributed to the delocalised nature of the ligand. While the poor solubility of the non-quaternised complex $^{Me2N-Ph,H}[N,N]FeCl_2$, **45**, resulted in an inefficient ATRP catalyst for styrene or MMA, the polymerisation characteristics suggested that some ATRP was occurring. There was no evidence for CCT, indicating that the strongly electron-donating nature of the *para*-dimethylamino *N*-substituent is effective in increasing the halogenophilicity of the catalyst.

Synthesis of $^{pipI,R''}[N,N]FeCl_2$ complexes with *N*-alkyl groups containing a quaternary amine were successful. With R″ = H or Me, both the tertiary and quaternary amine complexes (**52**, **53**, **55** and **56**) were poor ATRP catalysts for styrene, MMA and 2-HPMA. The high molecular weights and broad PDIs suggested essentially thermal polymerisations were occurring. A sterically hindered tertiary amine complex, $^{TEMP,H}[N,N]FeCl_2$, **59**, designed to probe whether coordination of the amine group could be responsible for the poor control exhibited similar polymerisation behaviour. The ineffectiveness of this family of piperidine-substituted complexes as ATRP catalysts was attributed to an inefficient deactivation step, resulting in high radical concentrations and rapid, uncontrolled propagation. The position of the atom transfer equilibrium was postulated to lie too far towards the oxidised metal complex and free radical (Scheme 6.17). It is also likely that a combination of poor solubility, poor stability in protic media and sensitivity towards air and moisture contributed to the ineffectiveness of these complexes.



Scheme 6.17 Possible pathways for radical polymerisation of styrene mediated by α-diimine Fe complexes where the ATRP equilibrium lies too far to the right.

More promising results were obtained using $^{pip,Ph}[N,N]FeCl_2$, **54**, which gave relatively well-controlled ATRP of styrene, and the analogous quaternised complex, $^{pip\text{-}I,Ph}[N,N]FeCl_2$, **57**, which showed good control over 2-HPMA polymerisation, although appeared to be unstable to MeOH. The presence of electron-withdrawing phenyl groups at the 2,3-positions of the α-diimine ligand backbone may balance the electron-donating piperidine groups, resulting in a complex where the halogenophilicity is "just right" for promotion of ATRP. Evidence for this balance in the electronic properties of the complex exists in that the styrene polymerisation data

using $^{pip,Ph}[N,N]FeCl_2$ closely resembled that obtained in Chapter 4 for the efficient ATRP complexes $^{R',Me2N\text{-}Ph}[N,N]FeCl_2$, where R′ = Cy or ^{t}Bu. Other complexes containing phenyl groups on the backbone such as $^{R',Ph}[N,N]FeCl_2$, where R′ = Cy, ^{t}Bu or Ph, result in styrene polymerisation predominantly terminated through CCT. Thus, the inclusion of the piperidine group as the *N*-substituent has shifted the balance of the equilibria towards ATRP.

The synthesis of an ammonium complex with an *N*-alkyl group, $^{IMe3N\text{-}nPr,Me}[N,N]FeCl_2$, **63**, also gave promising results for the ATRP of 2-HPMA in MeOH, although the PDI was rather broad (1.45). The data showed that solution polymerisations were better controlled than those carried out in bulk, indicating that complex **63** was stable to the methanolic polymerisation conditions. The next step with this catalyst would be to attempt the ATRP of 2-HPMA and other hydrophilic monomers in water/MeOH mixtures and then water.

With the hydroxy-functionalised complexes, the simple oximes $^{OH,Ph}[N,N]FeCl_2$ and $^{OH,Me}[N,N]FeCl_2$ proved to be efficient CCT catalysts for the polymerisation of styrene under ATRP conditions. Complexes **66** and **67** were unreactive towards MMA, presumably because of coordination of the functionalised monomer to the metal centre as evidenced by an immediate colour change upon monomer addition. The asymmetrical oximes displayed ATRP behaviour in MMA polymerisations, most likely because of their electron-donating *N*-alkyl groups. Again, the balance between the electron-withdrawing OH and Ph groups and the electron-donating alkyl groups resulted in a balance in the electronic properties of the complex which were "just right" for the promotion of ATRP. Although crystal structures of complexes **68** and **69** were not obtained, it is likely that the more sterically crowded coordination sphere around the metal centre prevented the coordination of MMA, which was postulated to occur with complexes **66** and **67**. The insolubility of $^{tBu,OH,Ph}[N,N]FeCl_2$, **69**, made it an inefficient catalyst for the ATRP of MMA, but ATRP-like behaviour was observed. $^{Cy,OH,Ph,H}[N,N]FeCl_2$, **68**, was found to be a reasonably good ATRP catalyst for MMA polymerisation, although the control over the reaction decreased when carried out in MeOH. Further work involving this catalyst would centre on exploring its efficacy for the ATRP of other hydrophilic monomers and using different polar/protic solvent systems.

Much work remains to be carried out before a water-soluble α-diimine iron complex, to rival the copper and ruthenium systems, can be used for the aqueous

ATRP of hydrophilic monomers. While the small successes in this chapter provide a starting point, the bulk of this thesis has shown how sensitive the α-diimine iron system is to relatively minor changes in the substituents at both the *N*- and 2,3-positions. One potential catalyst to target in future work would incorporate the water-solubilising ammonium groups on the backbone, allowing an *N*-cyclohexyl group to be retained (Figure 6.29).

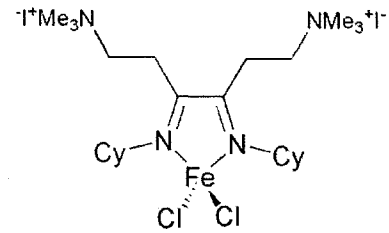


Figure 6.29 Potential ATRP catalyst designed for water solubility.

The remote position of the solubilising group would be expected to reduce any adverse electronic effects which may switch the polymerisation mechanism away from ATRP. By retaining the Cy substituent and incorporating an alkyl chain on the backbone, it is hoped that the efficiency of existing ATRP catalysts such as $^{Cy,H}[N,N]FeCl_2$, $^{Cy,Me}[N,N]FeCl_2$ and $^{Cy,Me2N\text{-}Ph}[N,N]FeCl_2$ would be maintained.

6.4 - References

(1) Cornils, B., *J. Mol. Catal. A: Chem.* **1999,** *143*, 1.

(2) Cornils, B.; Kuntz, E. G., *J. Organomet. Chem.* **1995,** *502*, 177.

(3) Brink, G.-J. t.; Arends, I. W. C. E.; Sheldon, R. A., *Science* **2000,** *287*, 1636.

(4) Held, A.; Mecking, S., *Chem. Eur. J.* **2000,** *6*, 4623.

(5) Held, A.; Bauers, F. M.; Mecking, S., *Chem. Commun.* **2000,** *4*, 301.

(6) Mohr, B.; Lynn, D. M.; Grubbs, R. H., *Organometallics* **1996,** *15*, 4317.

(7) ten Brink, G.-J.; Arends, I. W. C. E.; Papadogianakis, G.; Sheldon, R. A., *Chem. Commun.* **1998,** *21*, 2359.

(8) Penicaud, V.; Maillet, C.; Janvier, P.; Pipelier, M.; Bujoli, B., *Eur. J. Org. Chem.* **1999,** *7*, 1745.

(9) Zhang, X.; Xia, J.; Matyjaszewski, K., *Macromolecules* **1998,** *31*, 5167.

(10) Coca, S.; Jasieczek, C. B.; Beers, K. L.; Matyjaszewski, K., *J. Polym. Sci. A: Polym. Chem.* **1998,** *36*, 1417.

(11) Tsarevsky, N.; Matyjaszewski, K., *J. Polym. Sci. A: Polym. Chem.* **2006,** *44*, 5098.

(12) Nishikawa, T.; Ando, T.; Kamigaito, M.; Sawamoto, M., *Macromolecules* **1997,** *30*, 2244.

(13) Robinson, K. L.; Khan, M. A.; de PazBanez, M. V.; Wang, X. S.; Armes, S. P., *Macromolecules* **2001,** *34*, 3155.

(14) Save, M.; Weaver, J. V. M.; Armes, S. P., *Macromolecules* **2002,** *35*, 1152.

(15) Bednarek, M.; Jankova, K.; Hvilsted, S., *J. Polym. Sci. A: Polym. Chem.* **2007,** *45*, 333.

(16) Armes, S. P.; Wang, X.-S., *Macromolecules* **2000,** *33*, 6640.

(17) Perrier, S.; Armes, S. P.; Wang, X.-S.; Malet, F.; Haddleton, D. M., *J. Polym. Sci. A: Polym. Chem.* **2001,** *39*, 1696.

(18) Perrier, S.; Haddleton, D. M., *Macromol. Symp.* **2002,** *182*, 261.

(19) Wang, X. S.; Malet, F. L. G.; Armes, S. P., *Macromolecules* **2001,** *34*, 162.

(20) Rademacher, J. T.; Baum, M.; Pallack, M. E.; Brittain, W. J.; William J. Simonsick, J., *Macromolecules* **2000,** *33*, 284.

(21) Teodorescu, M.; Matyjaszewski, K., *Macromolecules* **1999,** *32*, 4826.

(22) Ashford, E. J.; Naldi, V.; O'Dell, R.; Billingham, N. C.; Armes, S. P., *Chem. Commun.* **1999**, 1285.

(23) Wang, X.-S.; Jackson, R. A.; Armes, S. P., *Macromolecules* **2000,** *33*, 255.

(24) Nishikawa, T.; Kamigaito, M.; Sawamoto, M., *Macromolecules* **1999,** *32*, 2204.

(25) Watanabe, K.; Nishikawa, T.; Matsuyama, M.; Kamigaito; M.; Sawamoto, M., *Polym. Prepr. Jpn.* **1997,** *46*, 148.

(26) Fuji, Y.; Watanabe, K.; Baek, K.-Y.; Ando, T.; Kamigaito, M.; Mitsuo Sawamoto, *J. Polym. Sci. A: Polym. Chem.* **2002,** *40*, 2055.

(27) Yoshitani, T.; Ando, T.; Kamigaito, M.; Sawamoto, M., *Polym. Prepr. Jpn.* **2003,** *52*, 1528.

(28) Kamigaito, M.; Ando, T.; Sawamoto, M., *The Chemical Record* **2004,** *4*, 159.

(29) Quémener, D.; Bousquet, A.; Héroguez, V.; Gnanou, Y., *Macromolecules* **2006,** *39*, 5589.

(30) Fuji, Y.; Ando, T.; Kamigaito, M.; Sawamoto, M., *Macromolecules* **2002,** *35*, 2949.

(31) O'Reilly, R. K. Synthesis of novel iron complexes and their use in atom transfer radical polymerisation. Ph.D. Thesis, University of London, 2003.

(32) O'Reilly, R. K.; Shaver, M. P.; White, A. J. P.; Gibson, V. C., *Macromolecules* **2007,** *40*, 7441.

(33) tom Dieck, H.; Renk, I. W., *Chem. Ber.* **1971,** *104*, 92.

(34) Gibson, V. C.; O'Reilly, R. K.; Reed, W.; Wass, D.; White, A. J. P.; Williams, D. J., *Chem. Commun.* **2002**, 1850.

(35) Gibson, V. C.; O'Reilly, R. K.; Wass, D. F.; White, A. J. P.; Williams, D. J., *Macromolecules* **2003,** *36*, 2591.

(36) Poli, R., *Angew. Chem. Int. Ed.* **2006,** *45*, 5058.

(37) Hardman, N. J.; Fang, X.; Scott, B. L.; Wright, R. J.; Martin, R. L.; Kubas, G. J., *Inorg. Chem.* **2005,** *44*, 8306.

(38) Heuts, J. P. A.; Forster, D. J.; Davis, T. P., *Macromolecules* **1999,** *32*, 2511.

(39) Larionov, S. V.; Myachina, L. I.; Romanenko, G. V.; Tkachev, A. V.; Sheludyakova, L. A.; Ikorskii, V. N.; Boguslavskii, E. G., *Russ. J. Coord. Chem.* **2001,** *27*, 423.

(40) Vaska, L.; Yamaji, T., *J. Am. Chem. Soc.* **1971,** *93*, 6673.

(41) Pomposo, F.; Stynes, D. V., *Inorg. Chem.* **1983,** *22*, 569.

(42) Thompson, D. W.; Stynes, D. V., *Inorg. Chem.* **1990,** *29*, 3815.

(43) Stynes, D. V.; Noglik, H.; Thompson, D. W., *Inorg. Chem.* **1991,** *30*, 4567.

(44) Gupta, B. D.; Yamuna, R.; Mandal, D., *Organometallics* **2006,** *25*, 706.

(45) Lindeman, S. V.; Struchkov, Y. T.; Voloshin, Y. Z., *Inorg. Chim. Acta* **1991,** *184*, 107.

(46) Lopez, C.; Alvarez, S.; Aguilo, M.; Solans, X.; Font-Altaba, M., *Inorg. Chim. Acta* **1987,** *127*, 153.

(47) Miller, J. S.; Goldberg, S. Z., *Inorg. Chem.* **1975,** *14*, 2294.

Chapter 7

Experimental

7.1 - General experimental details

All manipulations of air and/or moisture sensitive compounds were carried out under nitrogen using standard Schlenk and cannula techniques, or in a conventional nitrogen-filled glovebox. Elemental analyses were performed by the microanalytical service of the Chemistry department of London Metropolitan University. Crystal data were collected on Bruker P4 and Oxford Diffraction Xcalibur 3 or PX Ultra diffractometers. NMR spectra were recorded on Bruker AC250 (^{1}H, 250.1 MHz; ^{13}C, 60.9 MHz), DRX400 (^{1}H, 400.1 MHz; ^{13}C, 100.6 MHz) and AV-400 (^{1}H, 400.3 MHz; ^{13}C, 100.7 MHz) spectrometers, at 293 K unless otherwise stated. ^{1}H and ^{13}C chemical shifts are reported as δ (in ppm) and referenced to the residual proton signal and to the ^{13}C signal of the deuterated solvent, respectively. The following abbreviations have been used for multiplicities: s (singlet), d (doublet), t (triplet), m (unresolved multiplet), br (broad). Infra-red spectra were obtained as nujol mulls on CI plates or as KBr discs on a Perkin-Elmer 1710X FT-IR spectrometer. FAB (Fast Atom Bombardment), EI (Electron Ionisation) and CI (Chemical Ionisation) mass spectra were recorded on Micromass AutoSpec Premier and VG Platform spectrometers at Imperial College London. GPC data for polystyrene and PMMA samples were collected using Cirrus GPC/SEC software, Version 1.11, connected to a Shodex RI-101 detector, and were referenced to polystyrene or PMMA standards (PolymerLabs EasiCal, PS1 or PM1). Samples were injected onto two linear 10 micron columns, using chloroform as the eluant, at a flow rate of 1.0 cm^3min^{-1} at 35°C. GPC data for poly(hydroxypropylmethacrylate) were collected using a Polymer Labs GPC-50 with Mixed D 5 μL columns, using THF as the eluant and referenced to PMMA standards (PolymerLabs EasiCal, PM1). GC analyses were conducted on an Agilent 6890A gas chromatograph with an HP-5 column. EPR spectra were collected on Bruker ESP300E and Bruker Elexsys E600 spectrometers, using a Bruker ER6706KT (K-band) resonator. Variable temperature magnetic susceptibility data were collected using a Quantum Design MPMS-XL SQUID magnetometer equipped with a 7 T magnet. Mössbauer spectra were obtained using an ES-Technology MS-105 spectrometer, with a 125 MBq ^{57}Co source in a Rh matrix.

7.2 - Solvents and reagents

Pentane, toluene and heptane were dried by passing through a cylinder filled with commercially available Q-5 catalyst (13% Cu^{I} oxide on Al_2O_3) and activated Al_2O_3 (3 mm, pellets) in a stream of nitrogen. Other solvents were dried by refluxing over an appropriate drying agent and distilling: diethyl ether (Et_2O) and tetrahydrofuran (THF) were dried using sodium benzophenone ketyl, dichloromethane (CH_2Cl_2) and acetonitrile (MeCN) were dried over calcium hydride. Methanol was refluxed over sodium and then freshly distilled onto activated 3Å molecular sieves. All solvents were degassed before use. NMR solvents were dried over molecular sieves and degassed prior to use. Styrene and MMA were stirred over calcium hydride for 24 hours, vacuum-transferred, degassed and then stored in an inert atmosphere at –35°C. 2-HPMA was dried over $MgSO_4$, distilled and then passed through a basic alumina column before being stored over 3Å molecular sieves at 5°C. 1-PECl and EBrB were stirred over calcium hydride for 24 hours, vacuum-transferred, degassed and then stored over 3Å molecular sieves in an inert atmosphere at –35°C. AIBN and TosCl were purified through recrystallisation, dried under vacuum and then stored in an inert atmosphere at –35°C. Diazadiene ligands, RN=CH-CH=NR where R = ^{t}Bu or Cy, were prepared in bulk through modification of the literature procedures[1-3] and purified through recrystallisation. $FeCl_2(THF)_{1.5}$ was synthesised according to literature procedures.[4] $C_6H_5CHMeMgCl$ was also synthesised according to a literature procedure.[5] All amines and anilines were freshly distilled before use. All other reagents are commercially available and were used without further purification.

7.3 - Polymerisation procedures

All polymerisations were set up and performed under an atmosphere of oxygen-free, dry nitrogen. In an ampoule equipped with a magnetic stirrer bar, a solution of monomer, initiator and catalyst were placed. Solvent (if required) was used to rinse in the catalyst solution. The ampoules were heated in sand or oil baths, at 120°C (for styrene), 80°C (for MMA), or 50°C (for HPMA), with magnetic stirring. After stirring for the allotted period of time (15 min to 2 h), an aliquot (0.1 mL) was removed. Conversion was determined by integration of the monomer *versus* polymer backbone resonances in the ^{1}H NMR spectrum of the crude product in $CDCl_3$ or CD_3OD. Once the reaction was completed, polystyrene and PMMA were dissolved in THF and added dropwise to an approximately 20-fold excess of rapidly stirred

acidified methanol (1% HCl v/v). The precipitate that formed was filtered off and washed with methanol. Poly(hydroxypropylmethacrylate) was dissolved in THF and precipitated by addition to water. The precipitates were dried for 24 hours under vacuum. Samples were analysed by GPC.

7.4 - General procedure for alkyl decomposition experiments

$^{R',R''}[N,N]FeCl_3$ (0.50 mmol) was dissolved in THF (10 mL) and cooled to –78°C. Dropwise addition of a solution of RMgCl (0.50 mmol) in THF resulted in the precipitation of a white solid ($MgCl_2$). An aliquot (1 mL) was removed from the reaction mixture and quenched with distilled H_2O. Subsequent aliquots were removed and quenched over a range of temperatures. Depending on the stability of the corresponding alkyl complex, vivid colour changes corresponding to the formation of $^{R',R''}[N,N]FeCl_2$ were observed at various temperatures on warming. Aliquots were filtered through basic alumina and analyzed by GC or GC/MS. GC area counts were corrected against organic components present in unreacted RMgCl.

7.5 - Solution magnetic susceptibility measurements

According to the Evans' NMR method[6] 2 - 5 mg of complex was dissolved in a mixture of deuterated NMR solvent (CD_2Cl_2, $CDCl_3$ or $CD_3C_6D_5$) and cyclohexane or dichloromethane (95/5 v/v). A portion of this solution was transferred into a melting point capillary tube which was then placed into a Young's-tap NMR tube containing the NMR solvent/reference mixture. The chemical shift difference (Δf) for the cyclohexane or dichloromethane protons between the inner and outer tubes at room temperature was used to calculate the magnetic susceptibility, χ_m, according to equation (1):

$$\chi_m = 3 \times \Delta f \times (1000 \times f \times c)^{-1} \qquad (1)$$

where χ_m is the molar susceptibility of the sample in m^3 / mol

Δf is the difference in the chemical shift in Hz

f is the frequency of operation of the spectrometer in Hz

c is the concentration of the sample in mol / L

This can be used in equation (2) to calculate the magnetic moment, μ_{eff}, of a paramagnetic atom in a complex. All constants and equations are given in SI units.

$$\mu_{eff.} = 798 \times (T \times \chi_m)^{1/2} \qquad (2)$$

where $\mu_{eff.}$ is the magnetic moment in Bohr magnetons (B.M.)

T is the temperature in K

χ_m is the molar susceptibility of the sample in m^3 / mol

For all measurements the diamagnetic contributions of the ligands were neglected. The theoretical spin-only value for the magnetic moment of a paramagnetic atom can be calculated using equation (3):

$$\mu_{eff.} = (n(n+2))^{1/2} \quad (3)$$

where $\mu_{eff.}$ is the magnetic moment in Bohr magnetons (B.M.)

n is the number of unpaired electrons

7.6 - Synthetic procedures

7.6.1 - Experimental details for Chapter 2.

7.6.1.1 - Ligand synthesis.

Synthesis of 1,4-dicyclohexyl-2,3-diphenyl-1,4-diaza-1,3-butadiene, $^{Cy,Ph}[N,N]$, **1.** To a stirred solution of cyclohexyl amine (7.4 mL, 63 mmol) in CH_2Cl_2 (30 mL) at 0°C was added dropwise $TiCl_4$ (1M in CH_2Cl_2) (9.7 mL, 10 mmol). Benzil (1.7 g, 8 mmol) in CH_2Cl_2 (10 mL) was added dropwise, and the solution allowed to warm to room temperature. The solution was stirred overnight, and then water (20 mL) added. The precipitate was filtered out, and the aqueous layer of the filtrate extracted with CH_2Cl_2. Removal of the organic solvents under reduced pressure gave a sticky white crude product which was recrystallised from hot EtOH (40 mL) to give a white, crystalline product, 1.91 g, 63%. Anal. Calcd for $C_{26}H_{32}N_2$: C, 83.82; H, 8.66; N, 7.52. Found: C, 83.76; H, 8.62; N, 7.46. IR (nujol, cm^{-1}): 1616 ($\nu_{C=N}$). ^1H NMR ($CDCl_3$): δ 7.75 (4H, m, Ar-*H*), 7.35 (6H, m, Ar-*H*), 3.22 (2H, m, N-C*H*), 1.07-1.79 (20H, m, C*H*$_2$) ppm. $^{13}C\{^1H\}$ NMR ($CDCl_3$): δ 162.2 (s, N=*C*H), 137.2 (s, Ar-C_{ipso}), 130.3 (s, Ar-CH_{para}), 128.4, 127.7 (s, Ar-CH_{ortho}, Ar-CH_{meta}), 62.9 (s, N-*C*H), 34.0, 32.9 (s, N-CH*C*H$_2$), 25.7 (s, N-CHCH$_2$CH$_2$*C*H$_2$), 24.2, 24.1 (s, N-CHCH$_2$*C*H$_2$) ppm. MS (CI): *m/z* 373 $[M+H]^+$.

Synthesis of 1,4-dicyclohexyl-2,3-di(phenyl-4-fluoro)-1,4-diaza-1,3-butadiene, $^{Cy,F\text{-}Ph}[N,N]$, **2.** Ligand **2** was prepared as for **1**, using cyclohexyl amine (9.3 mL, 81.3 mmol), $TiCl_4$ solution (12.2 mL, 12.2 mmol) and *p*-fluorobenzil (2.50 g, 10.1 mmol). The sticky orange residue was recrystallised from hot MeOH (60 mL) to give white

crystals, 3.65 g, 88%. Anal. Calcd for $C_{26}H_{30}N_2F_2$: C, 76.44; H, 7.40; N, 6.86. Found: C, 76.61; H, 7.49; N, 6.76. IR (nujol, cm^{-1}): 1622 ($\nu_{C=N}$). ^1H NMR ($CDCl_3$): δ 7.75 (4H, m, Ar-*H*), 7.01 (4H, m, Ar-*H*), 3.17 (2H, m, NC*H*), 1.89-1.02 (20H, m, CH_2) ppm. $^{13}C\{^1H\}$ NMR ($CDCl_3$): δ 164.2 (d, $^1J_{C-F}$ 250.4, Ar-CH_{para}), 160.6 (s, N=CH), 133.2 (s, Ar-C_{ipso}), 129.6 (d, $^3J_{C-F}$ 7.7, Ar-CH_{ortho}), 115.5 (d, $^2J_{C-F}$ 21.9, Ar-CH_{meta}), 62.9 (s, NCH), 33.9, 33.0 (s, $NCHCH_2$), 25.6 (s, $NCH(CH_2)_2CH_2$), 24.1, 24.0 (s, $NCHCH_2CH_2$) ppm. MS (CI): *m/z* 409 $[M+H]^+$.

Synthesis of 1,4-di(*tert*-butyl)-2,3-diphenyl-1,4-diaza-1,3-butadiene, $^{tBu,Ph}[N,N]$, **3**. Ligand **3** was prepared as for **1**, using *tert*-butyl amine (10.03 mL, 96 mmol), $TiCl_4$ solution (14.30 mL, 14 mmol) and benzil (2.50 g, 12 mmol). The pale brown crude product was recrystallised from hot MeOH (50 mL) to give a white, crystalline solid, 2.35 g, 62%. Anal. Calcd for $C_{22}H_{28}N_2$: C, 82.45; H, 8.81; N, 6.26. Found: C, 82.47; H, 8.95; N, 6.16. IR (nujol, cm^{-1}): 1634 ($\nu_{C=N}$). ^1H NMR ($CDCl_3$): δ 7.77 (4H, m, Ar-*H*), 7.29 (6H, m, Ar-*H*), 1.25 (18H, 2, CH_3) ppm. $^{13}C\{^1H\}$ NMR ($CDCl_3$): δ 159.1 (s, N=CH), 140.4 (s, Ar-C_{ipso}), 129.6 (s, Ar-CH_{para}), 128.3, 127.7 (s, Ar-CH_{ortho}, Ar-CH_{meta}), 57.9 (s, CMe_3), 30.0 (s, CH_3) ppm. MS (CI): *m/z* 321 $[M+H]^+$.

Synthesis of 1,4-di(*tert*-butyl)-2,3-di(phenyl-4-fluoro)-1,4-diaza-1,3-butadiene, $^{tBu,F\text{-}Ph}[N,N]$, **4**. Ligand **4** was prepared as for **1**, using *t*-butyl amine (8.5 mL, 81 mmol), $TiCl_4$ solution (12.2 mL, 12 mmol) and *para*-fluorobenzil (2.50 g, 10 mmol). The sticky orange residue was recrystallised from hot MeOH (60 mL) to give white crystals, 1.53 g, 42%. Anal. Calcd for $C_{22}H_{26}N_2F_2$: C, 74.13; H, 7.35; N, 7.86. Found: C, 74.26; H, 7.32; N, 7.69. IR (nujol, cm^{-1}): 1626 ($\nu_{C=N}$). ^1H NMR ($CDCl_3$): δ 7.76 (4H, m, Ar-*H*), 7.01 (4H, m, Ar-*H*), 1.24 (18H, 2, CH_3) ppm. $^{13}C\{^1H\}$ NMR ($CDCl_3$): δ 163.8 (d, $^1J_{C-F}$ 250.5, Ar-CH_{para}), 157.5 (s, N=CH), 136.3 (s, Ar-C_{ipso}), 129.5 (d, $^3J_{C-F}$ 7.7, Ar-CH_{ortho}), 115.2 (d, $^2J_{C-F}$ 21.7, Ar-CH_{meta}), 58.0 (s, CMe_3), 29.9 (s, CH_3) ppm. MS (CI): *m/z* 357 $[M+H]^+$.

Synthesis of 1,4-diphenyl-2,3-diphenyl-1,4-diaza-1,3-butadiene, $^{Ph,Ph}[N,N]$, **5**. Aniline (3.65 mL, 40 mmol) was dissolved in toluene (150 mL) and stirred as benzil (3.15 g, 15 mmol) was added. *p*-TsOH (0.29 g, 1.5 mmol) was added and the solution heated under reflux using Dean-Stark apparatus for 75 h. The cooled

solution was filtered through silica, and the solvent was then removed under reduced pressure to give a waxy yellow solid. Recrystallisation from MeOH / EtOH (3:1 ratio, 200 mL) gave a bright yellow, crystalline product, 2.98 g, 55%. Anal. Calcd for $C_{26}H_{20}N_2$: C, 86.64; H, 5.59; N, 7.77. Found: C, 86.84; H, 5.74; N, 7.64. IR (nujol, cm^{-1}): 1612 ($\nu_{C=N}$). ^1H NMR ($CDCl_3$): δ 7.90 (4H, dd, $^3J_{H-H}$ 6.1, $^4J_{H-H}$ 1.3, Ar-H), 7.38-7.52 (6H, m, Ar-H), 6.97-7.16 (6H, m, Ar-H), 6.51-6.84 (4H, dd, $^3J_{H-H}$ 7.0, $^4J_{H-H}$ 1.2, Ar-H) ppm. $^{13}C\{^1H\}$ NMR ($CDCl_3$): δ 165.9 (s, N=*C*H), 163.9, 149.3 (s, Ar-C_{ipso}), 137.6, 131.1 (s, Ar-CH_{para}), 128.7, 128.4, 124.9, 120.1 (s, Ar-CH_{ortho}, Ar-CH_{meta}) ppm. MS (CI): *m/z* 362 $[M+H]^+$.

Synthesis of 1,4-di-(2,4,6-trimethylphenyl)-2,3-di(phenyl-4-fluoro)-1,4-diaza-1,3-butadiene, $^{Mes,F\text{-}Ph}[N,N]$, **6**. Ligand **6** was prepared as for **1**, using 2,4,6-trimethyl aniline (11.4 mL, 81 mmol), $TiCl_4$ solution (12.2 mL, 12 mmol) and *para*-fluorobenzil (2.50 g, 10 mmol). After removing the organic solvent a dark orange oil was isolated, containing a large amount of unreacted aniline, which was removed through distillation under reduced pressure to give a sticky orange residue. Addition of a small amount of MeOH (3 mL) induced precipitation of a yellow solid which was collected and then recrystallised from hot MeOH (50 mL) to give bright yellow crystals, 3.17 g, 65%. Anal. Calcd for $C_{32}H_{30}N_2F_2$: C, 79.97; H, 6.29; N, 5.83. Found: C, 79.89; H, 6.39; N, 5.76. IR (nujol, cm^{-1}): 1626($\nu_{C=N}$). ^1H NMR ($CDCl_3$): δ 8.28 (2H, m, Ar-*H*), 7.23 (2H, m, Ar-*H*), 6.68-6.90 (8H, m, Ar-*H*), 2.23, 2.20 (6H, m, CH_{3para}), 1.88, 1.80 (12H, s, CH_{3ortho}) ppm. $^{13}C\{^1H\}$ NMR ($CDCl_3$): δ 164.3, 163.7 (d, $^1J_{C-F}$ 174, Ar-CH_{para}), 161.9 (s, N=*C*H), 145.1, 144.5 (s, Ar-C_{ipso}), 132.8, 132.6 (s, Ar-CMe_{para}), 130.6, 129.7 (d, $^3J_{C-F}$ 33.5, Ar-CH_{ortho}), 129.0, 128.2 (s, Ar-CH_{meta}), 126.2, 125.3 (s, Ar-CMe_{ortho}), 115.8, 115.1 (d, $^2J_{C-F}$ 86.5, Ar-CH_{meta}), 20.7, 20.6 (s, Ar-CH_{3para}) 18.8, 18.5, (s, Ar-CH_{3ortho}) ppm. MS (CI): *m/z* 481 $[M+H]^+$.

7.6.1.2 - Synthesis of Fe^{II} complexes.

Synthesis of 1,4-dicyclohexyl-2,3-diphenyl-1,4-diaza-1,3-butadiene iron^{II} chloride, $^{Cy,Ph}[N,N]FeCl_2$, **7**. Ligand **1** (2.0 g, 5 mmol) and $FeCl_2(THF)_{1.5}$ (1.26 g, 5 mmol) were suspended in CH_2Cl_2 (*ca.* 40 mL) and stirred at room temperature for 24 h. The dark blue solution was filtered, and the remaining solid extracted with CH_2Cl_2 (3 × 10 mL). The washings and filtrate were combined and concentrated to *ca.* 15 mL,

and then pentane (30 mL) was added in to precipitate a bright purple solid which was collected by filtration and dried under vacuum to yield 1.90 g, 71%. Anal. Calcd for $C_{26}H_{32}N_2FeCl_2$: C, 62.54; H, 6.46; N, 5.61. Found: C, 62.65; H, 6.31; N, 5.54. IR (nujol, cm^{-1}): 1600 ($\nu_{C=N}$). ^1H NMR ($CDCl_3$): δ 193.00 (2H, br s, NC*H*), 15.37 (4H, br s, Ar-*H*), 7.76 (4H, br s, Ar-*H*), 6.45 (2H, br s, Ar-*H*), -5.84, -6.77, -13.37, -20.43, -49.81 (20H, br s, CH_2) ppm. MS (FAB^+): *m/z* 500 $[M+H]^+$, 463 $[M-Cl]^+$. $\mu_{eff.}$ = 5.02 B.M.

Synthesis of 1,4-dicyclohexyl-2,3-di(phenyl-4-fluoro)-1,4-diaza-1,3-butadiene iron^{II} chloride, $^{Cy,F\text{-}Ph}$[*N,N*]$FeCl_2$, **8.** Complex **8** was synthesised as for **7**, using ligand **2** (1.50 g, 4 mmol) and $FeCl_2(THF)_{1.5}$ (0.86 g, 4 mmol). Precipitation with pentane, filtration and drying yielded a purple solid, 1.52 g, 77%. Anal. Calcd for $C_{26}H_{30}N_2FeF_2Cl_2$: C, 58.34; H, 5.65; N, 5.23. Found: C, 58.47; H, 5.76; N, 5.28. IR (nujol, cm^{-1}): 1603 ($\nu_{C=N}$). ^1H NMR ($CDCl_3$): δ 193.93 (2H, br s, NC*H*), 16.26 (4H, br s, Ar-*H*), 15.37 (4H, br s, Ar-*H*), -5.57, -6.62, -13.26, -20.14, -47.56 (20H, br s, CH_2) ppm. MS (FAB^+): *m/z* 536 $[M+H]^+$, 499 $[M-Cl]^+$. $\mu_{eff.}$ = 5.02 B.M.

Synthesis of 1,4-di(*tert*-butyl)-2,3-diphenyl-1,4-diaza-1,3-butadiene iron^{II} chloride, ^{tBu,Ph}[*N,N*]$FeCl_2$, **9.** Complex **9** was synthesised in an analogous manner to **7**, using ligand **3** (1.0 g, 3 mmol) and $FeCl_2(THF)_{1.5}$ (0.73 g, 3 mmol). Precipitation with pentane, filtration and drying gave a purple solid, 0.89 g, 64%. Anal. Calcd for $C_{22}H_{28}N_2FeCl_2$: C, 59.08; H, 6.31; N, 6.26. Found: C, 59.14; H, 6.17; N, 6.16. IR (nujol, cm^{-1}): 1609 ($\nu_{C=N}$). ^1H NMR ($CDCl_3$): δ 19.22 (4H, br s, Ar-*H*), 17.57 (4H, br s, Ar-*H*), 7.63 (2H, br s, Ar-*H*), -17.04 (18H, br s, CH_3) ppm. MS (FAB^+): *m/z* 448 $[M+H]^+$, 411 $[M-Cl]^+$. $\mu_{eff.}$ = 5.13 B.M.

Synthesis of 1,4-di(*tert*-butyl)-2,3-di(phenyl-4-fluoro)-1,4-diaza-1,3-butadiene iron^{II} chloride, $^{tBu,F\text{-}Ph}$[*N,N*]$FeCl_2$, **10.** Complex **10** was synthesised in an analogous manner to **7**, using ligand **4** (1.00 g, 3 mmol) and $FeCl_2(THF)_{1.5}$ (0.66 g, 3 mmol). Precipitation with heptane, filtration and drying gave a purple solid, 0.98 g, 72%. Anal. Calcd for $C_{22}H_{26}N_2FeF_2Cl_2$: C, 54.68; H, 5.42; N, 5.80. Found: C, 54.67; H, 5.35; N, 5.88. IR (nujol, cm^{-1}): 1607 ($\nu_{C=N}$). ^1H NMR ($CDCl_3$): δ 19.17 (4H, br s, Ar-

H), 16.67 (4H, br s, Ar-*H*), -16.02 (18H, br s, C*H*$_3$) ppm. MS (FAB$^+$): *m/z* 484 [M+H]$^+$, 447 [M-Cl]$^+$. $\mu_{eff.}$ = 4.93 B.M.

Synthesis of 1,4-diphenyl-2,3-diphenyl-1,4-diaza-1,3-butadiene iron^{II} chloride, ^{Ph,Ph}[*N,N*]FeCl$_2$, **11.** Complex **11** was synthesised in an analogous manner to **7**, using ligand **5** (1.0 g, 3 mmol) and FeCl$_2$(THF)$_{1.5}$ (0.65 g, 3 mmol). Precipitation with pentane, filtration and drying gave a dark green solid, 0.99 g, 73%. Anal. Calcd for $C_{26}H_{20}N_2FeCl_2$: C, 64.10; H, 4.14; N, 5.75. Found: C, 63.97; H, 4.22; N, 5.79. IR (nujol, cm^{-1}): 1592 ($\nu_{C=N}$). MS (FAB$^+$): *m/z* 451 [M-Cl]$^+$, 811 [L$_2$FeCl]$^+$. $\mu_{eff.}$ = 4.98 B.M.

Synthesis of 1,4-di-(2,4,6-trimethylphenyl)-2,3-di(phenyl-4-fluoro)-1,4-diaza-1,3-butadiene iron^{II} chloride, $^{Mes,F-Ph}$[*N,N*]FeCl$_2$, **12.** Complex **12** was synthesised in an analogous manner to **7**, using ligand **6** (0.50 g, 1 mmol) and FeCl$_2$(THF)$_{1.5}$ (0.24 g, 1 mmol). Precipitation with pentane, filtration and drying gave a brown solid, 0.48 g, 76%. Anal. Calcd for $C_{32}H_{30}N_2F_2FeCl_2$: C, 63.28; H, 4.98; N, 4.61. Found: C, 63.57; H, 5.01; N, 4.21. IR (nujol, cm^{-1}): 1598 ($\nu_{C=N}$). MS (FAB$^+$): *m/z* 606 [M]$^+$, 571 [M-Cl]$^+$. $\mu_{eff.}$ = 5.10 B.M.

7.6.2 - Experimental details for Chapter 3.

7.6.2.1 - Synthesis of Fe^{III} complexes.

Synthesis of 1,4-dicyclohexyl-2,3-diphenyl-1,4-diaza-1,3-butadiene iron^{III} chloride, ^{Cy,Ph}[*N,N*]FeCl$_3$, **13.** To an intimate mixture of FeCl$_3$ (0.20 g, 1 mmol) and ligand **1** (0.50 g, 1 mmol) was added CH_2Cl_2 (30 mL) and the resulting solution stirred for 2 hours. Filtration of the red-brown solution followed by removal of solvent in vacuo gave a dark red residue which was washed with pentane (3 x 15 mL) to give a dark red solid, 0.45 g, 63%. Anal. Calcd for $C_{26}H_{32}N_2FeCl_3$: C, 58.40; H, 6.03; N, 5.24. Found: C, 58.24; H, 6.14; N, 5.19. IR (nujol, cm^{-1}): 1607 ($\nu_{C=N}$). MS (FAB$^+$): *m/z* 535 [M+H]$^+$, 463 [M-2Cl]$^+$, 428 [M-3Cl]$^+$. μ_{eff} = 4.14 B.M.

Synthesis of 1,4-dicyclohexyl-2,3-di(phenyl-4-fluoro)-1,4-diaza-1,3-butadiene iron^{III} chloride, $^{Cy,F-Ph}$[*N,N*]FeCl$_3$, **14.** To an intimate mixture of FeCl$_3$ (0.20 g, 1 mmol) and ligand **2** (0.50 g, 1 mmol) was added CH_2Cl_2 (20 mL) and the resulting

solution stirred for 2 hours. Filtration of the deep red solution followed by removal of solvent in vacuo gave a dark red paste. Washing with pentane (3 x 15 mL) gave 10 as a brick red solid in 70% yield. Anal. Cald for $C_{26}H_{30}N_2FeF_2Cl_3$: C, 54.72; H, 5.30; N, 4.91. Found: C, 54.64; H, 5.29; N, 4.99. IR (nujol, cm^{-1}): 1603 ($\nu_{C=N}$). MS (FAB^+): *m/z* 499 $[M\text{-}2Cl]^+$. μ_{eff} = 3.75 B.M.

Synthesis of 1,4-di(*tert*-butyl)-1,4-diaza-1,3-butadiene iron^{III} chloride, $^{tBu,H}[N,N]FeCl_3$, **15.** To an intimate mixture of $FeCl_3$ (0.97 g, 6 mmol) and ligand (1.0 g, 6 mmol) was added CH_2Cl_2 (30 mL) and the suspension stirred for 2 hours. Filtration of the resulting dark red solution followed by washing with CH_2Cl_2 (3 × 10 mL) and concentration of the solvent to *ca.* 15 mL gave **31** as an orange solid, which was washed with pentane (3 x 15 mL) and dried under vacuum, 1.25 g, 64%. Anal. Calcd for $C_{10}H_{20}N_2FeCl_3$: C, 36.34; H, 6.10; N, 8.40. Found: C, 36.32; H, 6.26; N, 8.40. IR (nujol, cm^{-1}): 1606 ($\nu_{C=N}$). MS (FAB^+): *m/z* 295 $[M\text{-}3Cl]^+$. μ_{eff} = 5.81 B.M.

Synthesis of 1,4-di(*tert*-butyl)-2,3-diphenyl-1,4-diaza-1,3-butadiene iron^{III} chloride, $^{tBu,Ph}[N,N]FeCl_3$, **16.** Ligand **3** (1.0 g, 3 mmol) and $FeCl_3$ (0.51 g, 3 mmol) were suspended in CH_2Cl_2 (*ca.* 30 mL) and stirred at room temperature for 2 h. The dark purple solution was filtered, and the remaining solid extracted with CH_2Cl_2 (3 × 10 mL). The washings and filtrate were combined and concentrated to yield a dark purple solid, 0.92 g, 61%. Anal. Calcd for $C_{22}H_{28}N_2FeCl_3$: C, 54.74; H, 5.85; N, 5.80. Found: C, 54.82; H, 5.83; N, 5.77. IR (nujol, cm^{-1}): 1604 ($\nu_{C=N}$). MS (FAB^+): *m/z* 484 $[M+H]^+$, 446 $[M\text{-}2Cl]^+$, 411 $[M\text{-}3Cl]^+$. μ_{eff} = 4.10 B.M. Recrystallisation of **16** from CH_2Cl_2/pentane gave yellow crystals of $^{tBu,Ph}[N,N]H^+[FeCl_4]^-$, **16a**, while recrystallisation from hot toluene gave red crystals of $^{tBu,Ph}[N,N]FeCl_2.{}^{tBu,Ph}[N,O]H^+[FeCl_4]^-$, **16b**.

Synthesis of 1,4-di(*tert*-butyl)-2,3-di(phenyl-4-fluoro)-1,4-diaza-1,3-butadiene iron^{III} chloride, $^{tBu,F\text{-}Ph}[N,N]FeCl_3$, **17.** To an intimate mixture of $FeCl_3$ (0.23 g, 1 mmol) and ligand **4** (0.50 g, 1 mmol) was added CH_2Cl_2 (20 mL) and the resulting solution stirred at 60°C for 1 hour. Filtration followed by concentration of solvent gave a dark blue-black solution. Addition of pentane (20 mL) precipitated a brown solid, which was removed by filtration to get a deep blue solution. Removal of

solvent gave **17** as a purple solid in 60% yield. Anal. Calcd for $C_{22}H_{26}N_2FeF_2Cl_3$: C, 50.95; H, 5.05; N, 5.40. Found: C, 51.07; H, 5.17; N, 5.40. IR (nujol, cm^{-1}): 1600 ($\nu_{C=N}$). MS (FAB^+): *m/z* 447 $[M-2Cl]^+$. μ_{eff} = 4.01 B.M. Recrystallisation of **17** from benzene gave red crystals which were crystallographically characterised as $^{tBu,F-Ph}[N,N]FeCl_2$, $FeCl_4^-$ and $^{tBu,F-Ph}[N,N]H^+$, **17a**.

Synthesis of 1,4-diphenyl-2,3-diphenyl-1,4-diaza-1,3-butadiene iron^{III} chloride, $^{Ph,Ph}[N,N]FeCl_3$, **18.** Complex **18** was synthesised as for complex **13**, using ligand **5** (0.25 g, mmol) and $FeCl_3$ (0.1 g, mmol). Filtration of the dark brown solution followed by removal of solvent in vacuo gave a black solid. Washing with pentane (3 x 15 mL) gave **18** as a black solid, 0.25 g, 70% yield. Anal. Calcd for $C_{26}H_{20}N_2FeCl_3$: C, 59.75; H, 3.86; N, 5.36. Found: C, 59.86; H, 4.00; N, 5.41. MS (FAB^+): *m/z* 486 $[M-Cl]^+$, 451 $[M-2Cl]^+$, 361 $[L+H]^+$. μ_{eff} = 4.21 B.M.

Synthesis of 1,4-di-(2,4,6-trimethylphenyl)-2,3-di(phenyl-4-fluoro)-1,4-diaza-1,3-butadiene iron^{III} chloride, $^{Mes,F-Ph}[N,N]FeCl_3$, **19.** Complex **19** was synthesised as for complex **13**, using ligand **6** (0.25 g, mmol) and $FeCl_3$ (0.1 g, mmol). Filtration of the dark brown solution followed by removal of solvent in vacuo gave a black solid. Washing with pentane (3 x 15 mL) gave **19** as a black solid, 0.19 g, 57% yield. Anal. Calcd for $C_{32}H_{30}N_2F_2FeCl_3$: C, 59.79; H, 4.70; N, 4.36. Found: C, 59.83; H, 4.66; N, 4.27. MS (FAB^+): *m/z* 606 $[M-Cl]^+$, 571 $[M-2Cl]^+$, 481 $[L+H]^+$. μ_{eff} = 4.34 B.M.

7.6.3 - Experimental details for Chapter 4.

7.6.3.1 - Ligand synthesis.

Synthesis of 1,4-dicyclohexyl-2,3-di(phenyl-4-bromo)-1,4-diaza-1,3-butadiene, $^{Cy,Br-Ph}[N,N]$, **20.** Ligand **20** was synthesised as for **1**, using cyclohexyl amine (7.5 mL, 65 mmol), $TiCl_4$ solution (9.8 mL, 10 mmol) and *para*-bromobenzil (3.0 g, 8 mmol). The sticky white crude product was recrystallised from hot MeOH (40 mL) to give a white, crystalline product, 3.48 g, 81%. Anal. Calcd for $C_{26}H_{30}N_2Br_2$: C, 58.88; H, 5.70; N, 5.28. Found: C, 58.72; H, 5.77; N, 5.18. IR (nujol, cm^{-1}): 1615 ($\nu_{C=N}$). ^1H NMR ($CDCl_3$): δ 7.63 (4H, d, $^3J_{H-H}$ 8.4, Ar-*H*), 7.49 (4H, d, $^3J_{H-H}$ 8.4, Ar-*H*), 3.18 (2H, m, N-C*H*), 1.07-1.83 (20H, m, CH_2) ppm. $^{13}C\{^1H\}$ NMR ($CDCl_3$): δ 160.6 (s, N=*C*H), 135.7 (s, Ar-C_{ipso}), 131.8, 129.1 (s, Ar-CH_{ortho}, Ar-CH_{meta}), 125.2

(s, Ar-C_{para}), 63.1 (s, N-*C*H), 33.9, 33.0 (s, N-CH*C*H$_2$), 25.6 (s, N-CHCH$_2$*C*H$_2$CH$_2$), 24.1, 24.0 (s, N-CHCH$_2$*C*H$_2$) ppm. MS (EI): *m/z* 530 $[M]^+$.

Synthesis of 1,4-dicyclohexyl-2,3-di(phenyl-4-methyl)-1,4-diaza-1,3-butadiene, $^{Cy,Me\text{-}Ph}[N,N]$, **21**. Ligand **21** was prepared as for **1**, using cyclohexyl amine (11.6 mL, 101 mmol), $TiCl_4$ solution (15.0 mL, 15 mmol) and *para*-methylbenzil (3.0 g, 13 mmol). The pale brown crude product was recrystallised from hot MeOH (50 mL) to give a white, crystalline solid, 3.15 g, 63%. Anal. Calcd for $C_{28}H_{36}N_2$: C, 83.95; H, 9.06; N, 6.99. Found: C, 84.03; H, 9.12; N, 7.07. IR (nujol, cm^{-1}): 1622 ($\nu_{C=N}$). ^1H NMR ($CDCl_3$): δ 7.70 (4H, d, $^3J_{H\text{-}H}$ 7.6, Ar-*H*), 7.16 (4H, d, $^3J_{H\text{-}H}$ 7.6, Ar-*H*), 3.25 (2H, m, N-C*H*), 2.36 (6H, s, ArCH_3), 1.08-1.83 (20H, m, CH_2) ppm. $^{13}C\{^1H\}$ NMR ($CDCl_3$): δ 162.3 (s, N=*C*H), 140.4 (s, Ar-C_{ipso}), 134.7 (s, Ar-C_{para}), 129.2, 127.7 (s, Ar-CH_{ortho}, Ar-CH_{meta}), 62.8 (s, N-*C*H), 34.1, 33.0 (s, N-CH*C*H$_2$), 25.8 (s, N-CHCH$_2$CH$_2$*C*H$_2$), 24.3, 24.2 (s, N-CHCH$_2$*C*H$_2$), 21.4 (s, *C*H$_3$) ppm. MS (EI): *m/z* 400 $[M]^+$.

Synthesis of 1,4-dicyclohexyl-2,3-di(phenyl-4-methoxy)-1,4-diaza-1,3-butadiene, $^{Cy,MeO\text{-}Ph}[N,N]$, **22**. Ligand **22** was prepared as for **1**, using cyclohexyl amine (8.5 mL, 74 mmol), $TiCl_4$ solution (11.1 mL, 11 mmol) and *para*-methoxybenzil (2.5 g, 9 mmol). The pale brown crude product was recrystallised from hot MeOH (50 mL) to give a white, crystalline solid, 2.43 g, 61%. Anal. Calcd for $C_{28}H_{36}N_2O_2$: C, 77.74; H, 8.39; N, 6.48. Found: C, 77.85; H, 8.44; N, 6.46. IR (nujol, cm^{-1}): 1624 ($\nu_{C=N}$). ^1H NMR ($CDCl_3$): δ 7.70 (4H, d, $^3J_{H\text{-}H}$ 8.9, Ar-*H*), 6.83 (4H, d, $^3J_{H\text{-}H}$ 8.9, Ar-*H*), 3.79 (6H, s, OCH_3), 3.18 (2H, m, N-C*H*), 1.04-1.78 (20H, m, CH_2) ppm. $^{13}C\{^1H\}$ NMR ($CDCl_3$): δ 161.7 (s, N=*C*H), 161.2 (s, Ar-C_{para}), 130.1 (s, Ar-C_{ipso}), 129.2, 113.7 (s, Ar-CH_{ortho}, Ar-CH_{meta}), 62.6 (s, N-*C*H), 55.2 (s, OCH_3) 34.1, 33.0 (s, N-CH*C*H$_2$), 25.7 (s, N-CHCH$_2$CH$_2$*C*H$_2$), 24.3, 24.1 (s, N-CHCH$_2$*C*H$_2$), 21.4 (s, *C*H$_3$) ppm. MS (CI): *m/z* 433 $[M+H]^+$.

Synthesis of 1,4-dicyclohexyl-2,3-di(phenyl-4-dimethylamino)-1,4-diaza-1,3-butadiene, $^{Cy,NMe2\text{-}Ph}[N,N]$, **23**. Ligand **23** was prepared as for **1**, using cyclohexyl amine (15.5 mL, 135 mmol), $TiCl_4$ solution (20 mL, 20 mmol) and *para*-dimethylaminobenzil (5.0 g, 17 mmol). The pale brown crude product was

recrystallised from hot MeOH/H_2O (95:5 v/v, 350 mL) to give a white, crystalline solid, 3.50 g, 45%. Anal. Calcd for $C_{30}H_{42}N_4$: C, 78.56; H, 9.23; N, 12.21. Found: C, 78.55; H, 9.12; N, 12.11. IR (nujol, cm^{-1}): 1596($\nu_{C=N}$). ^1H NMR ($CDCl_3$): δ 7.68 (4H, d, $^3J_{H-H}$ 8.8, Ar-*H*), 6.61 (4H, d, $^3J_{H-H}$ 8.8, Ar-*H*), 3.22 (2H, m, N-C*H*), 2.97 (12H, s, N-(C*H*$_3$)$_2$), 1.07-1.80 (20H, m, C*H*$_2$) ppm. $^{13}C\{^1H\}$ NMR ($CDCl_3$): δ 162.6 (s, N=CH), 151.6 (s, Ar-C_{para}), 125.4 (s, Ar-C_{ipso}), 129.2, 111.4 (s, Ar-CH_{ortho}, Ar-CH_{meta}), 62.4 (s, N-CH), 40.2 (s, CH_3) 34.3, 33.2 (s, N-$CHCH_2$), 25.8 (s, N-$CHCH_2CH_2CH_2$), 24.5, 24.4 (s, N-$CHCH_2CH_2$) ppm. MS (CI): *m/z* 459 $[M+H]^+$.

Synthesis of 1,4-di(*tert*-butyl)-2,3-di(phenyl-4-bromo)-1,4-diaza-1,3-butadiene, $^{tBu,Br-Ph}$[*N,N*], **24.** Ligand **24** was prepared as for **1**, using *tert*-butyl amine (6.9 mL, 65 mmol), $TiCl_4$ solution (9.8 mL, 10 mmol) and *para*-bromobenzil (3.0 g, 8 mmol). The sticky orange residue was recrystallised from hot MeOH (60 mL) to give white crystals, 2.62 g, 67%. Anal. Calcd for $C_{22}H_{26}N_2Br_2$: C, 55.25; H, 5.48; N, 5.86. Found: C, 55.16; H, 5.58; N, 5.98. IR (nujol, cm^{-1}): 1622 ($\nu_{C=N}$). ^1H NMR ($CDCl_3$): δ 7.64 (4H, d, $^3J_{H-H}$ 8.6, Ar-*H*), 7.48 (4H, d, $^3J_{H-H}$ 8.6, Ar-*H*), 1.26 (18H, s, C*H*$_3$) ppm. $^{13}C\{^1H\}$ NMR ($CDCl_3$): δ 157.5 (s, N=CH), 138.9 (s, Ar-C_{ipso}), 131.6, 129.2 (s, Ar-CH_{ortho}, Ar-CH_{meta}), 124.5 (s, Ar-C_{para}), 58.3 (s, CMe_3), 30.0 (s, CH_3) ppm. MS (EI): *m/z* 479 $[M+H]^+$.

Synthesis of 1,4-di(*tert*-butyl)-2,3-di(phenyl-4-methyl)-1,4-diaza-1,3-butadiene, $^{tBu,Me-Ph}$[*N,N*], **25.** Ligand **25** was prepared as for **1,** using *t*-butyl amine (10.6 mL, 101 mmol), $TiCl_4$ solution (15 mL, 15 mmol) and *para*-methylbenzil (3.0 g, 13 mmol). The sticky orange residue was recrystallised from hot MeOH (60 mL) to give white crystals, 2.73 g, 62%. Anal. Calcd for $C_{24}H_{32}N_2$: C, 82.71; H, 9.25; N, 8.04. Found: C, 82.64; H, 9.25; N, 8.13. IR (nujol, cm^{-1}): 1624 ($\nu_{C=N}$). ^1H NMR ($CDCl_3$): δ 7.73 (4H, d, d, $^3J_{H-H}$ 8.0, Ar-*H*), 7.18 (4H, d, $^3J_{H-H}$ 8.0, Ar-*H*), 2.39 (6H, s, ArC*H*$_3$), 1.31 (18H, s, C*H*$_3$) ppm. $^{13}C\{^1H\}$ NMR ($CDCl_3$): δ 159.2 (s, N=CH), 139.7 (s, Ar-C_{ipso}), 138.0 (s, Ar-C_{para}), 129.0, 127.7 (s, Ar-CH_{ortho}, Ar-CH_{meta}), 57.8 (s, CMe_3), 30.1 (s, Ar-CH_3), 29.9 (s, CH_3) ppm. MS (CI): *m/z* 349 $[M+H]^+$.

Synthesis of 1,4-di(*tert*-butyl)-2,3-di(phenyl-4-methoxy)-1,4-diaza-1,3-butadiene, $^{tBu,MeO\text{-}Ph}[N,N]$, **26.** Ligand **26** was prepared as for **1**, using *tert*-butyl amine (7.8 mL, 74 mmol), $TiCl_4$ solution (11mL, 11 mmol) and *para*-methoxybenzil (2.5 g, 9 mmol). The sticky orange residue was recrystallised from hot MeOH (60 mL) to give white crystals, 2.37 g, 67%. Anal. Calcd for $C_{24}H_{32}N_2O_2$: C, 75.75; H, 8.48; N, 7.36. Found: C, 75.83; H, 8.55; N, 7.28. IR (nujol, cm^{-1}): 1626 ($\nu_{C=N}$). ^1H NMR ($CDCl_3$): δ 7.71 (4H, d, $^3J_{H\text{-}H}$ 8.8, Ar-*H*), 6.84 (4H, d, $^3J_{H\text{-}H}$ 8.8, Ar-*H*), 3.80 (6H, s, O*CH*$_3$), 1.24 (18H, s, *CH*$_3$) ppm. $^{13}C\{^1H\}$ NMR ($CDCl_3$): δ 160.8 (s, N=*C*H), 158.6 (s Ar-*C*$_{para}$), 133.3 (s, Ar-*C*$_{ipso}$), 129.2, 113.5 (s, Ar-*C*H$_{ortho}$, Ar-*C*H$_{meta}$), 57.6 (s, *C*Me$_3$), 55.2 (s, O*C*H$_3$) 30.0 (s, *C*H$_3$) ppm. MS (CI): *m/z* 381 $[M+H]^+$.

Synthesis of 1,4-di(*tert*-butyl)-2,3-di(phenyl-4-dimethylamino)-1,4-diaza-1,3-butadiene, $^{tBu,NMe2\text{-}Ph}[N,N]$, **27.** Ligand **27** was prepared as for **1**, using *tert*-butyl amine (14.2 mL, 135 mmol), $TiCl_4$ solution (20 mL, 20 mmol) and *para*-dimethylaminobenzil (5.0 g, 17 mmol). The sticky orange residue was recrystallised from hot $MeOH/H_2O$ (95:5 v/v, 300 mL) to give white crystals, 3.93 g, 57%. Anal. Calcd for $C_{26}H_{38}N_4$: C, 76.80; H, 9.42; N, 13.78. Found: C, 76.66; H, 9.46; N, 13.83. IR (nujol, cm^{-1}): 1599 ($\nu_{C=N}$). ^1H NMR ($CDCl_3$): δ 7.68 (4H, d, $^3J_{H\text{-}H}$ 8.9, Ar-*H*), 6.64 (4H, m, $^3J_{H\text{-}H}$ 8.9, Ar-*H*), 2.98 (12H, s, N(*CH*$_3$)$_2$), 1.29 (18H, 2, *CH*$_3$) ppm. $^{13}C\{^1H\}$ NMR ($CDCl_3$): δ 159.4 (s, N=*C*H), 151.1 (s Ar-*C*$_{para}$), 129.0 (s, Ar-*C*$_{ipso}$), 128.9, 111.3 (s, Ar-*C*H$_{ortho}$, Ar-*C*H$_{meta}$), 57.2 (s, *C*Me$_3$), 40.2 (s, N(*C*H$_3$)$_2$) 30.2 (s, *C*H$_3$) ppm. MS (CI): *m/z* 407 $[M+H]^+$.

7.6.3.2 - Synthesis of Fe^{II} complexes.

Synthesis of 1,4-dicyclohexyl-2,3-di(phenyl-4-bromo)-1,4-diaza-1,3-butadiene iron^{II} chloride, $^{Cy,Br\text{-}Ph}[N,N]FeCl_2$, **28.** Complex **28** was prepared as reported for **7**, using ligand **20** (0.53 g, 1 mmol) and $FeCl_2(THF)_{1.5}$ (0.22 g, 1 mmol). Precipitation with heptane, filtration and drying yielded a bright purple solid, 0.37 g, 60%. Anal. Calcd for $C_{26}H_{30}N_2FeBr_2Cl_2$: C, 47.52; H, 4.60; N, 4.26. Found: C, 47.38; H, 4.64; N, 4.23. IR (nujol, cm^{-1}): 1590 ($\nu_{C=N}$). ^1H NMR ($CDCl_3$): δ 195.23 (2H, br s, NC*H*), 16.11 (4H, br s, Ar-*H*), 1.22 (4H, br s, Ar-*H*), 0.83, -5.48, -6.58, -13.27, -20.14, -45.76 (20H, br s, *CH*$_2$) ppm. MS (FAB^+): *m/z* 657 $[M+H]^+$, 621 $[M\text{-}Cl]^+$. $\mu_{eff.}$ = 4.96 B.M.

Synthesis of 1,4-dicyclohexyl-2,3-di(phenyl-4-methyl)-1,4-diaza-1,3-butadiene iron^{II} chloride, $^{Cy,Me\text{-}Ph}[N,N]FeCl_2$, **29.** Complex **29** was synthesised in an analogous manner to **7**, using ligand **21** (0.75 g, 2 mmol) and $FeCl_2(THF)_{1.5}$ (0.44 g, 2 mmol). Precipitation with heptane, filtration and drying gave a purple solid, 0.78 g, 79%. Anal. Calcd for $C_{28}H_{36}N_2FeCl_2$: C, 63.77; H, 6.88; N, 5.31. Found: C, 63.70; H, 6.67; N, 5.13. IR (nujol, cm^{-1}): 1606 ($\nu_{C=N}$). ^1H NMR ($CDCl_3$): δ 194.02 (2H, br s, NC*H*), 16.35 (4H, br s, Ar-*H*), 16.04 (4H, br s, Ar-*H*), 9.02 (6H, br s, ArCH_3), 7.20, -6.06, -7.00, -13.82, -21.21, -51.22 (20H, br s, CH_2) ppm. MS (FAB^+): *m/z* 491 $[M\text{-}Cl]^+$. $\mu_{eff.}$ = 5.10 B.M.

Synthesis of 1,4-dicyclohexyl-2,3-di(phenyl-4-methoxy)-1,4-diaza-1,3-butadiene iron^{II} chloride, $^{Cy,MeO\text{-}Ph}[N,N]FeCl_2$, **30.** Complex **30** was synthesised in an analogous manner to **7**, using ligand **22** (1.0 g, 2 mmol) and $FeCl_2(THF)_{1.5}$ (0.54 g, 2 mmol). Precipitation with heptane, filtration and drying gave a purple solid, 0.86 g, 66%. Anal. Calcd for $C_{28}H_{36}N_2O_2FeCl_2$ requires C, 60.12; H, 6.49; N, 5.01. Found: C, 60.17; H, 6.47; N, 4.95. IR (nujol, cm^{-1}): 1609 ($\nu_{C=N}$). ^1H NMR ($CDCl_3$): δ 194.71 (2H, br s, NC*H*), 15.95 (4H, br s, Ar-*H*), 15.75 (4H, br s, Ar-*H*), 6.43 (6H, br s, ArOCH_3), 7.19, -6.20, -7.26, -14.17, -21.83, -52.87 (20H, br s, CH_2) ppm. MS (FAB^+, m/z): 560 $[M+H]^+$, 523 $[M\text{-}Cl]^+$. $\mu_{eff.}$ = 5.06 B.M.

Synthesis of 1,4-dicyclohexyl-2,3-di(phenyl-4-dimethylamino)-1,4-diaza-1,3-butadiene iron^{II} chloride, $^{Cy,NMe2\text{-}Ph}[N,N]FeCl_2$, **31.** Complex **31** was synthesised in an analogous manner to **7**, using ligand **23** (0.50 g, 1 mmol) and $FeCl_2(THF)_{1.5}$ (0.26 g, 1 mmol). Precipitation with heptane, filtration and drying gave a dark red-brown solid, 0.48 g, 75%. Anal. Calcd for $C_{30}H_{42}N_4FeCl_2$: C, 61.55; H, 7.23; N, 9.57. Found: C, 61.47; H, 7.19; N, 9.60. IR (nujol, cm^{-1}): 1606 ($\nu_{C=N}$). ^1H NMR ($CDCl_3$): δ 192.28 (2H, br s, NC*H*), 15.53 (4H, br s, Ar-*H*), 8.65 (12H, br s, N(CH_3)$_2$), 2.12 (4H, br s, Ar-*H*), 4.34, -6.65, -7.88, -15.12, -23.8, -56.67 (20H, br s, CH_2) ppm. MS (FAB^+): *m/z* 549 $[M\text{-}Cl]^+$. $\mu_{eff.}$ = 5.25 B.M.

Synthesis of 1,4-di(*tert*-butyl)-2,3-di(phenyl-4-bromo)-1,4-diaza-1,3-butadiene iron^{II} chloride, $^{tBu,Br\text{-}Ph}[N,N]FeCl_2$, **32.** Complex **32** was synthesised in an analogous manner to **7**, using ligand **24** (0.75 g, 2 mmol) and $FeCl_2(THF)_{1.5}$ (0.37 g, 2 mmol).

Precipitation with heptane, filtration and drying gave a purple solid, 0.69 g, 73%. Anal. Calcd for $C_{22}H_{26}N_2FeBr_2Cl_2$: C, 43.67; H, 4.33; N, 4.63. Found: C, 43.67; H, 4.31; N, 4.45. IR (nujol, cm^{-1}): 1593 ($\nu_{C=N}$). ^1H NMR ($CDCl_3$): δ 18.91 (4H, br s, Ar-*H*), 17.25 (4H, br s, Ar-*H*), -15.43 (18H, br s, C*H*$_3$) ppm. MS (FAB^+): *m/z* 604 $[M+H]^+$, 569 $[M-Cl]^+$. $\mu_{eff.}$ = 5.14 B.M.

Synthesis of 1,4-di(*tert*-butyl)-2,3-di(phenyl-4-methyl)-1,4-diaza-1,3-butadiene iron^{II} chloride, $^{tBu,Me\text{-}Ph}$[*N,N*]$FeCl_2$, **33.** Complex **33** was synthesised in an analogous manner to **7**, using ligand **25** (0.75 g, 2 mmol) and $FeCl_2(THF)_{1.5}$ (0.51 g, 2 mmol). Precipitation with heptane, filtration and drying gave a purple solid, 0.71 g, 69%. Anal. Calcd for $C_{24}H_{32}N_2FeCl_2$: C, 60.65; H, 6.79; N, 5.89. Found: C, 60.51; H, 6.65; N, 5.77. IR (nujol, cm^{-1}): 1610 ($\nu_{C=N}$). ^1H NMR ($CDCl_3$): δ 19.24 (4H, br s, Ar-*H*), 17.85 (4H, br s, Ar-*H*), 9.69 (6H, br s, ArC*H*$_3$), -18.04 (18H, br s, C*H*$_3$) ppm. MS (FAB^+): *m/z* 476 $[M+H]^+$. $\mu_{eff.}$ = 5.28 B.M.

Synthesis of 1,4-di(*tert*-butyl)-2,3-di(phenyl-4-methoxy)-1,4-diaza-1,3-butadiene iron^{II} chloride, $^{tBu,MeO\text{-}Ph}$[*N,N*]$FeCl_2$, **34.** Complex **34** was synthesised in an analogous manner to **7**, using ligand **26** (0.50 g, 1 mmol) and $FeCl_2(THF)_{1.5}$ (0.31 g, 1 mmol). Precipitation with heptane, filtration and drying gave a purple solid, 0.52 g, 78%. Anal. Calcd for $C_{24}H_{32}N_2O_2FeCl_2$: C, 56.82; H, 6.36; N, 5.52. Found: C, 56.78; H, 6.44; N, 5.45. IR (nujol, cm^{-1}): 1607 ($\nu_{C=N}$). ^1H NMR ($CDCl_3$): δ 19.14 (4H, br s, Ar-*H*), 17.10 (4H, br s, Ar-*H*), 7.01 (12H, br s, OC*H*$_3$), -18.01 (18H, br s, C*H*$_3$) ppm. MS (FAB^+): *m/z* 506 $[M+H]^+$, 471 $[M-Cl]^+$. $\mu_{eff.}$ = 5.18 B.M.

Synthesis of 1,4-di(*tert*-butyl)-2,3-di(phenyl-4-dimethylamino)-1,4-diaza-1,3-butadiene iron^{II} chloride, $^{tBu,NMe2\text{-}Ph}$[*N,N*]$FeCl_2$, **35.** Complex **35** was synthesised in an analogous manner to **7**, using ligand **27** (0.50 g, 1 mmol) and $FeCl_2(THF)_{1.5}$ (0.29 g, 1 mmol). Precipitation with heptane, filtration and drying gave a dark red-brown solid, 0.43 g, 66%. Anal. Calcd for $C_{26}H_{38}N_4FeCl_2$: C, 58.55; H, 7.18; N, 10.50. Found: C, 58.67; H, 7.23; N, 10.40. IR (nujol, cm^{-1}): 1610 ($\nu_{C=N}$). ^1H NMR ($CDCl_3$): δ 18.88 (4H, br s, Ar-*H*), 17.13 (4H, br s, Ar-*H*), 7.82 (12H, br s, N(C*H*$_3$)$_2$), -20.09 (18H, br s, C*H*$_3$) ppm. MS (FAB^+): *m/z* 461 $[M-2Cl]^+$. $\mu_{eff.}$ = 4.99 B.M.

7.6.3.3 - Synthesis of Fe^{III} complexes.

Synthesis of 1,4-dicyclohexyl-2,3-di(phenyl-4-bromo)-1,4-diaza-1,3-butadiene iron^{III} chloride, $^{Cy,Br\text{-}Ph}[N,N]FeCl_3$, **36.** Ligand **20** (0.25 g, 0.5 mmol) and $FeCl_3$ (0.08 g, 0.5 mmol) were suspended in CH_2Cl_2 (*ca.* 25 mL) at -78C, and then allowed to warm to room temperature. The dark red-orange solution was stirred for an hour, filtered and then concentrated. The residue was washed with heptane (3 × 15 mL) to yield a dark red solid, 0.18 g, 55%. Anal. Calcd for $C_{26}H_{30}N_2FeBr_2Cl_3$: C, 45.09; H, 4.37; N, 4.05. Found: C, 45.15; H, 4.36; N, 3.94. $\mu_{eff.}$ = 4.10 B.M.

Synthesis of 1,4-dicyclohexyl-2,3-di(phenyl-4-methyl)-1,4-diaza-1,3-butadiene iron^{III} chloride, $^{Cy,Me\text{-}Ph}[N,N]FeCl_3$, **37.** Complex **37** was synthesised in an analogous manner to **36**, using ligand **21** (0.25 g, 0.6 mmol) and $FeCl_3$ (0.10 g, 0.6 mmol). The dark red-orange solution was stirred for an hour, filtered and then concentrated. The residue was washed with heptane (3 × 15 mL) to yield a dark red solid, 0.24 g, 68%. Anal. Calcd for $C_{28}H_{36}N_2FeCl_3$ requires C, 59.75; H, 6.45; N, 4.98. Found: C, 59.82; H, 6.55; N, 5.03. $\mu_{eff.}$ = 4.18 B.M.

Synthesis of 1,4-dicyclohexyl-2,3-di(phenyl-4-methoxy)-1,4-diaza-1,3-butadiene iron^{III} chloride, $^{Cy,MeO\text{-}Ph}[N,N]FeCl_3$, **38.** Complex **38** was synthesised in an analogous manner to **36**, using ligand **22** (0.25 g, 0.5 mmol) and $FeCl_3$ (0.10 g, 0.5 mmol). After stirring at room temperature for 2 h, the dark red-brown solution was filtered and heptane (*ca.* 5 mL) added in to precipitate a small amount of brown solid. Further concentration and washing with heptane gave a dark red solid, 0.25 g, 73%. Anal. Calcd for $C_{28}H_{38}N_2O_2FeCl_3$: C, 56.35; H, 6.42; N, 4.69. Found: C, 56.31; H, 6.44; N, 4.63. $\mu_{eff.}$ = 4.12 B.M.

Synthesis of 1,4-dicyclohexyl-2,3-di(phenyl-4-dimethylamino)-1,4-diaza-1,3-butadiene iron^{III} chloride, $^{Cy,NMe2\text{-}Ph}[N,N]FeCl_3$, **39.** Complex **39** was synthesised in an analogous manner to **36**, using ligand **23** (0.25 g, 0.5 mmol) and $FeCl_3$ (0.09 g, 0.5 mmol). The dark orange-brown solution was stirred at room temperature for 1 h and then filtered and concentrated to *ca.* 15 mL. Heptane was used to precipitate a dark red solid, which was collected by filtration and dried under vacuum to give 0.19

g, 56%. Anal. Calcd for $C_{30}H_{42}N_4FeCl_3$: C, 58.03; H, 6.82; N, 9.02. Found: C, 57.97; H, 6.72; N, 8.94. $\mu_{eff.}$ = 5.63 B.M.

Synthesis of 1,4-di(*tert*-butyl)-2,3-di(phenyl-4-bromo)-1,4-diaza-1,3-butadiene iron^{III} chloride, $^{tBu,Br\text{-}Ph}$[*N,N*]$FeCl_3$, **40.** Complex **40** was synthesised in an analogous manner to **16**, using ligand **24** (0.25 g, 0.7 mmol) and $FeCl_3$ (0.12 g, 0.7 mmol). After stirring at room temperature for 2 h, the dark blue-black solution was filtered and heptane (*ca.* 5 mL) added in to precipitate a small amount of brown solid. Further concentration and washing with heptane gave a dark blue solid, 0.10 g, 30%. Anal. Calcd for $C_{22}H_{26}N_2FeBr_2Cl_3$: C, 41.26; H, 4.09; N, 4.37. Found: C, 41.40; H, 4.05; N, 4.45. $\mu_{eff.}$ = 4.14 B.M.

Synthesis of 1,4-di(*tert*-butyl)-2,3-di(phenyl-4-methyl)-1,4-diaza-1,3-butadiene iron^{III} chloride, $^{tBu,Me\text{-}Ph}$[*N,N*]$FeCl_3$, **41.** Complex **41** was synthesised in an analogous manner to **16**, using ligand **25** (0.25 g, 0.7 mmol) and $FeCl_3$ (0.12 g, 0.7 mmol). After stirring at room temperature for 2 h, the dark blue-black solution was filtered and heptane (*ca.* 5 mL) added in to precipitate a small amount of brown solid. Further concentration and washing with heptane gave a dark blue solid, 0.14 g, 38%. Anal. Calcd for $C_{24}H_{32}N_2FeCl_3$: C, 56.44; H, 6.32; N, 5.48. Found: C, 56.60; H, 6.27; N, 5.45. $\mu_{eff.}$ = 4.05 B.M.

Synthesis of 1,4-di(*tert*-butyl)-2,3-di(phenyl-4-methoxy)-1,4-diaza-1,3-butadiene iron^{III} chloride, $^{tBu,MeO\text{-}Ph}$[*N,N*]$FeCl_3$, **42.** Complex **42** was synthesised in an analogous manner to **16**, using ligand **26** (0.32 g, 0.8 mmol) and $FeCl_3$ (0.14 g, 0.8 mmol). After stirring at room temperature for 2 h, the dark blue-black solution was filtered and heptane (*ca.* 5 mL) added in to precipitate a small amount of brown solid. Further concentration and washing with heptane gave a dark blue solid, 0.28 g, 61%. Anal. Calcd for $C_{24}H_{32}N_2O_2FeCl_3$: C, 53.11; H, 5.94; N, 5.16. Found: C, 52.89; H, 5.88; N, 5.11. $\mu_{eff.}$ = 3.87 B.M.

Synthesis of 1,4-di(*tert*-butyl)-2,3-di(phenyl-4-dimethylamino)-1,4-diaza-1,3-butadiene iron^{III} chloride, $^{tBu,NMe2\text{-}Ph}$[*N,N*]$FeCl_3$, **43.** Complex **43** was synthesised in an analogous manner to **16**, using ligand **27** (0.25 g, 0.6 mmol) and $FeCl_3$ (0.10 g, 0.6 mmol).After stirring at room temperature for 1 h, the dark orange-brown solution

was filtered, concentrated and washed with heptane to give a dark red-brown solid, 0.19 g, 54%. Anal. Calcd for $C_{26}H_{38}N_4FeCl_3$: C, 54.90; H, 6.73; N, 9.85. Found: C, 55.03; H, 6.66; N, 9.89. μ_{eff} = 5.71 B.M.

7.6.4 - Experimental details for Chapter 5.

Reaction of $^{Cy,F\text{-}Ph}$[*N,N*]FeCl$_2$(CHMePh) with TEMPO. $^{Cy,F\text{-}Ph}$[*N,N*]FeCl$_3$ (0.50 mmol) was dissolved in THF (10 mL) and cooled to –78°C. A solution of TEMPO (0.50 mmol) in THF (5 mL) was added to this mixture dropwise via cannula and an aliquot removed from the reaction. Addition of 1-PhEtMgCl (0.50 mmol) in THF resulted in the precipitation of a white solid ($MgCl_2$). The reaction mixture was warmed to room temperature and quenched with degassed H_2O. The organic fraction was separated, filtered through alumina, dried *in vacuo*, and recrystallised from Et_2O to yield 1-(1-phenylethoxy)-2,2,6,6-tetramethylpiperidine as a white solid in 61% yield. ^{1}H NMR ($CDCl_3$): δ 7.22-7.31 (5H, m, Ar-*H*), 4.77 (1H, q, $^3J_{H\text{-}H}$ 6.4, C*H*-CH_3), 1.77 (3H, d, $^3J_{H\text{-}H}$ 6.4, C*H*$_3$-CH), 1.46-1.56 (3 × 2H, m, C*H*$_2$), 1.02, 1.16, 1.29, 1.31 (4 × 3H, s, C*H*$_3$) ppm. ^{13}C{^{1}H} NMR ($CDCl_3$): δ 140.7 (s, Ar-*C*$_{ipso}$), 129.0 (s, Ar-*C*$_{para}$), 128.4, 126.5 (s, Ar-*C*H$_{ortho}$, Ar-*C*H$_{meta}$), 78.1 (s, *C*H), 48.9 (s, *C*Me$_2$), 34.1 (s, CMe$_2$*C*H$_2$), 25.8, 25.6, 24.1, 23.2 (C*C*H$_3$), 18.4 (CH*C*H$_3$), 15.9 (CH$_2$*C*H$_2$) ppm. MS (EI): *m/z* 261 [M]$^+$.

Reaction of $^{Cy,F\text{-}Ph}$[*N,N*]FeCl$_2$ with 1-PECl and TEMPO. To an ampoule equipped with a magnetic stirrer bar, toluene (3 mL), ^{Cy,H}[*N,N*]FeCl$_2$ (0.10 mmol), 1-phenylethyl chloride (0.10 mmol) and TEMPO (0.10 mmol) were added. The ampoule was sealed and heated in a sand bath at 120°C for 1 hour. The ampoule was then removed from heat and the contents were dissolved in THF, filtered through alumina, dried *in vacuo* and recrystallised from Et_2O to afford 1-(1-phenylethoxy)-2,2,6,6-tetramethylpiperidine in 56% yield. ^{1}H NMR ($CDCl_3$): δ 7.22-7.31 (5H, m, Ar-*H*), 4.77 (1H, q, $^3J_{H\text{-}H}$ 6.4, C*H*-CH_3), 1.77 (3H, d, $^3J_{H\text{-}H}$ 6.4, C*H*$_3$-CH), 1.46-1.56 (3 × 2H, m, C*H*$_2$), 1.02, 1.16, 1.29, 1.31 (4 × 3H, s, C*H*$_3$) ppm. ^{13}C{^{1}H} NMR ($CDCl_3$): δ 140.7 (s, Ar-*C*$_{ipso}$), 129.0 (s, Ar-*C*$_{para}$), 128.4, 126.5 (s, Ar-*C*H$_{ortho}$, Ar-*C*H$_{meta}$), 78.1 (s, *C*H), 48.9 (s, *C*Me$_2$), 34.1 (s, CMe$_2$*C*H$_2$), 25.8, 25.6, 24.1, 23.2 (C*C*H$_3$), 18.4 (CH*C*H$_3$), 15.9 (CH$_2$*C*H$_2$) ppm. MS (EI): *m/z* 261 [M]$^+$.

7.6.5 - Experimental details for Chapter 6.

7.6.5.1 - Synthesis of amine-substituted compounds.

Synthesis of 1,4-di-(4-dimethylaminophenyl)-1,4-diaza-1,3-butadiene, $^{NMe2Ph,H}[N,N]$, **44**. Dimethyl-*p*-phenylenediamine (9.05 g, 66 mmol) was suspended in MeOH (70 mL) and heated under reflux while glyoxal (3.81 mL, 33 mmol) was added. The solution darkened almost immediately, and a precipitate was visible. The solution was heated for a further 90 min then left stirring overnight, before the dark brown semisolid was collected by filtration, washed with cold MeOH (3 × 15 mL), dried under reduced pressure and then recrystallised from $CHCl_3$/petroleum spirit (40-60°C) to give a dark orange solid, 6.27 g, 65%. Anal. Calcd for $C_{18}H_{22}N_4$: C, 73.44; H, 7.53; N, 19.03. Found: C, 73.33; H, 7.48; N, 18.95. IR (nujol, cm^{-1}): 1605 ($\nu_{C=N}$). ^1H NMR ($CDCl_3$): δ 8.47 (2H, s, N=CH), 7.33 (4H, d, $^3J_{H-H}$ 3.3, o-Ar-*H*), 6.76 (4H, d, $^3J_{H-H}$ 3.3, *m*-Ar-*H*), 3.01 (12H, s, $N(CH_3)_2$) ppm. $^{13}C\{^1H\}$ NMR ($CDCl_3$): δ 154.98 (s, N=*C*H), 150.45 (s, Ar-C_{ipso}), 138.95 (s, Ar-C_{para}), 123.21, 112.45 (s, Ar-CH_{ortho}, Ar-CH_{meta}), 40.44 (s, CH_3) ppm. MS (CI): *m/z* 295 $[M+H]^+$.

Synthesis of 1,4-di-(4-dimethylaminophenyl)-1,4-diaza-1,3-butadiene iron^{II} chloride, $^{NMe2Ph,H}[N,N]FeCl_2$, **45**. Ligand **44** (1.00 g, 3 mmol) was dissolved in CH_2Cl_2 (40 mL) and added dropwise to a suspension of $FeCl_2(THF)_{1.5}$ (0.80 g, 3 mmol) in CH_2Cl_2 (15 mL), causing a colour change from pale pink to dark green. The ligand was washed in with CH_2Cl_2 (3 × 5 mL), and the solution stirred overnight at room temperature. Filtration yielded a dark green precipitate which was washed with cold CH_2Cl_2 (3 × 5 mL) and dried under vacuum, 1.21 g, 85%. [7] suitable for X-ray analysis were grown by slow cooling of a saturated acetonitrile solution. Anal. Calcd for $C_{18}H_{22}N_4FeCl_2$: C, 51.33; H, 5.27; N, 13.30. Found: C, 51.16; H, 5.31; N, 13.19. IR (nujol, cm^{-1}): 1603 ($\nu_{C=N}$). MS (FAB^+): *m/z* 422 $[M+H]^+$, 385 $[M-Cl]^+$. $\mu_{eff.}$ = 5.03 B.M.

Synthesis of 1,4-di-(4-benzylpiperidyl)-1,4-diaza-1,3-butadiene, $^{pip,H}[N,N]$, **46**. 4-aminobenzylpiperidine (2.95 mL, 14 mmol) was stirred at room temperature as glyoxal (0.83 mL, 7 mmol) was added dropwise. The solution became warm, and a precipitate began to form immediately. After 60 min the crude product was recrystallised from hot MeOH (25 mL) and the solution left at -5°C overnight. The

white, crystalline product was collected by filtration, washed with cold MeOH and dried under vacuum, 1.90g, 65%. Anal. Calcd for $C_{26}H_{34}N_4$: C, 77.57; H, 8.51; N, 13.92. Found: C, 77.64; H, 8.75; N, 13.95. IR (nujol, cm^{-1}): 1627 ($\nu_{C=N}$). ^1H NMR ($CDCl_3$): δ 7.97 (2H, s, N=C*H*), 7.21-7.35 (10H, m, Ar-*H*), 3.54 (4H, s, CH_2Ph), 3.20 (2H, m, N-C*H*), 2.92 (4H, m, N-CH_2), 2.11 (4H, m, N-CH_2), 1.81 (4H, m, N-CH_2CH_2), 1.78 (4H, m, N-CH_2CH_2) ppm. $^{13}C\{^1H\}$ NMR ($CDCl_3$): δ 160.6 (s, N=CH), 138.5 (s, Ar-C_{ipso}), 129.1, 128.2 (s, Ar-CH_{ortho}, Ar-CH_{meta}), 127.0 (s, Ar-CH_{para}), 67.3 (CH_2Ph), 63.1 (s, N-*C*H), 51.9 (s, N-CH_2), 33.1 (s, N-CH_2CH_2) ppm. MS (CI): *m/z* 403 $[M+H]^+$.

Synthesis of 1,4-di-(4-benzylpiperidyl)-2,3-dimethyl-1,4-diaza-1,3-butadiene, ^{pip,Me}[*N,N*], **47.** Ligand **47** was prepared by modification of a literature procedure.[8] To a stirred solution of 4-aminobenzylpiperidine (8.20 mL, 40 mmol) in CH_2Cl_2 (60 mL) at 0°C was added dropwise $TiCl_4$ (1M in CH_2Cl_2) (6.00 mL, 6 mmol). 2,3-butanedione (0.44 mL, 5 mmol) was added dropwise, and the solution allowed to warm to room temperature. The solution was stirred overnight, and then water (30 mL) added. The precipitate was filtered out, and the aqueous layer of the filtrate extracted with CH_2Cl_2. Removal of the organic solvents under reduced pressure gave a white, sticky residue which was recrystallised from hot MeOH to give a white, crystalline product which was dried under vacuum, 1.47g, 68%. Anal. Calcd for $C_{28}H_{38}N_4$: C, 78.09; H, 8.89; N, 13.01. Found: C, 77.92; H, 8.75; N, 12.96. IR (nujol, cm^{-1}): 1634 ($\nu_{C=N}$). ^1H NMR ($CDCl_3$): δ 7.35 (10H, m, Ar-*H*), 3.55 (4H, s, CH_2Ph), 3.50 (2H, m, N-C*H*), 2.90 (4H, m, N-CH_2), 2.18 (4H, m, N-CH_2), 2.06 (6H, s, CH_3), 1.76 (4H, m, N-CH_2CH_2), 1.64 (4H, m, N-CH_2CH_2) ppm. $^{13}C\{^1H\}$ NMR ($CDCl_3$): δ 166.0 (s, N=*C*H), 138.6 (s, Ar-C_{ipso}), 129.0, 128.1 (s, Ar-CH_{ortho}, Ar-CH_{meta}), 126.8 (s, Ar-CH_{para}), 63.3 (CH_2Ph), 57.8 (s, N-C*H*), 51.9 (s, N-CH_2), 32.5 (s, N-CH_2CH_2), 12.3 (s, CH_3) ppm. MS (CI): *m/z* 431 $[M+H]^+$.

Synthesis of 1,4-di-(4-benzylpiperidyl)-2,3-diphenyl-1,4-diaza-1,3-butadiene, ^{pip,Ph}[*N,N*], **48.** Ligand **48** was prepared as for **47**, using 4-aminobenzylpiperidine (8.20 mL, 40 mmol), $TiCl_4$ solution (6.00 mL, 6 mmol) and benzil (1.05g, 5 mmol). The sticky crude product was recrystallised from EtOH (85 mL) to give a white, crystalline solid which was dried under vacuum, 1.62g, 59%. Anal. Calcd for

$C_{38}H_{42}N_4$: C, 82.27; H, 7.63; N, 10.10. Found: C, 82.35; H, 7.74; N, 9.93. IR (nujol, cm^{-1}): 1616 ($\nu_{C=N}$). ^1H NMR ($CDCl_3$): δ 7.78 (4H, m, Ar-*H*), 7.23-7.40 (16H, m, Ar-*H*), 3.48 (4H, s, CH_2Ph), 3.24 (2H, m, N-C*H*), 2.93, 2.78 (4H, m, N-CH_2), 2.05-1.74 (8H, m, N-CH_2, N-CH_2CH_2), 1.83, 1.35 (4H, m, N-CH_2) ppm. $^{13}C\{^1H\}$ NMR ($CDCl_3$): δ 162.8 (s, N=CH), 138.5, 136.8 (s, Ar-C_{ipso}), 130.6 (s, Ar-CH_{para}), 129.2, 128.5, 128.2, 127.7 (s, Ar-CH_{ortho}, Ar-CH_{meta}), 127.0(s, Ar-CH_{para}), 63.3 (s, CH_2Ph), 60.9, 60.8 (s, N-*C*H), 51.6, 51.4 (s, N-CH_2), 33.3, 32.3 (s, N-CH_2CH_2) ppm. MS (CI): *m/z* 555 $[M+H]^+$.

Synthesis of 1,4-di-(4-benzyl-4-methyl-piperidinium iodide)-1,4-diaza-1,3-butadiene, $^{pip\text{-}I,H}$[*N,N*], **49.** Ligand **46** (3.00g, 8 mmol) was dissolved in CH_2Cl_2 (25 mL) and stirred at room temperature as MeI (0.93 mL, 16 mmol) in CH_2Cl_2 (10 mL) was added dropwise. A white precipitate was visible almost immediately, and after stirring for 24 h the solution was filtered, washed with CH_2Cl_2 (3 × 10 mL), and dried under vacuum, 4.99g, 98%. Anal. Calcd for $C_{28}H_{40}N_4I_2$: C, 48.99; H, 5.87; N, 8.16. Found: C, 48.99; H, 5.80; N, 8.19. IR (nujol, cm^{-1}): 1631 ($\nu_{C=N}$). ^1H NMR (d_6-dmso): δ 7.99 (2H, s, N=C*H*), 7.54 (10H, m, Ar-*H*), 4.66 (4H, s, CH_2Ph), 3.44 (10H, m, N-C*H* and N-CH_2), 3.02 (6H, s, CH_3), 1.99 (8H, m, N-CH_2CH_2) ppm. $^{13}C\{^1H\}$ NMR (d_6-dmso): δ 161.8 (s, N=*C*H), 156.6 (s, Ar-C_{ipso}), 133.2, 130.3 (s, Ar-CH_{ortho}, Ar-CH_{meta}), 128.9 (s, Ar-CH_{para}), 70.0 (CH_2Ph), 63.0 (s, N-*C*H), 55.9 (s, N-CH_2), 40.5 (s, N-CH_2CH_2), 26.4 (s, CH_3) ppm. MS (FAB^+): *m/z* 559 $[M-I]^+$.

Synthesis of 1,4-di-(4-benzyl-4-methyl-piperidinium iodide)-2,3-dimethyl-1,4-diaza-1,3-butadiene, $^{pip\text{-}I,Me}$[*N,N*], **50.** An analogous procedure to that described for **49** was followed, using ligand **47** (1.0 g, 2 mmol) and methyl iodide (0.28 mL, 4 mmol) to give the off-white product, 1.46 g, 94%. Anal. Calcd for $C_{30}H_{44}N_4I_2$: C, 50.43; H, 6.21; N, 7.66. Found: C, 50.31; H, 6.23; N, 7.84. IR (nujol, cm^{-1}): 1643 ($\nu_{C=N}$). ^1H NMR (d_6-dmso): δ 7.53 (10H, m, Ar-H), 4.67 (4H, s, CH_2Ph), 3.80 (2H, m, N-CH), 3.44 (8H, m, N-CH_2), 3.02 (6H, s, CH_3), 2.06 (6H, s, N=CCH_3), 1.99 (8H, m, N-CH_2CH_2) ppm. $^{13}C\{^1H\}$ NMR (d_6-dmso): δ 167.4 (s, N=*C*H), 133.1, 130.3 (s, Ar-CH_{ortho}, Ar-CH_{meta}), 128.9 (s, Ar-CH_{para}), 127.6 (s, Ar-C_{ipso}), 57.7 (CH_2Ph), 55.3, 53.8 (s, CH_2), 45.5 (s, N-*C*H), 26.8 (s, N^+CH_3), 12.6 (s, CH_3) ppm. MS (FAB^+): *m/z* 587 $[M-I]^+$.

Synthesis of 1,4-di-(4-benzyl-4-methyl-piperidinium iodide)-2,3-diphenyl-1,4-diaza-1,3-butadiene, $^{pip\text{-}I,Ph}[N,N]$ iodide, **51**. An analogous procedure to that described for **49** was followed, using ligand **48** (3.0 g, 5 mmol) and methyl iodide (0.67 mL, 10 mmol) to give a white product, 4.36 g, 96%. Anal. Calcd for $C_{40}H_{48}N_4I_2$: C, 57.29; H, 5.77; N, 6.68. Found: C, 57.39; H, 5.93; N, 6.64. IR (nujol, cm^{-1}): 1622 ($\nu_{C=N}$). ^1H NMR (d_6-dmso): δ 7.93-7.40 (20H, m, Ar-H), 4.64 (4H, s, CH_2Ph), 3.60-3.34 (10H, m, N-CH and N-CH_2), 3.06 (6H, s, CH_3), 2.25-1.69 (8H, m, N-CH_2CH_2) ppm. $^{13}C\{^1H\}$ NMR (d_6-dmso): δ 163.5 (s, N=*C*H), 135.3, 133.5 (s, Ar-C_{ipso}), 133.1, 130.28, 129.1, 127.6 (s, Ar-CH_{ortho}, Ar-CH_{meta}), 131.6, 128.9, (s, Ar-CH_{para}), 65.8 (CH_2Ph), 57.2 (s, N-*C*H), 56.8 (s, N-CH_2), 49.1 (s, N-CH_2CH_2), 27.0 (s, CH_3) ppm. MS (FAB^+): *m/z* 711 $[M\text{-}I]^+$.

Synthesis of 1,4-di-(4-benzylpiperidyl)-1,4-diaza-1,3-butadiene iron^{II} chloride, $^{pip,H}[N,N]FeCl_2$, **52**. Ligand **46** (1.00 g, 2.5 mmol) was dissolved in CH_2Cl_2 (15 mL) and added dropwise to a stirred solution of $FeCl_2(THF)_{1.5}$ (0.58 g, 2.5 mmol) in CH_2Cl_2 (10 mL). The solution became a deep blue colour immediately, and after stirring at 25°C for 24 h, the solvent was concentrated to 10 mL and pentane (20 mL) added to precipitate a purple solid, which was washed with pentane (3 × 10 mL) and dried under vacuum, 0.98 g, 74%. Crystals suitable for X-ray analysis were grown by layering a saturated dichloromethane solution with pentane, and allowing slow diffusion to occur. Anal. Calcd for $C_{26}H_{34}N_4FeCl_2$: C, 59.00; H, 6.47; N, 10.58. Found: C, 58.84; H, 6.39; N, 10.79. IR (nujol, cm^{-1}): 1645 ($\nu_{C=N}$). MS (FAB^+): *m/z* 403 $[L+H]^+$. μ_{eff} = 4.96 B.M.

Synthesis of 1,4-di-(4-benzylpiperidyl)-2,3-dimethyl-1,4-diaza-1,3-butadiene iron^{II} chloride, $^{pip,Me}[N,N]FeCl_2$, **53**. Complex **53** was prepared as for **52**, using ligand **47** (0.50 g, 1 mmol) and $FeCl_2(THF)_{1.5}$ (0.27 g, 1 mmol). After stirring at room temperature overnight, the dark blue solution was concentrated to 10 mL and pentane (20 mL) added in to precipitate a pink solid. The precipitate was isolated by filtration, washed with pentane (3 × 10 mL) and dried under vacuum, 0.51 g, 76%. Crystals suitable for X-ray analysis were grown by layering a saturated dichloromethane solution with pentane, and allowing slow diffusion to occur. Anal.

Calcd for $C_{28}H_{38}N_4FeCl_2$: C, 60.34; H, 6.87; N, 10.05. Found: C, 60.17; H, 7.03; N, 9.93. IR (nujol, cm^{-1}): 1637 ($\nu_{C=N}$). MS (FAB^+): *m/z* 521 $[M\text{-}Cl]^+$. μ_{eff} = 5.01 B.M.

Synthesis of 1,4-di-(4-benzylpiperidyl)-2,3-diphenyl-1,4-diaza-1,3-butadiene iron^{II} chloride, $^{pip,Ph}[N,N]FeCl_2$, **54.** Complex **54** was prepared using the method described for **52**, using ligand **48** (0.50 g, 1 mmol) and $FeCl_2(THF)_{1.5}$ (0.21 g, 1 mmol). Extraction in CH_2Cl_2, concentration and precipitation gave a green solid, 0.54 g, 88%. Anal. Calcd for $C_{38}H_{42}N_4FeCl_2$: C, 66.97; H, 6.21; N, 8.22. Found: C, 66.78; H, 6.16; N, 8.22. IR (nujol, cm^{-1}): 1616 ($\nu_{C=N}$). MS (FAB^+): *m/z* 585 $[L+H]^+$. μ_{eff} = 4.76 B.M.

Synthesis of 1,4-di-(4-benzyl-4-methyl-piperidinium iodide)-1,4-diaza-1,3-butadiene iron^{II} chloride, $^{pip\text{-}I,H}[N,N]FeCl_2$, **55.** Ligand **49** (1.00 g, 1.5 mmol) and $FeCl_2(THF)_{1.5}$ (0.34 g, 1.5 mmol) were stirred at room temperature in THF (30 mL). A purple colour was immediately visible. After stirring for 24 h, the lilac precipitate was isolated by filtration, washed with THF (3 × 10 mL) and dried under vacuum, 0.87 g, 74%. Anal. Calcd for $C_{28}H_{40}N_4FeCl_2I_2$: C, 41.36; H, 4.96; N, 6.89. Found: C, 41.38; H, 4.96; N, 6.73. IR (nujol, cm^{-1}): 1635 ($\nu_{C=N}$). MS (FAB^+): *m/z* 686 $[M\text{-}I]^+$. μ_{eff} = 5.13 B.M.

Synthesis of 1,4-di-(4-benzyl-4-methyl-piperidinium iodide)-2,3-dimethyl-1,4-diaza-1,3-butadiene iron^{II} chloride, $^{pip\text{-}I,Me}[N,N]FeCl_2$, **56.** Ligand **50** (0.5 g, 0.6 mmol) and $FeCl_2(THF)_{1.5}$ (0.14 g, 0.6 mmol) were stirred at room temperature in MeOH (25 mL) for 24 h. The solution was filtered, and the remaining solid washed with MeOH (3 × 10 mL). Concentration of the solution and precipitation using ether gave the product as a brown solid, 0.39 g, 68%. Anal. Calcd for $C_{40}H_{48}N_4FeCl_2I_2$: C, 49.77; H, 5.01; N, 5.80. Found: C, 49.91; H, 4.93; N, 5.70. IR (nujol, cm^{-1}): 1627 ($\nu_{C=N}$). MS (FAB^+): *m/z* 838 $[M\text{-}I]^+$. μ_{eff} = 4.98 B.M.

Synthesis of 1,4-di-(4-benzyl-4-methyl-piperidinium iodide)-2,3-diphenyl-1,4-diaza-1,3-butadiene iron^{II} chloride, $^{pip\text{-}I,Ph}[N,N]FeCl_2$, **57.** Complex **57** was prepared as for **56**, using ligand **51** (0.5 g, 6 mmol) and $FeCl_2(THF)_{1.5}$ (0.14 g, 6 mmol). After filtration, washing and concentrating, the product was obtained as a brown solid,

0.37 g, 64%. Anal. Calcd for $C_{40}H_{48}N_4I_2FeCl_2$: C, 49.77; H, 5.01; N, 5.80. Found: C, 49.91; H, 4.93; N, 5.70. IR (nujol, cm^{-1}): 1637 ($\nu_{C=N}$). MS (FAB^+): *m/z* 711 $[L\text{-}I]^+$. μ_{eff} = 5.07 B.M.

Synthesis of 1,4-di-(2,2,6,6-tetramethylpiperidyl)-1,4-diaza-1,3-butadiene, $^{TEMP,H}[N,N]$, **58.** An analogous procedure as described for ligand **46** was followed, using 4-amino-2,2,6,6-tetramethylpiperidine (2.5 mL, 15 mmol) and glyoxal (0.84 mL, 7.5 mmol). The sticky crude residue was recrystallised from hot Et_2O/MeOH (8:1) and white crystals of the product were obtained, 1.62 g, 66%. Anal. Calcd for $C_{20}H_{38}N_4$: C, 71.80; H, 11.45; N, 16.75. Found: C, 71.90; H, 11.41; N, 16.44. IR (nujol, cm^{-1}): 3300, 3250 ($\nu_{N\text{-}H}$), 1630 ($\nu_{C=N}$). ^1H NMR ($CDCl_3$): δ 7.97 (2H, s, N=C*H*), 3.64 (2H, m, N-C*H*), 1.08-1.66 (32H, m, CH_2 and CH_3) ppm. $^{13}C\{^1H\}$ NMR ($CDCl_3$): δ 160.64 (s, N=*C*H), 62.6 (s, N-*C*Me_2), 50.3 (s, N-*C*H), 45.6 (s, CH_2), 35.0, 28.7 (s, CH_3) ppm. MS (CI): *m/z* 335 $[M+H]^+$.

Synthesis of 1,4-di-(2,2,6,6-tetramethylpiperidyl)-1,4-diaza-1,3-butadiene iron^{II} chloride, $^{TEMP,H}[N,N]FeCl_2$, **59.** Ligand **58** (0.75 g, 2.2 mmol) and $FeCl_2(THF)_{1.5}$ (0.53 g, 2.2 mmol) were suspended in THF (40 mL) and heated at 60°C overnight. After cooling, filtering and concentrating the dark blue solution, pentane was added to precipitate the product as a purple solid, 0.78 g, 75%. Anal. Calcd for $C_{20}H_{38}N_4FeCl_2$: C, 52.07; H, 8.30; N, 12.15. Found: C, 51.96; H, 8.34; N, 12.23. IR (nujol, cm^{-1}): 3332, 3316 ($\nu_{N\text{-}H}$), 1637 ($\nu_{C=N}$). MS (FAB^+): *m/z* 460 $[M+H]^+$, 335 $[L+H]^+$. μ_{eff} = 5.12 B.M.

Synthesis of 1,4-di-(3-dimethylaminopropane)-2,3-dimethyl-1,4-diaza-1,3-butadiene, $^{NMe2\text{-}nPr,Me}[N,N]$, **60.** As literature procedure.[9] Butanedione (1.89 mL, 22 mmol) was dissolved in EtOH (60 mL) and stirred at room temperature as *N,N*-dimethylaminopropyl amine (5.42 mL, 44 mmol) was added. The yellow solution was then heated under reflux for 5 h, during which time the colour darkened to brown. Removal of the solvent under reduced pressure gave a dark brown oil which was vacuum distilled (74°C at 0.01 mmHg) to give a pale yellow oil, 1.72 g, 31%. Anal. Calcd for $C_{14}H_{30}N_4$: C, 66.09; H, 11.89; N, 22.02. Found: C, 65.90; H, 11.81; N, 21.97. IR (nujol, cm^{-1}): 1617 ($\nu_{C=N}$). ^1H NMR ($CDCl_3$): δ 3.37 (4H, t, $^3J_{H\text{-}H}$ 7.0,

N-C*H*$_2$), 2.33 (4H, m, C=N-C*H*$_2$), 2.19 (12H, s, NC*H*$_3$), 1.99 (6H, s, CC*H*$_3$), 1.80 (4H, m, NCH$_2$C*H*$_2$) ppm. ^{13}C{^{1}H} NMR ($CDCl_3$): δ 168.0 (s, *C*=N), 57.4 (s, *C*H$_2$NMe$_2$), 50.3 (s, N*C*H$_2$), 45.5 (s, N*C*H$_3$), 28.8 (s, NCH$_2$*C*H$_2$), 12.6 (s, C*C*H$_3$) ppm. MS (CI): *m/z* 255 $[M+H]^+$. μ_{eff} = 5.01 B.M.

Synthesis of 1,4-di-(3-trimethylaminopropane ammonium iodide)-2,3-dimethyl-1,4-diaza-1,3-butadiene, $^{NMe3I\text{-}nPr,Me}$[*N,N*], **61**. Ligand **60** (0.50 g, 2 mmol) was dissolved in CH_2Cl_2 (30 mL) and stirred at room temperature as MeI (0.25 mL, 4 mmol) was added dropwise. After 15 min, formation of a white solid had occurred. The reaction was stirred for a further 3 h and then the product was collected by filtration, washed with CH_2Cl_2 (3 × 10 mL) and dried under vacuum, 0.60 g, 57%. Anal. Calcd for $C_{16}H_{36}N_4I_2$: C, 35.70; H, 6.74; N, 10.41. Found: C, 35.84; H, 6.66; N, 10.22. IR (nujol, cm^{-1}): 1621 ($\nu_{C=N}$). ^{1}H NMR (d$_6$-dmso): δ 3.42 (8H, m, N-C*H*$_2$, C=N-C*H*$_2$), 3.12 (18H, s, NC*H*$_3$), 2.09 (4H, m, NCH$_2$C*H*$_2$), 2.03 (6H, s, CC*H*$_3$) ppm. ^{13}C{^{1}H} NMR (d$_6$-dmso): δ168.8 (s, *C*=N), 64.7 (s, *C*H$_2$NMe$_2$), 52.8 (s, N*C*H$_3$), 49.1 (s, N*C*H$_2$), 24.3 (s, NCH$_2$*C*H$_2$), 13.3 (s, C*C*H$_3$) ppm. MS (FAB$^+$): *m/z* 411 $[M-I]^+$. μ_{eff} = 5.14 B.M.

Synthesis of 1,4-di-(3-dimethylaminopropane)-2,3-dimethyl-1,4-diaza-1,3-butadiene iron^{II} chloride, $^{NMe2\text{-}nPr,Me}$[*N,N*]$FeCl_2$, **62**. Ligand **60** (0.5 g, 2 mmol) was dissolved in CH_2Cl_2 (20 mL) and added dropwise to a suspension of $FeCl_2(THF)_{1.5}$ (0.46 g, 2 mmol) in CH_2Cl_2 (10 mL). The dark blue solution was stirred at room temperature overnight and then filtered and concentrated to *ca.* 10 mL. Heptane was added in to precipitate the product, 0.46 g, 61%. Anal. Calcd for $C_{14}H_{30}N_4FeCl_2$: C, 44.11; H, 7.93; N, 14.70. Found: C, 43.95; H, 7.82; N, 14.82. ^{1}H NMR ($CDCl_3$): δ 148.6, 106.2, 82.5, 3.9, -20.3, -41.8, IR (nujol, cm^{-1}): 1622 ($\nu_{C=N}$). MS (FAB$^+$): *m/z* 345 $[M-Cl]^+$. μ_{eff} = 5.07 B.M.

Synthesis of 1,4-di-(3-trimethylaminopropane ammonium iodide)-2,3-dimethyl-1,4-diaza-1,3-butadiene iron^{II} chloride, $^{NMe3I\text{-}nPr,Me}$[*N,N*]$FeCl_2$, **63**. Ligand **61** (0.20 g, 0.4 mmol) and $FeCl_2(THF)_{1.5}$ (0.09 g, 0.4 mmol) were dissolved in MeOH (25 mL) and the red-purple solution stirred at room temperature for 3 h. The solution was then filtered and concentrated, before the product was obtained by precipitation

using ether (15 mL), 0.16 g, 65 %. Anal. Calcd for $C_{16}H_{36}N_2FeCl_2I_2$: C, 28.90; H, 5.46; N, 8.42. Found: C, 28.71; H, 5.99; N, 8.29. IR (nujol, cm^{-1}): 1634 ($\nu_{C=N}$). MS (FAB^+): *m/z* 629 $[M\text{-}Cl]^+$, 537 $[M\text{-}I]^+$. μ_{eff} = 5.01 B.M.

7.6.5.2 - Synthesis of hydroxy-substituted compounds.

Synthesis of 1-cyclohexyl-4-hydroxy-2-phenyl-1,4-diaza-1,3-butadiene, $^{Cy,OH,Ph,H}[N,N]$, **64**. 2-isonitrosoacetophenone (2.5 g, 17 mmol) and cyclohexylamine (15.4 mL, 134 mmol) were dissolved in CH_2Cl_2 and stirred at 0°C as $TiCl_4$ solution (20.0 mL, 20 mmol) was added dropwise. A colour change from yellow to black occurred as the addition progressed. The solution was stirred at room temperature for 48 h, then water (40 mL) was added in. The precipitate was filtered, and the aqueous layer of the filtrate extracted with CH_2Cl_2. Removal of the solvent gave a sticky, dark orange oil which was recrystallised from hot MeOH (50 mL) to give a pale yellow solid, 1.51 g, 40%. Anal. Calcd for $C_{14}H_{18}N_2O$: C, 73.01; H, 7.88; N, 12.16. Found: C, 73.07; H, 7.91; N, 12.02. IR (nujol, cm^{-1}): 3210 br ($\nu_{O\text{-}H}$), 1609, 1593 ($\nu_{C=N}$). ^1H NMR (d_6-dmso): δ 8.21 (1H, s, O*H*), 7.65 (1H, s, *H*C=N), 7.64-7.15 (5H, m, Ar-*H*), 3.44 (1H, m, NC*H*), 1.87-1.23 (10H, m, CH_2) ppm. $^{13}C\{^1H\}$ NMR (d_6-dmso): δ 163.1 (s, *C*=N), 158.1 (s, Ar-C_{ipso}), 152.3 (s, *C*=NOH), 143.0 (s, Ar-CH_{para}), 128.1, 127.3, (s, Ar-CH_{ortho}, Ar-CH_{meta}), 60.4 (s, NCH), 33.2, 25.1, 23.9 (s, CH_2) ppm. MS (CI): *m/z* 231 $[M+H]^+$.

Synthesis of benzil monoxime $^{Ph}[O,NOH]$. Benzil (5.0 g, 24 mmol) and sodium acetate (1.97 g, 24 mmol) were dissolved in EtOH (100 mL) and stirred at room temperature as a solution of hydroxylamine hydrochloride (1.65 g, 24 mmol) in $EtOH/H_2O$ (25 mL, 4:1) was added dropwise. After addition was complete, the solution was stirred at room temperature for 2 hours, during which time a white precipitate formed. The suspension was filtered, and the filtrate concentrated to give a sticky, yellow solid, which was recrystallised from Et_2O/hexane to yield a white solid, 4.45 g, 83%. Anal. Calcd for $C_{14}H_{11}NO_2$: C, 74.65; H, 4.92; N, 6.22. Found: C, 74.47; H, 4.85; N, 6.13. IR (nujol, cm^{-1}): 3251 br ($\nu_{O\text{-}H}$), 1675 ($\nu_{C=O}$), 1635 ($\nu_{C=N}$). ^1H NMR (d_6-dmso): δ 11.90 (1H, br s, O*H*), 7.87-7.39 (10H, m, Ar-*H*) ppm. $^{13}C\{^1H\}$ NMR (d_6-dmso): δ 195.4 (s, *C*=O), 154.7 (s, *C*=NOH), 134.7 (s, Ar-CH_{para}), 134.4,

131.5 (s, Ar-C_{ipso}), 130.0 (s, Ar-CH_{para}), 129.4, 129.1, 128.8, 125.6 (s, Ar-CH_{ortho}, Ar-CH_{meta}) ppm. MS (CI): *m/z* 226 $[M+H]^+$.

Synthesis of 1-(*tert*-butyl)-4-hydroxy-2,3-diphenyl-1,4-diaza-1,3-butadiene, $^{tBu,OH,Ph}[N,N]$, **65.** Benzil monoxime (2.5 g, 11 mmol) and *t*-butyl amine (9.34 mL, 88 mmol) were stirred at 0°C in CH_2Cl_2 (60 mL) as $TiCl_4$ solution (13.3 mL, 13 mmol) was added dropwise. The colour of the solution darkened from yellow to orange as a white precipitate formed, and the mixture was stirred at room temperature for 64 h. Water (30 mL) was added, and the solid removed by filtration. Separation and concentration of the organic layer gave a sticky orange residue which was recrystallised from hot EtOH (75 mL) to yield an off-white solid, 1.99 g, 64%. Anal. Calcd for $C_{18}H_{20}N_2O$: C, 77.11; H, 7.19; N, 9.99. Found: C, 77.19; H, 7.28; N, 9.89. IR (nujol, cm^{-1}): 3111 br (ν_{O-H}), 1614, 1595 ($\nu_{C=N}$). ^1H NMR (d_6-dmso): δ 11.7 (1H, br s, O*H*), 7.65-7.35 (10H, m, Ar-*H*), 1.20 (9H, s, CH_3) ppm. $^{13}C\{^1H\}$ NMR (d_6-dmso): δ 155.1 (s, *C*=N), 154.7 (s, *C*=NOH), 137.5, 134.2 (s, Ar-C_{ipso}), 129.8, 129.4 (s, Ar-CH_{para}), 128.8, 128.3, 126.8, 125.7 (s, Ar-CH_{ortho}, Ar-CH_{meta}), 57.2 (s, CMe_3), 29.7 (s, CH_3) ppm. MS (CI): *m/z* 281 $[M+H]^+$.

Synthesis of 1,4-hydroxy-2,3-dimethyl-1,4-diaza-1,3-butadiene iron^{II} chloride, $^{OH,Me}[N,N]FeCl_2$, **66.** Dimethyl glyoxime (1.00 g, 9 mmol) and $FeCl_2(THF)_{1.5}$ (2.02 g, 9 mmol) were suspended in THF (40 mL) and stirred at room temperature for 5 h. The bright red solution was filtered and concentrated to 15 mL, whereupon precipitation of a bright orange solid occurred. This solid was collected by filtration, washed with pentane (3 × 10 mL) and dried under vacuum, 1.06 g, 51%. Crystals suitable for X-ray analysis were grown by layering a saturated THF solution with pentane, and allowing slow diffusion to occur. Anal. Calcd for $C_4H_8N_2O_2FeCl_2$: C, 19.78; H, 3.32; N, 11.53. Found: C, 22.43; H, 3.73; N, 10.05. IR (nujol, cm^{-1}): 3148 br (ν_{O-H}), 1614 ($\nu_{C=N}$). MS (FAB^+): *m/z* 207 $[M-Cl]^+$. μ_{eff} = 4.99 B.M.

Synthesis of 1,4-hydroxy-2,3-diphenyl-1,4-diaza-1,3-butadiene iron^{II} chloride $^{OH,Ph}[N,N]FeCl_2$, **67.** Complex **67** was synthesised in an analogous manner to **66**, using diphenyl glyoxime (1.00 g, 4.0 mmol) and $FeCl_2(THF)_{1.5}$ (0.98 g, 4.0 mmol). The bright red solution was filtered, concentrated and then pentane (40 mL) was

added to precipitate the product as a bright orange solid, which was collected by filtration, washed with pentane (3 × 10 mL) and dried under vacuum, g, 88%. Crystals suitable for X-ray analysis were grown by layering a saturated THF solution with pentane, and allowing slow diffusion to occur. Anal. Calcd for $C_{14}H_{12}N_2O_2FeCl_2$: C, 45.82; H, 3.30; N, 7.63. Found: C, 45.89; H, 3.22; N, 7.55. IR (nujol, cm^{-1}): 3398 br (ν_{O-H}), 1637 ($\nu_{C=N}$). MS (FAB^+): *m/z* 207 $[L-H_2O]^+$. μ_{eff} = 4.93 B.M.

Synthesis of 1-cyclohexyl-4-hydroxy-2-phenyl-1,4-diaza-1,3-butadiene iron^{II} chloride, $^{Cy,OH,Ph,H}[N,N]FeCl_2$, **68.** Procedure as for complex **66**, using ligand **64** (0.34 g, 1.5 mmol) and $FeCl_2(THF)_{1.5}$ (0.35 g, 1.5 mmol) in 30 mL of THF. Solution turned dark blue-purple and was stirred overnight at room temperature, before being filtered, concentrated (to 10 mL) and the product precipitated using pentane (30 mL), washed with pentane (3 × 10 mL) and dried under vacuum, 0.17 g, 59%. Anal. Calcd for $C_{14}H_{18}N_2OFeCl_2$: C, 47.09; H, 5.08; N, 7.85. Found: C, 46.96; H, 5.15; N, 7.76. IR (nujol, cm^{-1}): 3197 br (ν_{O-H}), 1605, 1599 ($\nu_{C=N}$). MS (FAB^+, CI): *m/z* 231 $[L+H]^+$. μ_{eff} = 5.08 B.M.

Synthesis of 1-(*tert*-butyl)-4-hydroxy-2,3-diphenyl-1,4-diaza-1,3-butadiene iron^{II} chloride, $^{tBu,OH,Ph}[N,N]FeCl_2$, **69.** Procedure as for complex **66**, using ligand **65** (0.20 g, 0.7 mmol) and $FeCl_2(THF)_{1.5}$ (0.17 g, 0.7 mmol) in 25 mL of THF. The solution slowly turned pale blue and was stirred overnight at room temperature, before being filtered, concentrated (to 10 mL) and the product precipitated using pentane (30 mL), washed with pentane (3 × 10 mL) and dried under vacuum, 0.17 g, 59%. Anal. Calcd for $C_{18}H_{20}N_2OFeCl_2$: C, 53.10; H, 4.95; N, 6.88. Found: C, 52.95; H, 5.04; N, 6.95. IR (nujol, cm^{-1}): 3393 br (ν_{O-H}) 1643, 1613 ($\nu_{C=N}$). MS (FAB^+, CI): *m/z*281 $[L-H]^+$. μ_{eff} = 4.85 B.M.

7.7 - References

(1) Hsieh, A. T. T.; West, B. O., *J. Organomet. Chem.* **1976,** *112*, 285.

(2) Gibson, V. C.; O'Reilly, R. K.; Reed, W.; Wass, D.; White, A. J. P.; Williams, D. J., *Chem. Commun.* **2002**, 1850.

(3) Gibson, V. C.; O'Reilly, R. K.; Wass, D. F.; White, A. J. P.; Williams, D. J., *Macromolecules* **2003,** *36*, 2591.

(4) Cotton, F. A.; Luck, R. L.; Son, K.-A.-. *Inorg. Chim. Acta* **1991,** *179*, 11.

(5) Baker, K. V.; Brown, J. M.; Hughes, N.; Skarnulis, A. J.; Sexton, A., *J. Org. Chem.* **1991,** *56*, 4585.

(6) Evans, D. F., *J. Chem. Soc.* **1959**, 2003.

(7) Breuer, J.; Fruhauf, H.-W.; Smeets, W. J. J.; Spek, A. L., *Inorg. Chim. Acta* **1999,** *291*, 438.

(8) Kimpe, N. D.; D'Hondt, L.; Stanoeva, E., *Tetrahedron Lett.* **1991,** *31*, 3879.

(9) Hardman, N. J.; Fang, X.; Scott, B. L.; Wright, R. J.; Martin, R. L.; Kubas, G. J., *Inorg. Chem.* **2005,** *44*, 8306.

Chapter 8

Appendices

8.1 - Appendix 1: Crystal Structure Data

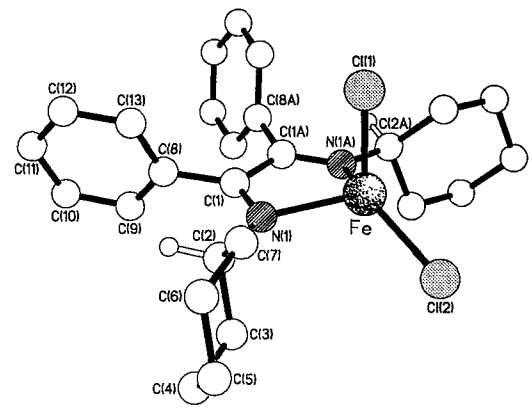
8.1.1 - Crystal structure data for Chapter 2.

data	7	8	9	10	11
code	VG0438	VG0564	VG0447	VG0539	VG0422
formula	$C_{26}H_{32}Cl_2FeN_2$	$C_{26}H_{30}Cl_2F_2FeN_2$	$C_{22}H_{28}Cl_2FeN_2$	$C_{22}H_{26}Cl_2F_2FeN_2$	$C_{26}H_{20}Cl_2FeN_2$
solvent	0.5MeOH	—	$0.33C_7H_8$	—	$2C_6H_6$
formula weight	515.31	535.27	477.93	483.20	643.41
colour, habit	purple needles	red platy needles	purple plates	purple needles	green needles
crystal size / mm	0.36 × 0.12 × 0.04	0.45 × 0.05 × 0.01	0.23 × 0.23 × 0.02	0.43 × 0.06 × 0.03	0.25 × 0.04 × 0.02
temp. / K	173	173	173	173	293
crystal system	tetragonal	orthorhombic	monoclinic	monoclinic	monoclinic
space group	$P\bar{4}2_1m$ (no. 113)	$Cmc2_1$ (no. 36)	$P2_1/c$ (no. 14)	$P2_1/m$ (no. 11)	I2/a
***a* / Å**	20.3559(6)	22.037(6)	9.9410(4)	9.8171(4)	10.9545(14)
***b* / Å**	—	12.3887(14)	33.2392(14)	18.9918(12)	17.1146(19)
***c* / Å**	6.5223(4)	9.471(2)	22.5763(11)	12.4198(7)	18.278(2)
α / deg	—	—	—	—	—
β / deg	—	—	95.832(4)	90.393(4)	98.062(10)
γ / deg	—	—	—	—	—
***V* / Å^3**	2702.6(2)	2585.7(10)	7421.3(6)	2315.5(2)	3393.0(7)
Z	4 [b]	4 [b]	12 [c]	4 [d]	4
***D*$_c$ / g cm^{-3}**	1.266	1.375	1.283	1.386	1.260
radiation used	Mo-Kα	Mo-Kα	Cu-Kα	Mo-Kα	Cu-Kα
μ / mm^{-1}	0.774	0.821	6.958	0.908	5.218
2θ max / deg	65	66	142	65	142
no. of unique reflns measured	4873	3964	14082	8230	3228
obs, $\|F_o\| > 4\sigma(\|F_o\|)$	4722	1305	12605	4556	2312
no. of variables	164	234	800	298	170
***R*$_1$, *wR*$_2$ [f]**	0.077, 0.173	0.060, 0.108	0.076, 0.138	0.060, 0.161	0.0763, 0.1387

Full bond lengths and angles for complex 7, ^{Cy,Ph}[*N*,*N*]$FeCl_2$:

bond length (Å)			angle (°)		
Fe-N(1)#1	2.077(3)	N(1)#1-Fe-N(1)	78.43(15)	C(13)-C(8)-C(9)	119.6(3)
Fe-N(1)	2.077(3)	N(1)#1-Fe-Cl(2)	119.24(9)	C(13)-C(8)-C(1)	119.0(3)
Fe-Cl(2)	2.2183(15)	N(1)-Fe-Cl(2)	119.24(9)	C(9)-C(8)-C(1)	121.4(3)
Fe-Cl(1)	2.2551(16)	N(1)#1-Fe-Cl(1)	101.79(9)	C(8)-C(9)-C(10)	119.5(4)
N(1)-C(1)	1.284(4)	N(1)-Fe-Cl(1)	101.79(9)	C(11)-C(10)-C(9)	120.6(4)
N(1)-C(2)	1.480(4)	Cl(2)-Fe-Cl(1)	125.62(7)	C(12)-C(11)-C(10)	119.3(4)
C(1)-C(8)	1.481(4)	C(1)-N(1)-C(2)	122.3(3)	C(11)-C(12)-C(13)	120.9(5)
C(1)-C(1)#1	1.521(6)	C(1)-N(1)-Fe	112.3(2)	C(8)-C(13)-C(12)	120.1(4)
C(2)-C(7)	1.512(5)	C(2)-N(1)-Fe	124.4(2)		
C(2)-C(3)	1.531(6)	N(1)-C(1)-C(8)	124.8(3)		

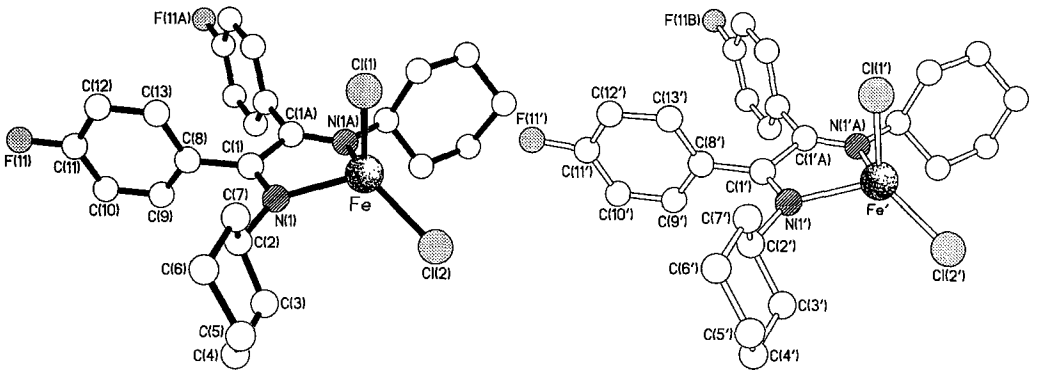
C(3)-C(4)	1.532(6)	N(1)-C(1)-C(1)#1	115.47(17)
C(4)-C(5)	1.501(6)	C(8)-C(1)-C(1)#1	119.72(17)
C(5)-C(6)	1.513(6)	N(1)-C(2)-C(7)	109.9(3)
C(6)-C(7)	1.533(5)	N(1)-C(2)-C(3)	107.1(3)
C(8)-C(13)	1.374(5)	C(7)-C(2)-C(3)	111.1(3)
C(8)-C(9)	1.390(5)	C(2)-C(3)-C(4)	111.4(4)
C(9)-C(10)	1.391(5)	C(5)-C(4)-C(3)	112.4(4)
C(10)-C(11)	1.381(7)	C(4)-C(5)-C(6)	112.0(4)
C(11)-C(12)	1.365(8)	C(5)-C(6)-C(7)	111.9(3)
C(12)-C(13)	1.391(6)	C(2)-C(7)-C(6)	111.9(3)



Full bond lengths and angles for complex **8**, $^{Cy,F\text{-}Ph}[N,N]FeCl_2$:

bond length (Å)	I	II	bond angle (°)	I	II
Fe-N(1)	2.064(8)	2.094(11)	N(1)-Fe-N(1)#1	79.0(4)	76.9(6)
Fe-N(1)#1	2.064(8)	2.094(11)	N(1)-Fe-Cl(1)	105.6(2)	102.3(4)
Fe-Cl(1)	2.209(5)	2.278(8)	N(1)#1-Fe-Cl(1)	105.6(2)	102.3(4)
Fe-Cl(2)	2.247(6)	2.145(8)	N(1)-Fe-Cl(2)	118.7(2)	122.4(4)
N(1)-C(1)	1.302(12)	1.280(15)	N(1)#1-Fe-Cl(2)	118.7(2)	122.4(4)
N(1)-C(2)	1.495(7)	1.495(12)	Cl(1)-Fe-Cl(2)	121.1(2)	121.0(3)
C(1)-C(8)	1.494(12)	1.473(15)	C(1)-N(1)-C(2)	120.7(8)	118.6(11)
C(1)-C(1)#1	1.517(15)	1.58(3)	C(1)-N(1)-Fe	111.9(5)	115.5(8)
C(2)-C(3)	1.472(9)	1.498(13)	C(2)-N(1)-Fe	126.3(8)	124.9(9)
C(2)-C(7)	1.501(12)	1.512(15)	N(1)-C(1)-C(8)	127.5(7)	131.3(12)
C(3)-C(4)	1.544(9)	1.562(13)	N(1)-C(1)-C(1)#1	115.2(4)	113.6(7)
C(4)-C(5)	1.507(15)	1.485(18)	C(8)-C(1)-C(1)#1	117.2(4)	115.2(9)
C(5)-C(6)	1.527(11)	1.471(14)	C(3)-C(2)-N(1)	108.4(6)	106.4(10)
C(6)-C(7)	1.555(9)	1.551(13)	C(3)-C(2)-C(7)	115.2(10)	110.4(11)
C(8)-C(9)	1.332(14)	1.344(16)	N(1)-C(2)-C(7)	107.7(7)	108.8(11)
C(8)-C(13)	1.398(9)	1.396(13)	C(2)-C(3)-C(4)	112.1(6)	111.8(10)
C(9)-C(10)	1.376(15)	1.397(17)	C(5)-C(4)-C(3)	111.3(8)	113.9(12)
C(10)-C(11)	1.357(9)	1.366(14)	C(4)-C(5)-C(6)	107.5(9)	111.3(14)
C(11)-C(12)	1.350(13)	1.321(16)	C(5)-C(6)-C(7)	110.8(7)	112.1(12)
C(11)-F(11)	1.356(14)	1.356(16)	C(2)-C(7)-C(6)	110.4(7)	113.0(12)
C(12)-C(13)	1.398(14)	1.424(17)	C(9)-C(8)-C(13)	120.1(10)	119.6(14)
			C(9)-C(8)-C(1)	123.1(7)	122.4(12)
			C(13)-C(8)-C(1)	116.8(9)	117.6(12)

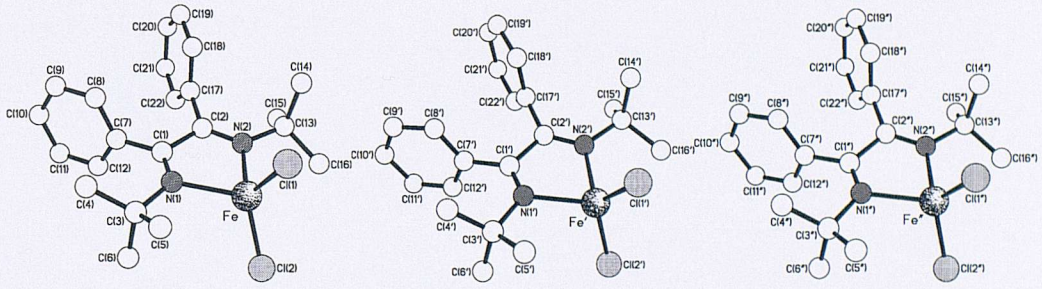
C(8)-C(9)-C(10)	122.3(8)	122.3(13)
C(11)-C(10)-C(9)	117.8(11)	118.3(14)
C(12)-C(11)-F(11)	119.2(8)	116.5(13)
C(12)-C(11)-C(10)	122.1(11)	120.4(15)
F(11)-C(11)-C(10)	118.7(10)	123.1(15)
C(11)-C(12)-C(13)	119.8(8)	122.7(14)
C(12)-C(13)-C(8)	117.8(9)	116.5(13)



Full bond lengths and angles for complex **9**, $^{tBu,Ph}[N,N]FeCl_2$:

bond length (Å)	I	II	III	bond angle (°)	I	II	III
Fe-N(2)	2.112(3)	2.114(3)	2.120(3)	N(2)-Fe-N(1)	78.45(12)	78.95(12)	78.75(12)
Fe-N(1)	2.130(3)	2.115(3)	2.121(3)	N(2)-Fe-Cl(2)	116.79(9)	112.15(9)	114.19(10)
Fe-Cl(2)	2.2390(12)	2.2630(12)	2.2428(13)	N(1)-Fe-Cl(2)	110.56(9)	107.55(9)	104.92(10)
Fe-Cl(1)	2.2460(12)	2.2450(12)	2.2451(14)	N(2)-Fe-Cl(1)	107.11(10)	110.09(9)	110.98(10)
C(1)-N(1)	1.283(5)	1.285(5)	1.269(5)	N(1)-Fe-Cl(1)	113.71(9)	114.47(9)	117.11(9)
C(1)-C(7)	1.497(5)	1.496(5)	1.510(5)	Cl(2)-Fe-Cl(1)	122.11(5)	124.53(5)	122.63(6)
C(1)-C(2)	1.532(6)	1.525(5)	1.532(5)	N(1)-C(1)-C(7)	128.3(4)	126.8(3)	127.7(3)
N(1)-C(3)	1.499(5)	1.515(5)	1.508(5)	N(1)-C(1)-C(2)	116.3(3)	116.2(3)	117.1(3)
C(2)-N(2)	1.282(5)	1.282(5)	1.284(5)	C(7)-C(1)-C(2)	115.4(3)	116.9(3)	115.1(3)
C(2)-C(17)	1.497(5)	1.504(5)	1.492(5)	C(1)-N(1)-C(3)	126.0(3)	125.6(3)	125.8(3)
N(2)-C(13)	1.501(5)	1.507(5)	1.505(5)	C(1)-N(1)-Fe	113.7(3)	113.0(3)	113.3(3)
C(3)-C(4)	1.525(6)	1.511(6)	1.516(6)	C(3)-N(1)-Fe	119.9(2)	120.5(2)	120.3(2)
C(3)-C(6)	1.534(6)	1.517(6)	1.521(6)	N(2)-C(2)-C(17)	127.9(4)	128.4(4)	127.5(4)
C(3)-C(5)	1.539(6)	1.539(6)	1.535(6)	N(2)-C(2)-C(1)	116.6(3)	117.1(3)	116.1(3)
C(7)-C(12)	1.380(6)	1.381(6)	1.388(6)	C(17)-C(2)-C(1)	115.5(3)	114.4(3)	116.4(3)
C(7)-C(8)	1.393(6)	1.382(6)	1.394(6)	C(2)-N(2)-C(13)	125.7(3)	126.1(3)	125.5(3)
C(8)-C(9)	1.378(6)	1.396(7)	1.386(7)	C(2)-N(2)-Fe	114.3(3)	113.2(3)	113.3(3)
C(9)-C(10)	1.382(8)	1.374(8)	1.378(9)	C(13)-N(2)-Fe	119.8(2)	120.6(2)	120.8(2)
C(10)-C(11)	1.372(8)	1.367(8)	1.376(9)	N(1)-C(3)-C(4)	115.1(3)	113.8(3)	113.0(3)
C(11)-C(12)	1.393(6)	1.390(6)	1.383(7)	N(1)-C(3)-C(6)	107.3(3)	109.0(3)	109.1(3)
C(13)-C(15)	1.521(6)	1.529(6)	1.507(8)	C(4)-C(3)-C(6)	111.1(3)	112.3(4)	112.2(4)
C(13)-C(16)	1.527(6)	1.531(6)	1.517(6)	N(1)-C(3)-C(5)	106.0(3)	104.7(3)	105.7(3)
C(13)-C(14)	1.529(7)	1.516(6)	1.516(8)	C(4)-C(3)-C(5)	108.0(3)	107.7(4)	108.0(4)
C(17)-C(18)	1.386(6)	1.378(6)	1.382(6)	C(6)-C(3)-C(5)	109.1(4)	109.0(4)	108.5(4)
C(17)-C(22)	1.394(6)	1.387(5)	1.387(5)	C(12)-C(7)-C(8)	119.9(4)	119.7(4)	119.8(4)

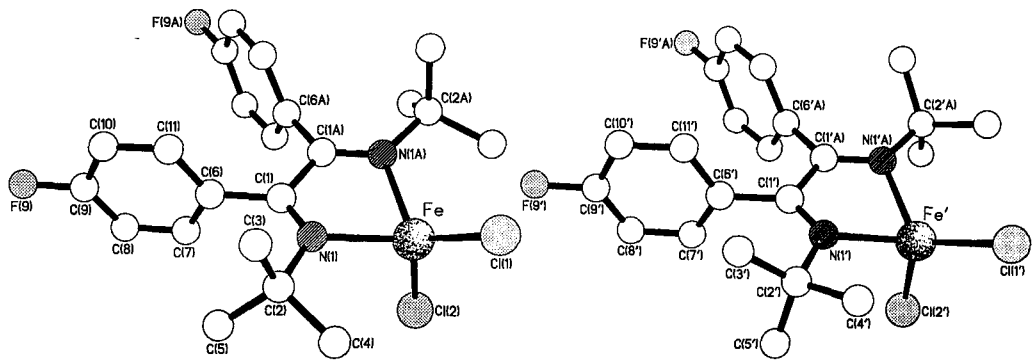
C(18)-C(19)	1.383(6)	1.377(6)	1.397(6)	C(12)-C(7)-C(1)	119.7(4)	118.7(4)	118.7(4)
C(19)-C(20)	1.389(8)	1.385(6)	1.384(6)	C(8)-C(7)-C(1)	120.2(4)	121.6(4)	121.4(4)
C(20)-C(21)	1.372(8)	1.371(6)	1.366(7)	C(9)-C(8)-C(7)	120.3(4)	119.0(5)	119.4(5)
C(21)-C(22)	1.373(6)	1.375(6)	1.387(6)	C(8)-C(9)-C(10)	119.4(5)	121.0(5)	120.6(6)
				C(11)-C(10)-C(9)	120.9(5)	119.8(5)	120.2(5)
				C(10)-C(11)-C(12)	119.9(5)	120.0(5)	119.9(6)
				C(7)-C(12)-C(11)	119.6(5)	120.5(5)	120.1(5)
				N(2)-C(13)-C(15)	113.6(4)	113.2(3)	114.4(4)
				N(2)-C(13)-C(16)	105.5(3)	106.2(3)	105.8(4)
				C(15)-C(13)-C(16)	108.0(4)	107.9(4)	111.0(5)
				N(2)-C(13)-C(14)	108.4(4)	108.0(3)	107.7(4)
				C(15)-C(13)-C(14)	111.6(4)	111.7(4)	110.5(6)
				C(16)-C(13)-C(14)	109.5(4)	109.6(4)	107.1(5)
				C(18)-C(17)-C(22)	119.7(4)	119.2(4)	119.7(4)
				C(18)-C(17)-C(2)	119.2(4)	119.0(3)	119.9(4)
				C(22)-C(17)-C(2)	121.1(4)	121.6(3)	120.3(4)
				C(19)-C(18)-C(17)	120.1(4)	120.9(4)	119.7(4)
				C(18)-C(19)-C(20)	119.7(5)	119.5(4)	120.1(4)
				C(21)-C(20)-C(19)	120.1(4)	119.8(4)	119.9(4)
				C(20)-C(21)-C(22)	120.7(5)	120.7(4)	120.6(4)
				C(21)-C(22)-C(17)	119.8(5)	119.9(4)	120.0(4)



Full bond lengths and angles for complex **10**, $^{tBu,F\text{-}Ph}[N,N]FeCl_2$:

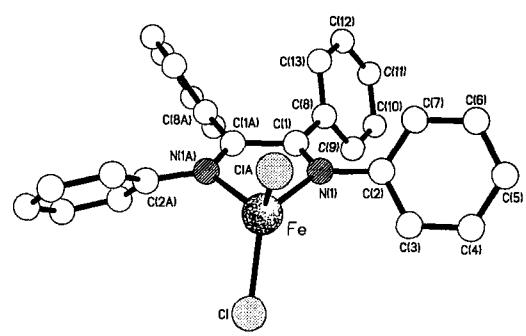
bond length (Å)	**I**	**II**	**bond angle (°)**	**I**	**II**
Fe-N(1)	2.103(2)	2.100(2)	N(1)-Fe-N(1)#1	79.39(13)	79.45(13)
Fe-N(1)#1	2.103(2)	2.100(2)	N(1)-Fe-Cl(2)	104.16(8)	103.17(8)
Fe-Cl(2)	2.2329(14)	2.2341(13)	N(1)#1-Fe-Cl(2)	104.16(8)	103.17(8)
Fe-Cl(1)	2.2393(13)	2.2474(13)	N(1)-Fe-Cl(1)	119.57(8)	122.50(8)
N(1)-C(1)	1.280(4)	1.285(4)	N(1)#1-Fe-Cl(1)	119.57(8)	122.50(8)
N(1)-C(2)	1.505(4)	1.507(4)	Cl(2)-Fe-Cl(1)	121.56(6)	118.44(5)
C(1)-C(6)	1.492(4)	1.493(4)	C(1)-N(1)-C(2)	125.9(2)	125.0(2)
C(1)-C(1)#1	1.521(6)	1.521(6)	C(1)-N(1)-Fe	111.0(2)	110.58(19)
C(2)-C(5A)	1.475(10)	1.530(10)	C(2)-N(1)-Fe	122.42(18)	122.83(19)
C(2)-C(3)	1.488(5)	1.526(5)	N(1)-C(1)-C(6)	127.3(3)	127.6(3)
C(2)-C(4)	1.519(5)	1.538(5)	N(1)-C(1)-C(1)#1	117.11(17)	116.91(17)
C(2)-C(5)	1.544(5)	1.502(5)	C(6)-C(1)-C(1)#1	115.63(16)	115.46(16)
C(2)-C(3A)	1.547(10)	1.491(11)	C(5A)-C(2)-C(3)	136.1(7)	142.6(8)
C(2)-C(4A)	1.558(10)	1.519(11)	C(5A)-C(2)-N(1)	111.5(7)	105.3(8)
C(6)-C(7)	1.376(5)	1.386(4)	C(3)-C(2)-N(1)	107.0(3)	108.6(3)

C(6)-C(11)	1.389(4)	1.398(5)	C(5A)-C(2)-C(4)	76.6(7)	111.6(9)
C(7)-C(8)	1.369(5)	1.387(5)	C(3)-C(2)-C(4)	112.1(4)	73.2(8)
C(8)-C(9)	1.363(5)	1.347(6)	N(1)-C(2)-C(4)	106.2(3)	106.3(9)
C(9)-F(9)	1.367(4)	1.366(4)	C(5A)-C(2)-C(5)	32.4(6)	37.3(7)
C(9)-C(10)	1.369(5)	1.378(6)	C(3)-C(2)-C(5)	111.5(3)	112.1(4)
C(10)-C(11)	1.379(4)	1.388(5)	N(1)-C(2)-C(5)	113.5(3)	113.5(3)
			C(4)-C(2)-C(5)	106.6(4)	134.4(9)
			C(5A)-C(2)-C(3A)	110.6(8)	111.7(8)
			C(3)-C(2)-C(3A)	31.6(6)	38.8(6)
			N(1)-C(2)-C(3A)	112.9(6)	113.9(7)
			C(4)-C(2)-C(3A)	132.8(6)	107.9(8)
			C(5)-C(2)-C(3A)	81.3(6)	75.5(7)
			C(5A)-C(2)-C(4A)	111.0(7)	75.7(7)
			C(3)-C(2)-C(4A)	76.2(6)	108.8(4)
			N(1)-C(2)-C(4A)	106.7(6)	106.0(3)
			C(4)-C(2)-C(4A)	37.9(5)	37.8(8)
			C(5)-C(2)-C(4A)	133.6(6)	107.6(4)
			C(3A)-C(2)-C(4A)	103.8(7)	134.8(7)
			C(7)-C(6)-C(11)	118.5(3)	119.2(3)
			C(7)-C(6)-C(1)	119.8(3)	119.3(3)
			C(11)-C(6)-C(1)	121.6(3)	121.3(3)
			C(8)-C(7)-C(6)	121.7(3)	120.8(3)
			C(9)-C(8)-C(7)	118.3(3)	118.4(4)
			C(8)-C(9)-F(9)	119.2(3)	119.2(4)
			C(8)-C(9)-C(10)	122.4(3)	123.4(3)
			F(9)-C(9)-C(10)	118.4(3)	117.3(4)
			C(9)-C(10)-C(11)	118.5(3)	118.2(4)
			C(10)-C(11)-C(6)	120.5(3)	119.9(3)



Full bond lengths and angles for complex **11**, $^{Ph,Ph}[N,N]FeCl_2$:

bond length (Å)			angle (°)		
Fe-N(1)#1	2.116(3)	N(1)#1-Fe-N(1)	76.71(16)	C(35)-C(36)-C(31)	120
Fe-N(1)	2.116(3)	N(1)#1-Fe-Cl#1	117.98(8)	C(32')-C(31')-C(36')	120
Fe-Cl#1	2.2253(11)	N(1)-Fe-Cl#1	108.16(8)	C(31')-C(32')-C(33')	120
Fe-Cl	2.2253(11)	N(1)#1-Fe-Cl	108.16(8)	C(32')-C(33')-C(34')	120
N(1)-C(1)	1.293(4)	N(1)-Fe-Cl	117.98(8)	C(35')-C(34')-C(33')	120
N(1)-C(2)	1.420(3)	Cl#1-Fe-Cl	120.29(7)	C(34')-C(35')-C(36')	120
C(1)-C(8)	1.476(4)	C(1)-N(1)-C(2)	123.4(3)	C(35')-C(36')-C(31')	120
C(1)-C(1)#1	1.507(7)	C(1)-N(1)-Fe	116.0(2)		
C(2)-C(3)	1.39	C(2)-N(1)-Fe	120.2(2)		
C(2)-C(7)	1.39	N(1)-C(1)-C(8)	125.4(3)		
C(3)-C(4)	1.39	N(1)-C(1)-C(1)#1	115.6(2)		
C(4)-C(5)	1.39	C(8)-C(1)-C(1)#1	118.87(17)		
C(5)-C(6)	1.39	C(3)-C(2)-C(7)	120		
C(6)-C(7)	1.39	C(3)-C(2)-N(1)	117.71(19)		
C(8)-C(9)	1.39	C(7)-C(2)-N(1)	122.14(19)		
C(8)-C(13)	1.39	C(2)-C(3)-C(4)	120		
C(9)-C(10)	1.39	C(5)-C(4)-C(3)	120		
C(10)-C(11)	1.39	C(6)-C(5)-C(4)	120		
C(11)-C(12)	1.39	C(5)-C(6)-C(7)	120		
C(12)-C(13)	1.39	C(6)-C(7)-C(2)	120		
C(21)-C(22)	1.343(8)	C(9)-C(8)-C(13)	120		
C(21)-C(23)#2	1.370(8)	C(9)-C(8)-C(1)	119.0(2)		
C(22)-C(23)	1.349(8)	C(13)-C(8)-C(1)	120.9(2)		
C(23)-C(21)#2	1.370(8)	C(8)-C(9)-C(10)	120		
C(31)-C(32)	1.39	C(9)-C(10)-C(11)	120		
C(31)-C(36)	1.39	C(12)-C(11)-C(10)	120		
C(32)-C(33)	1.39	C(11)-C(12)-C(13)	120		
C(33)-C(34)	1.39	C(12)-C(13)-C(8)	120		
C(34)-C(35)	1.39	C(22)-C(21)-C(23)#2	120.3(6)		
C(35)-C(36)	1.39	C(21)-C(22)-C(23)	120.3(5)		
C(31')-C(32')	1.39	C(22)-C(23)-C(21)#2	119.4(6)		
C(31')-C(36')	1.39	C(32)-C(31)-C(36)	120		
C(32')-C(33')	1.39	C(33)-C(32)-C(31)	120		
C(33')-C(34')	1.39	C(32)-C(33)-C(34)	120		
C(34')-C(35')	1.39	C(35)-C(34)-C(33)	120		
C(35')-C(36')	1.39	C(36)-C(35)-C(34)	120		



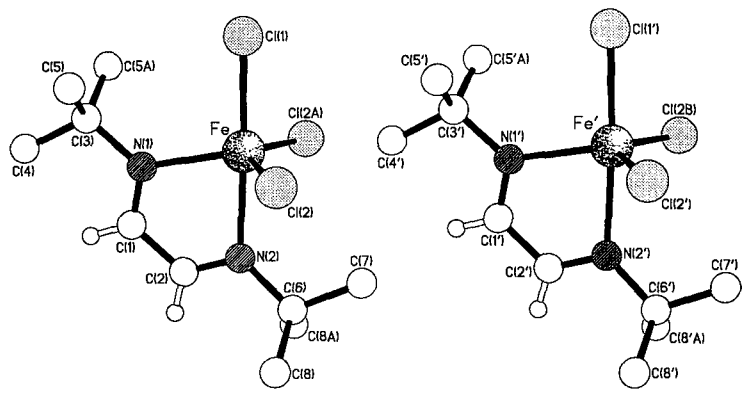
8.1.2 - Crystal structure data for Chapter 3.

data	15	16a	16b	17a
code	VG0540	VG0511b	VG0512	VG0542
formula	$C_{10}H_{20}Cl_3FeN_2$	$[C_{22}H_{29}N_2](FeCl_4)$	$[C_{22}H_{28}Cl_2N_2Fe](FeCl_4)[C_{18}H_{20}NO]$	$[C_{22}H_{26}Cl_2F_2N_2Fe](FeCl_4)[C_{22}H_{27}F_2N_2]$
solvent	—	—	—	$0.5C_6H_6$
formula weight	330.48	519.12	911.21	1077.36
colour, habit	orange needles	yellow blocks	red shards	red plates
crystal size / mm	0.35 × 0.01 × 0.01	0.25 × 0.22 × 0.11	0.28 × 0.24 × 0.19	0.14 × 0.14 × 0.06
temperature / K	173	173	173	173
crystal system	orthorhombic	orthorhombic	triclinic	orthorhombic
space group	*Cmc*2_1 (no. 36)	*Pna*2_1 (no. 33)	*P*1 (no. 1)	*Pccn* (no. 56)
***a* / Å**	10.2994(13)	17.7580(6)	9.9631(5)	19.1664(10)
***b* / Å**	19.845(3)	11.5780(4)	11.3338(7)	30.5452(14)
***c* / Å**	14.723(2)	12.9030(4)	11.4274(6)	17.9330(9)
α / deg	—	—	68.818(5)	—
β / deg	—	—	83.507(4)	—
γ / deg	—	—	67.022(5)	—
***V* / Å^3**	3009.2(7)	2652.88(15)	1107.14(11)	10498.7(9)
Z	8 [c]	4	1	8
***D*$_c$ / g cm^{-3}**	1.459	1.300	1.367	1.363
radiation used	Mo-Kα	Mo-Kα	Mo-Kα	Mo-Kα
μ / mm^{-1}	1.513	0.982	1.050	0.907
2θ max / deg	66	65	66	66
no. of unique reflns measured	4282	8939	8597	18613
obs, $\|F_o\| > 4\sigma(\|F_o\|)$	2870	8823	8547	5450
no. of variables	175	279	486	583
***R*$_1$, *wR*$_2$ [d]**	0.097, 0.099	0.083, 0.188	0.031, 0.079	0.081, 0.131

Full bond lengths and angles for complex **15**, ^{tBu,H}[*N,N*]FeCl$_3$:

bond length (Å)	I	II	bond angle (°)	I	II
Fe-N(1)	2.145(6)	2.141(6)	N(1)-Fe-Cl(2)	114.76(7)	117.06(7)
Fe-Cl(2)	2.2053(19)	2.2109(19)	N(1)-Fe-Cl(2)#1	114.76(7)	117.06(7)
Fe-Cl(2)#1	2.2053(19)	2.2109(19)	Cl(2)-Fe-Cl(2)#1	127.08(14)	122.69(13)
Fe-N(2)	2.243(7)	2.275(7)	N(1)-Fe-N(2)	77.2(2)	77.7(2)
Fe-Cl(1)	2.285(3)	2.294(3)	Cl(2)-Fe-N(2)	86.82(10)	87.03(11)
N(1)-C(1)	1.272(10)	1.276(9)	Cl(2)#1-Fe-N(2)	86.82(10)	87.03(11)
N(1)-C(3)	1.501(10)	1.506(10)	N(1)-Fe-Cl(1)	100.65(19)	98.7(2)
N(2)-C(2)	1.247(9)	1.265(9)	Cl(2)-Fe-Cl(1)	94.13(6)	94.68(7)
N(2)-C(6)	1.514(10)	1.492(11)	Cl(2)#1-Fe-Cl(1)	94.13(6)	94.68(7)
C(1)-C(2)	1.455(12)	1.456(12)	N(2)-Fe-Cl(1)	177.83(19)	176.4(2)
C(3)-C(4)	1.529(11)	1.526(11)	C(1)-N(1)-C(3)	118.4(7)	118.5(7)
C(3)-C(5)	1.531(8)	1.520(7)	C(1)-N(1)-Fe	112.3(6)	111.6(6)
C(3)-C(5)#1	1.531(8)	1.520(7)	C(3)-N(1)-Fe	129.4(4)	130.0(5)
C(6)-C(8)	1.533(8)	1.531(8)	C(2)-N(2)-C(6)	119.0(7)	118.0(7)

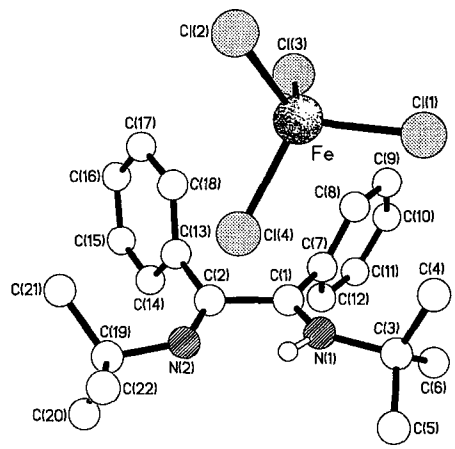
C(6)-C(8)#1	1.533(8)	1.531(8)	C(2)-N(2)-Fe	109.3(6)	108.2(6)
C(6)-C(7)	1.537(11)	1.500(11)	C(6)-N(2)-Fe	131.7(4)	133.8(5)
			N(1)-C(1)-C(2)	120.0(8)	121.8(7)
			N(2)-C(2)-C(1)	121.3(8)	120.7(7)
			N(1)-C(3)-C(4)	113.5(6)	112.6(6)
			N(1)-C(3)-C(5)	107.7(4)	106.7(4)
			C(4)-C(3)-C(5)	108.2(4)	108.9(4)
			N(1)-C(3)-C(5)#1	107.7(4)	106.7(4)
			C(4)-C(3)-C(5)#1	108.2(4)	108.9(4)
			C(5)-C(3)-C(5)#1	111.6(7)	113.1(7)
			N(2)-C(6)-C(8)	108.0(5)	108.3(5)
			N(2)-C(6)-C(8)#1	108.0(5)	108.3(5)
			C(8)-C(6)-C(8)#1	112.4(7)	109.8(8)
			N(2)-C(6)-C(7)	110.4(6)	111.0(7)
			C(8)-C(6)-C(7)	109.0(5)	109.8(5)
			C(8)#1-C(6)-C(7)	109.0(5)	109.8(5)



Full bond lengths and angles for complex **16a**, $[C_{22}H_{29}N_2](FeCl_4)$:

bond length (Å)			**angle (°)**		
Fe-Cl(1)	2.1829(7)	Cl(1)-Fe-Cl(4)	109.37(4)	C(4)-C(3)-C(5')	73.0(5)
Fe-Cl(4)	2.1921(8)	Cl(1)-Fe-Cl(2)	109.82(3)	C(5)-C(3)-C(5')	42.7(5)
Fe-Cl(2)	2.1930(7)	Cl(4)-Fe-Cl(2)	109.18(3)	C(6)-C(3)-C(5')	143.0(5)
Fe-Cl(3)	2.1971(8)	Cl(1)-Fe-Cl(3)	110.31(3)	C(12)-C(7)-C(8)	120.2(2)
N(1)-C(1)	1.274(3)	Cl(4)-Fe-Cl(3)	109.40(5)	C(12)-C(7)-C(1)	119.3(2)
N(1)-C(3)	1.504(3)	Cl(2)-Fe-Cl(3)	108.73(4)	C(8)-C(7)-C(1)	120.5(2)
C(1)-C(7)	1.474(3)	C(1)-N(1)-C(3)	134.87(19)	C(7)-C(8)-C(9)	119.1(3)
C(1)-C(2)	1.531(3)	N(1)-C(1)-C(7)	124.25(18)	C(10)-C(9)-C(8)	120.6(3)
N(2)-C(2)	1.261(3)	N(1)-C(1)-C(2)	113.84(18)	C(11)-C(10)-C(9)	119.4(3)
N(2)-C(19)	1.490(3)	C(7)-C(1)-C(2)	121.91(19)	C(10)-C(11)-C(12)	121.4(4)
C(2)-C(13)	1.489(3)	C(2)-N(2)-C(19)	128.9(2)	C(7)-C(12)-C(11)	119.0(3)
C(3)-C(6')	1.490(10)	N(2)-C(2)-C(13)	130.66(19)	C(18)-C(13)-C(14)	120.3(3)
C(3)-C(4')	1.492(10)	N(2)-C(2)-C(1)	113.40(19)	C(18)-C(13)-C(2)	120.0(2)
C(3)-C(4)	1.514(4)	C(13)-C(2)-C(1)	115.94(19)	C(14)-C(13)-C(2)	119.7(2)
C(3)-C(5)	1.516(5)	C(6')-C(3)-C(4')	115.4(8)	C(15)-C(14)-C(13)	119.6(3)
C(3)-C(6)	1.531(5)	C(6')-C(3)-N(1)	107.9(6)	C(16)-C(15)-C(14)	120.1(3)

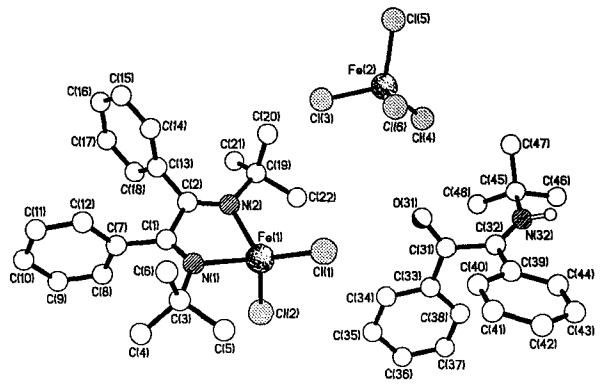
C(3)-C(5')	1.551(9)	C(4')-C(3)-N(1)	110.4(8)	C(15)-C(16)-C(17)	120.5(3)
C(7)-C(12)	1.383(3)	C(6')-C(3)-C(4)	142.4(6)	C(18)-C(17)-C(16)	119.4(4)
C(7)-C(8)	1.390(3)	C(4')-C(3)-C(4)	39.5(7)	C(17)-C(18)-C(13)	120.0(3)
C(8)-C(9)	1.396(5)	N(1)-C(3)-C(4)	108.1(2)	N(2)-C(19)-C(22)	105.2(2)
C(9)-C(10)	1.381(7)	C(6')-C(3)-C(5)	69.1(6)	N(2)-C(19)-C(20)	107.20(19)
C(10)-C(11)	1.361(6)	C(4')-C(3)-C(5)	140.5(8)	C(22)-C(19)-C(20)	109.5(3)
C(11)-C(12)	1.396(4)	N(1)-C(3)-C(5)	104.3(2)	N(2)-C(19)-C(21)	113.8(2)
C(13)-C(18)	1.389(4)	C(4)-C(3)-C(5)	111.7(4)	C(22)-C(19)-C(21)	110.6(3)
C(13)-C(14)	1.393(3)	C(6')-C(3)-C(6)	43.6(5)	C(20)-C(19)-C(21)	110.3(3)
C(14)-C(15)	1.391(5)	C(4')-C(3)-C(6)	74.1(7)		
C(15)-C(16)	1.374(7)	N(1)-C(3)-C(6)	112.1(2)		
C(16)-C(17)	1.405(7)	C(4)-C(3)-C(6)	110.8(3)		
C(17)-C(18)	1.385(5)	C(5)-C(3)-C(6)	109.7(4)		
C(19)-C(22)	1.522(5)	C(6')-C(3)-C(5')	110.7(6)		
C(19)-C(20)	1.527(4)	C(4')-C(3)-C(5')	110.9(7)		
C(19)-C(21)	1.535(5)	N(1)-C(3)-C(5')	100.6(5)		



Full bond lengths and angles for complex **16b**, $[C_{22}H_{28}Cl_2N_2Fe](FeCl_4)[C_{18}H_{20}NO]$:

bond length (Å)			**angle (°)**		
Fe(1)-N(2)	2.0970(18)	N(2)-Fe(1)-N(1)	79.46(6)	C(21)-C(19)-C(20')	74.8(5)
Fe(1)-N(1)	2.1046(16)	N(2)-Fe(1)-Cl(1)	122.29(5)	C(21')-C(19)-C(20')	107.6(4)
Fe(1)-Cl(1)	2.2348(7)	N(1)-Fe(1)-Cl(1)	122.29(5)	N(2)-C(19)-C(20')	113.9(3)
Fe(1)-Cl(2)	2.2971(6)	N(2)-Fe(1)-Cl(2)	105.16(5)	C(22)-C(19)-C(20')	135.0(4)
N(1)-C(1)	1.287(3)	N(1)-Fe(1)-Cl(2)	103.64(5)	Cl(6)-Fe(2)-Cl(3)	108.83(3)
N(1)-C(3)	1.500(3)	Cl(1)-Fe(1)-Cl(2)	117.13(3)	Cl(6)-Fe(2)-Cl(4)	112.91(4)
C(1)-C(7)	1.490(3)	C(1)-N(1)-C(3)	125.92(17)	Cl(3)-Fe(2)-Cl(4)	107.42(3)
C(1)-C(2)	1.527(2)	C(1)-N(1)-Fe(1)	111.34(12)	Cl(6)-Fe(2)-Cl(5)	109.63(4)
N(2)-C(2)	1.285(2)	C(3)-N(1)-Fe(1)	121.74(14)	Cl(3)-Fe(2)-Cl(5)	107.58(3)
N(2)-C(19)	1.513(2)	N(1)-C(1)-C(7)	127.54(17)	Cl(4)-Fe(2)-Cl(5)	110.29(3)
C(2)-C(13)	1.492(3)	N(1)-C(1)-C(2)	116.14(16)	O(31)-C(31)-C(33)	124.9(2)
C(3)-C(4)	1.509(4)	C(7)-C(1)-C(2)	116.29(17)	O(31)-C(31)-C(32)	116.0(2)
C(3)-C(6)	1.521(4)	C(2)-N(2)-C(19)	125.84(18)	C(33)-C(31)-C(32)	118.78(18)
C(3)-C(5)	1.530(4)	C(2)-N(2)-Fe(1)	112.97(13)	C(32)-N(32)-C(45)	132.3(2)

C(7)-C(12)	1.395(3)	C(19)-N(2)-Fe(1)	121.16(13)	N(32)-C(32)-C(39)	120.8(2)
C(7)-C(8)	1.400(3)	N(2)-C(2)-C(13)	128.27(17)	N(32)-C(32)-C(31)	123.0(2)
C(8)-C(9)	1.384(3)	N(2)-C(2)-C(1)	116.36(17)	C(39)-C(32)-C(31)	115.86(18)
C(9)-C(10)	1.387(4)	C(13)-C(2)-C(1)	115.25(16)	C(34)-C(33)-C(38)	120.7(2)
C(10)-C(11)	1.396(4)	N(1)-C(3)-C(4)	115.8(2)	C(34)-C(33)-C(31)	119.52(19)
C(11)-C(12)	1.385(4)	N(1)-C(3)-C(6)	105.2(2)	C(38)-C(33)-C(31)	119.81(19)
C(13)-C(18)	1.393(3)	C(4)-C(3)-C(6)	113.0(4)	C(35)-C(34)-C(33)	119.5(2)
C(13)-C(14)	1.396(3)	N(1)-C(3)-C(5)	106.63(19)	C(34)-C(35)-C(36)	119.8(2)
C(14)-C(15)	1.391(4)	C(4)-C(3)-C(5)	107.9(3)	C(37)-C(36)-C(35)	120.8(2)
C(15)-C(16)	1.380(5)	C(6)-C(3)-C(5)	107.9(3)	C(36)-C(37)-C(38)	119.7(2)
C(16)-C(17)	1.388(5)	C(12)-C(7)-C(8)	119.0(2)	C(37)-C(38)-C(33)	119.4(2)
C(17)-C(18)	1.396(4)	C(12)-C(7)-C(1)	122.99(19)	C(44)-C(39)-C(40)	119.6(2)
C(19)-C(20)	1.478(5)	C(8)-C(7)-C(1)	117.99(17)	C(44)-C(39)-C(32)	121.5(2)
C(19)-C(22')	1.497(8)	C(9)-C(8)-C(7)	120.9(2)	C(40)-C(39)-C(32)	118.9(2)
C(19)-C(21)	1.507(6)	C(8)-C(9)-C(10)	119.8(2)	C(41)-C(40)-C(39)	119.6(3)
C(19)-C(21')	1.508(6)	C(9)-C(10)-C(11)	119.7(2)	C(40)-C(41)-C(42)	120.3(3)
C(19)-C(22)	1.538(4)	C(12)-C(11)-C(10)	120.6(2)	C(43)-C(42)-C(41)	120.1(3)
C(19)-C(20')	1.556(7)	C(11)-C(12)-C(7)	120.0(2)	C(44)-C(43)-C(42)	120.0(3)
Fe(2)-Cl(6)	2.1805(8)	C(18)-C(13)-C(14)	120.3(2)	C(39)-C(44)-C(43)	120.3(2)
Fe(2)-Cl(3)	2.1928(7)	C(18)-C(13)-C(2)	121.49(19)	C(48)-C(45)-N(32)	113.8(2)
Fe(2)-Cl(4)	2.1990(8)	C(14)-C(13)-C(2)	118.2(2)	C(48)-C(45)-C(46)	111.9(3)
Fe(2)-Cl(5)	2.2040(7)	C(15)-C(14)-C(13)	119.1(3)	N(32)-C(45)-C(46)	104.9(2)
O(31)-C(31)	1.217(3)	C(16)-C(15)-C(14)	121.0(3)	C(48)-C(45)-C(47)	110.1(3)
C(31)-C(33)	1.481(3)	C(15)-C(16)-C(17)	119.7(3)	N(32)-C(45)-C(47)	105.6(2)
C(31)-C(32)	1.526(3)	C(16)-C(17)-C(18)	120.2(3)	C(46)-C(45)-C(47)	110.2(3)
N(32)-C(32)	1.295(3)	C(13)-C(18)-C(17)	119.6(2)		
N(32)-C(45)	1.515(3)	C(20)-C(19)-C(22')	75.0(5)		
C(32)-C(39)	1.464(3)	C(20)-C(19)-C(21)	111.7(5)		
C(33)-C(34)	1.397(3)	C(22')-C(19)-C(21)	132.0(5)		
C(33)-C(38)	1.398(3)	C(20)-C(19)-C(21')	139.5(4)		
C(34)-C(35)	1.387(3)	C(22')-C(19)-C(21')	111.0(5)		
C(35)-C(36)	1.393(4)	C(21)-C(19)-C(21')	34.0(4)		
C(36)-C(37)	1.387(4)	C(20)-C(19)-N(2)	108.4(3)		
C(37)-C(38)	1.392(3)	C(22')-C(19)-N(2)	107.8(4)		
C(39)-C(44)	1.390(4)	C(21)-C(19)-N(2)	113.8(2)		
C(39)-C(40)	1.415(3)	C(21')-C(19)-N(2)	107.4(3)		
C(40)-C(41)	1.384(4)	C(20)-C(19)-C(22)	108.8(4)		
C(41)-C(42)	1.394(5)	C(22')-C(19)-C(22)	35.3(4)		
C(42)-C(43)	1.393(4)	C(21)-C(19)-C(22)	108.2(4)		
C(43)-C(44)	1.390(4)	C(21')-C(19)-C(22)	78.7(4)		
C(45)-C(48)	1.510(4)	N(2)-C(19)-C(22)	105.7(2)		
C(45)-C(46)	1.517(4)	C(20)-C(19)-C(20')	39.1(4)		
C(45)-C(47)	1.522(5)	C(22')-C(19)-C(20')	109.2(5)		

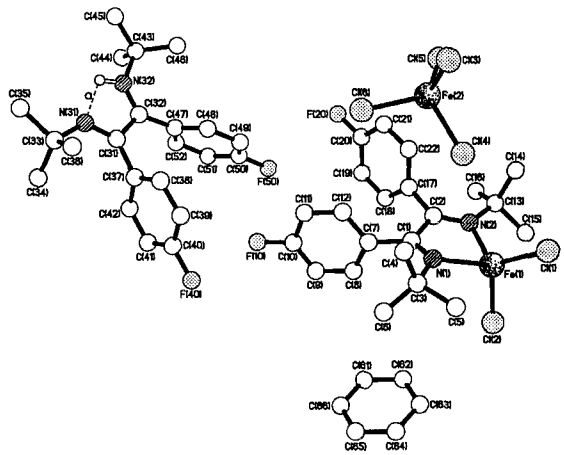


Full bond lengths and angles for complex **17a**,$[C_{22}H_{26}Cl_2F_2N_2Fe](FeCl_4)$ $[C_{22}H_{27}F_2N_2]$:

bond length (Å)			angle (°)		
Fe(1)-N(1)	2.100(4)	N(1)-Fe(1)-N(2)	79.62(17)	Cl(5)-Fe(2)-Cl(6)	108.48(8)
Fe(1)-N(2)	2.101(4)	N(1)-Fe(1)-Cl(1)	121.04(12)	Cl(5)-Fe(2)-Cl(4)	109.97(7)
Fe(1)-Cl(1)	2.2436(15)	N(2)-Fe(1)-Cl(1)	119.16(12)	Cl(6)-Fe(2)-Cl(4)	109.68(7)
Fe(1)-Cl(2)	2.2502(16)	N(1)-Fe(1)-Cl(2)	105.43(11)	Cl(5)-Fe(2)-Cl(3)	109.56(7)
N(1)-C(1)	1.276(6)	N(2)-Fe(1)-Cl(2)	109.36(11)	Cl(6)-Fe(2)-Cl(3)	110.00(7)
N(1)-C(3)	1.509(6)	Cl(1)-Fe(1)-Cl(2)	116.35(6)	Cl(4)-Fe(2)-Cl(3)	109.14(6)
N(2)-C(2)	1.273(6)	C(1)-N(1)-C(3)	125.4(4)	C(31)-N(31)-C(33)	126.3(4)
N(2)-C(13)	1.495(6)	C(1)-N(1)-Fe(1)	111.8(3)	C(32)-N(32)-C(43)	133.3(4)
C(1)-C(7)	1.484(7)	C(3)-N(1)-Fe(1)	121.1(3)	N(31)-C(31)-C(37)	131.8(5)
C(1)-C(2)	1.545(7)	C(2)-N(2)-C(13)	126.5(4)	N(31)-C(31)-C(32)	112.7(4)
C(2)-C(17)	1.497(7)	C(2)-N(2)-Fe(1)	112.7(3)	C(37)-C(31)-C(32)	115.4(4)
C(3)-C(5')	1.466(11)	C(13)-N(2)-Fe(1)	120.8(3)	N(32)-C(32)-C(47)	125.2(5)
C(3)-C(6)	1.474(9)	N(1)-C(1)-C(7)	128.9(5)	N(32)-C(32)-C(31)	114.9(4)
C(3)-C(4')	1.509(10)	N(1)-C(1)-C(2)	115.6(4)	C(47)-C(32)-C(31)	119.9(4)
C(3)-C(5)	1.532(9)	C(7)-C(1)-C(2)	115.4(4)	N(31)-C(33)-C(34)	110.7(4)
C(3)-C(4)	1.543(9)	N(2)-C(2)-C(17)	129.2(5)	N(31)-C(33)-C(36)	110.0(4)
C(3)-C(6')	1.588(10)	N(2)-C(2)-C(1)	116.7(4)	C(34)-C(33)-C(36)	111.7(5)
C(7)-C(12)	1.396(7)	C(17)-C(2)-C(1)	114.1(4)	N(31)-C(33)-C(35)	105.0(4)
C(7)-C(8)	1.398(7)	C(5')-C(3)-C(6)	125.8(11)	C(34)-C(33)-C(35)	109.6(5)
C(8)-C(9)	1.389(7)	C(5')-C(3)-C(4')	113.9(8)	C(36)-C(33)-C(35)	109.7(5)
C(9)-C(10)	1.345(8)	C(6)-C(3)-C(4')	71.0(7)	C(38)-C(37)-C(42)	119.0(5)
C(10)-F(10)	1.362(6)	C(5')-C(3)-N(1)	108.6(10)	C(38)-C(37)-C(31)	120.4(5)
C(10)-C(11)	1.372(8)	C(6)-C(3)-N(1)	117.2(6)	C(42)-C(37)-C(31)	120.5(5)
C(11)-C(12)	1.374(7)	C(4')-C(3)-N(1)	115.3(8)	C(37)-C(38)-C(39)	120.8(5)
C(13)-C(14)	1.513(7)	C(5')-C(3)-C(5)	24.7(7)	C(40)-C(39)-C(38)	118.1(6)
C(13)-C(16)	1.516(7)	C(6)-C(3)-C(5)	111.0(7)	C(41)-C(40)-F(40)	118.2(6)
C(13)-C(15)	1.542(7)	C(4')-C(3)-C(5)	132.1(9)	C(41)-C(40)-C(39)	123.4(6)
C(17)-C(18)	1.382(7)	N(1)-C(3)-C(5)	105.8(5)	F(40)-C(40)-C(39)	118.4(7)
C(17)-C(22)	1.395(6)	C(5')-C(3)-C(4)	82.5(7)	C(40)-C(41)-C(42)	117.3(6)
C(18)-C(19)	1.375(7)	C(6)-C(3)-C(4)	110.0(7)	C(41)-C(42)-C(37)	121.3(6)
C(19)-C(20)	1.382(7)	C(4')-C(3)-C(4)	40.4(6)	N(32)-C(43)-C(44)	107.6(4)
C(20)-F(20)	1.354(6)	N(1)-C(3)-C(4)	105.4(6)	N(32)-C(43)-C(46)	112.1(4)

C(20)-C(21)	1.361(7)	C(5)-C(3)-C(4)	106.7(6)	C(44)-C(43)-C(46)	112.1(5)
C(21)-C(22)	1.378(7)	C(5')-C(3)-C(6')	107.9(8)	N(32)-C(43)-C(45)	102.5(4)
Fe(2)-Cl(5)	2.1703(17)	C(6)-C(3)-C(6')	35.2(6)	C(44)-C(43)-C(45)	111.3(4)
Fe(2)-Cl(6)	2.1787(17)	C(4')-C(3)-C(6')	106.0(7)	C(46)-C(43)-C(45)	110.8(4)
Fe(2)-Cl(4)	2.1968(16)	N(1)-C(3)-C(6')	104.5(6)	C(48)-C(47)-C(52)	118.8(5)
Fe(2)-Cl(3)	2.2115(16)	C(5)-C(3)-C(6')	85.3(7)	C(48)-C(47)-C(32)	120.4(4)
N(31)-C(31)	1.266(5)	C(4)-C(3)-C(6')	143.0(7)	C(52)-C(47)-C(32)	120.6(4)
N(31)-C(33)	1.485(6)	C(12)-C(7)-C(8)	118.4(5)	C(49)-C(48)-C(47)	120.8(5)
N(32)-C(32)	1.274(6)	C(12)-C(7)-C(1)	123.7(5)	C(50)-C(49)-C(48)	119.4(5)
N(32)-C(43)	1.508(6)	C(8)-C(7)-C(1)	117.3(4)	F(50)-C(50)-C(49)	119.9(5)
C(31)-C(37)	1.496(6)	C(9)-C(8)-C(7)	120.5(5)	F(50)-C(50)-C(51)	118.1(5)
C(31)-C(32)	1.543(7)	C(10)-C(9)-C(8)	118.4(6)	C(49)-C(50)-C(51)	122.0(5)
C(32)-C(47)	1.472(6)	C(9)-C(10)-F(10)	118.3(7)	C(50)-C(51)-C(52)	118.6(5)
C(33)-C(34)	1.516(7)	C(9)-C(10)-C(11)	123.6(6)	C(51)-C(52)-C(47)	120.2(5)
C(33)-C(36)	1.532(7)	F(10)-C(10)-C(11)	118.1(6)		
C(33)-C(35)	1.541(7)	C(10)-C(11)-C(12)	118.1(6)		
C(37)-C(38)	1.370(6)	C(11)-C(12)-C(7)	120.9(5)		
C(37)-C(42)	1.393(7)	N(2)-C(13)-C(14)	106.6(4)		
C(38)-C(39)	1.376(7)	N(2)-C(13)-C(16)	115.4(4)		
C(39)-C(40)	1.373(8)	C(14)-C(13)-C(16)	112.6(5)		
C(40)-C(41)	1.364(8)	N(2)-C(13)-C(15)	106.2(4)		
C(40)-F(40)	1.371(6)	C(14)-C(13)-C(15)	108.7(5)		
C(41)-C(42)	1.375(7)	C(16)-C(13)-C(15)	106.9(5)		
C(43)-C(44)	1.509(7)	C(18)-C(17)-C(22)	118.4(5)		
C(43)-C(46)	1.512(7)	C(18)-C(17)-C(2)	122.0(5)		
C(43)-C(45)	1.532(7)	C(22)-C(17)-C(2)	119.3(5)		
C(47)-C(48)	1.386(6)	C(19)-C(18)-C(17)	121.5(5)		
C(47)-C(52)	1.410(6)	C(18)-C(19)-C(20)	118.1(5)		
C(48)-C(49)	1.377(7)	F(20)-C(20)-C(21)	119.7(6)		
C(49)-C(50)	1.365(7)	F(20)-C(20)-C(19)	117.9(5)		
C(50)-F(50)	1.347(6)	C(21)-C(20)-C(19)	122.3(5)		
C(50)-C(51)	1.384(7)	C(20)-C(21)-C(22)	118.8(5)		
C(51)-C(52)	1.384(7)	C(21)-C(22)-C(17)	120.8(5)		

N-H found from delta-F map and refined with a free isotropic thermal parameter subject to an X-H distance constraint (0.90 Å).



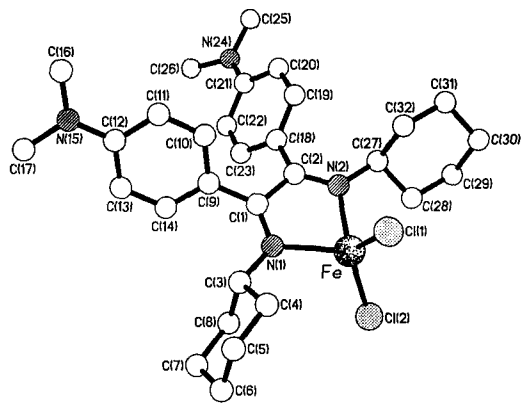
8.1.3 - Crystal structure data for Chapter 4.

data	31	35
code	VG0612	VG0607
formula	$C_{30}H_{42}Cl_2FeN_4$	$C_{26}H_{38}Cl_2FeN_4$
solvent	C_7H_8	C_7H_8
formula weight	677.56	625.49
colour, habit	red blocks	red blocks
crystal size / mm	0.30 × 0.28 × 0.09	0.35 × 0.34 × 0.34
temperature / K	173	173
crystal system	triclinic	triclinic
space group	$P\bar{1}$ (no. 2)	$P\bar{1}$ (no. 2)
***a* / Å**	11.4162(17)	10.5713(19)
***b* / Å**	13.2441(18)	13.9909(10)
***c* / Å**	13.751(2)	23.405(4)
α / deg	94.147(12)	83.312(9)
β / deg	108.738(13)	81.799(14)
γ / deg	111.334(14)	88.431(9)
***V* / Å^3**	1791.4(4)	3402.7(8)
Z	2	4
***D*$_c$ / g cm^{-3}**	1.256	1.221
radiation used	Cu-Kα	Mo-Kα
μ / mm^{-1}	4.972	0.627
2θ max / deg	142	64
no. of unique reflns measured	6584	20199
obs, $\|F_o\| > 4\sigma(\|F_o\|)$	6087	12259
no. of variables	408	857
***R*$_1$, *wR*$_2$ [f]**	0.030, 0.083	0.083, 0.188

Full bond lengths and angles for complex **31**, $^{Cy,Me2N\text{-}Ph}[N,N]FeCl_2$:

bond length (Å)			angle (°)		
Fe-N(1)	2.1040(14)	N(1)-Fe-N(2)	78.37(5)	C(19)-C(18)-C(2)	124.33(13)
Fe-N(2)	2.1050(13)	N(1)-Fe-Cl(1)	115.42(4)	C(20)-C(19)-C(18)	121.65(14)
Fe-Cl(1)	2.2438(6)	N(2)-Fe-Cl(1)	105.81(4)	C(19)-C(20)-C(21)	121.22(14)
Fe-Cl(2)	2.2548(6)	N(1)-Fe-Cl(2)	107.39(4)	N(24)-C(21)-C(22)	121.09(15)
N(1)-C(1)	1.2890(19)	N(2)-Fe-Cl(2)	119.93(4)	N(24)-C(21)-C(20)	122.08(15)
N(1)-C(3)	1.4785(19)	Cl(1)-Fe-Cl(2)	122.06(2)	C(22)-C(21)-C(20)	116.83(14)
N(2)-C(2)	1.2911(19)	C(1)-N(1)-C(3)	122.67(12)	C(23)-C(22)-C(21)	121.50(14)
N(2)-C(27)	1.4769(19)	C(1)-N(1)-Fe	113.66(10)	C(22)-C(23)-C(18)	121.62(14)
C(1)-C(9)	1.476(2)	C(3)-N(1)-Fe	121.09(9)	C(21)-N(24)-C(26)	121.14(15)
C(1)-C(2)	1.535(2)	C(2)-N(2)-C(27)	123.10(12)	C(21)-N(24)-C(25)	120.96(15)
C(2)-C(18)	1.4754(19)	C(2)-N(2)-Fe	114.67(10)	C(26)-N(24)-C(25)	117.16(15)
C(3)-C(8)	1.527(2)	C(27)-N(2)-Fe	121.31(9)	N(2)-C(27)-C(28)	109.31(12)
C(3)-C(4)	1.529(2)	N(1)-C(1)-C(9)	126.33(13)	N(2)-C(27)-C(32)	109.01(13)
C(4)-C(5)	1.532(2)	N(1)-C(1)-C(2)	115.41(12)	C(28)-C(27)-C(32)	110.09(13)

C(5)-C(6)	1.522(3)	C(9)-C(1)-C(2)	118.12(12)	C(27)-C(28)-C(29)	111.16(14)
C(6)-C(7)	1.522(3)	N(2)-C(2)-C(18)	127.70(13)	C(30)-C(29)-C(28)	111.39(16)
C(7)-C(8)	1.534(2)	N(2)-C(2)-C(1)	114.76(12)	C(29)-C(30)-C(31)	111.40(15)
C(9)-C(14)	1.397(2)	C(18)-C(2)-C(1)	117.39(12)	C(30)-C(31)-C(32)	111.53(15)
C(9)-C(10)	1.397(2)	N(1)-C(3)-C(8)	108.74(13)	C(31)-C(32)-C(27)	110.52(15)
C(10)-C(11)	1.380(2)	N(1)-C(3)-C(4)	109.26(13)		
C(11)-C(12)	1.404(2)	C(8)-C(3)-C(4)	110.70(14)		
C(12)-N(15)	1.374(2)	C(3)-C(4)-C(5)	110.79(15)		
C(12)-C(13)	1.405(2)	C(6)-C(5)-C(4)	111.44(16)		
C(13)-C(14)	1.380(2)	C(5)-C(6)-C(7)	111.02(16)		
N(15)-C(16)	1.442(3)	C(6)-C(7)-C(8)	111.37(16)		
N(15)-C(17)	1.449(3)	C(3)-C(8)-C(7)	110.92(15)		
C(18)-C(23)	1.399(2)	C(14)-C(9)-C(10)	117.38(14)		
C(18)-C(19)	1.400(2)	C(14)-C(9)-C(1)	123.57(13)		
C(19)-C(20)	1.379(2)	C(10)-C(9)-C(1)	118.98(13)		
C(20)-C(21)	1.409(2)	C(11)-C(10)-C(9)	121.39(15)		
C(21)-N(24)	1.372(2)	C(10)-C(11)-C(12)	121.29(15)		
C(21)-C(22)	1.407(2)	N(15)-C(12)-C(11)	121.52(16)		
C(22)-C(23)	1.375(2)	N(15)-C(12)-C(13)	121.29(15)		
N(24)-C(26)	1.426(2)	C(11)-C(12)-C(13)	117.18(14)		
N(24)-C(25)	1.444(2)	C(14)-C(13)-C(12)	121.09(15)		
C(27)-C(28)	1.524(2)	C(13)-C(14)-C(9)	121.55(14)		
C(27)-C(32)	1.532(2)	C(12)-N(15)-C(16)	120.51(16)		
C(28)-C(29)	1.532(2)	C(12)-N(15)-C(17)	119.94(16)		
C(29)-C(30)	1.519(3)	C(16)-N(15)-C(17)	118.38(16)		
C(30)-C(31)	1.521(3)	C(23)-C(18)-C(19)	117.14(13)		
C(31)-C(32)	1.531(2)	C(23)-C(18)-C(2)	118.50(13)		



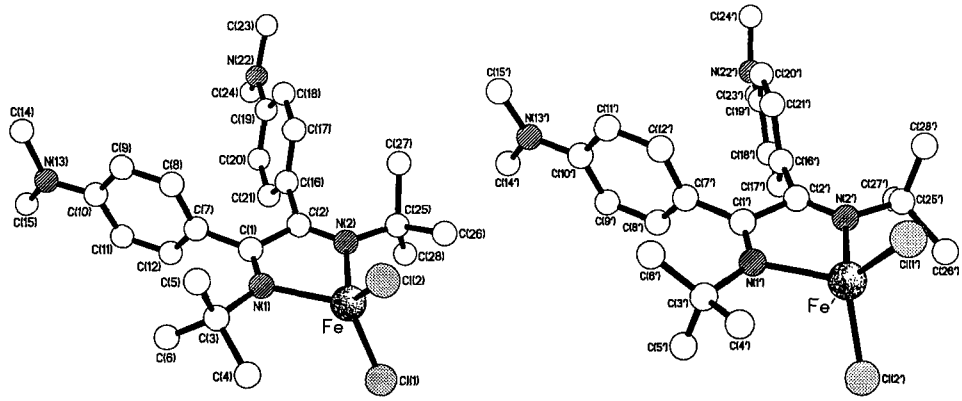
Full bond lengths and angles for complex **35**, $^{tBu,Me2N\text{-}Ph}[N,N]FeCl_2$:

bond length (Å)	**I**	**II**	**bond angle (°)**	**I**	**II**
Fe-N(2)	2.112(3)	2.109(3)	N(2)-Fe-N(1)	78.29(11)	78.57(12)
Fe-N(1)	2.123(3)	2.125(3)	N(2)-Fe-Cl(2A)	108.6(2)	106.2(3)
Fe-Cl(2A)	2.257(4)	2.265(5)	N(1)-Fe-Cl(2A)	119.3(2)	115.3(2)
Fe-Cl(1)	2.263(3)	2.290(3)	N(2)-Fe-Cl(1)	107.2(2)	106.9(2)
Fe-Cl(2)	2.275(4)	2.245(4)	N(1)-Fe-Cl(1)	118.6(2)	121.8(2)

Fe-Cl(1A)	2.279(3)	2.213(3)	Cl(2A)-Fe-Cl(1)	116.16(13)	117.85(16)
N(1)-C(1)	1.284(4)	1.291(5)	N(2)-Fe-Cl(2)	119.1(2)	118.1(2)
N(1)-C(3)	1.520(4)	1.510(5)	N(1)-Fe-Cl(2)	109.1(2)	107.5(2)
N(2)-C(2)	1.285(4)	1.271(4)	Cl(2A)-Fe-Cl(2)	14.98(8)	14.66(11)
N(2)-C(25)	1.515(4)	1.513(5)	Cl(1)-Fe-Cl(2)	118.40(13)	118.13(16)
C(1)-C(7)	1.502(4)	1.499(5)	N(2)-Fe-Cl(1A)	118.3(2)	120.1(3)
C(1)-C(2)	1.537(5)	1.549(5)	N(1)-Fe-Cl(1A)	107.3(2)	110.2(3)
C(2)-C(16A)	1.506(5)	1.493(7)	Cl(2A)-Fe-Cl(1A)	118.78(14)	119.64(17)
C(2)-C(16)	1.525(4)	1.524(4)	Cl(1)-Fe-Cl(1A)	16.37(7)	17.82(13)
C(3)-C(5)	1.462(8)	1.451(8)	Cl(2)-Fe-Cl(1A)	116.23(13)	114.87(16)
C(3)-C(6A)	1.478(8)	1.463(9)	C(1)-N(1)-C(3)	125.0(3)	125.8(3)
C(3)-C(4)	1.557(7)	1.580(7)	C(1)-N(1)-Fe	114.5(2)	113.5(2)
C(3)-C(4A)	1.559(7)	1.547(9)	C(3)-N(1)-Fe	120.5(2)	120.7(2)
C(3)-C(5A)	1.565(9)	1.591(9)	C(2)-N(2)-C(25)	126.1(3)	125.3(3)
C(3)-C(6)	1.566(7)	1.541(8)	C(2)-N(2)-Fe	114.7(2)	115.3(2)
C(7)-C(8)	1.379(5)	1.376(6)	C(25)-N(2)-Fe	119.1(2)	119.4(2)
C(7)-C(12)	1.386(5)	1.375(6)	N(1)-C(1)-C(7)	127.3(3)	126.9(3)
C(8)-C(9)	1.375(5)	1.390(6)	N(1)-C(1)-C(2)	116.2(3)	116.6(3)
C(9)-C(10)	1.399(6)	1.396(7)	C(7)-C(1)-C(2)	116.5(3)	116.5(3)
C(10)-N(13)	1.388(5)	1.393(5)	N(2)-C(2)-C(16A)	127.4(4)	128.5(5)
C(10)-C(11)	1.402(6)	1.389(7)	N(2)-C(2)-C(16)	127.1(3)	129.3(4)
C(11)-C(12)	1.389(5)	1.400(6)	C(16A)-C(2)-C(16)	6.1(4)	7.3(6)
N(13)-C(15)	1.437(6)	1.411(8)	N(2)-C(2)-C(1)	116.3(3)	115.8(3)
N(13)-C(14)	1.443(6)	1.457(7)	C(16A)-C(2)-C(1)	116.2(4)	115.7(5)
C(16)-C(17)	1.39	1.39	C(16)-C(2)-C(1)	116.5(3)	114.6(4)
C(16)-C(21)	1.39	1.39	C(5)-C(3)-C(6A)	136.4(6)	142.9(7)
C(17)-C(18)	1.39	1.39	C(5)-C(3)-N(1)	109.2(4)	108.3(5)
C(18)-C(19)	1.39	1.39	C(6A)-C(3)-N(1)	110.4(5)	108.6(5)
C(19)-C(20)	1.39	1.39	C(5)-C(3)-C(4)	113.0(5)	110.5(5)
C(19)-N(22)	1.421(5)	1.428(5)	C(6A)-C(3)-C(4)	73.2(5)	63.9(5)
C(20)-C(21)	1.39	1.39	N(1)-C(3)-C(4)	104.6(4)	103.4(4)
N(22)-C(24)	1.445(9)	1.449(8)	C(5)-C(3)-C(4A)	74.4(6)	60.3(6)
N(22)-C(23)	1.452(9)	1.443(9)	C(6A)-C(3)-C(4A)	110.4(5)	112.3(6)
C(16A)-C(17A)	1.39	1.39	N(1)-C(3)-C(4A)	106.3(4)	105.4(5)
C(16A)-C(21A)	1.39	1.39	C(4)-C(3)-C(4A)	41.0(4)	52.2(5)
C(17A)-C(18A)	1.39	1.39	C(5)-C(3)-C(5A)	33.8(5)	48.2(6)
C(18A)-C(19A)	1.39	1.39	C(6A)-C(3)-C(5A)	111.3(6)	110.4(6)
C(19A)-C(20A)	1.39	1.39	N(1)-C(3)-C(5A)	113.1(5)	115.3(5)
C(19A)-N(22A)	1.438(9)	1.437(9)	C(4)-C(3)-C(5A)	136.3(6)	139.8(6)
C(20A)-C(21A)	1.39	1.39	C(4A)-C(3)-C(5A)	105.1(5)	104.7(6)
N(22A)-C(23A)	1.441(11)	1.435(12)	C(5)-C(3)-C(6)	112.4(6)	114.9(6)
N(22A)-C(24A)	1.451(11)	1.450(12)	C(6A)-C(3)-C(6)	33.3(5)	44.0(6)
C(25)-C(27A)	1.409(8)	1.456(9)	N(1)-C(3)-C(6)	112.8(4)	113.6(5)
C(25)-C(28)	1.414(7)	1.478(7)	C(4)-C(3)-C(6)	104.5(5)	105.3(5)
C(25)-C(26A)	1.579(7)	1.567(8)	C(4A)-C(3)-C(6)	134.2(5)	139.1(6)
C(25)-C(26)	1.582(7)	1.559(7)	C(5A)-C(3)-C(6)	80.9(6)	69.4(6)
C(25)-C(27)	1.601(7)	1.567(7)	C(8)-C(7)-C(12)	117.7(3)	118.2(4)
C(25)-C(28A)	1.601(7)	1.568(8)	C(8)-C(7)-C(1)	121.5(3)	120.7(4)

C(30)-C(31)	1.510(14)	1.53(2)	C(12)-C(7)-C(1)	120.8(3)	121.1(3)
C(31)-C(32)	1.39	1.39	C(9)-C(8)-C(7)	121.3(4)	121.8(4)
C(31)-C(36)	1.39	1.39	C(8)-C(9)-C(10)	122.4(4)	120.6(4)
C(32)-C(33)	1.39	1.39	N(13)-C(10)-C(9)	122.5(4)	121.3(4)
C(33)-C(34)	1.39	1.39	N(13)-C(10)-C(11)	121.7(4)	121.5(5)
C(34)-C(35)	1.39	1.39	C(9)-C(10)-C(11)	115.8(3)	117.2(4)
C(35)-C(36)	1.39	1.39	C(12)-C(11)-C(10)	121.5(4)	121.4(4)
			C(7)-C(12)-C(11)	121.3(4)	120.7(4)
			C(10)-N(13)-C(15)	120.3(4)	121.1(5)
			C(10)-N(13)-C(14)	120.0(4)	119.9(5)
			C(15)-N(13)-C(14)	117.5(4)	119.0(5)
			C(17)-C(16)-C(21)	120	120
			C(17)-C(16)-C(2)	119.7(3)	120.0(3)
			C(21)-C(16)-C(2)	120.3(3)	119.9(3)
			C(18)-C(17)-C(16)	120	120
			C(19)-C(18)-C(17)	120	120
			C(20)-C(19)-C(18)	120	120
			C(20)-C(19)-N(22)	119.3(4)	120.2(4)
			C(18)-C(19)-N(22)	120.7(4)	119.8(4)
			C(19)-C(20)-C(21)	120	120
			C(20)-C(21)-C(16)	120	120
			C(19)-N(22)-C(24)	121.2(6)	120.5(6)
			C(19)-N(22)-C(23)	119.9(6)	119.8(5)
			C(24)-N(22)-C(23)	117.0(6)	117.2(6)
			C(17A)-C(16A)-C(21A)	120	120
			C(17A)-C(16A)-C(2)	119.8(4)	118.5(7)
			C(21A)-C(16A)-C(2)	120.2(4)	121.4(7)
			C(16A)-C(17A)-C(18A)	120	120
			C(19A)-C(18A)-C(17A)	120	120
			C(20A)-C(19A)-C(18A)	120	120
			C(20A)-C(19A)-N(22A)	120.1(5)	118.9(6)
			C(18A)-C(19A)-N(22A)	119.9(5)	121.0(6)
			C(19A)-C(20A)-C(21A)	120	120
			C(20A)-C(21A)-C(16A)	120	120
			C(19A)-N(22A)-C(23A)	119.9(8)	120.8(10)
			C(19A)-N(22A)-C(24A)	120.4(7)	121.1(9)
			C(23A)-N(22A)-C(24A)	118.6(8)	117.9(10)
			C(27A)-C(25)-C(28)	136.3(6)	138.2(6)
			C(27A)-C(25)-N(2)	111.8(5)	110.6(5)
			C(28)-C(25)-N(2)	111.2(4)	109.5(4)
			C(27A)-C(25)-C(26A)	112.9(5)	111.0(6)
			C(28)-C(25)-C(26A)	62.7(5)	69.2(5)
			N(2)-C(25)-C(26A)	104.3(4)	104.2(5)
			C(27A)-C(25)-C(26)	62.5(5)	69.7(6)
			C(28)-C(25)-C(26)	113.0(5)	110.0(5)
			N(2)-C(25)-C(26)	104.7(3)	105.2(4)
			C(26A)-C(25)-C(26)	54.5(4)	44.0(5)
			C(27A)-C(25)-C(27)	41.1(4)	38.2(5)

C(28)-C(25)-C(27)	113.0(5)	112.9(5)
N(2)-C(25)-C(27)	111.9(4)	113.2(4)
C(26A)-C(25)-C(27)	141.5(5)	138.0(5)
C(26)-C(25)-C(27)	102.5(5)	105.6(5)
C(27A)-C(25)-C(28A)	114.1(5)	113.9(6)
C(28)-C(25)-C(28A)	40.2(4)	37.6(5)
N(2)-C(25)-C(28A)	110.9(4)	111.5(5)
C(26A)-C(25)-C(28A)	102.0(5)	105.0(5)
C(26)-C(25)-C(28A)	141.7(5)	137.5(5)
C(27)-C(25)-C(28A)	77.2(4)	78.9(5)
C(32)-C(31)-C(36)	120	120
C(32)-C(31)-C(30)	124.8(10)	124.4(12)
C(36)-C(31)-C(30)	115.2(11)	115.6(12)
C(31)-C(32)-C(33)	120	120
C(34)-C(33)-C(32)	120	120
C(33)-C(34)-C(35)	120	120
C(34)-C(35)-C(36)	120	120
C(35)-C(36)-C(31)	120	120
C(42)-C(41)-C(46)	119.4(8)	
C(42)-C(41)-C(40)	121.5(8)	
C(46)-C(41)-C(40)	119.1(8)	
C(41)-C(42)-C(43)	122.2(9)	
C(42)-C(43)-C(44)	122.2(9)	
C(45)-C(44)-C(43)	118.8(8)	
C(44)-C(45)-C(46)	117.9(7)	
C(41)-C(46)-C(45)	119.6(8)	



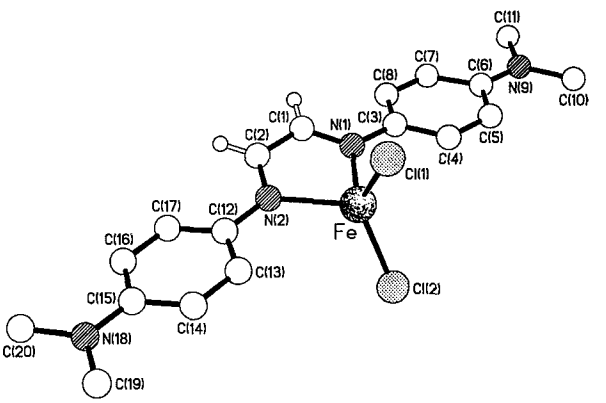
8.1.4 - Crystal structure data for Chapter 6.

data	45	52	53	66	67
code	VG0408	VG0412	VG0423b	VG0638b	VG0637
formula	$C_{18}H_{22}Cl_2FeN_4$	$C_{26}H_{34}Cl_2FeN_4$	$C_8H_{38}Cl_2FeN_4$	$C_{16}H_{32}Cl_4Fe_2N_4O_6$	$C_{36}H_{40}Cl_4Fe_2N_4O_6$
solvent	—	—	—	—	THF
formula weight	421.15	529.32	557.37	629.96	950.32
colour, habit	blue/green prisms	purple blocky needles	pink blocky needles	orange blocks	red blocks
crystal size / mm	0.47 × 0.23 × 0.20	0.73 × 0.40 × 0.20	0.27 × 0.17 × 0.13	0.25 × 0.24 × 0.17	0.27 × 0.16 × 0.14
temp. / K	203	203	173	173	173
crystal system	orthorhombic	orthorhombic	monoclinic	monoclinic	triclinic
space group	Pna2(1)	Pbcn	C2/c	P2(1)/n	P-1
a / Å	13.267(3)	13.6458(11)	29.2799(7)	9.4526(3)	9.5460(14)
b / Å	20.517(3)	9.9479(13)	8.0944(5)	10.0444(4)	11.4692(19)
c / Å	7.3789(8)	19.445(2)	12.2316(15)	13.7772(5)	22.129(3)
α / deg	—	—	—	—	102.820(13)
β / deg	—	—	107.399(5)	91.454(3)°	92.546(12)
γ / deg	—	—	—	—	108.997(14)
V / Å^3	2008.5(5)	2639.5(5)	2766.3(4)	1307.66(8)	2215.7(6)
Z	4	4	4	2	2
D_c / g cm^{-3}	1.393	1.332	1.338	1.600	1.424
radiation used	Mo-Kα	Mo-Kα	Mo-Kα	Mo-Kα	Mo-Kα
μ / mm^{-1}	1.025	0.795	0.762	1.555	0.947
2θ max / deg	50	50	66	64	64
no. of unique reflns measured	1909	2322	4658	4247	13957
obs, $\|F_o\| > 4\sigma(\|F_o\|)$	1169	1445	4376	3599	10293
no. of variables	230	139	160	172	548
R_1, wR_2	0.048, 0.072	0.049, 0.092	0.042, 0.102	0.028, 0.074	0.038, 0.105

Full bond lengths and angles for complex **45**, $^{Me2N\text{-}Ph,H}[N,N]FeCl_2$:

bond length (Å)			angle (°)		
Fe-N(2)	2.111(7)	N(2)-Fe-N(1)	79.5(2)	C(17)-C(12)-C(13)	117.1(8)
Fe-N(1)	2.143(8)	N(2)-Fe-Cl(1)	109.6(2)	C(17)-C(12)-N(2)	123.2(9)
Fe-Cl(1)	2.214(2)	N(1)-Fe-Cl(1)	110.4(2)	C(13)-C(12)-N(2)	119.7(8)
Fe-Cl(2)	2.233(2)	N(2)-Fe-Cl(2)	113.4(2)	C(14)-C(13)-C(12)	121.7(9)
N(1)-C(1)	1.294(14)	N(1)-Fe-Cl(2)	112.4(2)	C(13)-C(14)-C(15)	121.9(9)
N(1)-C(3)	1.398(12)	Cl(1)-Fe-Cl(2)	123.25(9)	N(18)-C(15)-C(16)	121.9(9)
C(1)-C(2)	1.447(11)	C(1)-N(1)-C(3)	123.4(8)	N(18)-C(15)-C(14)	122.2(9)
N(2)-C(2)	1.302(12)	C(1)-N(1)-Fe	109.5(6)	C(16)-C(15)-C(14)	115.9(8)
N(2)-C(12)	1.399(12)	C(3)-N(1)-Fe	126.7(6)	C(17)-C(16)-C(15)	122.4(9)
C(3)-C(8)	1.390(13)	N(1)-C(1)-C(2)	119.2(10)	C(16)-C(17)-C(12)	120.9(10)
C(3)-C(4)	1.392(14)	C(2)-N(2)-C(12)	122.2(8)	C(15)-N(18)-C(19)	119.9(9)
C(4)-C(5)	1.353(13)	C(2)-N(2)-Fe	110.0(6)	C(15)-N(18)-C(20)	122.9(10)

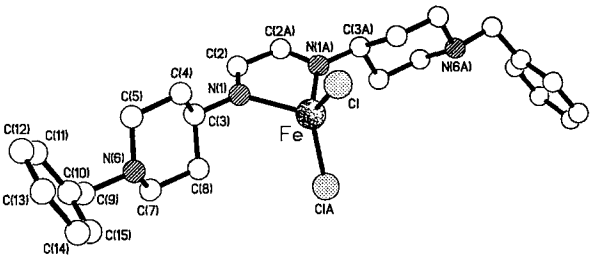
C(5)-C(6)	1.443(14)	C(12)-N(2)-Fe	127.3(6)	C(19)-N(18)-C(20)	116.9(9)
C(6)-N(9)	1.332(13)	N(2)-C(2)-C(1)	119.5(10)		
C(6)-C(7)	1.436(16)	C(8)-C(3)-C(4)	117.7(8)		
C(7)-C(8)	1.364(16)	C(8)-C(3)-N(1)	123.5(9)		
N(9)-C(10)	1.450(15)	C(4)-C(3)-N(1)	118.8(8)		
N(9)-C(11)	1.459(15)	C(5)-C(4)-C(3)	121.8(9)		
C(12)-C(17)	1.392(15)	C(4)-C(5)-C(6)	122.5(10)		
C(12)-C(13)	1.397(14)	N(9)-C(6)-C(7)	123.3(10)		
C(13)-C(14)	1.375(12)	N(9)-C(6)-C(5)	123.1(10)		
C(14)-C(15)	1.407(14)	C(7)-C(6)-C(5)	113.6(9)		
C(15)-N(18)	1.361(13)	C(8)-C(7)-C(6)	122.7(9)		
C(15)-C(16)	1.395(15)	C(7)-C(8)-C(3)	121.4(10)		
C(16)-C(17)	1.389(14)	C(6)-N(9)-C(10)	120.9(9)		
N(18)-C(19)	1.453(16)	C(6)-N(9)-C(11)	121.0(10)		
N(18)-C(20)	1.460(17)	C(10)-N(9)-C(11)	118.1(8)		



Full bond lengths and angles for complex **52**, $^{pip,H}[N,N]FeCl_2$:

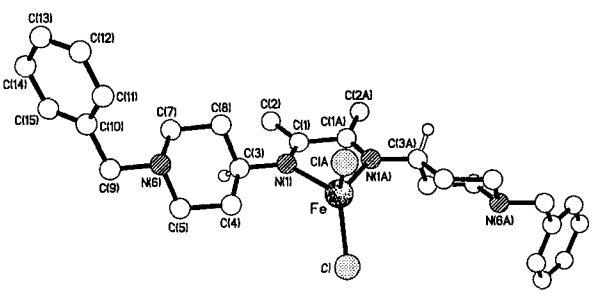
bond length (Å)			**angle (°)**		
Fe-N(1)	2.130(3)	N(1)-Fe-N(1)#1	78.59(16)	C(11)-C(10)-C(15)	120
Fe-N(1)#1	2.130(3)	N(1)-Fe-Cl#1	111.71(9)	C(11)-C(10)-C(9)	121.3(2)
Fe-Cl#1	2.2258(12)	N(1)#1-Fe-Cl#1	111.11(8)	C(15)-C(10)-C(9)	118.7(2)
Fe-Cl	2.2258(12)	N(1)-Fe-Cl	111.11(8)	C(10)-C(11)-C(12)	120
N(1)-C(2)	1.270(5)	N(1)#1-Fe-Cl	111.71(9)	C(13)-C(12)-C(11)	120
N(1)-C(3)	1.478(5)	Cl#1-Fe-Cl	123.72(8)	C(14)-C(13)-C(12)	120
C(2)-C(2)#1	1.489(7)	C(2)-N(1)-C(3)	117.8(3)	C(13)-C(14)-C(15)	120
C(3)-C(4)	1.517(5)	C(2)-N(1)-Fe	112.2(2)	C(14)-C(15)-C(10)	120
C(3)-C(8)	1.520(5)	C(3)-N(1)-Fe	129.6(2)		
C(4)-C(5)	1.523(5)	N(1)-C(2)-C(2)#1	118.3(2)		
C(5)-N(6)	1.462(5)	N(1)-C(3)-C(4)	111.7(3)		
N(6)-C(7)	1.468(5)	N(1)-C(3)-C(8)	109.9(3)		
N(6)-C(9)	1.475(5)	C(4)-C(3)-C(8)	108.0(3)		
C(7)-C(8)	1.523(5)	C(3)-C(4)-C(5)	109.5(3)		
C(9)-C(10)	1.521(4)	N(6)-C(5)-C(4)	113.0(3)		
C(10)-C(11)	1.39	C(5)-N(6)-C(7)	110.0(3)		
C(10)-C(15)	1.39	C(5)-N(6)-C(9)	110.7(3)		

C(11)-C(12)	1.39	C(7)-N(6)-C(9)	109.1(3)
C(12)-C(13)	1.39	N(6)-C(7)-C(8)	112.0(3)
C(13)-C(14)	1.39	C(3)-C(8)-C(7)	109.7(3)
C(14)-C(15)	1.39	N(6)-C(9)-C(10)	112.8(3)



Full bond lengths and angles for complex **53**, $^{pip,Me}[N,N]FeCl_2$:

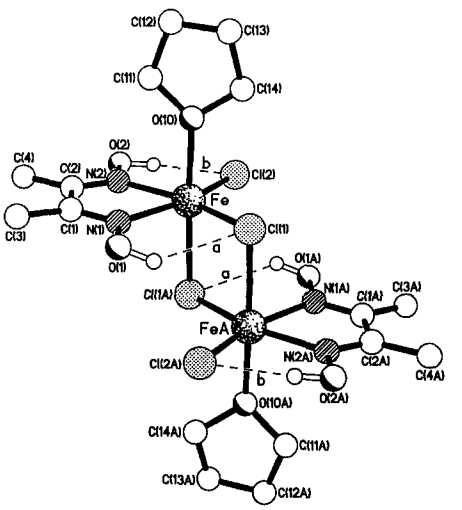
bond length (Å)		angle (°)			
Fe-N(1)	2.1051(11)	N(1)-Fe-N(1)#1	77.76(6)	N(6)-C(9)-C(10)	113.04(12)
Fe-N(1)#1	2.1058(11)	N(1)-Fe-Cl#1	109.28(3)	C(15)-C(10)-C(11)	118.84(15)
Fe-Cl#1	2.2491(4)	N(1)#1-Fe-Cl#1	114.97(3)	C(15)-C(10)-C(9)	120.18(15)
Fe-Cl	2.2500(4)	N(1)-Fe-Cl	115.00(3)	C(11)-C(10)-C(9)	120.97(14)
C(1)-N(1)	1.2846(16)	N(1)#1-Fe-Cl	109.32(3)	C(10)-C(11)-C(12)	120.10(15)
C(1)-C(2)	1.4944(17)	Cl#1-Fe-Cl	122.17(2)	C(13)-C(12)-C(11)	120.44(17)
C(1)-C(1)#1	1.524(2)	N(1)-C(1)-C(2)	126.76(11)	C(14)-C(13)-C(12)	119.70(16)
N(1)-C(3)	1.4799(15)	N(1)-C(1)-C(1)#1	115.81(7)	C(13)-C(14)-C(15)	120.18(17)
C(3)-C(8)	1.5264(17)	C(2)-C(1)-C(1)#1	117.43(7)	C(10)-C(15)-C(14)	120.72(17)
C(3)-C(4)	1.5267(17)	C(1)-N(1)-C(3)	120.19(10)		
C(4)-C(5)	1.5303(19)	C(1)-N(1)-Fe	115.25(8)		
C(5)-N(6)	1.4618(18)	C(3)-N(1)-Fe	124.56(8)		
N(6)-C(7)	1.4599(18)	N(1)-C(3)-C(8)	110.69(10)		
N(6)-C(9)	1.4677(18)	N(1)-C(3)-C(4)	110.78(10)		
C(7)-C(8)	1.5192(18)	C(8)-C(3)-C(4)	108.03(10)		
C(9)-C(10)	1.511(2)	C(3)-C(4)-C(5)	109.78(11)		
C(10)-C(15)	1.384(2)	N(6)-C(5)-C(4)	111.79(11)		
C(10)-C(11)	1.386(2)	C(7)-N(6)-C(5)	110.59(10)		
C(11)-C(12)	1.394(2)	C(7)-N(6)-C(9)	110.54(12)		
C(12)-C(13)	1.379(3)	C(5)-N(6)-C(9)	109.83(11)		
C(13)-C(14)	1.370(3)	N(6)-C(7)-C(8)	110.64(11)		
C(14)-C(15)	1.392(3)	C(7)-C(8)-C(3)	109.31(11)		



Full bond lengths and angles for complex **66**, $^{OH,Me}[N,N]FeCl_2$:

bond length (Å)				angle (°)	
Fe-N(2)	2.1497(12)	N(2)-Fe-O(10)	89.92(4)	O(2)-N(2)-Fe	123.30(9)
Fe-O(10)	2.1866(10)	N(2)-Fe-N(1)	71.00(5)	N(2)-C(2)-C(1)	113.54(12)
Fe-N(1)	2.1991(11)	O(10)-Fe-N(1)	91.65(4)	N(2)-C(2)-C(4)	124.78(15)
Fe-Cl(2)	2.3735(4)	N(2)-Fe-Cl(2)	88.99(3)	C(1)-C(2)-C(4)	121.65(14)
Fe-Cl(1)	2.4072(4)	O(10)-Fe-Cl(2)	91.69(3)	C(11')-O(10)-C(14)	94.1(3)
Fe-Cl(1)#1	2.5430(4)	N(1)-Fe-Cl(2)	159.70(3)	C(11')-O(10)-C(11)	17.8(2)
Cl(1)-Fe#1	2.5430(4)	N(2)-Fe-Cl(1)	159.46(3)	C(14)-O(10)-C(11)	105.6(2)
N(1)-C(1)	1.2899(18)	O(10)-Fe-Cl(1)	87.96(3)	C(11')-O(10)-C(14')	109.2(3)
N(1)-O(1)	1.3854(16)	N(1)-Fe-Cl(1)	88.64(3)	C(14)-O(10)-C(14')	21.0(2)
C(1)-C(2)	1.476(2)	Cl(2)-Fe-Cl(1)	111.482(15)	C(11)-O(10)-C(14')	116.2(2)
C(1)-C(3)	1.492(2)	N(2)-Fe-Cl(1)#1	94.44(3)	C(11')-O(10)-Fe	121.8(2)
N(2)-C(2)	1.2877(18)	O(10)-Fe-Cl(1)#1	174.76(3)	C(14)-O(10)-Fe	120.57(13)
N(2)-O(2)	1.3829(16)	N(1)-Fe-Cl(1)#1	87.04(3)	C(11)-O(10)-Fe	122.73(12)
C(2)-C(4)	1.490(2)	Cl(2)-Fe-Cl(1)#1	91.292(14)	C(14')-O(10)-Fe	118.9(2)
O(10)-C(11')	1.415(6)	Cl(1)-Fe-Cl(1)#1	86.943(12)	O(10)-C(11)-C(12)	106.5(3)
O(10)-C(14)	1.439(3)	Fe-Cl(1)-Fe#1	93.057(12)	C(11)-C(12)-C(13)	106.3(3)
O(10)-C(11)	1.462(3)	C(1)-N(1)-O(1)	114.24(11)	C(12)-C(13)-C(14)	102.6(3)
O(10)-C(14')	1.480(5)	C(1)-N(1)-Fe	119.00(10)	O(10)-C(14)-C(13)	105.0(2)
C(11)-C(12)	1.509(5)	O(1)-N(1)-Fe	126.54(8)	O(10)-C(11')-C(12')	103.1(5)
C(12)-C(13)	1.516(6)	N(1)-C(1)-C(2)	114.39(12)	C(13')-C(12')-C(11')	99.6(6)
C(13)-C(14)	1.528(5)	N(1)-C(1)-C(3)	124.03(15)	C(14')-C(13')-C(12')	105.9(6)
C(11')-C(12')	1.543(10)	C(2)-C(1)-C(3)	121.57(14)	O(10)-C(14')-C(13')	104.8(4)
C(12')-C(13')	1.524(11)	C(2)-N(2)-O(2)	115.09(12)		
C(13')-C(14')	1.488(8)	C(2)-N(2)-Fe	121.60(10)		

O-H found from delta-F map and refined with a free isotropic thermal parameter subject to an O-H distance constraint (0.90 Å).

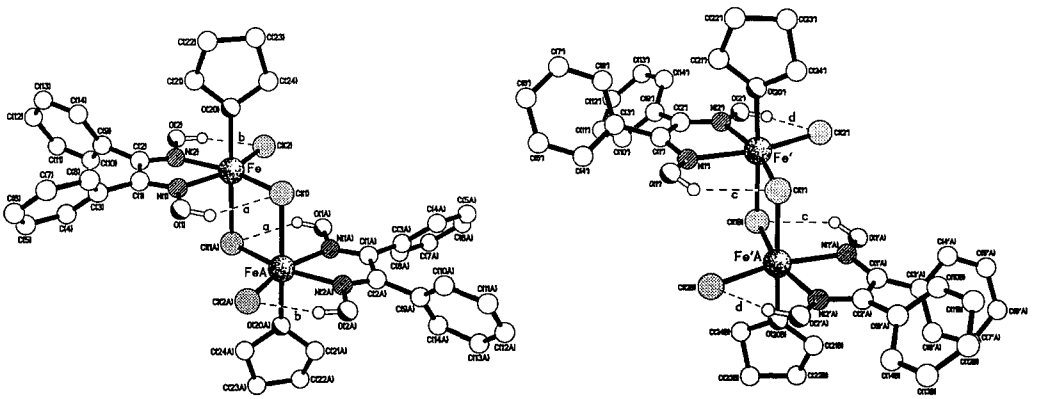


Full bond lengths and angles for complex **67**, $^{OH,Ph}[N,N]FeCl_2$:

bond length (Å)	I	II	bond angle (°)	I	II
Fe-N(2)	2.1464(15)	2.1479(14)	N(2)-Fe-N(1)	70.97(6)	71.21(5)
Fe-N(1)	2.1726(14)	2.1865(14)	N(2)-Fe-O(20)	91.29(6)	90.03(5)
Fe-O(20)	2.1875(14)	2.1654(14)	N(1)-Fe-O(20)	87.06(5)	88.26(6)
Fe-Cl(2)	2.3490(7)	2.3519(7)	N(2)-Fe-Cl(2)	87.60(5)	88.98(4)
Fe-Cl(1)	2.4044(7)	2.3884(6)	N(1)-Fe-Cl(2)	158.56(4)	160.14(4)
Fe-Cl(1)#1	2.5509(6)	2.5419(6)	O(20)-Fe-Cl(2)	93.01(4)	93.30(4)
Cl(1)-Fe#1	2.5509(6)	2.5419(6)	N(2)-Fe-Cl(1)	161.87(4)	161.87(4)
N(1)-C(1)	1.297(2)	1.292(2)	N(1)-Fe-Cl(1)	90.90(4)	90.66(4)
N(1)-O(1)	1.3841(19)	1.3852(19)	O(20)-Fe-Cl(1)	87.67(4)	88.92(4)
C(1)-C(3)	1.471(2)	1.479(2)	Cl(2)-Fe-Cl(1)	110.53(2)	109.15(2)
C(1)-C(2)	1.490(2)	1.487(2)	N(2)-Fe-Cl(1)#1	92.33(5)	91.26(4)
N(2)-C(2)	1.291(2)	1.2932(19)	N(1)-Fe-Cl(1)#1	88.75(4)	90.04(4)
N(2)-O(2)	1.387(2)	1.3849(18)	O(20)-Fe-Cl(1)#1	173.27(4)	177.42(4)
C(2)-C(9)	1.476(2)	1.475(2)	Cl(2)-Fe-Cl(1)#1	92.81(2)	88.96(2)
C(3)-C(8)	1.388(2)	1.382(2)	Cl(1)-Fe-Cl(1)#1	87.13(2)	89.16(2)
C(3)-C(4)	1.391(2)	1.394(2)	Fe-Cl(1)-Fe#1	92.87(2)	90.84(2)
C(4)-C(5)	1.390(3)	1.388(2)	C(1)-N(1)-O(1)	114.97(13)	114.76(13)
C(5)-C(6)	1.369(3)	1.371(3)	C(1)-N(1)-Fe	120.70(12)	118.50(11)
C(6)-C(7)	1.383(3)	1.384(3)	O(1)-N(1)-Fe	124.23(9)	122.24(9)
C(7)-C(8)	1.385(2)	1.391(3)	N(1)-C(1)-C(3)	125.91(15)	125.17(15)
C(9)-C(10)	1.387(3)	1.399(2)	N(1)-C(1)-C(2)	113.03(14)	113.24(14)
C(9)-C(14)	1.389(3)	1.392(3)	C(3)-C(1)-C(2)	121.05(14)	121.41(14)
C(10)-C(11)	1.381(3)	1.390(3)	C(2)-N(2)-O(2)	115.12(14)	116.37(13)
C(11)-C(12)	1.368(4)	1.367(4)	C(2)-N(2)-Fe	121.65(12)	121.23(11)
C(12)-C(13)	1.367(4)	1.374(4)	O(2)-N(2)-Fe	122.01(10)	120.69(9)
C(13)-C(14)	1.386(3)	1.396(3)	N(2)-C(2)-C(9)	124.54(16)	125.58(15)
O(20)-C(21)	1.420(2)	1.425(3)	N(2)-C(2)-C(1)	113.06(14)	112.53(13)
O(20)-C(24)	1.447(2)	1.449(2)	C(9)-C(2)-C(1)	122.33(14)	121.82(13)
C(21)-C(22)	1.500(3)	1.518(3)	C(8)-C(3)-C(4)	119.24(15)	119.83(15)
C(22)-C(23)	1.503(3)	1.516(3)	C(8)-C(3)-C(1)	120.17(14)	118.44(14)
C(23)-C(24)	1.488(3)	1.502(3)	C(4)-C(3)-C(1)	120.57(16)	121.72(16)
O(30)-C(34)	1.387(9)	1.447(11)	C(5)-C(4)-C(3)	119.69(18)	119.67(18)
O(30)-C(31)	1.493(9)	1.469(11)	C(6)-C(5)-C(4)	120.61(17)	120.40(17)
C(31)-C(32)	1.630(10)	1.607(12)	C(5)-C(6)-C(7)	120.13(18)	120.19(17)
C(32)-C(33)	1.456(12)	1.364(14)	C(6)-C(7)-C(8)	119.8(2)	119.94(19)
C(33)-C(34)	1.519(10)	1.599(12)	C(7)-C(8)-C(3)	120.55(17)	119.93(17)
O(30")-C(34")	1.458(12)		C(10)-C(9)-C(14)	119.48(18)	119.73(16)
O(30")-C(31")	1.460(12)		C(10)-C(9)-C(2)	121.22(16)	118.82(16)
C(31")-C(32")	1.691(14)		C(14)-C(9)-C(2)	119.29(17)	121.42(15)
C(32")-C(33")	1.408(16)		C(11)-C(10)-C(9)	120.2(2)	119.5(2)
C(33")-C(34")	1.538(14)		C(12)-C(11)-C(10)	119.9(2)	120.6(2)
			C(13)-C(12)-C(11)	120.4(2)	120.26(19)
			C(12)-C(13)-C(14)	120.7(2)	120.7(2)
			C(13)-C(14)-C(9)	119.2(2)	119.2(2)
			C(21)-O(20)-C(24)	107.93(16)	109.11(15)

C(21)-O(20)-Fe	126.04(11)	128.85(11)
C(24)-O(20)-Fe	122.81(12)	121.61(12)
O(20)-C(21)-C(22)	105.81(17)	107.38(17)
C(21)-C(22)-C(23)	103.72(18)	102.8(2)
C(24)-C(23)-C(22)	105.93(17)	102.51(18)
O(20)-C(24)-C(23)	107.20(18)	104.84(16)
C(34)-O(30)-C(31)	105.9(7)	99.9(8)
O(30)-C(31)-C(32)	95.2(6)	101.9(7)
C(33)-C(32)-C(31)	97.8(6)	107.2(7)
C(32)-C(33)-C(34)	104.5(6)	99.8(7)
O(30)-C(34)-C(33)	107.1(6)	99.2(7)
C(34")-O(30")-C(31")	107.7(9)	
O(30")-C(31")-C(32")	95.1(8)	
C(33")-C(32")-C(31")	97.5(9)	
C(32")-C(33")-C(34")	101.5(9)	
O(30")-C(34")-C(33")	106.0(8)	

O-H found from delta-F map and refined with a free isotropic thermal parameter subject to an O-H distance constraint (0.90 Å).



8.2 - Appendix 2: Hammett Substituent Constants

8.2.1 - Substituent constant data for Chapter 4.

X	σ_m	σ_p	X	σ_m	σ_p
H	0	0	NHOH	-0.04	-0.34
Me	-0.069	-0.17	NO_2	0.71	0.778
Et	-0.07	-0.151	O^-	-0.71	-0.52
Pr	-0.05	-0.151	OH	0.121	-0.37
^{i}Pr	-0.1	-0.197	**OMe**	0.115	-0.268
^{t}Bu	-0.1	-0.197	OEt	0.1	-0.24
Ph	0.06	-0.01	OPh	0.252	-0.32
C_6F_5	-0.12	-0.03	OCOMe	0.39	0.31
CN	0.56	0.66	OCF_3	0.40	0.35
CH_2CN		0.01	**F**	0.337	0.062
CHO	0.36	0.22	Cl	0.373	0.227
COMe	0.376	0.502	**Br**	0.391	0.232
$CONH_2$	0.28	0.36	I	0.352	0.18
COOH	0.37	0.45	SH	0.25	0.15
COO^-	-0.10	0	SMe	0.15	0
COOMe	0.32	0.39	$^{+}SMe_3$	1.0	0.9
CF_3	0.43	0.54	SCOMe	0.39	0.44
CH_2SiMe_3	-0.19	-0.22	SOMe	0.52	0.49
N_2^+	1.76	1.91	SCF_3	0.40	0.50
NH_2	-0.16	-0.66	SO_2Me	0.56	0.68
NHMe	-0.3	-0.84	SO_2CF_3	0.79	0.93
NMe_2	-0.05	-0.83	SO_2NH_2	0.55	0.62
$^{+}NMe_3$	0.88	0.82	SO_3^-	0.05	0.09
NHCOMe	0.21	0	SeMe	0.1	0
$NHNH_2$	-0.02	-0.55	$SiMe_3$	-0.04	-0.07

Standard Hammett σ-constants, based on ionization of benzoic acids